THE UNIVERSITY
of EDINBURGH

Solvent Effects on Hydrogen Bonding

Nicole Yvette Meredith

Doctor of Philosophy

The University of Edinburgh

2019

Declaration

I declare that this thesis has been composed entirely by myself.

I confirm that a substantial volume of the research presented herein has been carried out by myself, and any contributions from other researchers have been outlined at the beginning of each chapter.

I declare that this work has not been submitted for any other degree or professional qualification.

Date: ……. Signature: …….

Contents

Acknowledgements

A huge thanks to Dr Scott Cockroft for his focus and determination, for constructive scientific chats, and for steering the projects into fruitful chapters.

I extend this thanks to the rest of the Cockroft group: Thanks to Becky for enlightening fumehood discussions, Karina for her positivity, Qingshu for his kindness, Stefan for helpful scientific inputs, Dominic for sharing both desk space and industrial collaborators, Justin for his understanding and Antoine for his friendship and fondues!

A special thanks is due to the University of Edinburgh staff, in particular Dr Lorna Murray and Mr Juraj Bella, for their help with NMR experiments.

Importantly, I would like to thank Syngenta and EPSRC for the funding and Dr Kenny Ling and Dr Chris Baker for useful conversations.

Cheers to all my closest friends, for providing me with fun escapes away from PhD stress.

Finally, I thank my Mum and Dad and the rest of my family for their support and encouragement.

Abstract

Determining the strength of H-bonds in solution can be challenging due to competing solvent interactions, especially in biologically relevant polar solvents such as water. In this thesis, various molecular balance designs are used to quantify the strength of H-bonds in solution.

Chapter 1 presents a literature review on optimising H-bond interactions, with a focus on experimental systems previously used to quantify the strength of H-bonds in different solvents.

Chapter 2 investigates the effectiveness of implicit solvation models for predicting the thermodynamic behaviour of different solvents using a simple series of molecular balances. Computationally determined equilibrium energies are compared with experimental values. Generally, the implicit solvation models are found to have good correlations in non-polar solvents, but poorer results are observed when moving onto more polar solvents.

Chapter 3 provides an experimental study of organic and aqueous solvent effects on intramolecular H-bonding between amide and anilines. Several series of compounds are investigated, where both H-bond geometry and conformational flexibility are varied. Thermodynamic information is derived from the balances and the experimental data examined further by plotting against computational results and fitting with a semi-empirical solvation model.

Chapter 4 presents a study on solvent effects on H-bond cooperativity. A phenol, catechol and pyrogallol molecular balance series are synthesised and experimental energies are derived. Three different types of behaviour are observed depending on the acceptor ability of the solvent.

Lay Summary

Hydrogen bonds (H-bonds) are prevalent non-covalent interactions in biology, supramolecular polymer chemistry and molecular recognition. In biology and chemistry, H-bonds are often solvated and therefore the extent to which individual interactions contribute is hard to quantify. Understanding fundamental H-bond interactions is important to determine how these processes work and also to aid rational drug design.

The research presented in this thesis aims to quantify H-bond interactions in solution through the use of molecular torsion balances. A molecular torsion balance adopts two distinct conformations and allows the measurement of weak interactions which is useful when studying H-bonds in competitive solvents. Several designs of molecular balances are synthesised to probe electronic, distance and solvent effects on the strength of H-bonds. Computational and experimental methods are used to analyse the systems.

The results of this thesis may have important implications in understanding protein-ligand binding, and could be of use in the agrochemical and medicinal industries. The experimentally determined values could be used as benchmarks to improve current computational solvation methods.

Abbreviations

1D	1-dimensional
2D	2-dimensional
$\Delta\delta$	change in chemical shift
α_2^H	H-bond donor constant
β_2^H	H-bond acceptor constant
AM1	Austin Model 1
A	adenine
Ac	acetyl
Ar	aromatic
B3LYP	Becke, three-parameter, Lee-Yang-Parr exchange-correlation functional
Bu	butyl
c_{ed}	cohesive energy density
COSY	correlation spectroscopy
CSD	Cambridge Structural Database
d	doublet
dba	dibenzylideneacetone
DCM	dichloromethane
DFT	density functional theory
DMEDA	N,N'-dimethylethylene diamine
DMF	dimethylformamide
DMSO	dimethyl sulfoxide
DNA	deoxyribonucleic acid
EDG	electron donating group
ESP	electrostatic potential
EWG	electron withdrawing group
FBS	Fetal Bovine Serum
HF	Hartree-Fock
HMBC	heteronuclear multiple-bond correlation spectroscopy
HRMS	high resolution mass spectrometry
HSQC	heteronuclear single-quantum correlation spectroscopy
IEF-PCM	integral equation formalism- polarizable continuum model
IR	infrared spectroscopy
m	multiplet
m	meta
m.p.	melting point
Me	methyl
MO	molecular orbital
NMR	nuclear magnetic resonance
o	ortho
o/n	overnight
p	para

PBS	phosphate buffered saline
PCM	polarizable continuum model
PEG	polyethylene glycol
Ph	phenyl
ppm	parts per million
Py	pyridyl
q	quartet
r.t.	room temperature
s	singlet
S. D.	standard deviation
SM8	solvation model 8
SM12	solvation model 12
SMD	solvent model based on density
t	triplet
TFA	trifluoroacetic acid
THF	tetrahydrofuran
TLC	thin layer chromatography
VT-NMR	variable temperature NMR

Chapter 1

Quantifying H-Bond Interactions

Abstract

Hydrogen bonds are ubiquitous in nature. In biological systems, water competes strongly with H-bonds therefore the extent to which H-bonds regulate molecular interactions is difficult to quantify. Thus, various experimental model systems have been developed to probe H-bonds in solution. The following chapter provides an introduction into the energetics of H-bonding interactions in solution. A variety of different systems are reported. The focus has been on studies where quantitative binding energies in H-bonded systems have been determined in both non-polar and polar solvents.

Contributions: This chapter is a literature review complied by Nicole Yvette Meredith (NYM).

1.1 Introduction

The hydrogen bond was first discovered over 100 years ago.[1,2,3] From the 1920's onwards, Latimer and Rodebush,[1] Huggins[3] and Pauling[4,2] all played pioneering roles in developing the classical view of the hydrogen bond. The classical view stated that H-bonds were directional, attractive interactions X-H–A formed by strongly electropositive atoms on one side, and electronegative atoms on the other (X= O, N, halogen; A = O, N, S, halide etc.). Over a century later, further research highlighted that the hydrogen bond was a much broader phenomenon. H-bonds are now known that are so strong that they resemble covalent character, whereas others are so weak that they are hard to distinguish from van der Waals interactions.[5] Jeffery defined H-bonds as weak, strong, and in between depending on the distance and directionality of the H-bond.[6] Advancements in diffraction techniques allowed the geometry and directionality of N–H···O=C H-bonds to be analysed in a large data set of crystals.[7-8] Taylor[9] found that there was a statistical significant tendency for H-bonds to occur in the directions of the sp^2 lone pairs, and this directionality became more pronounced as the H-bond distance decreased. Whilst techniques such as X-ray crystallography provide useful insights into H-bond geometry and directionality,[10] the study of H-bonds in solution is complicated by solvent effects which can significantly change the nature of these interactions.

In nature, H-bonds are solvated. H-bonds play key roles in DNA base pairing,[11] protein interactions,[12,13] enzyme catalysis,[14,15] protein-ligand binding,[16] and in determining the properties of bulk liquids.[17] Using various computational[18] and experimental systems, the energetic contributions to H-bonding can be derived to further our understanding of these biologically important associations. Quantifying the binding energies of H-bonds is also key for the design and optimisation of application-oriented systems. In the following sections, various different strategies are described to quantify the H-bond interaction energy values from synthetic and protein-based supramolecular complexes.

1.2 H-Bond Energies in Small Molecules

Thousands of H-bond binding constants between small molecules have been measured in organic solvents using spectroscopic techniques. Laurence[19] determined the binding constants for primary amine acceptors using 4-fluorophenol as a reference H-bond donor in carbon tetrachloride. However, it was Abraham and Raevsky who carried out the most comprehensive investigation of H-bond energies between small molecules. Abraham[20-21] studied intermolecular H-bonding between a wide range of different compounds against a reference H-bond donor, e.g. 4-nitrophenol, and a reference H-bond acceptor molecule, e.g. *N*-methylpyrrolidone, in non-polar solvents such as carbon tetrachloride. NMR titrations were carried out between the donor/acceptor molecules with the solute to measure the 1:1 association constants. This enabled the determination of H-bond donor and acceptor parameters, α_2^H and β_2^H using equation 1.1.

$$\log K = c\alpha_2^H\beta_2^H + c' \quad (1.1)$$

where *K* is the association constant for the formation of a 1 : 1 complex, and c and c' are constants that depend on the solvent.

Hunter[22] used Abrahams work to develop an electrostatic solvent competition model describing solvent effects on intermolecular H-bonding. Abraham's α_2^H and β_2^H constants were plotted against the calculated maximum and minimum on the molecular electrostatic potential surfaces respectively, showing reasonable linear correlations despite the low-level Austin Model 1 (AM1) semi-empirical method used to calculate the electrostatic potentials (Figure 1.1).

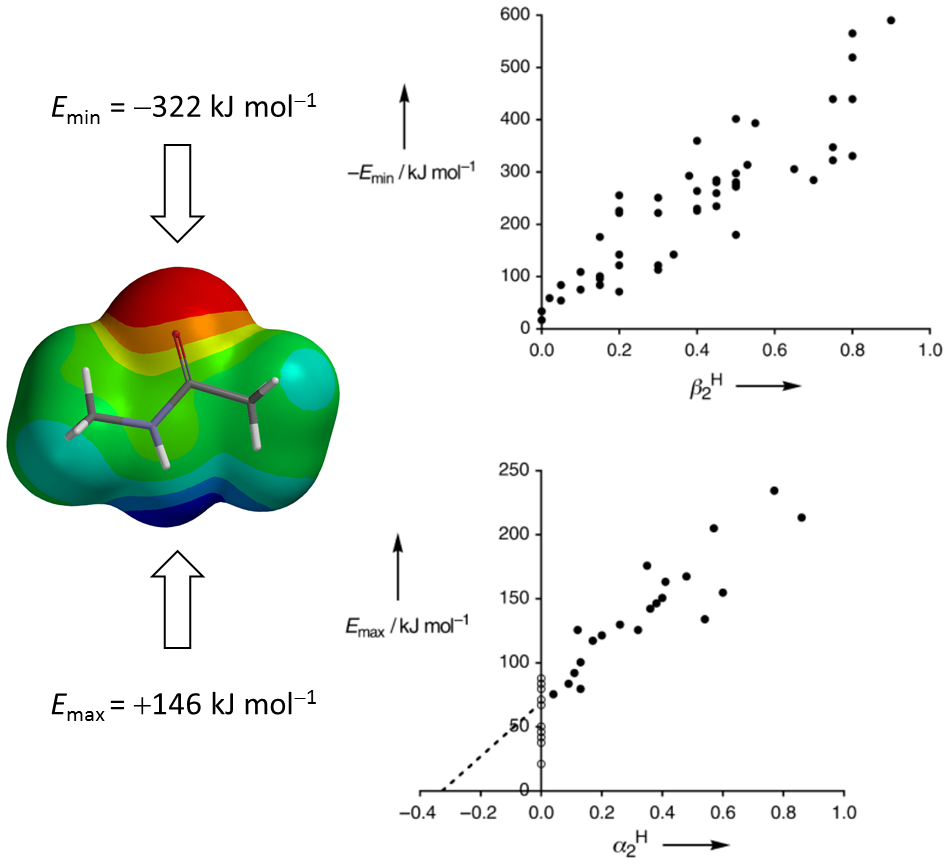

Figure 1.1: Hunter plotted the Austin Model 1 (AM1) calculated molecular electrostatic potential surfaces, maxima (E_{max}) and minima (E_{min}), of a range of simple molecules containing only one functional group against the corresponding experimentally determined values of α_2^H and β_2^H constants.[22] For simple functional groups, the primary mode of interaction is hydrogen-bond contacts between the maxima (blue) and minima (red) in the electrostatic potential surfaces of the molecules.

A higher E_{max} corresponds to a stronger H-bond donor, whereas a lower E_{min} value corresponds to a stronger H-bond acceptor. The α and β values were therefore derived for any molecule from the corresponding calculated electrostatic surface potentials, or determined experimentally by carrying out NMR titrations. This suggested that a simple electrostatic model provided a good quantitative description of the thermodynamic properties of H-bonds in solution. It is important to note that the correlation intersected the E_{max} axis at 100 kJ mol^{-1}, which was the calculated E_{max} value for carbon tetrachloride. This means that the solute H-bond scales have origins that are determined by the solvent used to make the measurements. From Figure 1.1,

it is implicated that for equilibria in solution, there is a competition between solute-solute and solvent-solute interactions. This led to Hunter proposing Equation 1.2:

$$\Delta G = -(\alpha - \alpha_s)(\beta - \beta_s) + 6 \text{ kJ mol}^{-1} \quad (1.2)$$

Where α and β are the H-bond donor and acceptor constants of the H-bond donor and acceptor respectively, and α_s and β_s are the H-bond donor and acceptor constants of the solvent. The equation was used to produce a generalised functional group interaction profile that describes whether a non-covalent interaction between two solutes is favourable or not in a given solvent (Figure 1.3). In zone **A**, solute-solvent interactions are shown to dominate, and therefore the equilibrium lies towards the reactants, and the interaction between solutes is not favourable. However, in zone **B**, solute-solute interactions are favourable. The top right square corresponds to interactions where the $\alpha\beta$ term dominates, whereas zone **C** represents the solvophobic zone, where solvent-solvent interactions dominate the position of the equilibrium. Figure 1.4A gives an indication of the strengths of different organic H-bond acceptors, whereas Figure 1.4B represents the magnitudes of different H-bond donor organic molecules.

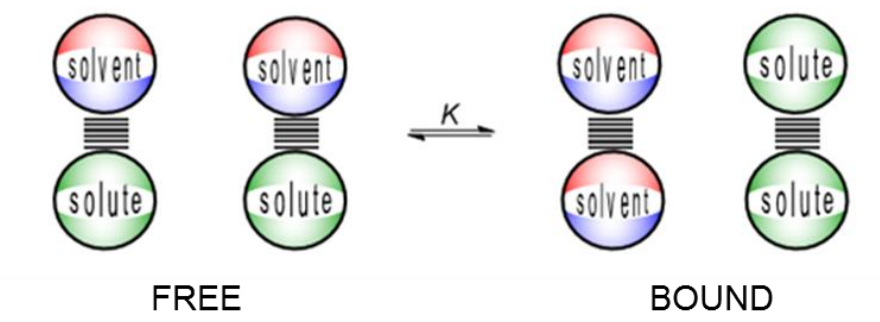

Figure 1.2: Intermolecular H-bond interactions in solution are a competition between solute–solvent interactions in the free state, and solute–solute and solvent–solvent interactions in the bound state.[22]

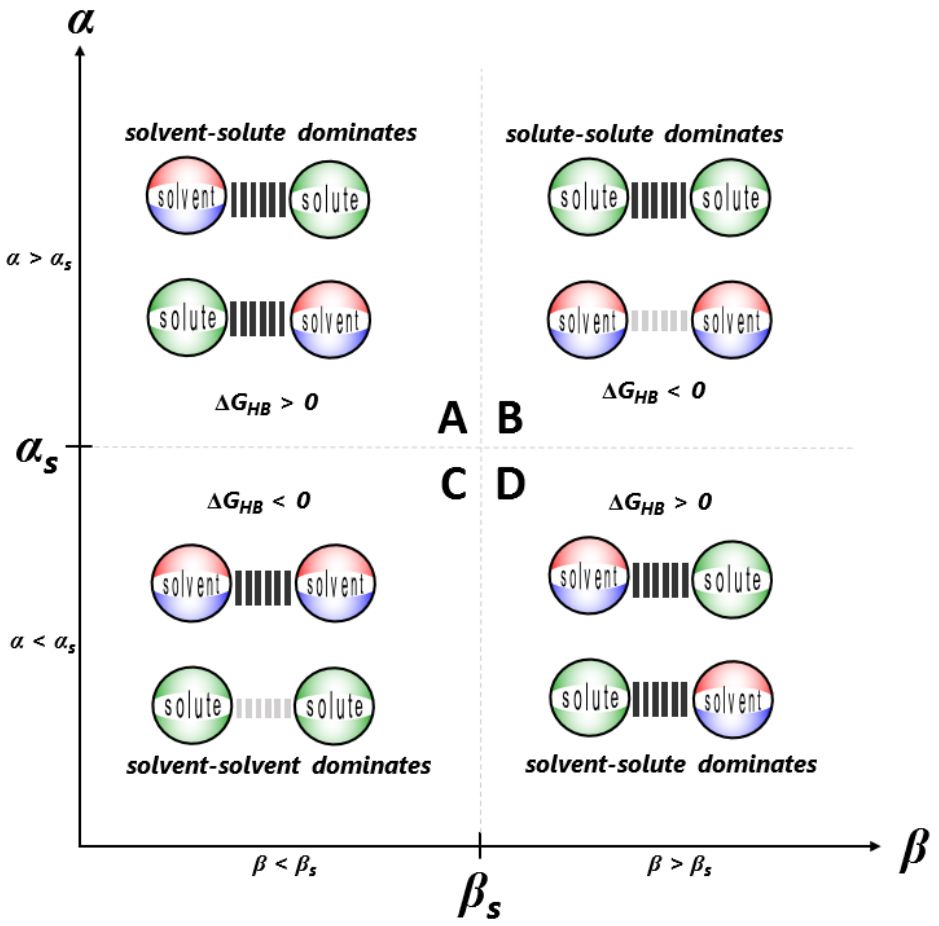

Figure 1.3: Generalised interaction profile illustrating how the free energy of interaction between two functional groups varies as a function of their H-bond parameters, α and β. In zone **A**, solvent-solute interactions dominate and solute-solute interactions are unfavourable. In zone **B**, solute-solute interaction dominate. In zone **C**, solvent-solvent interactions dominate leading to attractive solute-solute interactions. The values of the H-bond parameters for the solvent, α_s and β_s set the boundaries between four different quadrants.[22]

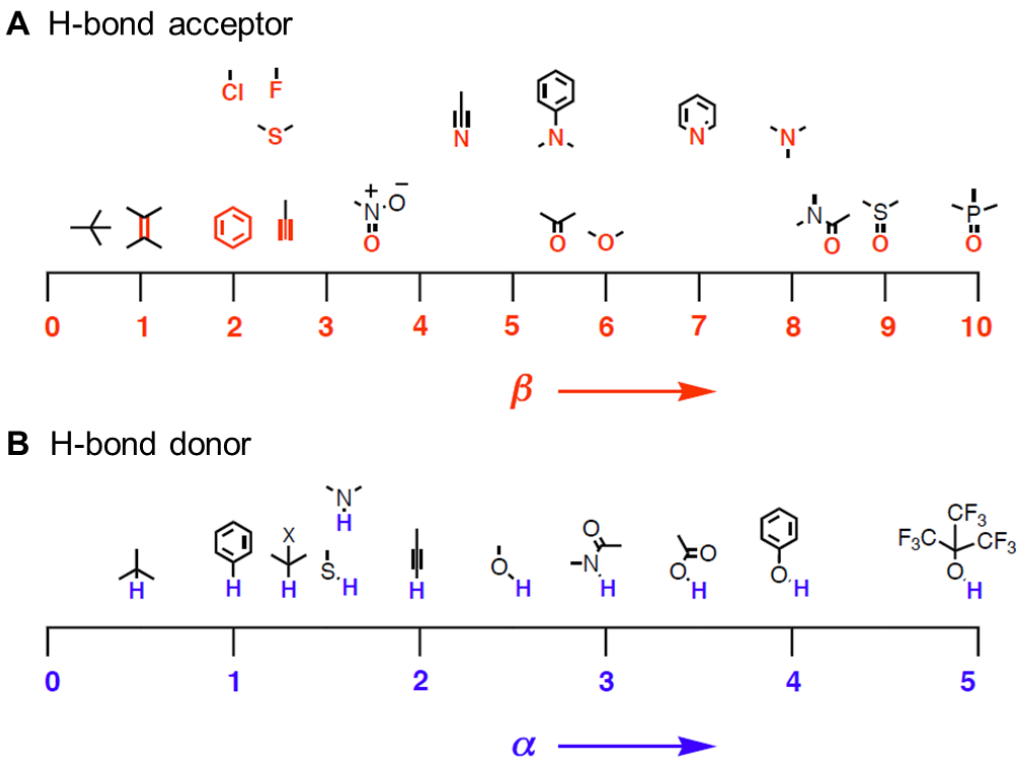

Figure 1.4: A H-bond acceptor constants for a range of functional groups. **B** H-bond donor constants for a range of H-bond donors.

Hunter carried out further investigations on intermolecular H-bonding between small molecules in organic solvents and solvent mixtures, where Equation 1.2 was experimentally validated.[23-24] NMR titrations were used to determine H-bond energies between an exceptionally strong H bond donor, *per*-fluoro-*tert*-butyl alcohol, and a strong acceptor, *tri*-*n*-butlyphosphine (Figure 1.5A). This donor and acceptor did not self-associate and formed a 1:1 complex featuring a single well-defined H-bond between the phenol and P=O group. Large changes were observed in the ^{31}P chemical shift which allowed complexation to be monitored readily (Figure 1.5B), it was also possible to measure complexation in polar solvents due to the exceptional strength of the donor and acceptor.

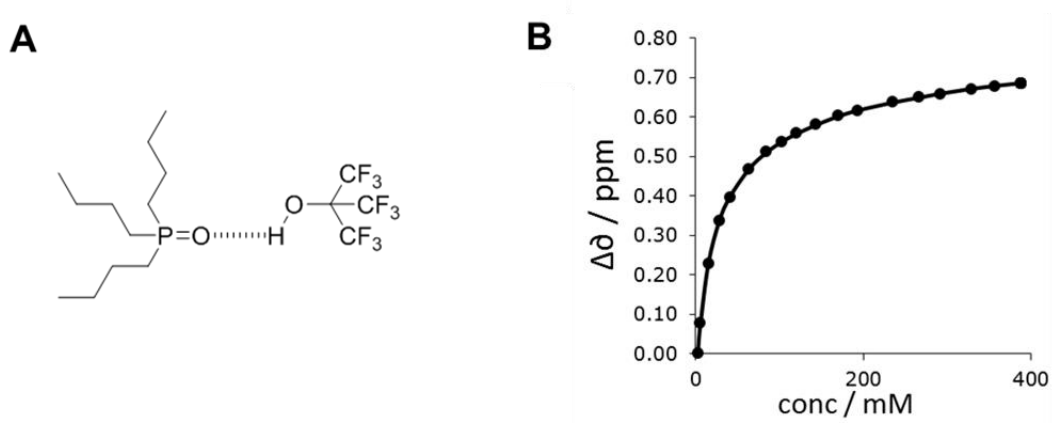

Figure 1.5: A Intermolecular H-bonding system used by Hunter *et al*[25] to investigate H-bonding between a strong H-bond donor, *per*-fluoro-*tert*-butyl alcohol, and a strong H-bond acceptor, *tri*-*n*-butlyphosphine in a variety of solvents. **B** An example binding curve obtained from ^{31}P NMR titration experiments. A plot of the concentration of *tri*-*n*-butlyphosphine against the change in ^{31}P chemical shift allows the binding constant between the H-bond donor and H-bond acceptor to be obtained.

Intermolecular H-bonding between perfluoro-*tert*-butyl alcohol and tri-*n*-butylphosphine oxide was also investigated in solvent mixtures.[25] Association constants were determined in solvent mixtures of chloroform and tetrahydrofuran, the stability of the complex was found to be highest in pure chloroform (K = 250 M^{-1}) and lowest in a 2:1 mixture of chloroform and tetrahydrofuran (K = 15 M^{-1}). This finding implicated that the addition of a less polar solvent (chloroform) to a more polar solvent (tetrahydrofuran) produced a significantly more polar mixture. This behaviour was explained using Hunter's simple solvent-competition model (Equation 1.2), the equation was based on the relative H-bond donor/acceptor abilities of the solvent and solute. Therefore, as chloroform (α = 2.2, β = 0.8) and tetrahydrofuran (α = 0.9, β = 5.3) had very different H-bond donor/acceptor constants, perfluoro-*tert*-butyl alcohol (good donor) was preferentially solvated by tetrahydrofuran (good acceptor) and tri-*n*-butylphosphine oxide (good acceptor) was solvated by chloroform (good donor). Using Equation 1.2 a log K value was determined that compared well with the experimental results.

Further intermolecular H-bonding interactions were studied between 4-phenyl azophenol (Figure 1.6) and *tri*-*n*-butylphosphine oxide in polar liquids.[26] Association constants of complexation between donor and acceptor were measured in *n*-octane/*n*-

decanol, *n*-octane/*n*-hexanoic acid, and *n*-octane/2-ethylhexyl acetamide solvent mixtures. It was found that the polar solvents associated differently in alkanes. Carboxylic acids formed dimers in concentrated solution, secondary amides formed linear polymers and the alcohols formed cyclic tetramers at concentrations above 1 mM. The association of the polar liquids in alkanes then interact with the donor and acceptor solutes differently (Figure 1.6). The carboxylic acid and secondary amide dimers have no hydrogen-bond acceptor groups free to bind to the hydrogen bond donor, resulting in a lower polarity solvent. The alcohols associate in a cyclic tetramer, therefore the oxygen sites are able to hydrogen bond to a competing hydrogen-bond acceptor group resulting in a higher polarity solvent mixture.

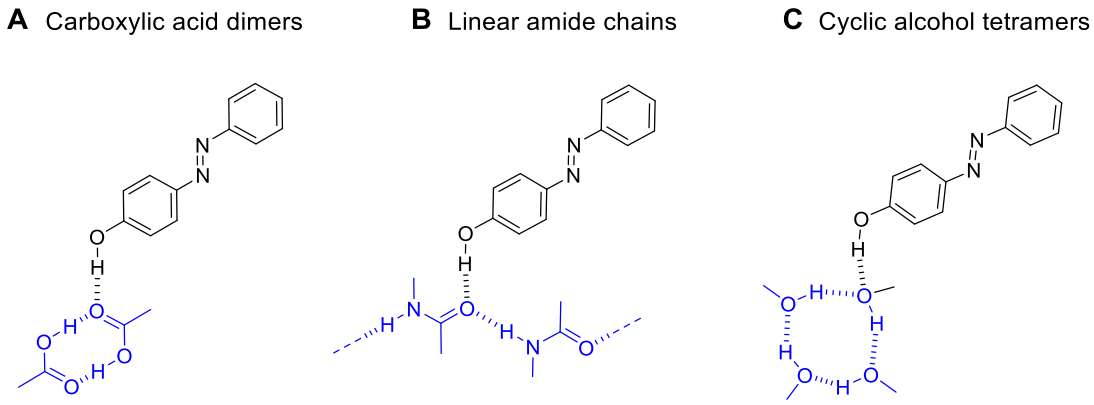

Figure 1.6: H-bond solvation modes of 4-phenyl azophenol in different alkane solvent mixtures, studied by Hunter *et al*.[26] 4-phenyl azophenol bonds to **A** *n*-hexanoic acid, **B** 2-ethylhexyl acetamide and **C** *n*-decanol.

Equation 1.3 has also been used to determine the β constants for both metal fluoride complex H-bond acceptors[27] and various anionic H-bond acceptors in organic solvents.[28] For the metal fluoride complexes, it was found that group 10 metal fluorides exhibit exceptionally strong H-bond character, the strongest H-bond acceptor is nickel fluoride with R = Et (β = 12.1), and palladium fluoride with R = Cy (β = 11.6). These group 10 metal fluorides have similar strength to the strongest organic H-bond acceptors (Figure 1.7) such as trimethylphosphine (β = 10.7), this strength was attributed to the polarity of the M–F bonds. The group 4 metal difluorides were found to be weaker H-bond acceptors relative to the group 10 metal fluorides. The Cp* (β = 6.9–5.4) series displayed slightly stronger H-bond acceptor ability, compared to the Cp series (β = 4.7–5.8), due to the electron releasing nature of Cp*.

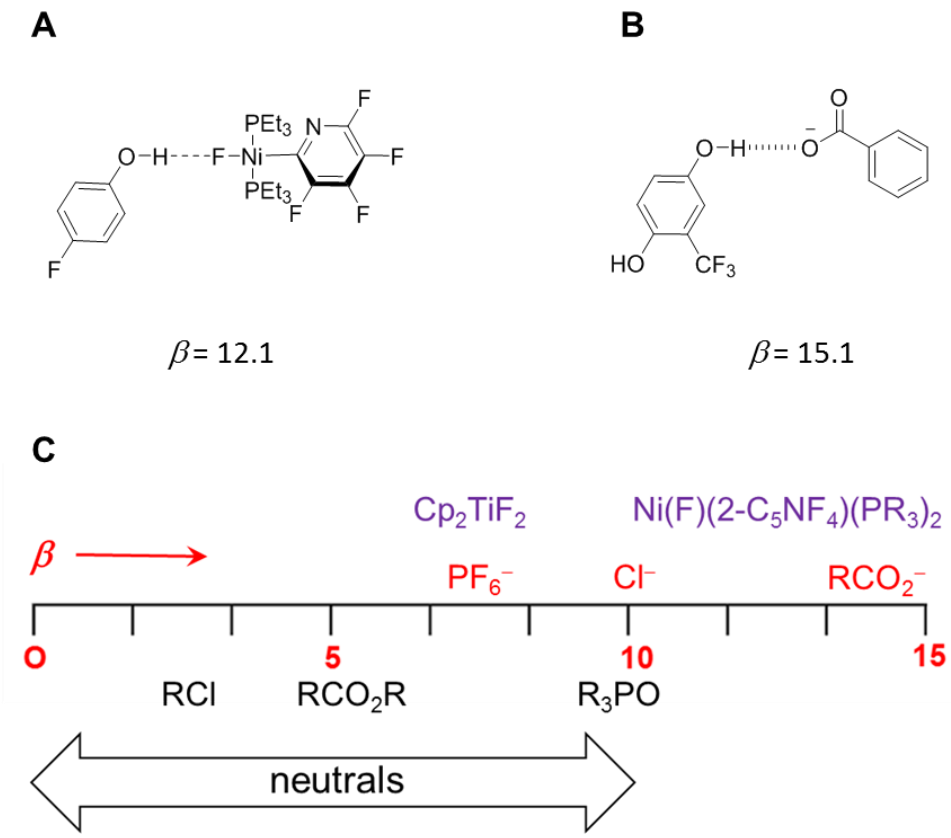

Figure 1.7: The phenols used by Hunter[27] to determine the β values of **A** group 10 metal fluoride H-bond acceptors and **B** anion acceptors. **C** A scale showing the range of β values determined for organic H-bond acceptors, metal fluoride H-bond acceptors and anion H-bond acceptors.

For the PF_6^-, Cl^- and RCO_2^- anions investigated (Figure 1.7), the carboxylates were found to be the strongest H-bond acceptors ($\beta = 15.0$), with strengths greater than those of all previously studied neutral species, whereas PF_6^- was found to be the weakest anion ($\beta = 7.0$). Sulfonate anions were also investigated where the β constants were found to vary ($\beta = 9.4 - 10.4$),, showing that the electronic effects of substituents are similar to the neutral H-bond acceptors. The counter cations were systematically varied to investigate the influence on ion pairing on the measured β values, and ion pairing was found to only compete with H-bond formation for small polar countercations (tetraethylammonium) in less polar solvents such as chloroform.

Other groups have used pK_a values to evaluate the strength of H-bonds between complexes.[10] The strength of a D-H···A bond (where D corresponds to an H-bond

donor and A corresponds to an H-bond acceptor) bond has been suggested to increase with decreasing ΔpK_a. Where ΔpK_a is defined using Equation 1.3:

$$\Delta pK_a = pK_a\,(D{-}H) - pK_a\,(A{-}H^+) \qquad (1.3)$$

Gilli *et al* published a paper on predicting H-bond strengths based on the pK_a values of H-bond donor and acceptors. It was confirmed experimentally that the strength of the H-bond increases as ΔpK_a approaches zero.[10] Intramolecular H-bonds in a series of substituted salicylate molecules were studied as a function of ΔpK_a in DMSO and water.[29] A strong linear relationship was found on plotting log$K$ values against ΔpK_a values, steeper slopes were found for DMSO relative to water which indicate that hydrogen bonds undergo larger changes in organic media as the charge density on the donor or acceptor atom increases (Figure 1.8).

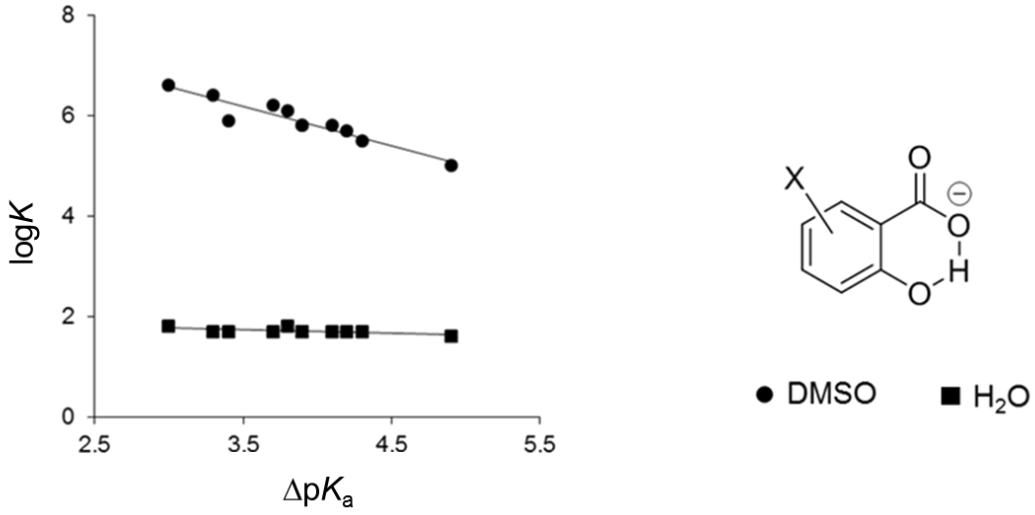

Figure 1.8: Logarithms of stability constants of intramolecular H-bonds in a series of salicylate molecules in DMSO and H_2O plotted against differences of pK_a values of donor and acceptor molecules.[29]

The preceding section, described the determination of α and β for different H-bond donor and acceptor molecules, as well as the effects of solvation on specific binding events. Other research groups have studied steric and electronic effects on H-bonding energies in $CDCl_3$. To investigate electronic effects, Pluth[30] synthesised a number of H-bond donors with differing electronic groups and carried out binding studies with the H-bond acceptor diethyl barbital (Figure 1.9). Binding energies were

found to be higher for compounds bearing electron-withdrawing groups relative to those containing electron-donating groups, since pulling electronic density away from the H-bond donor makes a proton more electropositive and therefore a better H-bond donor. The binding energies were then plotted against the corresponding σ_p values to give a curved Hammett plot. The authors partitioned the curve into regions with different positive slopes with ρ values of 1.08 ± 0.08 for the compounds bearing electron-donating groups and 0.37 ± 0.02 for those bearing the electron-withdrawing groups. This change in gradient suggested a structural change in the binding conformation, which was supported using B3LYP/6-31G* calculations that employed the IEF-PCM implicit solvation model for $CHCl_3$. This study revealed how electronic changes not only affect the thermodynamics of H-bonds but also structural changes too.[30]

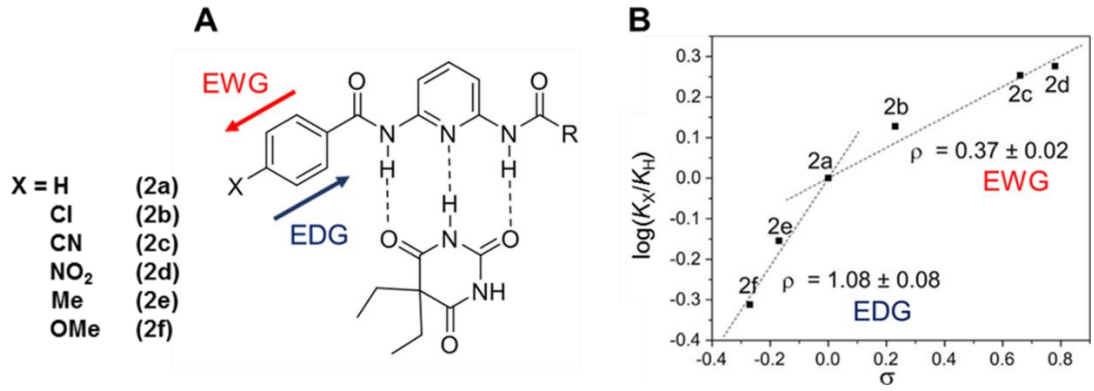

Figure 1.9: A H-bond donor and acceptor used by Pluth[30] to investigate H-bond binding. Effects of electron donating (EDG) and withdrawing (EWG) groups on the electron density of 2,6-diamidopyridine receptors. **B** Hammett plot of H-bond donors **2a-f** binding to H-bond acceptor diethyl barbital. Donors **2a-f** are shown above with varying X groups.

1.3 Host-Guest Interactions

Many groups have studied H-bond interaction energies in solution using supramolecular complexes. In contrast to binding between small molecules, supramolecular complexes often involve multiple interaction sites.

C–O···H$^+$ Hydrogen Bonding

Cationic H-bonding between crown ether-ammonium complexes has been studied. Schneider[31] measured the binding energies between 18-crown-6 complexes

and ammonium cations in a series of solvents using titration calorimetry. The binding energies were found to have large entropic contributions, counteracting the enthalpy of complexation. A strong correlation was found between the binding energy with the number of available $^{+}$N-H bonds. Solvent effects on the system were also investigated. Binding constants were obtained in polar solvents such as water, 2-propanol, *t*-butyl alcohol, *n*-octanol, DMF, DMSO, and pyridine and were found to vary by factors of up to 1000. These solvent effects on the association constants were described as a linear function of the accepting ability of the solvent molecules, β. These results highlighted the predictive ability of simple solvent parameters (Figure 1.10).

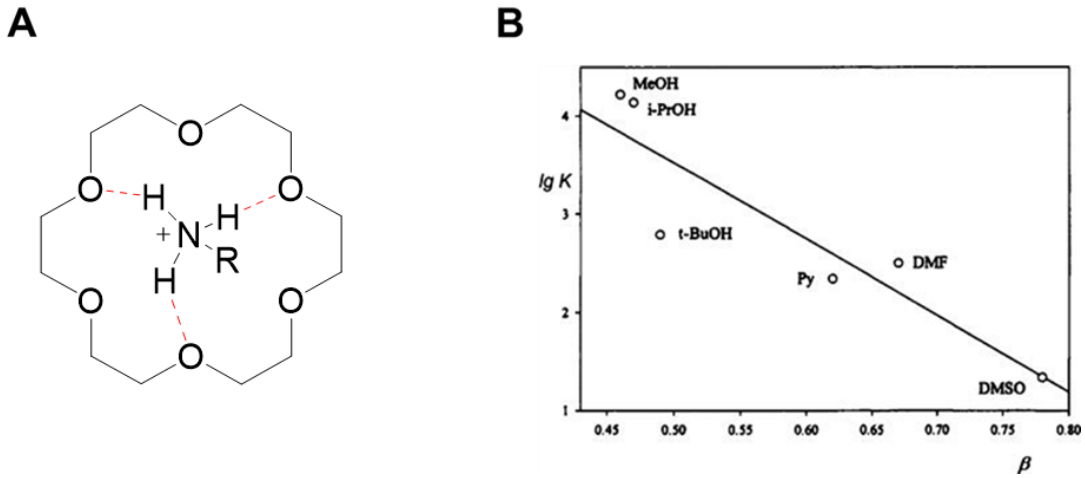

Figure 1.10: A Cationic binding between crown ether ammonium complexes. R group corresponds to benzyl ammonium chloride. **B** Solvent effect on lg *K* values of H-bond between 18-crown-6 and benzyl ammonium chloride against the solvent basicity parameter β of the solvent.[31]

C–H···A⁻ Hydrogen Bonding

Various supramolecular structures have been designed to study anionic H-bonding.[32-33] Luminescent and colorimetric sensors have also been investigated to study anions in organic and aqueous media using H-bonds.[34-35]Johnson and Haley investigated substituent effects on aryl CH hydrogen bonding by synthesising supramolecular structures (Figure 1.11).[36] The methoxy-substituted phenylureas acted as hydrogen bond donors to direct the anion into the binding site, whereas the *t*-butyl groups were incorporated to provide solubility in organic solvents. The R-groups were then systematically varied with electron withdrawing/donating groups.

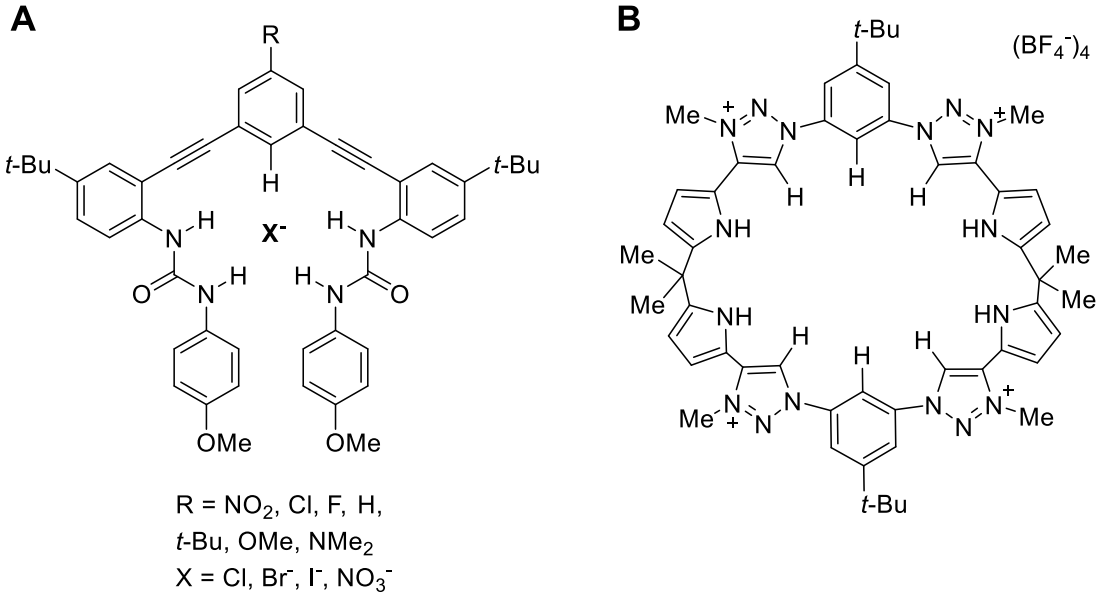

Figure 1.11: **A** Supramolecular complex designed by Johnson and Haley[35] used to study H-bonding between ureas and anions. **B** Sessler[36] synthesised a pyrrole-based triazolium-phane receptor used to study H-bonding between anions and NH bonds.

The binding of anions into the receptors was investigated in water saturated $CDCl_3$ mixtures using NMR and UV/vis titrations. It was found that the resonance contribution of a substituent played a role in dictating the H-bond strength: the more electron withdrawing the R group, the stronger the binding to the anion. The strength of the CH hydrogen bonds was tunable across a range of 4.3-5.1 kJ mol^{-1} by altering the R group. Also, the selectivity of the receptors for the anions followed the trend of $Cl^- > NO_3^- > Br^- >> I^-$ for all hosts. The results provided important insights into accomplishing CH hydrogen bond optimisation.

Sessler[33] and co-workers synthesised a pyrrole-based triazolium-phane receptor that bound anions via NH and CH hydrogen bonds. The receptor was shown to display a highly solvent-dependent selectivity for tetrahedral oxyanions in comparison to monoanions and trigonal planar anions; e.g. $\Delta G = -40$ kJ mol^{-1} for HSO_4^-, and 36 kJ mol^{-1} for chloride binding in acetonitrile. The complexation energy of HSO_4^- was weakened to −31 kJ mol^{-1} in the more competitive acetone/water (2:3) solvent mixture, while chloride binding was no longer detectable.

The Hunter group synthesised a water-soluble supramolecular complex that bound cyclic dipeptides in water (Figure 1.12).[37] NMR titrations were carried out to determine the binding energies with various guests, the values were then compared against previously determined H-bond energies in chloroform using an organic analogue (where R = CH_2 in Figure 1.12). The binding energies in water were found to be substantially smaller than in chloroform, this was consistent with an increase in solvent competition for the hydrogen-bonding sites. It was also found that there was not a uniform change in selectivity across the guests studied. It was found that the energy penalty for desolvation upon complexation was greatest for the most polar guest molecules.

R = CH_2, $N^+Me_2Cl^-$

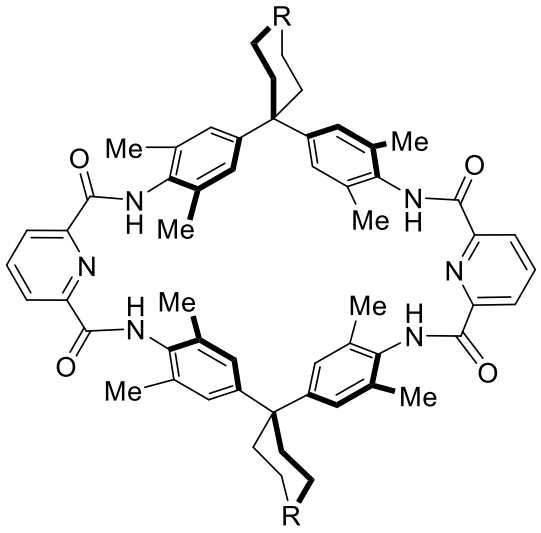

Figure 1.12: Water soluble (R=$N^+Me_2Cl^-$) and organic (R=CH_2) supramolecular structures used by Hunter *et al*. [37]

Both organic and water soluble receptors have been designed that effectively bind to carbohydrates via H-bonds and CH···π interactions.[38-39] Mazik *et al*[38]

synthesised carbohydrate receptors involving a macrocyclic building block and two flexible side arms (Figure 1.13). These receptors bound to the sugars via a multitude of interactions involving H-bonds and CH···π interactions. The sugars were extracted from aqueous solution into organic media and experimental binding energies determined using ^{1}H NMR and fluorescence spectroscopy. Binding energies were also determined in homogeneous organic media. Very strong 1:1 complexes were found with β-glucoside, where the binding energy was determined to be –28.5 kJ mol^{-1}. Meanwhile, the Davis[40] group managed to synthesise water-soluble synthetic lectins that bound glucose molecules in water; the structure and binding studies of these complexes are detailed in Chapter 4.

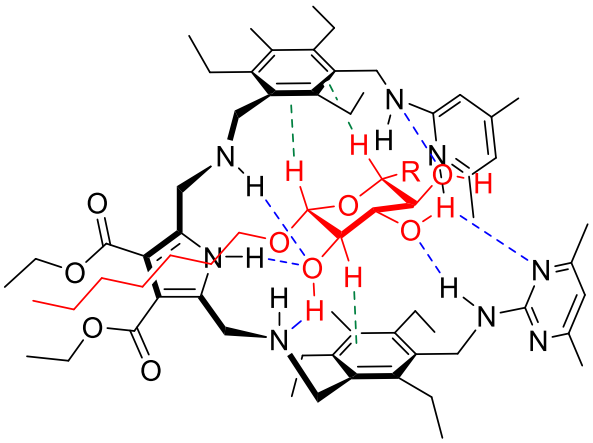

Figure 1.13: Artificial receptor synthesised by Mazik *et al*[38] used to bind carbohydrate molecules.

1.4 H-bonding in Proteins

Encouraged by the pharmaceutical and agrochemical industries, many groups have researched H-bonding binding energies from protein complexes to aid rational drug design.[41,42,43] X-ray crystallography has been used to shed light on biological structures whereas thermodynamic information has been extracted using affinity screening.[44,45] Computational efforts to understand H-bond energetic contributions to protein folding and protein-ligand binding have also been carried out.[46,47]

Kelly[48] investigated the dependence of hydrogen bond strength on the polarity of the microenvironment using protein backbone and side chain mutagenesis (Figure 1.14). Amide-to-ester mutation of the backbone perturbed hydrogen bonding, whereas

altering the side chain groups perturbed the microenvironment polarity. A thermodynamic cycle revealed that hydrogen bonds were stronger by up to 5.1 kJ mol^{-1} in hydrophobic surroundings compared to when they were exposed to solvent. This finding has important implications on the forces driving protein folding.

Raines has carried out studies on carbonyl-carbonyl interactions[49] and H-bond interactions in proteins.[50] H-bond interactions in proteins were studied using quantum mechanical calculations, IR spectroscopy and ^{1}H NMR spectroscopy. Density functional theory (DFT) calculations were carried out on a peptide backbone model, followed by natural bond orbital (NBO) analysis to show that the C5 H-bond interaction could make a significant contribution to the stability of these conformations (Figure 1.14).

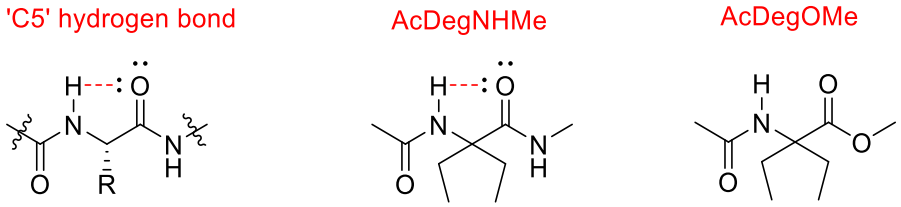

Figure 1.14: Peptides studied by Raines showing the putative C5 hydrogen bond, characterised by overlap of the p-type carbonyl lone pair and N-H sigma star orbital.[50]

Experimental studies were then performed on diethylglycine residues to probe the C5 hydrogen bond. Infrared spectroscopy and nuclear magnetic resonance spectroscopy were used to show that the C5 hydrogen bond in the AcDegNHMe residue was stronger relative to the AcDegOMe residue, which was consistent with the predicted NBO analysis. D_2O exchange rate experiments also confirmed that both residues were forming the C5 H-bonding geometry. H-bonding was also investigated in β-sheets, where biophysical analyses demonstrated that selective attenuation or enhancement of the C5 H-bonds affected the stability. It was therefore found that these interactions provided conformational stability to a typical protein.[50]

Using high resolution protein crystal structures, Raines[51] investigated the contributions of H-bonds and carbonyl-carbonyl n→π* interactions in asparagine residues (Figure 1.15). These residues were capable of accepting a hydrogen bond from a donor and also capable of donating an n→π* interaction to a carbonyl group.

Natural bond orbital (NBO) analysis was carried out to determine the relative energetic contributions of the H-bonds and the n→π* interactions to these residues. Unsurprisingly, H-bonds were found to be the stronger interaction. The n→π* interactions were determined to be worth ~5−25% of a hydrogen bond and the stronger hydrogen bonds tended to obscure the n→π* interactions. In contrast, weaker H-bonds correlated with stronger n→π* interactions. It was therefore concluded that both these interactions contribute to the stability of protein backbones, and that n→π* interactions should be included in force fields for biomolecular modelling.

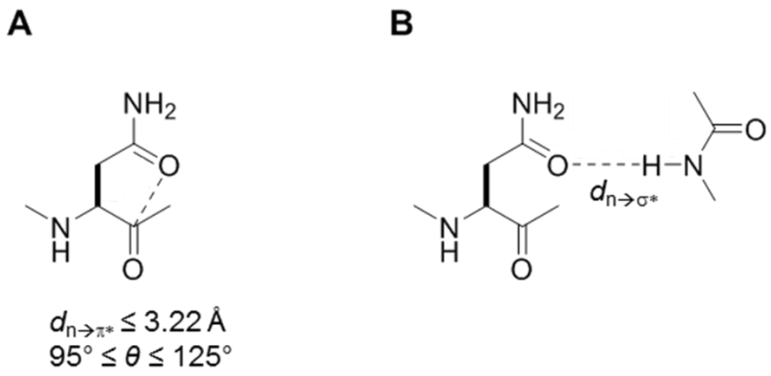

Figure 1.15: Interactions studied by Raines[52]. Parameters defining **A** n→ π * interactions and **B** hydrogen bonds in asparagine side chain systems.

N−H···N hydrogen bonds have been investigated in proteins by Romesberg[53] using deuterated variants of proline. Experimentally, IR spectroscopy was carried out to reveal blue shifts in C−D bonds due to hyperconjugation with N electron density. Computational studies on dipeptide mimics supported the experimental finding that H-bonds were forming; as DFT and NBO analysis showed orbital overlap, indicative of n → σ* interactions expected for H-bond formation between N−H···N bonds. These results suggested that these interactions contribute to the stability of proteins and should not be overlooked.

Raines has studied the competition between H-bonding and n→π* carbonyl-carbonyl interactions by designing and synthesising a model system based around the amino acid proline (Figure 1.16).[52] The keto and enol forms of the structures synthesised interconverted slowly enough on the NMR timescale so that they could be easily distinguished. The proton highlighted in red was easily assigned in conformers where either an intramolecular H-bond or proposed n→π* carbonyl-carbonyl

interaction was present. It was found that the population of the *trans* enol species decreased upon an improved n→π* interaction. It was therefore concluded that an increase in n→π* energy of 2.9 kJ mol^{-1} resulted in the ~20% decrease in the population of the hydrogen-bonded tautomer. This suggested a substantial electron density competition between n→π* interactions and hydrogen bonds. These results impacted current thought on the folding and stability of proteins.

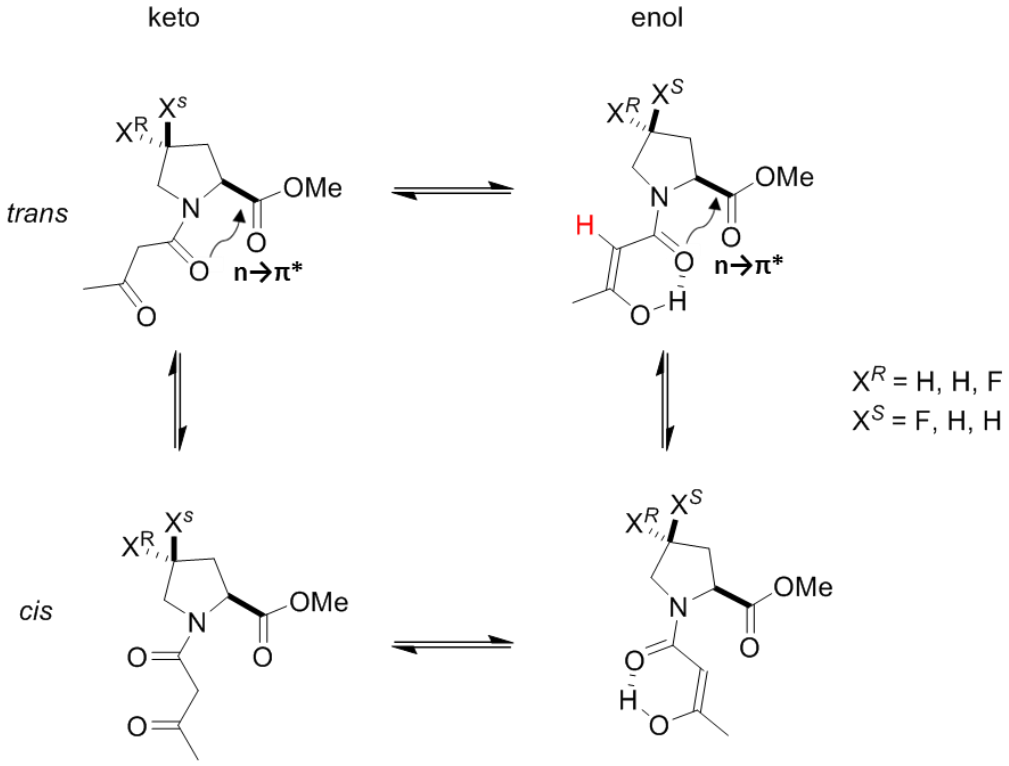

Figure 1.16: Keto and enols designed by Raines[52] to study the competition between H-bonds and n→ π * interactions.

1.5 H-bonding in Nucleic Acids and H-bond Arrays

Inspired by the naturally occurring H-bond arrays in nucleic acids, DNA and RNA (Figure 1.17),[11] chemists have explored the binding thermodynamics of synthetic compounds that incorporate arrays of H-bonds. Many triple H-bonded complexes have been synthesised, where the arrangement of donor and acceptor groups affected the stability of the complexes.

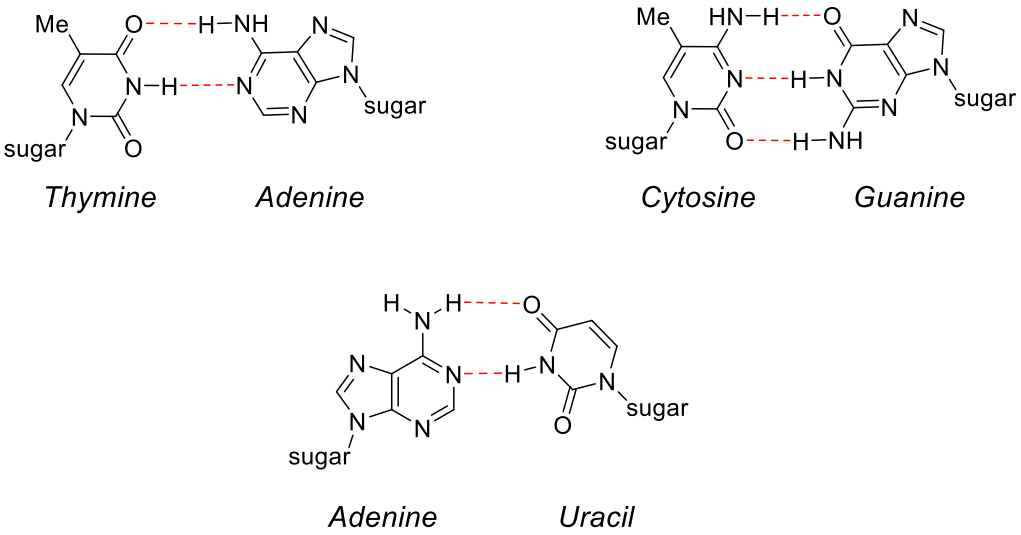

Figure 1.17: Complementary H-bonding in DNA and RNA base pairs.[11]

It was proposed by Jorgensen[54] that the strongest complexes would be those containing only attractive secondary interactions and experimental binding studies in numerous complexes were consistent with this proposal. For example, the triple H-bond guanine-cystosine complex (Figure 1.18B) has a AAD-DDA arrangement of donors (D) and acceptors (A) and has been found to have stronger binding constant (K_a = 10^4 M^{-1} in chloroform) relative to uracil-2,6-diaminopyrdine (Figure 1.18A), which has a ADA-DAD arrangement and lower binding constant (K_a = 1.7 x 10^2 M^{-1} in chloroform). This added stability was attributed to additional stabilisation from secondary attractive interactions. Complexes that had AAA-DDD were found to have the highest stabilities with binding constants determined to be K_a > 10^5 M^{-1} in chloroform (Figure 1.18C).

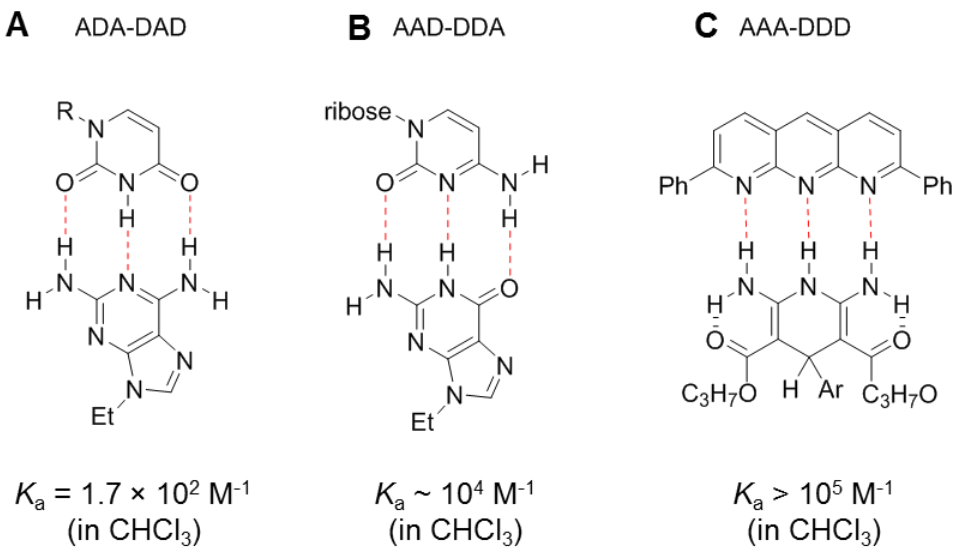

Figure 1.18: A Jorgensen[54] investigated ADA-DAD and **B** AAD-DDA arrangements of H-bond acceptor and donor groups in nucleobase pairing. **C** Zimmerman synthesised a triply H-bonded AAA-DDD module.[56]

Quadruple H-bonded complexes have been investigated by Meijer,[55] who reported ureidopyrimidinone, which forms AADD-AADD complexes with a high binding constant of K_a = 6 x 10^7 M^{-1} in chloroform (Figure 1.19). Similarly, Zimmerman[56,57] reported the synthesis of a quadryuply H-bonded complex with an ADDA-DAAD arrangement of groups and high association constant were found in chloroform ($K_a \sim 10^7\ M^{-1}$), the high stability of these arrays allowed them to be utilised in alternating multiblock copolymers.[58] However, consistent with Jorgensen's above noted proposal, the strongest quadruple H-bonds were found for the complexes that only exhibited primary and secondary attractive interactions (Figure 1.19A and B). Leigh *et al*[59] synthesised a complex that formed a quadruple AAAA-DDDD H-bond array and exhibited exceptionally strong binding in non-polar dichloromethane ($K_a > 3 \times 10^{12}\ M^{-1}$). This complex was also stable in polar solvents acetonitrile ($K_a = 1.5 \times 10^6\ M^{-1}$) and 10% (v/v) DMSO/$CHCl_3$ ($K_a = 3.4 \times 10^5\ M^{-1}$).

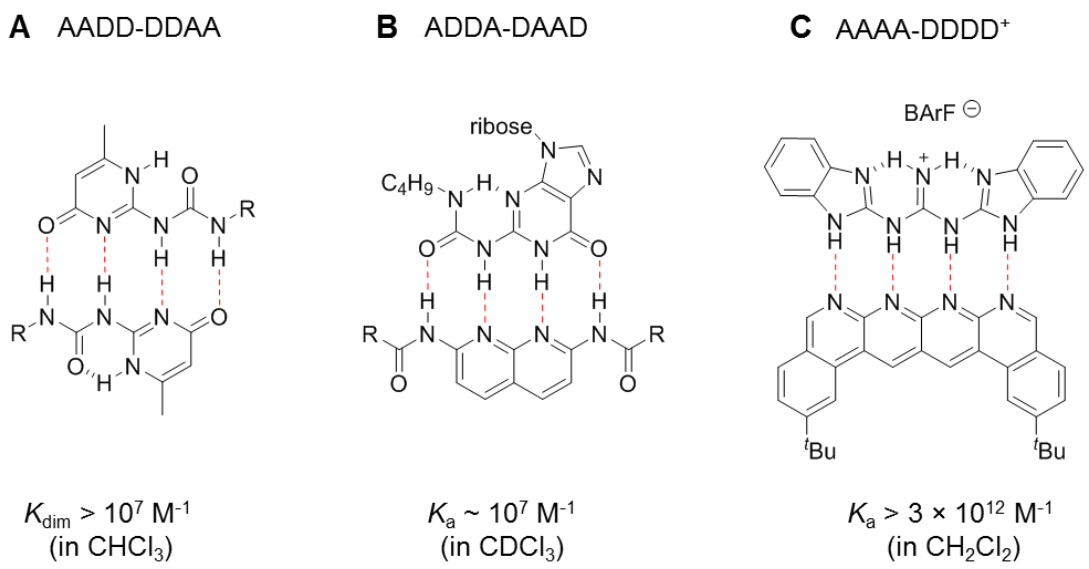

Figure 1.19: A Quadruple H-bond module synthesised by Meijer[55] **B** H-bond complex designed by Zimmerman[56,57] **C** Quadruple H-bond complex synthesised by Leigh *et al*, exceptionally strong association constants were determined even in polar solvents.[59]

Gong[60] reported an even larger molecular duplex that contained six H-bonds that was found to be highly stable (K_a = 1.3 ± 0.7 × 10^9 M^{-1}) in $CDCl_3$, where intramolecular H-bonds played a key role in the preorganised, planar arrangement of the amide groups (Figure 1.20). The duplexes were also investigated in aqueous solution on addition of competing H-bonding groups.[61] This sextuple H-bonded motif was incorporated into the chain ends of poly(styrene) (PS) and poly(ethylene glycol) (PEG) to form complementary homopolymers that could then self-assemble to form a AB diblock copolymer.[62] Such polymers provide the possibility of responsiveness to external stimuli, such as pH and solvent.

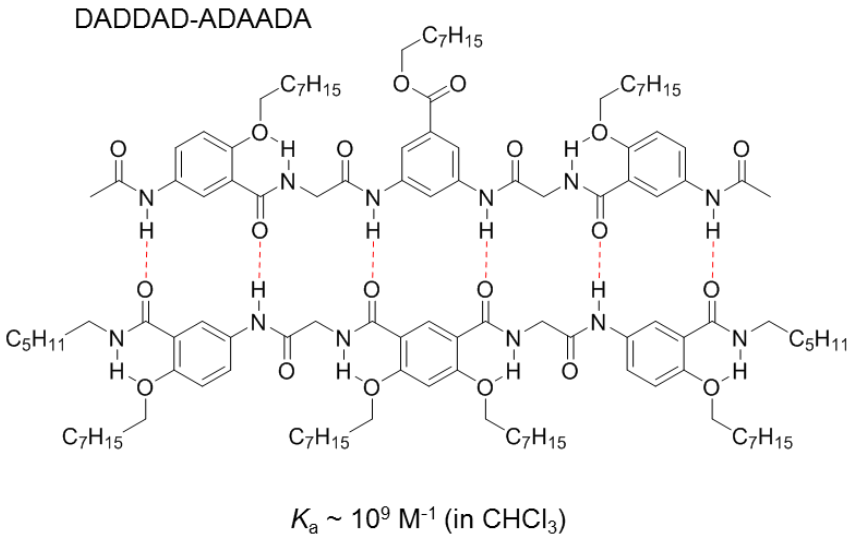

Figure 1.20: H-bonded molecular duplex synthesised by Gong *et al,*[60] containing six H-bonds.

H-bonding arrays have also been exploited for anion recognition. Schmuck[63] synthesised a series of guanidiniocarbonyl pyrrole receptors (Figure 1.21) that bound carboxylates by ion pairing and multiple H-bonds. The binding energies were determined in 40% (v/v) water/DMSO using NMR titration studies. The strongest association constants were found to be $K_a \approx 10^3$ M^{-1}. The receptor structure was varied, allowing estimates for the energetic contributions of individual binding interactions to be derived. It was found that each H-bond differed significantly in their energetic contribution to the overall complexation process.

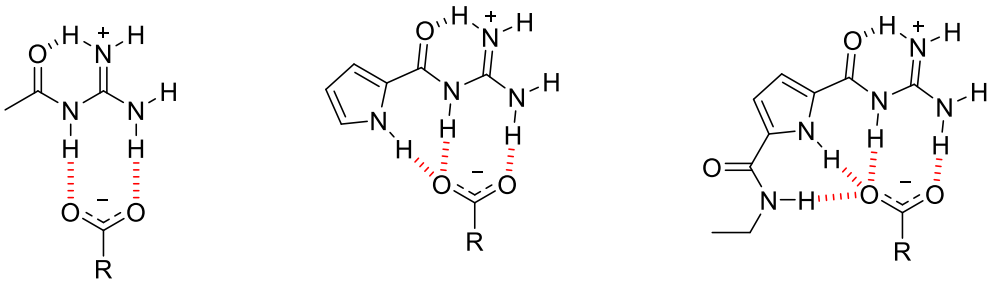

Figure 1.21: Guanidiniocarbonyl pyrrole receptors synthesised by Schmuck[63] that bound carboxylates by H-bonding in 40% water/DMSO (v/v).

Schmuck[64] also designed and synthesised a cationic receptor that bound dipeptides and amino acids via hydrogen bonds (Figure 1.22). The binding energies with various substrates were studied by UV titration in water (and small amounts of

DMSO for solubility purposes). The receptor bound carboxylates very effectively in water with association constants of $K_a > 10^4$ M^{-1}. This binding was an order of magnitude stronger than the receptor binding to simple amino acids ($K_a \approx 5\text{-}7 \times 10^3$ M^{-1}). It was also found that complex stability depended on the side chains present, in the order Gly < Ala < Val.

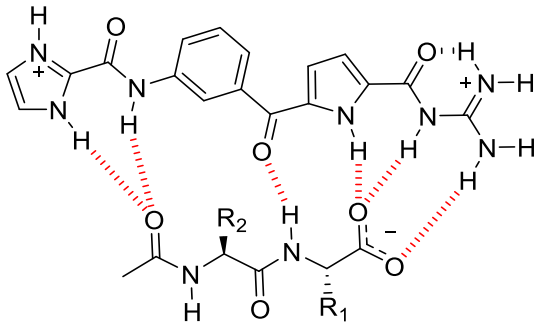

Figure 1.22: Cationic receptor synthesised by Schmuck[64] that bound to dipeptides in water.

1.6 Dissecting H-bond Energies Using Thermodynamic Cycles

Sometimes it is possible for the specific contributions of H-bonding interactions to be dissected from a background of other contributing aspects using thermodynamic cycles. Fersht and co-workers first proposed a thermodynamic cycle known as a double-mutant cycle for dissecting interactions as shown in Figure 1.23.[65] The differences in the thermodynamic binding parameters are measured between the interaction of interest (X–Y), and three control compounds: control X', Y' and XY', which therefore leads to Equation 1.4 for the double mutant cycle:

$$\Delta\Delta G_{X\text{-}Y} = \Delta G_{XY \rightarrow X'Y} - \Delta G_{XY' \rightarrow X'Y'}$$

$$= \Delta G_{XY \rightarrow XY'} - \Delta G_{X'Y \rightarrow X'Y'} \qquad (1.4)$$

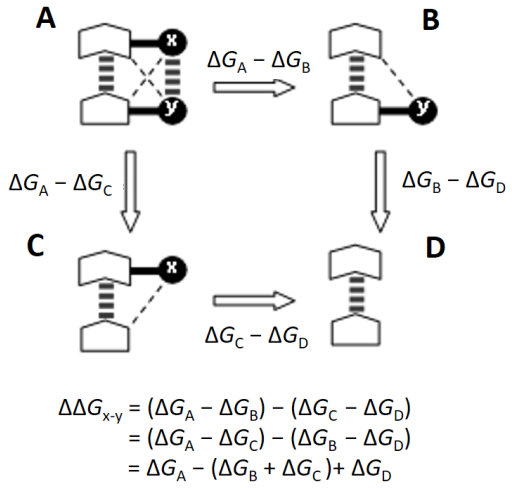

$$\Delta\Delta G_{x\text{-}y} = (\Delta G_A - \Delta G_B) - (\Delta G_C - \Delta G_D)$$
$$= (\Delta G_A - \Delta G_C) - (\Delta G_B - \Delta G_D)$$
$$= \Delta G_A - (\Delta G_B + \Delta G_C) + \Delta G_D$$

Figure 1.23: Double mutant cycle for the measurement of the X-Y interaction. The bold dashed lines represent the main non-covalent interactions whereas the thinner lines represent the secondary interactions.[65]

Double mutant cycles provide a general strategy for the dissection and quantification of a specific interaction of interest in a complex system containing multiple secondary interactions. Accordingly, the approach can also be applied to gaining understanding of molecular recognition processes in chemical systems.[66] Indeed, many H-bonded supramolecular systems have used this method for the quantification of chelate cooperativity in multiply H-bonded complexes.[67,68] Binding cooperativity in a supramolecular system is defined as occurring when the complex is more stable than the sum of the individual interactions. The effective molarity of a system (EM) is the parameter used to quantify cooperativity, and can be determined experimentally through the use of double mutant cycles. A high EM value corresponds to favourable intramolecular interactions with respect to intermolecular interactions.

Double mutant cycles have been used on various H-bonded supramolecular metalloporhyrins with pyridine ligands to investigate chelate cooperativity in polar solvents,[69] as well as the effects of non-covalent preorganisation and conformational restriction on supramolecular effective molarities.[70,71] The influence of non-covalent preorganisation on supramolecular effective molarities for formation of intramolecular H-bonds was investigated using complexes of the type shown in Figure 1.24.

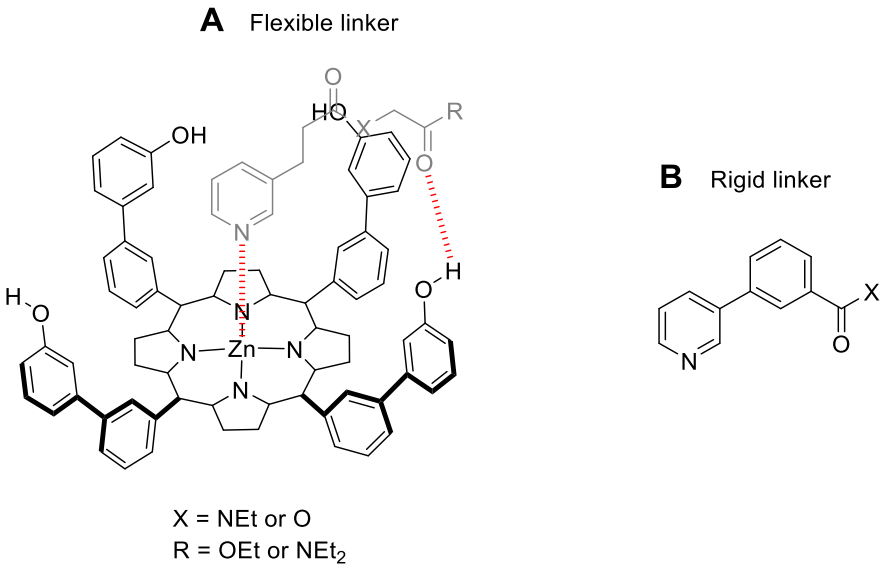

Figure 1.24: A Structure of zinc porphyrin-pyridine complex investigated by Hunter[70] that formed an 'intramolecular' H-bond to a carbonyl group. **B** Rigid linker also studied by Hunter[71] to investigate the effects of conformational flexibility on effective molarities.

The pyridine linkers formed intramolecular H-bonds with the phenol H-bond donor groups. Different acceptor linker groups (esters and amides) were used to vary the degree of preorganisation, the amide linkers were more preorganised (90-100% populated the H-bonded state) compared to the ester linkers (60-70% populated the H-bonded state). UV/vis absorption and fluorescence titrations were carried out in toluene and trichloroethylene to determine association constants. Effective molarities were then calculated using double mutant cycles (Figure 1.25) to reveal that the terminal intramolecular H-bond acceptors were independent of the nature of the linker indicating the preorganisation had no effect on chelate cooperativity. The same zinc-porphyrin structure was investigated with a more rigid linker that had one degree less torsional freedom (Figure 1.24B).[71] The effective molarities were found to be an order of magnitude lower for the flexible linker compared to the rigid linker. This indicated that intramolecular H-bonds were stronger for the rigid-linker complexes and that the cost of freezing a rotor in supramolecular complexes is of the order of 5 kJ mol^{-1}.

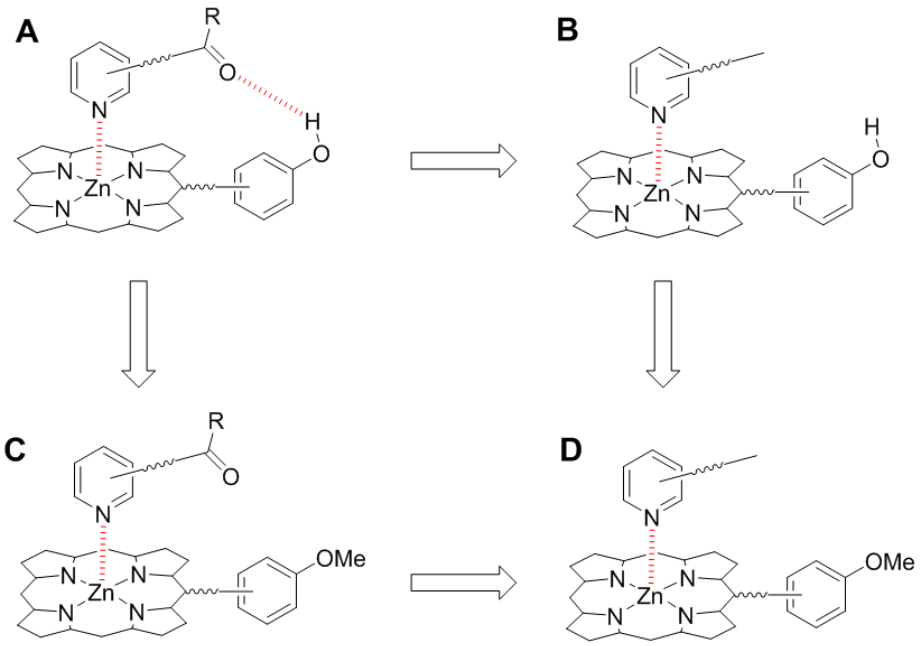

$$\Delta\Delta G = \Delta G^{\circ}_{A} - \Delta G^{\circ}_{B} - \Delta G^{\circ}_{C} + \Delta G^{\circ}_{D}$$

Figure 1.25: Chemical double mutant cycle (DMC) used by Hunter[69] to determine the free energy contribution of an intramolecular H-bond to the stability of **A**.

The effects of conformational flexibility on intramolecular H-bonding between a phenol donor and amide acceptor were also investigated by Cockroft using a thermodynamic cycle (Figure 1.26).[72] Due to fast exchange of the conformers on the NMR timescale, the interaction energies between the phenol donor groups and the amide acceptor groups were determined via competitive binding experiments. The energy of the intramolecular H-bond was determined from the weakening effect that the internal H-bond had on a competing intermolecular interaction. The determined energies were then compared to the number of rotatable bonds. It was found that compounds with up to five rotatable bonds between the donor and acceptor contained strong hydrogen bonds (−5 to −9 kJ mol^{-1}), however H-bonds were worth less than −1 kJ mol^{-1} when the donor and acceptor groups were separated by >6 rotating bonds. Effective molarities of internal H-bonds were determined to be <3 M which was below the ~10–100 M upper limit proposed for non-covalent interactions.[73] Overall, it was concluded that only extremely strong acceptors were able to compete with the strong internal H-bonds.

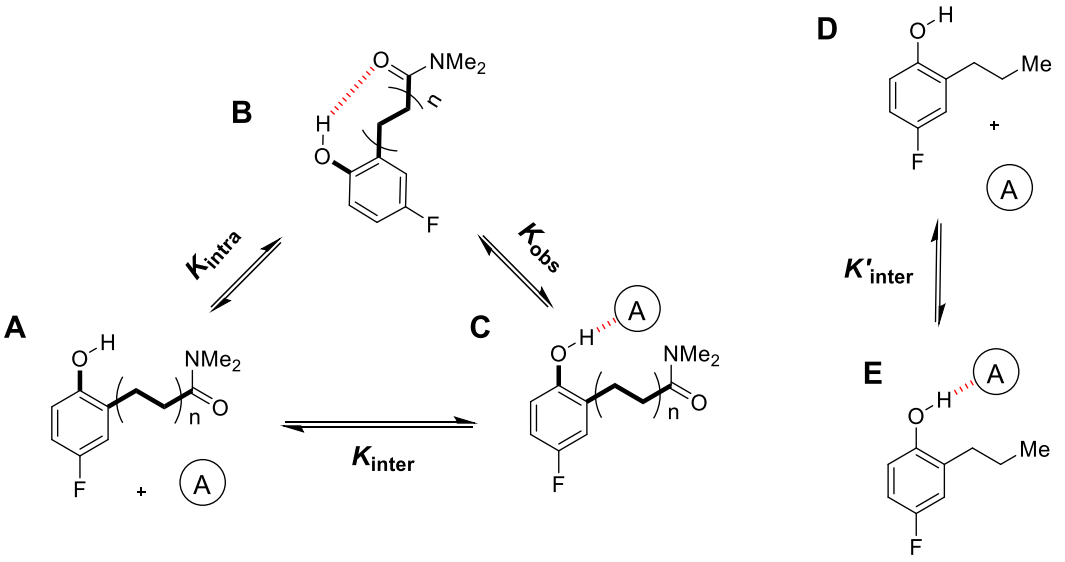

Figure 1.26: Intramolecular H-bonding between phenol and amide used to investigate conformational flexibility by Cockroft.[72]

Gellman *et al* also investigated the relative stability of H-bonds in flexible molecules. Specifically, the strength of H-bond conformers in triamides were studied in DCM (Figure 1.27). They carried out variable-temperature NMR experiments, followed by van't Hoff analysis, to determine the entropic and enthalpic contributions to folding. They found that the most enthalpically stable conformer did not maximize the number of H-bonds, this contradicted what was often presumed, and it could be reasoned this was due to a more favourable H-bond geometry in the larger ring.[74,75]

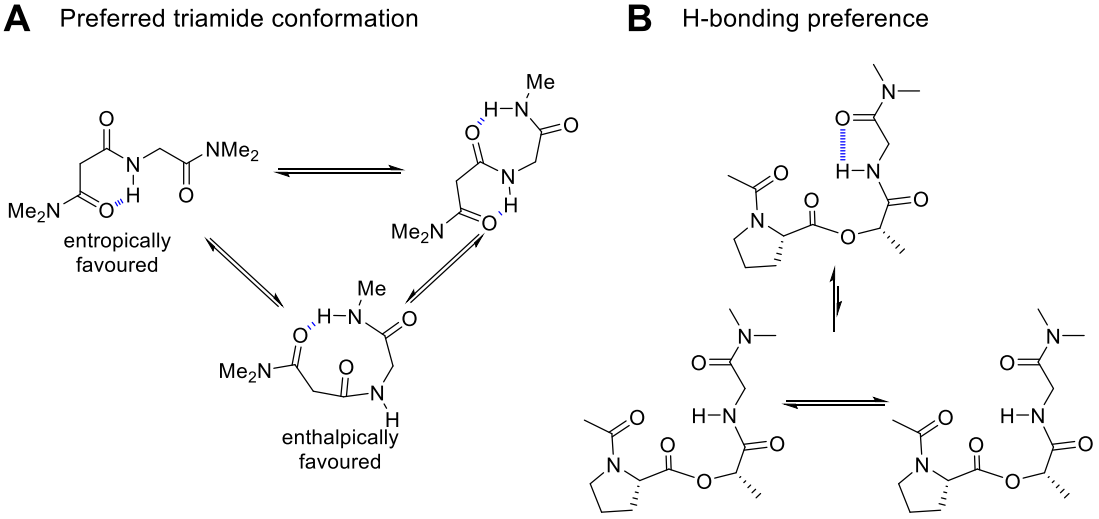

Figure 1.27: Structures used by Gellman[74,75] to study H-bonding between triamides in DCM.

1.7 Foldamers and Molecular Balances

An alternative method for quantifying non-covalent interactions, such as H-bonds, is by using molecular balances. A molecular balance is a molecule that can adopt two clearly distinguishable conformations (Figure 1.28), usually via restricted rotation about a single bond that allows distinct conformational populations to be directly quantified by NMR spectroscopy.[76]

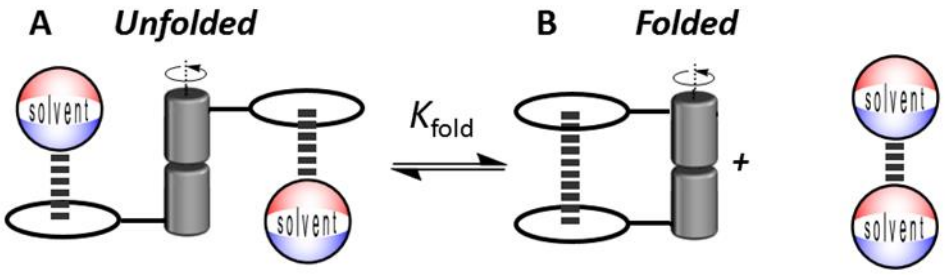

Figure 1.28: Molecular torsion balance equilibrium. **A** The unfolded conformation interacts with the solvent. **B** The folded conformation of the molecular balance forming intramolecular interactions.

The rotational barrier about the single bond, $\Delta G^{\ddagger}$, and the differences in ground state conformational energies, ΔG, are illustrated in Figure 1.29. The ground state free energies are determined by taking the integrals of the two distinct conformer peaks on the NMR spectrum to calculate the equilibrium constant, K, and then using equation $\Delta G = -RT\ln K$ allows for the determination of the Gibbs free energies.[76]

The molecular balance approach to studying non-covalent interactions offers advantages over the other approaches as the geometry of the interaction of interest can be controlled. Also, weak interactions that are too small to overcome the entropic penalty associated with intermolecular interactions can often be measured more accurately by measuring the position of a conformational equilibrium compared to titration-based methods.[76]

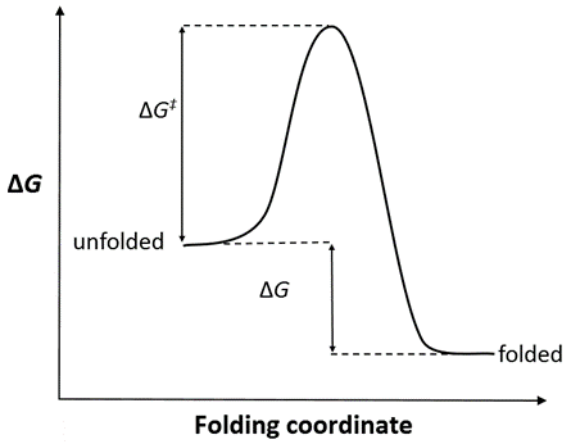

Figure 1.29: A folding energy profile for a molecular balance showing the rotational energy barrier ($\Delta G^{\ddagger}$) and the folding free energy (ΔG).

Molecular balances have been used to study a wide range of interactions[76], including van der Waals interactions,[77] solvophobic effects,[78] stacking interactions,[79] CH···aryl interactions,[80-81] and chalcogen-bonding.[82] Highlighted below is a summary of molecular balance systems designed to quantify H-bonds interactions.

Functional Group···π Interactions

Cornago and Elguero studied NH···π interactions using molecular balances shown in Figure 1.30. The percentage of **A** and **B** in dichloromethane, hexamethylphosphoramide, dimethyl sulfoxide and chloroform was determined using ^{1}H NMR spectroscopy. Substituent effects were analysed with Hammett substituent constants, for 5-(2-benzylphenyl) groups, the strength of the NH···π hydrogen bond depended on the electronic effect of the R-substituent.[83]

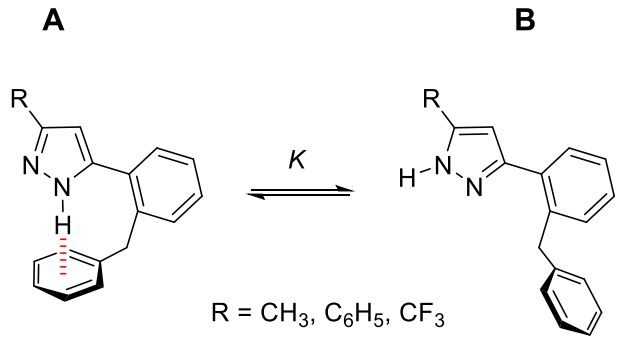

Figure 1.30: Molecular balances synthesised by Cornago and Elguero[83] to study NH···π interactions.

Motherwell *et al*[84] designed a dibenzobicyclo[3,2,2]nonane scaffold to study intramolecular H-bonding with π systems, amongst other interactions (Figure 1.31). The interconversion between the two states was fast on the NMR timescale, therefore accurate population ratios were determined from the ^{1}H-NMR *J*-couplings of the conformers. When Y = Me and Z = OH, the π intramolecular hydrogen bond dominated in non-polar solvents such as chloroform and benzene. However, on shifting to solvents that acted as good H-bond acceptors (pyridine, methanol), the solvent competed with the hydrogen bond and the equilibrium was shifted more towards the other conformation. When Z = NH_2, smaller populations of the hydrogen bonded conformer were observed in all solvents indicating a weaker interaction relative to the OH···π interaction.

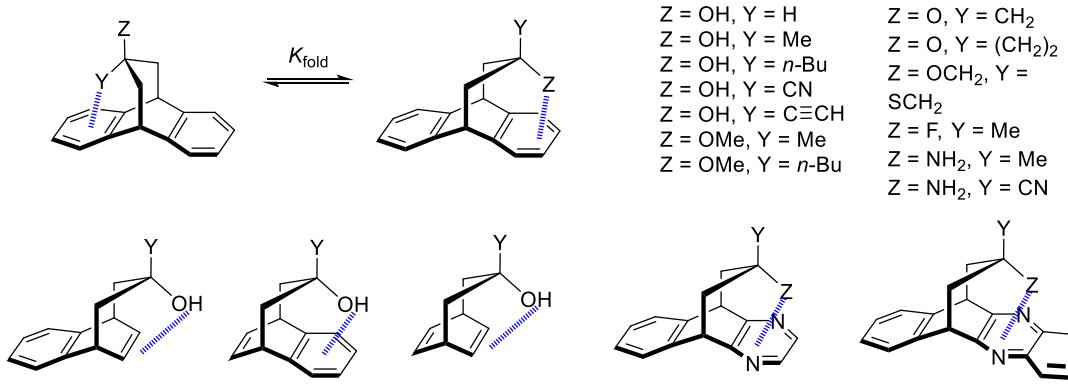

Figure 1.31: Molecular balances synthesised by Motherwell *et al*[84] used to study OH··· arene interactions.

The same scaffold was used to compare OH···π interactions in arenes against alkenes.[85] It was found that the π-facial intramolecular H-bond from a hydroxy group to an arene was stronger (by 1.2 kJ mol^{-1}) than that to an alkene. Also, the stability trend in the hydrocarbon···aryl interactions was sp3< sp2< sp(alkyne) < sp(CN), the latter being consistently more stable than the OH···aryl interaction. The results revealed similar solvent effects to that shown previously; the folding energies depended on the H-bond acceptor parameter, β.

The design was modified to investigate the non-covalent interaction of a hydroxy group with π-deficient pyrazine and quinoxaline unit[86] (Figure 1.31). The hydroxy group on the top-pan balance was shown to interact with heteroaromatic ring

in every solvent. This solvent independent behaviour was attributed to a lone pair···heteroaryl interaction, rather than a hydrogen bond. Similar results were observed with dimethoxy balance (that cannot form an H-bond), further confirming that this was a lone pair···heteroaryl interaction. A strong attractive interaction between an alkyne and quinoxaline was also observed, that outweighed the intramolecular H-bond.

Shimizu *et al.*[87] designed a molecular balance to investigate solvent OH···π interactions between protic solvents and aromatic surfaces (Figure 1.32). A system was designed where there was competition between the CH···π interactions in the folded state against OH···π interactions in the unfolded state.

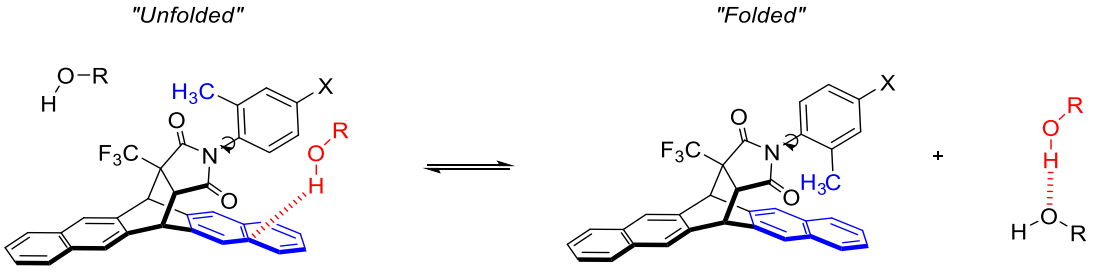

Figure 1.32: Molecular balance designed by Shimizu used to study OH-aryl interactions.[87]

Folding energies were determined in protic and aprotic solvents and it was found that the folding energies increased with increasing solvent polarity which was in agreement with other studies. Plots of the folding energies against the cohesive energy density, C_{ed}, solvent parameter revealed two distinct trendlines for the protic and aprotic solvents. Also, surprisingly, the gradient of the protic solvent trendline was shallower compared to the apolar solvents. These weaker than expected solvophobic effects were attributed to the formation of OH···π interactions between the solvent and exposed aromatic surfaces in the unfolded conformer. This was further confirmed by a strong linear fit on plotting the experimental data against energies calculated using a two-parameter model, $-\Delta G = a(c_{ed}) + b(\alpha_M) + c$ where a, b, and c are fitting coefficients and c_{ed} and α_M are the solvent parameters describing solvophobicity and solvent-solute hydrogen bonding respectively.

In an early example, OH···F hydrogen bonding was investigated by Abraham *et al* using the conformational equilibria shown in Figure 1.33.[88] The conformers shown in the equilibria were directly observed in non-polar and polar solvents using low temperature ^{1}H NMR spectroscopy. In non-polar solvents CCl_4, the Gibbs free energy was determined to be 6.5 kJ mol^{-1}, and in polar solvent acetone it was determined to be 5.0 kJ mol^{-1}. The *eq-eq* conformer proposed to be found to be the most stable form due to H-bond formation. Gibbs free energies were also determined for mono-substituted cyclohexanes, and comparison with trans-2-fluorocyclohexanol gave the OH···F hydrogen-bonding attraction in the *eq,eq* conformer a free energy of 6.5 kJ mol^{-1}. However, it should be noted that orbital interactions, or repulsion between the oxygen and fluorine lone pair electrons may also contribute to the observed conformational preferences.

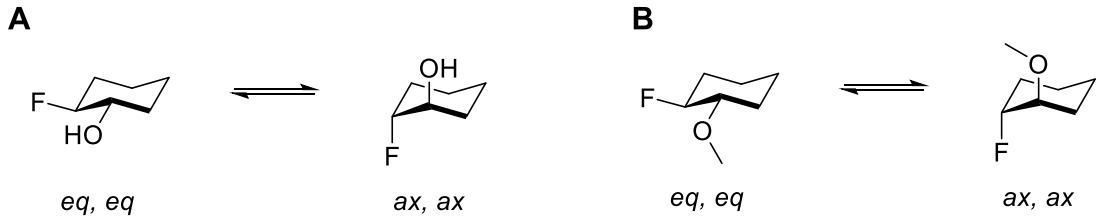

Figure 1.33: Conformational equilibria in **A** *trans*-2-fluorocyclohexanol and **B** the methyl ether used to study OH···F hydrogen bonding.[88]

NH···CO interactions

Wilcox *et al* designed a molecular balance to investigate intramolecular H-bonding between amino acids in an antiparallel *β*–sheet motif.[89] Slow rotation about an *N*-aryl bond resulted in two distinct conformations (Figure 1.34) visible on the NMR spectra. The design was therefore a useful system for measuring H-bond stability between two competing sequences. Molecular balances were synthesized that incorporated bromine substituents *ortho* to the upper side chains, in order to preorganise and promote the side chains for hydrogen bonding. A comparison was made against a control molecular balance with no bromine atoms, and it was found that H-bond alignment was improved with the addition of the bromine atoms. Conformational analysis was carried out on the molecular balance in chloroform and dichloromethane, using ^{1}H NMR spectroscopy. The H-bonded conformer was found to be the major conformer relative to the unbound conformation (96:4), due to the H-bond stabilizing the structure. This study was limited as no thermodynamic information was derived from the system and the strength of the H-bonds were not quantified.

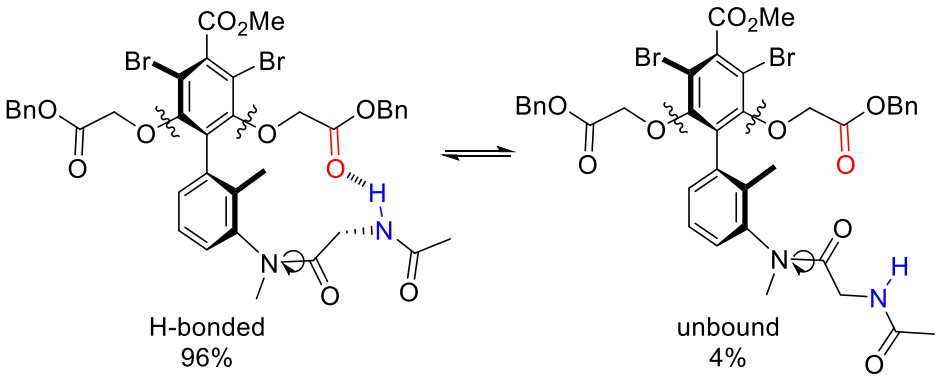

Figure 1.34: Molecular torsion balance designed by Wilcox[89] to investigate H-bonding between amides.

A. D. Hamilton and S. Thompson[90] also used synthetic molecular torsion balances to investigate H-bond stability in amides (Figure 1.35). In this design, two amide donors competed for a single acceptor group, in which the populations of the conformations were determined by the relative H-bond donor ability of the two benzamide NHs. The R groups, R^1 and R^2, were varied to probe steric and electronic

effects. Since the conformers in which the H-bond of interest was either broken or formed were not in slow exchange on the NMR timescale, the position of the conformational equilibria was instead estimated by comparing the ^{1}H NMR amide NH resonances with control compounds in chloroform. Experimental conformational free energies were found in the range of –0.7 – +2.5 kJ mol^{-1}, and they were found to correlate well with Hammett substituent constants. However, this study was limited to non-polar organic solvents and involved lengthy synthetic routes.

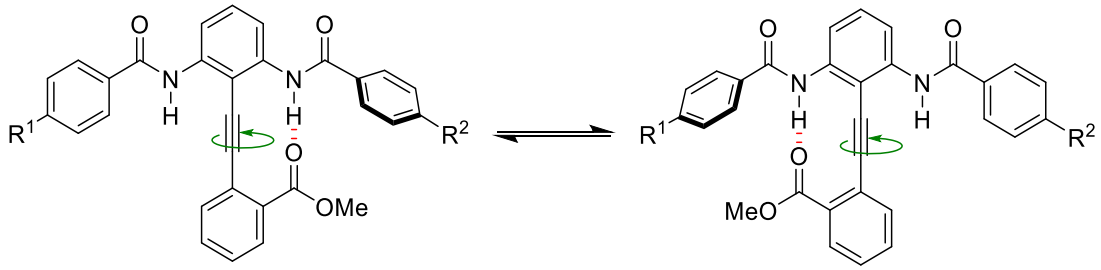

Figure 1.35: Molecular balance used by A. D. Hamiliton and S. Thompson[90] to investigate the relative H-bond strength between amides.

N,*N*-di-arylformamide molecular balances

The Cockroft[91] group have used simple molecular torsion balances (Figure 1.36) to study solvent effects on non-covalent interactions. A *para* and *ortho* series of molecular balances were synthesised with varying X substituents and energies were determined in a range of solvents. Significant changes in the experimentally determined free energies were seen across the solvents investigated, balances bearing an electron withdrawing group in the *para* position showed an increased preference for the H-conformer in polar solvents, whereas the opposite trend was observed for the *ortho* series. Hunter's solvation model was adapted for the molecular balances and applied to the system (Equation 1.5).

$$\Delta G_{exp} = \Delta E + \beta_s \Delta\alpha + \alpha_s \Delta\beta \qquad (1.5)$$

Where α_s and β_s are the hydrogen bond donor and acceptor constants respectively. Using linear regression, values for ΔE, $\Delta\alpha$ and $\Delta\beta$ were determined which gave information on the differences in intramolecular interactions and the changes in solvation on the donor and acceptor parts of the balance. This approach provided a

high-quality fit against experimental data ($R^2 = 0.96$) and the derived ΔE values, which described the intramolecular interactions correlated well with conformational energies calculated at the DFT/B3LYP/6-31G* level of theory.

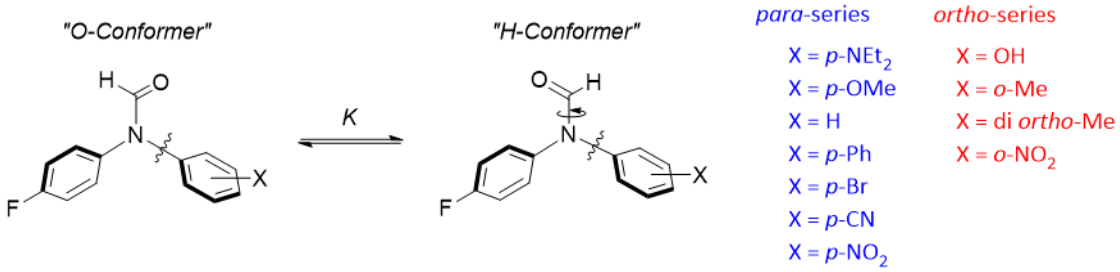

Figure 1.36: Simple molecular torsion balances used to study solvent effects on non-covalent interactions.[91]

A similar series of *para*-substituted molecular balances was used to study the electrostatic modulation of aromatic rings via explicit solvation of the substituents.[92] Energies were determined in non-polar solvents, $CDCl_3$, DCM and C_6D_6 and it was observed that the carbonyl oxygen preferred to be above the most electron-deficient ring. Electrostatic surface potentials (ESPs) were calculated (DFT/B3LYP/6-31G*) at the *ortho* position relative to the formamide and plotted against the experimentally determined energies, ΔG, to give strong linear correlations. The correlations were improved using an explicit solvation model that included a single solvent molecular on the substituent ($R^2 = 0.99$).

H-bonding was also investigated using the *N*,*N*-di-arylformamide molecular balances.[93] Phenol, catechol and pyrogallol molecular balances were synthesised and used to study cooperative H-bonding (Figure 1.37).

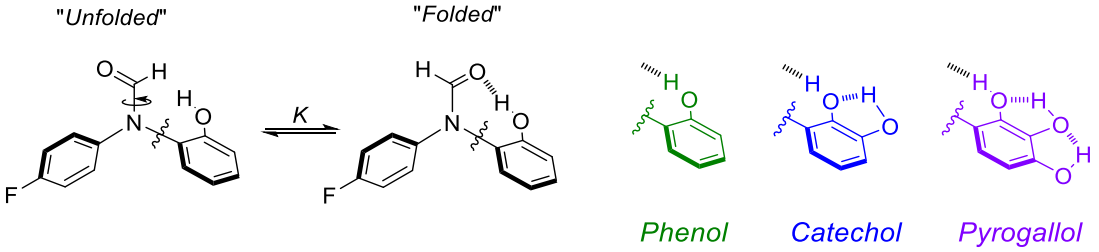

Figure 1.37: Molecular balances synthesised by Cockroft to study cooperative H-bonding.[93]

The position of the conformational equilibrium in these phenol balances enabled the measurement of the energy of the H-bond at the end of a linear chain of one, two or

three H-bonds. The phenol balance was found to have a strong preference for the folded conformer in $CDCl_3$, ΔG = –4.2 kJ mol^{-1}. The strength of the H-bond approximately doubled in magnitude for the catechol molecular balance, ΔG = –8.1 kJ mol^{-1}. However, on addition of an H-bond to the system, the strength of the H-bond slightly decreased. These trends persisted in solvent mixtures of $CDCl_3$ with small amounts of CD_3CN. Experimental controls and computation confirmed that the observed binary energetic behaviour depends entirely on whether a chain of (two or more) H-bonds was present, and ruled out significant through-bond substituent effects. This molecular balance design is studied further in chapter five.

Foldamers

An alternative approach to studying H-bonding is to design and synthesise larger folding molecules known as foldamers. Foldamers can adopt discrete secondary structures based on different types of H-bonding such as F···H–N H-bonds,[94] O···H–N H-bonds[95] and pyridine-N···H–N hydrogen-bonds.[96] Foldamers can also adapt their conformation in response to environmental triggers, and can therefore be used in a catalogue of applications.

Clayden *et al* synthesised peptide-like foldamers, global conformational changes were observed by either insertion or deletion of a single H-bond induced by changes in pH or by photochemical deprotection.[97] Oligourea foldamers were also synthesised (Figure 1.38) that formed hydrogen bonds, two different conformations were visible on the NMR timescale and the barrier to conversion was investigated in various solvents using variable temperature NMR experiments. The barrier to rotation was determined to be $\Delta G^{\ddagger}_{298}$= 70 kJ mol^{-1} in chloroform.[98] The relative population of the two conformers was determined by the competing hydrogen-bonding properties of the terminal groups.

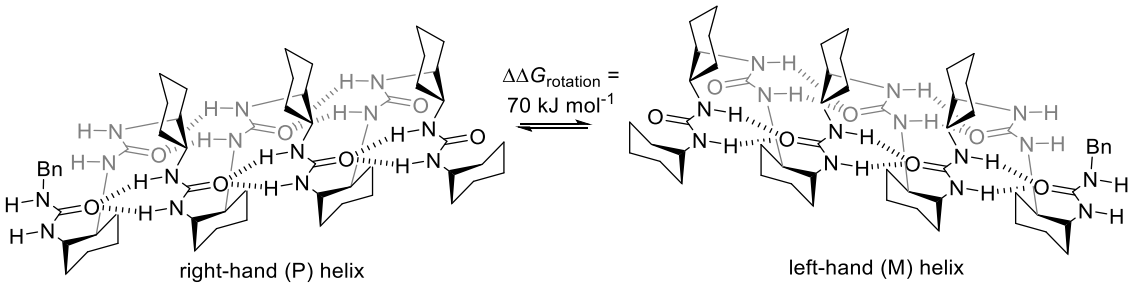

Figure 1.38: H-bonded foldamer designed by Clayden *et al* which showed a 70 kJ mol^{-1} barrier to rotation between opposite helical conformations.[98]

1.8 Conclusion

Hydrogen bonds are prevalent interactions in nature, where they play important roles in molecular recognition. The study of inter/intra molecular hydrogen bonds between donor and acceptor groups in solution is often complicated by solvent effects, where the solvent competes for H-bond interaction sites. Many experimental models have been developed to quantify H-bond interactions in solution. Molecular balances offer advantages as they can be carefully designed to allow for the quantification of specific H-bonds, including those too weak to measure using intermolecular techniques. Therefore, H-bond energies can be determined in polar solvents allowing us to further our understanding of fundamental H-bond interactions in biology.

1.9 References

1. Latimer, W. M.; Rodebush, W. H. Polarity and Ionisation from the Standpoint of the Lewis Theory of Valence. *Journal of the American Chemical Society*. **1920**, *42* (7), 1419-1433.

2. Pauling, L. The Structure and Entropy of Ice and of Other Crystals with Some Randomness of Atomic Arrangement. *Journal of the American Chemical Society*. **1935**, *57* (12), 2680-2684.

3. Huggins, M. L. Hydrogen Bridges in Organic Compounds. *The Journal of Organic Chemistry*. **1936**, *01* (5), 407-456.

4. Pauling, L. The Shared-Electron Chemical Bond. *Proceedings of the National Academy of Sciences of the United States of America*. **1928**, *14* (4), 359-362.

5. Grabowski, S. J. What Is the Covalency of Hydrogen Bonding? *Chemical Reviews*. **2011**, *111* (4), 2597-2625.

6. Dannenberg, J. J. An Introduction to Hydrogen Bonding. *Journal of the American Chemical Society*. **1998**, *120* (22), 5604-5604.

7. Jeffrey, G. A.; Maluszynska, H. A survey of the geometry of hydrogen bonds in the crystal structures of barbiturates, purines and pyrimidines. *Journal of Molecular Structure*. **1986**, *147* (1), 127-142.

8. Taylor, R.; Kennard, O.; Versichel, W. *Geometry of the N-H···O=C hydrogen bond. 2. Three-center ("bifurcated") and four-center ("trifurcated") bonds*, 1984; Vol. 106, p 244-248.

9. Taylor, R.; Kennard, O.; Versichel, W. Geometry of the imino-carbonyl (N-H...O:C) hydrogen bond. 1. Lone-pair directionality. *Journal of the American Chemical Society*. **1983**, *105* (18), 5761-5766.

10. Gilli, P.; Pretto, L.; Bertolasi, V.; Gilli, G. Predicting Hydrogen-Bond Strengths from Acid−Base Molecular Properties. The pKa Slide Rule: Toward the Solution of a Long-Lasting Problem. *Accounts of Chemical Research*. **2009**, *42* (1), 33-44.

11. Watson, J. D.; Crick, F. H. C. Molecular Structure of Nucleic Acids: A Structure for Deoxyribose Nucleic Acid. *Nature*. **1953**, *171*, 737.

12. Mundlapati, V. R.; Ghosh, S.; Bhattacherjee, A.; Tiwari, P.; Biswal, H. S. Critical Assessment of the Strength of Hydrogen Bonds between the Sulfur Atom of Methionine/Cysteine and Backbone Amides in Proteins. *The Journal of Physical Chemistry Letters*. **2015**, *6* (8), 1385-1389.

13. Biswal, H. S.; Gloaguen, E.; Loquais, Y.; Tardivel, B.; Mons, M. Strength of NH···S Hydrogen Bonds in Methionine Residues Revealed by Gas-Phase IR/UV Spectroscopy. *The Journal of Physical Chemistry Letters.* **2012**, *3* (6), 755-759.

14. Trylska, J.; Grochowski, P.; McCammon, J. A. The role of hydrogen bonding in the enzymatic reaction catalyzed by HIV-1 protease. *Protein Science: A Publication of the Protein Society.* **2004**, *13* (2), 513-528.

15. Wells, T. N. C.; Fersht, A. R. Hydrogen bonding in enzymatic catalysis analysed by protein engineering. *Nature.* **1985**, *316*, 656.

16. Chen, D.; Oezguen, N.; Urvil, P.; Ferguson, C.; Dann, S. M.; Savidge, T. C. Regulation of protein-ligand binding affinity by hydrogen bond pairing. *Science Advances.* **2016**, *2* (3).

17. Wernet, P.; Nordlund, D.; Bergmann, U.; Cavalleri, M.; Odelius, M.; Ogasawara, H.; Näslund, L. Å.; Hirsch, T. K.; Ojamäe, L.; Glatzel, P.; Pettersson, L. G. M.; Nilsson, A. The Structure of the First Coordination Shell in Liquid Water. *Science.* **2004**, *304* (5673), 995-999.

18. Pandey, S. K.; Manogaran, D.; Manogaran, S.; Schaefer, H. F. Quantification of Hydrogen Bond Strength Based on Interaction Coordinates: A New Approach. *The Journal of Physical Chemistry A.* **2017**, *121* (32), 6090-6103.

19. Graton, J.; Laurence, C.; Berthelot, M.; Le Questel, J.-Y.; Besseau, F.; D. Raczynska, E. Hydrogen-bond basicity pK_{HB} scale of aliphatic primary amines. *Journal of the Chemical Society, Perkin Transactions 2.* **1999**, (5), 997-1002.

20. Abraham, M. H. Scales of solute hydrogen-bonding: their construction and application to physicochemical and biochemical processes. *Chemical Society Reviews.* **1993**, *22* (2), 73-83.

21. H. Abraham, M.; Berthelot, M.; Laurence, C.; J. Taylor, P. Analysis of hydrogen-bond complexation constants in 1,1,1-trichloroethane: the $\alpha_{2H}\beta_{2H}$ relationship. *Journal of the Chemical Society, Perkin Transactions 2.* **1998**, (1), 187-192.

22. Hunter, C. A. Quantifying Intermolecular Interactions: Guidelines for the Molecular Recognition Toolbox. *Angewandte Chemie International Edition.* **2004**, *43* (40), 5310-5324.

23. Cook, J. L.; Hunter, C. A.; Low, C. M. R.; Perez-Velasco, A.; Vinter, J. G. Solvent Effects on Hydrogen Bonding. *Angewandte Chemie International Edition.* **2007**, *46* (20), 3706-3709.

24. Cabot, R.; Hunter, C. A.; Varley, L. M. Hydrogen bonding properties of non-polar solvents. *Organic & Biomolecular Chemistry.* **2010**, *8* (6), 1455-1462.

25. Cook, J. L.; Hunter, C. A.; Low, C. M. R.; Perez-Velasco, A.; Vinter, J. G. Preferential Solvation and Hydrogen Bonding in Mixed Solvents. *Angewandte Chemie International Edition.* **2008**, *47* (33), 6275-6277.

26. Amenta, V.; Cook, J. L.; Hunter, C. A.; Low, C. M. R.; Sun, H.; Vinter, J. G. Interplay of Self-Association and Solvation in Polar Liquids. *Journal of the American Chemical Society.* **2013**, *135* (32), 12091-12100.

27. Smith, D. A.; Beweries, T.; Blasius, C.; Jasim, N.; Nazir, R.; Nazir, S.; Robertson, C. C.; Whitwood, A. C.; Hunter, C. A.; Brammer, L.; Perutz, R. N. The Contrasting Character of Early and Late Transition Metal Fluorides as Hydrogen Bond Acceptors. *Journal of the American Chemical Society.* **2015**, *137* (36), 11820-11831.

28. Pike, S. J.; Hutchinson, J. J.; Hunter, C. A. H-Bond Acceptor Parameters for Anions. *Journal of the American Chemical Society.* **2017**, *139* (19), 6700-6706.

29. Shan, S. O.; Herschlag, D. The change in hydrogen bond strength accompanying charge rearrangement: Implications for enzymatic catalysis. *Proceedings of the National Academy of Sciences.* **1996**, *93* (25), 14474-14479.

30. McGrath, J. M.; Pluth, M. D. Linear Free Energy Relationships Reveal Structural Changes in Hydrogen-Bonded Host–Guest Interactions. *The Journal of Organic Chemistry.* **2014**, *79* (23), 11797-11801.

31. Rüdiger, V.; Schneider, H.-J.; Solov'ev, V. P.; Kazachenko, V. P.; Raevsky, O. A. Crown Ether–Ammonium Complexes: Binding Mechanisms and Solvent Effects. *European Journal of Organic Chemistry.* **1999**, *1999* (8), 1847-1856.

32. Lee, S.; Chen, C.-H.; Flood, A. H. A pentagonal cyanostar macrocycle with cyanostilbene CH donors binds anions and forms dialkylphosphate [3]rotaxanes. *Nature Chemistry.* **2013**, *5*, 704.

33. Cai, J.; Hay, B. P.; Young, N. J.; Yang, X.; Sessler, J. L. A pyrrole-based triazolium-phane with NH and cationic CH donor groups as a receptor for tetrahedral oxyanions that functions in polar media. *Chemical Science.* **2013**, *4* (4), 1560-1567.

34. Gunnlaugsson, T.; Glynn, M.; Tocci, G. M.; Kruger, P. E.; Pfeffer, F. M. Anion recognition and sensing in organic and aqueous media using luminescent and colorimetric sensors. *Coordination Chemistry Reviews.* **2006**, *250* (23), 3094-3117.

35. Duke, R. M.; Veale, E. B.; Pfeffer, F. M.; Kruger, P. E.; Gunnlaugsson, T. Colorimetric and fluorescent anion sensors: an overview of recent developments in the use of 1,8-naphthalimide-based chemosensors. *Chemical Society Reviews.* **2010**, *39* (10), 3936-3953.

36. Tresca, B. W.; Hansen, R. J.; Chau, C. V.; Hay, B. P.; Zakharov, L. N.; Haley, M. M.; Johnson, D. W. Substituent Effects in CH Hydrogen Bond Interactions: Linear

Free Energy Relationships and Influence of Anions. *Journal of the American Chemical Society.* **2015**, *137* (47), 14959-14967.

37. Allott, C.; Adams, H.; A. Hunter, C.; A. Thomas, J.; L. Bernad Jr, P.; Rotger, C. Hydrogen-bond recognition of cyclic dipeptides in water. *Chemical Communications.* **1998,** (22), 2449-2450.

38. Lippe, J.; Mazik, M. Carbohydrate Receptors Combining Both a Macrocyclic Building Block and Flexible Side Arms as Recognition Units: Design, Syntheses, and Binding Studies. *The Journal of Organic Chemistry.* **2015**, *80* (3), 1427-1439.

39. Destecroix, H.; Renney, C. M.; Mooibroek, T. J.; Carter, T. S.; Stewart, P. F. N.; Crump, M. P.; Davis, A. P. Affinity Enhancement by Dendritic Side Chains in Synthetic Carbohydrate Receptors. *Angewandte Chemie International Edition.* **2015**, *54* (7), 2057-2061.

40. Ferrand, Y.; Crump, M. P.; Davis, A. P. A Synthetic Lectin Analog for Biomimetic Disaccharide Recognition. *Science* **2007**, *318* (5850), 619-622.

41. Abraham, M. H.; Ibrahim, A.; Zissimos, A. M.; Zhao, Y. H.; Comer, J.; Reynolds, D. P. Application of hydrogen bonding calculations in property based drug design. *Drug Discovery Today.* **2002**, *7* (20), 1056-1063.

42. Bajorath, J. Integration of virtual and high-throughput screening. *Nat Rev Drug Discov.* **2002**, *1* (11), 882-894.

43. Banerjee, S.; Veale, E. B.; Phelan, C. M.; Murphy, S. A.; Tocci, G. M.; Gillespie, L. J.; Frimannsson, D. O.; Kelly, J. M.; Gunnlaugsson, T. Recent advances in the development of 1,8-naphthalimide based DNA targeting binders, anticancer and fluorescent cellular imaging agents. *Chemical Society Reviews.* **2013**, *42* (4), 1601-1618.

44. Shortridge, M. D.; Hage, D. S.; Harbison, G. S.; Powers, R. Estimating Protein−Ligand Binding Affinity Using High-Throughput Screening by NMR. *Journal of Combinatorial Chemistry.* **2008**, *10* (6), 948-958.

45. Diamante, L.; Gatti-Lafranconi, P.; Schaerli, Y.; Hollfelder, F. In vitro affinity screening of protein and peptide binders by megavalent bead surface display. *Protein Engineering, Design and Selection.* **2013**, *26* (10), 713-724.

46. Chen, D.; Oezguen, N.; Urvil, P.; Ferguson, C.; Dann, S. M.; Savidge, T. C. Regulation of protein-ligand binding affinity by hydrogen bond pairing. *Science Advances.* **2016**, *2* (3), e1501240.

47. Liu, Z.; Wang, G.; Li, Z.; Wang, R. Geometrical Preferences of the Hydrogen Bonds on Protein−Ligand Binding Interface Derived from Statistical Surveys and Quantum Mechanics Calculations. *Journal of Chemical Theory and Computation.* **2008**, *4* (11), 1959-1973.

48. Gao, J.; Bosco, D. A.; Powers, E. T.; Kelly, J. W. Localized thermodynamic coupling between hydrogen bonding and microenvironment polarity substantially stabilizes proteins. *Nat Struct Mol Biol.* **2009**, *16* (7), 684-690.

49. Choudhary, A.; Gandla, D.; Krow, G. R.; Raines, R. T. Nature of Amide Carbonyl−Carbonyl Interactions in Proteins. *Journal of the American Chemical Society.* **2009**, *131* (21), 7244-7246.

50. Newberry, R. W.; Raines, R. T. A prevalent intraresidue hydrogen bond stabilizes proteins. *Nat Chem Biol.* **2016**, *12* (12), 1084-1088.

51. Bartlett, G. J.; Newberry, R. W.; VanVeller, B.; Raines, R. T.; Woolfson, D. N. Interplay of Hydrogen Bonds and n→π* Interactions in Proteins. *Journal of the American Chemical Society.* **2013**, *135* (49), 18682-18688.

52. Newberry, R. W.; Orke, S. J.; Raines, R. T. n→π* Interactions Are Competitive with Hydrogen Bonds. *Organic Letters.* **2016**, *18* (15), 3614-3617.

53. Adhikary, R.; Zimmermann, J.; Liu, J.; Forrest, R. P.; Janicki, T. D.; Dawson, P. E.; Corcelli, S. A.; Romesberg, F. E. Evidence of an Unusual N–H···N Hydrogen Bond in Proteins. *Journal of the American Chemical Society.* **2014**, *136* (39), 13474-13477.

54. Jorgensen, W. L.; Pranata, J. Importance of secondary interactions in triply hydrogen bonded complexes: guanine-cytosine vs uracil-2,6-diaminopyridine. *Journal of the American Chemical Society.* **1990**, *112* (5), 2008-2010.

55. Sijbesma, R. P.; Beijer, F. H.; Brunsveld, L.; Folmer, B. J. B.; Hirschberg, J. H. K. K.; Lange, R. F. M.; Lowe, J. K. L.; Meijer, E. W. Reversible Polymers Formed from Self-Complementary Monomers Using Quadruple Hydrogen Bonding. *Science.* **1997**, *278* (5343), 1601-1604.

56. Park, T.; Zimmerman, S. C.; Nakashima, S. A Highly Stable Quadruply Hydrogen-Bonded Heterocomplex Useful for Supramolecular Polymer Blends. *Journal of the American Chemical Society.* **2005**, *127* (18), 6520-6521.

57. Park, T.; Todd, E. M.; Nakashima, S.; Zimmerman, S. C. A Quadruply Hydrogen Bonded Heterocomplex Displaying High-Fidelity Recognition. *Journal of the American Chemical Society.* **2005**, *127* (51), 18133-18142.

58. Park, T.; Zimmerman, S. C. A Supramolecular Multi-Block Copolymer with a High Propensity for Alternation. *Journal of the American Chemical Society.* **2006**, *128* (43), 13986-13987.

59. Blight, B. A.; Hunter, C. A.; Leigh, D. A.; McNab, H.; Thomson, P. I. T. An AAAA–DDDD quadruple hydrogen-bond array. *Nat Chem.* **2011**, *3* (3), 244-248.

60. Zeng, H.; Miller, R. S.; Flowers, R. A.; Gong, B. A Highly Stable, Six-Hydrogen-Bonded Molecular Duplex. *Journal of the American Chemical Society*. **2000**, *122* (11), 2635-2644.

61. Li, M.; Yamato, K.; Ferguson, J. S.; Gong, B. Sequence-Specific Association in Aqueous Media by Integrating Hydrogen Bonding and Dynamic Covalent Interactions. *Journal of the American Chemical Society*. **2006**, *128* (39), 12628-12629.

62. Yang, X.; Hua, F.; Yamato, K.; Ruckenstein, E.; Gong, B.; Kim, W.; Ryu, C. Y. Supramolecular AD Diblock Copolymers. *Angewandte Chemie International Edition.* **2005**, *44* (13), 1907-1907.

63. Schmuck, C. Carboxylate Binding by 2-(Guanidiniocarbonyl)pyrrole Receptors in Aqueous Solvents: Improving the Binding Properties of Guanidinium Cations through Additional Hydrogen Bonds. *Chemistry – A European Journal*. **2000**, *6* (4), 709-718.

64. Schmuck, C.; Geiger, L. Dipeptide Binding in Water by a de Novo Designed Guanidiniocarbonylpyrrole Receptor. *Journal of the American Chemical Society* **2004**, *126* (29), 8898-8899.

65. J. Carter, P.; Winter, G.; Wilkinson, A.; Fersht, A. *The use of double mutants to detect structural changes in the active site of the tyrosyl-tRNA synthetase (Bacillus stearothermophilus)*. 1984; Vol. 38, pp 835-40.

66. Cockroft, S. L.; Hunter, C. A. Chemical double-mutant cycles: dissecting non-covalent interactions. *Chemical Society Reviews.* **2007**, *36* (2), 172-188.

67. Camara-Campos, A.; Musumeci, D.; Hunter, C. A.; Turega, S. Chemical Double Mutant Cycles for the Quantification of Cooperativity in H-Bonded Complexes. *Journal of the American Chemical Society.* **2009**, *131* (51), 18518-18524.

68. Hunter, C. A.; Misuraca, M. C.; Turega, S. M. Influence of H-Bond Strength on Chelate Cooperativity. *Journal of the American Chemical Society.* **2011**, *133* (50), 20416-20425.

69. Henkel, S.; Misuraca, M. C.; Ding, Y.; Guitet, M.; Hunter, C. A. Enhanced Chelate Cooperativity in Polar Solvents. *Journal of the American Chemical Society* **2017**, *139* (19), 6675-6681.

70. Sun, H.; Navarro, C.; Hunter, C. A. Influence of non-covalent preorganization on supramolecular effective molarities. *Organic & Biomolecular Chemistry*. **2015**, *13* (17), 4981-4992.

71. Adams, H.; Chekmeneva, E.; Hunter, C. A.; Misuraca, M. C.; Navarro, C.; Turega, S. M. Quantification of the Effect of Conformational Restriction on Supramolecular Effective Molarities. *Journal of the American Chemical Society*. **2013**, *135* (5), 1853-1863.

72. Hubbard, T. A.; Brown, A. J.; Bell, I. A. W.; Cockroft, S. L. The Limit of Intramolecular H-Bonding. *Journal of the American Chemical Society.* **2016**, *138* (46), 15114-15117.

73. Misuraca, M. C.; Grecu, T.; Freixa, Z.; Garavini, V.; Hunter, C. A.; van Leeuwen, P. W. N. M.; Segarra-Maset, M. D.; Turega, S. M. Relationship Between Conformational Flexibility and Chelate Cooperativity. *The Journal of Organic Chemistry.* **2011**, *76* (8), 2723-2732.

74. Gellman, S. H.; Adams, B. R.; Dado, G. P. Temperature-dependent changes in the folding pattern of a simple triamide. *Journal of the American Chemical Society.* **1990**, *112* (1), 460-461.

75. Yang, J.; Gellman, S. H. Energetic Superiority of Two-Center Hydrogen Bonding Relative To Three-Center Hydrogen Bonding in a Model System. *Journal of the American Chemical Society.* **1998**, *120* (35), 9090-9091.

76. Mati, I. K.; Cockroft, S. L. Molecular balances for quantifying non-covalent interactions. *Chemical Society Reviews.* **2010**, *39* (11), 4195-4205.

77. Yang, L.; Adam, C.; Nichol, G. S.; Cockroft, S. L. How much do van der Waals dispersion forces contribute to molecular recognition in solution? *Nat Chem.* **2013**, *5* (12), 1006-1010.

78. Yang, L.; Adam, C.; Cockroft, S. L. Quantifying Solvophobic Effects in Nonpolar Cohesive Interactions. *Journal of the American Chemical Society.* **2015**, *137* (32), 10084-10087.

79. Yang, L.; Brazier, J. B.; Hubbard, T. A.; Rogers, D. M.; Cockroft, S. L. Can Dispersion Forces Govern Aromatic Stacking in an Organic Solvent? *Angewandte Chemie International Edition.* **2016**, *55* (3), 912-916.

80. Paliwal, S.; Geib, S.; Wilcox, C. S. Molecular Torsion Balance for Weak Molecular Recognition Forces. Effects of "Tilted-T" Edge-to-Face Aromatic Interactions on Conformational Selection and Solid-State Structure. *Journal of the American Chemical Society.* **1994**, *116* (10), 4497-4498.

81. Emenike, B. U.; Bey, S. N.; Spinelle, R. A.; Jones, J. T.; Yoo, B.; Zeller, M. Cationic CH···π interactions as a function of solvation. *Physical Chemistry Chemical Physics.* **2016**, *18* (45), 30940-30945.

82. Pascoe, D. J.; Ling, K. B.; Cockroft, S. L. The Origin of Chalcogen-Bonding Interactions. *Journal of the American Chemical Society.* **2017**, *139* (42), 15160-15167.

83. Cornago, P.; Claramunt, R. M.; Bouissane, L.; Elguero, J. A molecular balance to measure the strength of N–H···π hydrogen bonds based on the tautomeric equilibria of C-benzylphenyl substituted NH-pyrazoles. *Tetrahedron.* **2008**, *64* (17), 3667-3673.

84. Motherwell, W. B.; Moïse, J.; Aliev, A. E.; Nič, M.; Coles, S. J.; Horton, P. N.; Hursthouse, M. B.; Chessari, G.; Hunter, C. A.; Vinter, J. G. Noncovalent Functional-Group–Arene Interactions. *Angewandte Chemie International Edition.* **2007**, *46* (41), 7823-7826.

85. Aliev, A. E.; Arendorf, J. R. T.; Pavlakos, I.; Moreno, R. B.; Porter, M. J.; Rzepa, H. S.; Motherwell, W. B. Surfing π Clouds for Noncovalent Interactions: Arenes versus Alkenes. *Angewandte Chemie.* **2015**, *127* (2), 561-565.

86. Pavlakos, I.; Arif, T.; Aliev, A. E.; Motherwell, W. B.; Tizzard, G. J.; Coles, S. J. Noncovalent Lone Pair···(No-π!)-Heteroarene Interactions: The Janus-Faced Hydroxy Group. *Angewandte Chemie International Edition* **2015**, *54* (28), 8169-8174.

87. Maier, J. M.; Li, P.; Vik, E. C.; Yehl, C. J.; Strickland, S. M. S.; Shimizu, K. D. Measurement of Solvent OH−π Interactions Using a Molecular Balance. *Journal of the American Chemical Society.* **2017**, *139* (19), 6550-6553.

88. Abraham, R. J.; Smith, T. A. D.; Thomas, W. A. Conformational analysis. Part 28. OH···F hydrogen bonding and the conformation of trans-2-fluorocyclohexanol. *Journal of the Chemical Society, Perkin Transactions 2.* **1996**, (9), 1949-1955.

89. Lypson, A. B.; Wilcox, C. S. Synthesis and NMR Analysis of a Conformationally Controlled β-Turn Mimetic Torsion Balance. *The Journal of Organic Chemistry.* **2017**, *82* (2), 898-909.

90. Luccarelli, J.; Jones, I. M.; Thompson, S.; Hamilton, A. D. Unpicking the determinants of amide NH···O=C hydrogen bond strength with diphenylacetylene molecular balances. *Organic & Biomolecular Chemistry.* **2017**, (15), 9156-9163

91. Mati, I. K.; Adam, C.; Cockroft, S. L. Seeing through solvent effects using molecular balances. *Chemical Science.* **2013**, *4* (10), 3965-3972.

92. Muchowska, K. B.; Adam, C.; Mati, I. K.; Cockroft, S. L. Electrostatic Modulation of Aromatic Rings via Explicit Solvation of Substituents. *Journal of the American Chemical Society.* **2013**, *135* (27), 9976-9979.

93. Dominelli-Whiteley, N.; Brown, J. J.; Muchowska, K. B.; Mati, I. K.; Adam, C.; Hubbard, T. A.; Elmi, A.; Brown, A. J.; Bell, I. A. W.; Cockroft, S. L. Strong Short-Range Cooperativity in Hydrogen-Bond Chains. *Angewandte Chemie International Edition.* **2017**, *56* (26), 7658-7662.

94. Li, C.; Ren, S.-F.; Hou, J.-L.; Yi, H.-P.; Zhu, S.-Z.; Jiang, X.-K.; Li, Z.-T. F···H–N Hydrogen Bonding Driven Foldamers: Efficient Receptors for Dialkylammonium Ions. *Angewandte Chemie International Edition.* **2005**, *44* (35), 5725-5729.

95. Fisher, B. F.; Guo, L.; Dolinar, B. S.; Guzei, I. A.; Gellman, S. H. Heterogeneous H-Bonding in a Foldamer Helix. *Journal of the American Chemical Society*. **2015**, *137* (20), 6484-6487.

96. Garric, J.; Léger, J.-M.; Huc, I. Molecular Apple Peels. *Angewandte Chemie International Edition*. **2005**, *44* (13), 1954-1958.

97. Le Bailly, B. A. F.; Byrne, L.; Clayden, J. Refoldable Foldamers: Global Conformational Switching by Deletion or Insertion of a Single Hydrogen Bond. *Angewandte Chemie International Edition*. **2016**, *55* (6), 2132-2136.

98. Wechsel, R.; Žabka, M.; Ward, J. W.; Clayden, J. Competing Hydrogen-Bond Polarities in a Dynamic Oligourea Foldamer: A Molecular Spring Torsion Balance. *Journal of the American Chemical Society*. **2018**, *140* (10), 3528-3531.

Chapter 2

Limitations of Implicit Solvation Models

Abstract

Most biological and chemical systems are solvated. Modelling solvation computationally is important for drug development and agrochemical development as potential candidates need to meet the required solubility criteria. Low solubility leads to low bio-availability, reducing effectiveness. Herein, the computational predictions provided by implicit solvation models are compared with experimentally determined conformational equilibria. Strong linear correlations are found in non-polar solvents such as benzene, however, poorer correlations are found for polar solvents such as methanol. The polarisable continuum model (PCM) method was shown to perform the best in all solvents compared with the solvation mode based on density (SMD), solvation model 8 (SM8) and solvation model 12 (SM12).

Full computational and supplementary details are given in Supporting Information A, pages 126-135.

Contributions: The computational results presented in this chapter were obtained by Nicole Yvette Meredith (NYM). The synthesis and experimental free energies of the para molecular balance series were previously determined.[1,2]

2.1 Introduction

Understanding the complicated influence of solvents on the behaviour of biological and chemical systems remains a challenge. Solvation is important in protein-ligand binding,[3] catalysis,[4] photochemistry,[5] and in determining the rates of reactions.[6,7] It is also important in determining the position of supramolecular and conformational equilibria.[1,8,9,10] The following chapter describes methods used to model solvation computationally, with a focus on implicit solvation models. A good solvation model should be able to balance accuracy and efficiency to provide a realistic description of the solvation behaviour; a good model can therefore then be directly used for experimental testing and/or validation.

Explicit solvation modelling

Explicit solvation models have been developed that treat each solvent molecule individually (Figure 2.1A). The explicit treatment of the solvent should provide the most descriptive, realistic and accurate model for the investigation of solvation, however such modelling is associated with a large number of degrees of freedom and is therefore computationally expensive. Explicit solvation models consider solvation in terms of free energy calculations and typically use molecular dynamics or Monte Carlo statistical methods. Explicit solvation has been used to determine the solvation energies of solutes,[11,12] pK_a values,[13,14] to study the conformations of cyclodextrins[15] and in the solvation of biomolecules.[16,17]

Meirovitch[16] performed molecular dynamic simulations of protein surface loops using explicit solvent water molecules. They found that the loop backbone was stabilised with a surprisingly small number of water molecules, at this hydration level, computational times compared well with an implicit solvation model. Thus, using minimalist explicit models could result in a more accurate description of protein loops of this type.

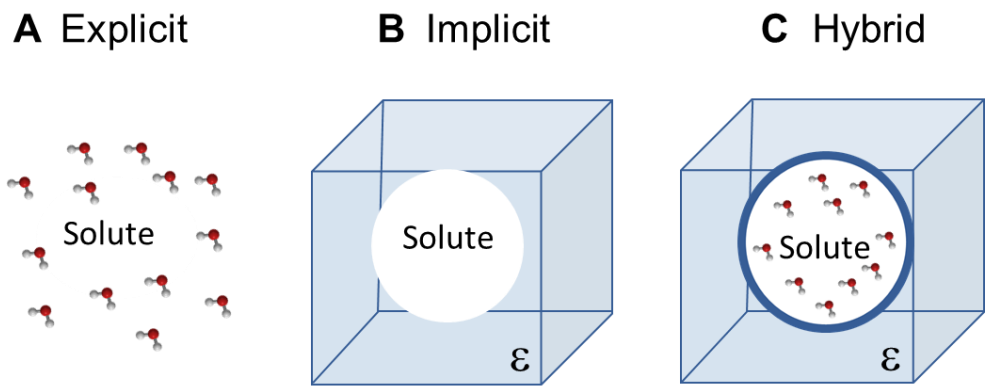

Figure 2.1: A Schematic of an explicit solvation model where each solvent molecule is treated individually. **B** Implicit solvation model where the solvent is treated as a continuous polarisable medium with a fixed dielectric constant, ε. **C** Hybrid solvation model where solvent molecules in the inner solvation sphere are treated individually, and solvent molecules in the outer sphere are treated as a continuous polarisable medium with a fixed dielectric constant, ε.

Cockroft[2] used a simple explicit solvation model to study how solvation of substituents affects the electrostatic potential of aromatic rings (Figure 2.2). Synthetic molecular torsion balances were synthesised and experimental energies of the conformational equilibria determined in non-polar solvents using ^{19}F NMR spectroscopy. The experimental energies were then plotted against the calculated electrostatic surface potential *meta* to the substituent. The electrostatic surface potentials were measured both in the gas phase and with an explicit chloroform and benzene molecule included (Figure 2.2A). Strikingly, it was found that incorporation of the non-polar solvent molecules improved the linear correlations. This study also included the implicit solvation model, SM8 (see below), however in all the solvents tested the correlations were found to be weaker relative to even the gas phase calculations. Whilst this study found stronger correlations for the simple explicit solvation model, it was limited to non-polar solvents and therefore lacked biological relevance.

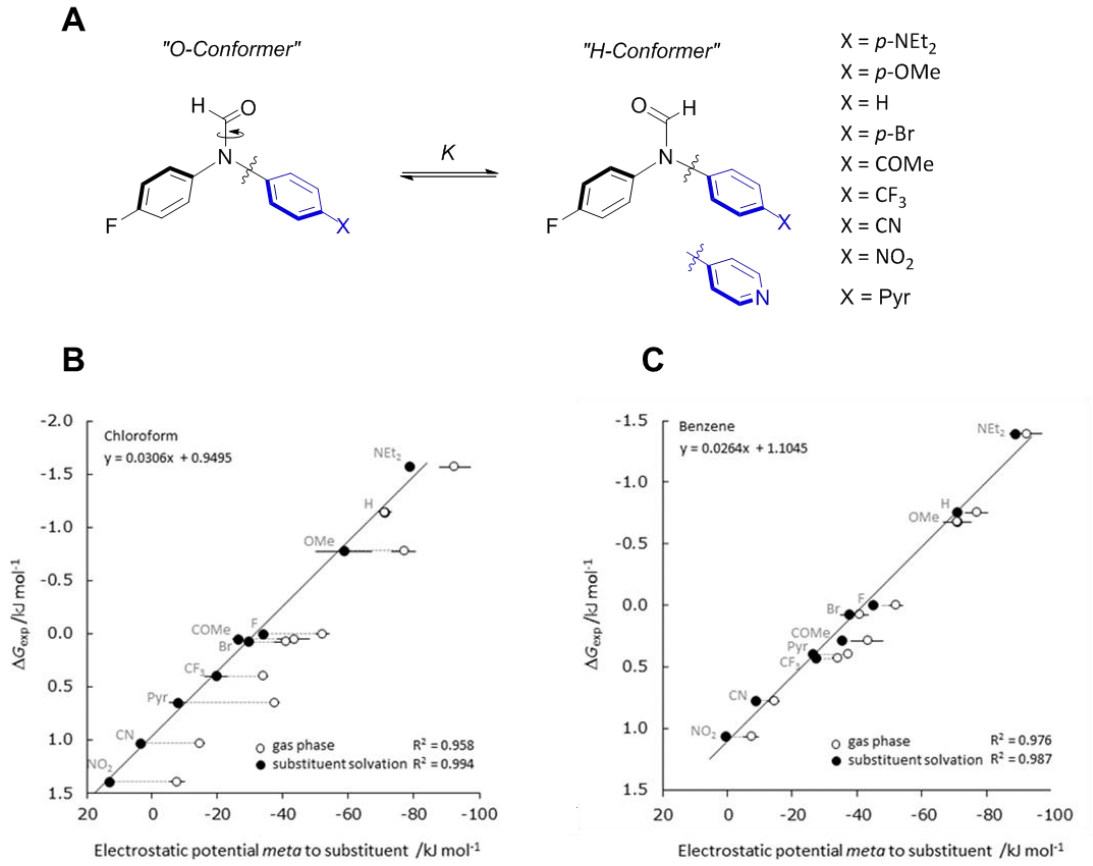

Figure 2.2: A Molecular balances used by Cockroft[2] to investigate solvation on substituents and the effects on the electrostatic surface potential of aromatic rings. **B** Correlation of the experimentally determined Gibbs free energies plotted against B3LYP/6-31G* electrostatic surface potentials taken *meta* to the substituent. The open circles correspond to gas phase calculations whilst the black circles correspond to calculations involving chloroform molecules. **C** Correlation of the experimentally determined Gibbs free energies plotted against B3LYP/6-31G* electrostatic surface potentials taken *meta* to the substituent. The open circles correspond to gas phase calculations whilst the black circles correspond to calculations involving benzene molecules.

Implicit solvation modelling

In contrast to explicit models, implicit solvation models treat the solvent as a continuous medium (Figure 2.1B). The solvent is considered as a uniform polarizable medium of fixed dielectric constant ε. Inside the solvent, a solute molecule is treated quantum mechanically and placed in a suitably shaped cavity. Implicit solvation models differ depending on factors such as the size and shape of the cavity.[18,19] The solute has a charge distribution which causes electric polarization of the surrounding solvent. The polarized solvent then exerts a field called the reaction field on the solute.

Implicit solvation models are generally considered as computationally inexpensive relative to explicit solvation methods, and a good approximation where it models isotropic and bulk solvent. Implicit solvation models have been used in biomolecular simulations as reported by Kleinjung,[20-21] protein surface interfaces[22] and also to calculate small molecule hydration energies.[23]

Examples of implicit solvation models include the Polarisable Continuum Model (PCM),[24] solvation model 8 (SM8),[25] solvation model 12 (SM12),[26] and the Solvation Model based on Density (SMD).[27]

Polarisable Continuum Model (PCM)

The polarisable continuum model (PCM)[28–29] and conductor-like PCM (C-PCM)[30] are generally regarded as the most successful implicit solvation models. As mentioned above, a solute molecule placed in a cavity interacts with the surrounding solvent with constant dielectric constant, ε. C-PCM and PCM define the cavities as envelopes of spheres centred on atoms or atomic groups. The PCM model is based on the Poisson-Boltzmann equation. Houk benchmarked the C-PCM for aqueous solvation free energies of neutral and ionic organic molecules[31] and found that the mean absolute deviations from experiment were 10.9 kJ mol^{-1}. Truhlar and Cramar also investigated the aqueous and organic solvation free energies of solutes using PCM and compared the accuracy against other implicit solvation models.[32] PCM has been used to model solvation in a number of different systems. It has been used in the pK_a determination of thiols,[13] to study solvent effects on both the optical rotations of chiral molecules,[33] and also on the excited-state double proton transfer mechanism.[34]

Solvation model based on Density (SMD)

The universal solvation model based on electron density, SMD, also solves the Poisson-Boltzmann equation, similar to the PCM implicit solvation model mentioned above.[27] However, the model treats the cavity with a set of specifically parameterised radii and is therefore more refined relative to the PCM method. Schlegel *et al* used the SMD solvation model with explicit water molecules to calculate the pK_a values of selenols in aqueous solution. The pK_a values were calculated using different functionals (ωB97XD, B3LYP, and M06-2X) and basis sets (6-31+G(d,p) and 6-

311++G(d,p)). The best results for SMD/M06-2X/ 6-31+G(d,p) were found using one explicit water molecule, whereas it was found that the best results for ωB97XD and B3LYP with 6-31+G(d,p) were determined using three explicit waters. Using these parameters, the SMD solvation model was effectively used to produce reliable pK_a values for the substituted selenols.[14]

Solvation model 8 (SM8)

Solvation model 8 (SM8) is a universal solvation model; it can be employed to model any liquid condensed phase for which bulk properties are available.[25] The reaction field generated by a charge distribution contained within a cavity placed in the surrounding continuous medium with fixed ε, is related to the quantum mechanical charge distribution by the generalised born equation. The quantum mechanical charge distribution is represented by atom centred monopoles. SM8 was used to effectively compute solvation free energies, partition coefficients, pK_a values and oxidation and reduction potentials.[35]

Solvation model 12 (SM12)

Similar to the SM8 method, solvation model 12 (SM12)[26] is a self-consistent reaction field (SCRF) implicit solvation model that employs the generalised Born approximation for the bulk electrostatic contribution to the free energy of solvation. It offers advantages over the earlier model as it can be used with extended basis sets, is parameterised against a more diverse training set and has been also defined for the entire periodic table. The SM8, SMD and C-PCM implicit solvation models outlined above were used in one study to predict the aqueous oxidation potentials of neutral organic compounds.[35,36]

Hybrid solvation models

The thermodynamic properties of liquids can also be approximated using hybrid methodologies. These models involve elements of implicit and explicit techniques with the aim of minimising computational cost whilst retaining some spatial resolution of the solvent. Quantum mechanics and molecular mechanics models are generally used for hybrid solvation methods. Free energies of solvation were investigated by Da Silva[37] by explicitly representing solvent molecules in the first solvation shell within continuum solvation calculations. Calculations were determined for 60 ionic species

and the unsigned average errors were calculated to be 8.8 kJ mol^{-1} for anions and 11.7 mol^{-1} for cations.[37]

2.2 Aims

Limited work has been done to assess and compare the performance of implicit solvation models for the computation of conformational equilibrium energies. Herein, solvent effects on conformational equilibria were studied computationally using simple molecular torsion balances. Four different implicit solvation models: PCM, SMD, SM8 and SM12 were employed, in a range of different solvents, and the results were compared against experimental conformational energies to evaluate their predictive capacity.

2.3 Results and discussion

Molecular balances, as reviewed in Chapter 1, are molecules that can adopt two distinct states that are distinguishable by NMR spectroscopy, usually via restricted rotation about a single bond.[8] The Cockroft[1-2] group have designed and synthesised a series of simple *ortho* and *para* molecular torsion balances (Figure 2.3), and investigated solvent effects on the conformational equilibrium experimentally. Due to slow rotation about the formyl group, two peaks appear on the NMR spectrum. ^{19}F NMR spectroscopy was therefore used to integrate peaks and determine the equilibrium constant K, using K = [H conformer]/[O conformer] from which the experimental energies were calculated using $\Delta G = -RT\ln K_a$.[1-2]

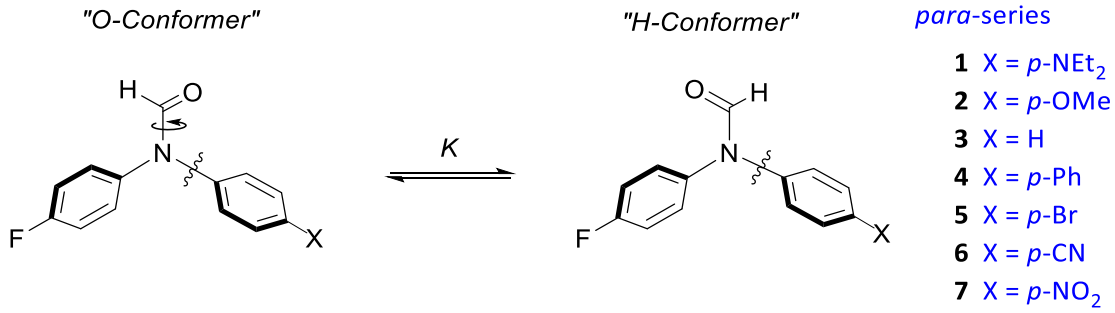

Figure 2.3: Previously synthesised *para* molecular balance series used in the present computational study.

The conformational energies can also be calculated computationally in the gas phase and in the solution phase by employing solvation models. As mentioned above, Cockroft[2] previously used a simple explicit solvation model and implicit solvation model SM8 to investigate the solvation effects of substituents on the electrostatic surface potentials of aromatic rings. This study was limited to non-polar solvents: benzene, chloroform and dichloromethane. In the following work, a similar molecular balance series was used to investigate the effectiveness and accuracy of implicit solvation models: SM8, SM12, SMD and PCM by direct comparison of the computational and experimental Gibbs free energies.

The relative computationally inexpensive nature of the calculations employed allowed calculations to be readily performed in a multitude of solvents with varied polarities. For the present study, the simple *para*-substituted molecular balance series shown in Figure 2.3 were chosen to investigate solvent effects computationally.

Calculations that employed PCM, SMD, SM8 and SM12 implicit solvation models were performed on the 'O' and 'H' conformers that had been geometry optimised at the DFT/B3LYP/6-31G* level of theory. The calculated conformational energies were then determined using Equation 2.1 for solvents, benzene, acetone, acetonitrile, carbon tetrachloride, chloroform, DCM, ethanol, ethyl acetate, methanol and THF.

$$\Delta E = \text{`}E_{H\,\text{conformer}}\text{'} - \text{`}E_{\text{O conformer}}\text{'} \quad (2.1)$$

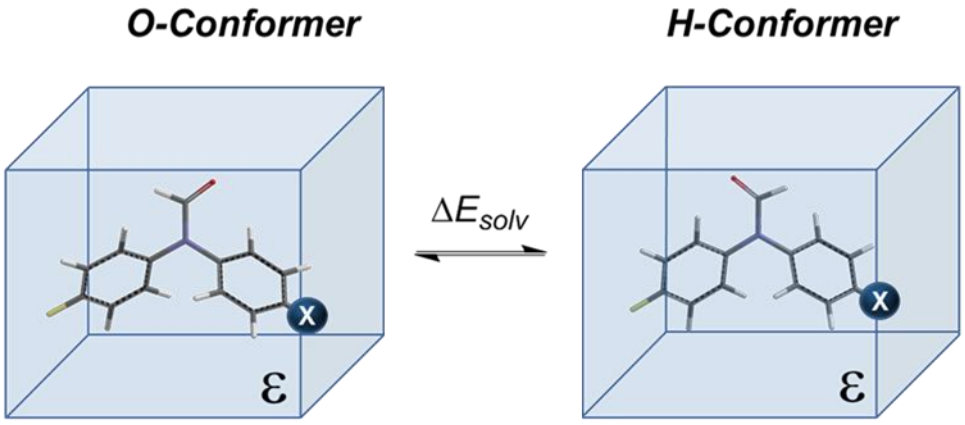

Figure 2.4: Calculated conformational energies employing implicit solvation models PCM, SMD, SM8 and SM12 using DFT/6-31G*/B3LYP.

The calculated conformational energies were then plotted against the previously determined experimental energies to evaluate the quality of each implicit solvation model (Figure 2.5). Figure 2.5 spans over three pages and shows data for ten different solvents with varying polarity. From the plots, R^2 values and gradients were derived to evaluate the effectiveness of each solvation model. A high R^2 value corresponded to a strong linear correlation and meant the implicit solvation models were predicting the general trends of the experimental conformational energies well. The closer the value of the gradient was to 1, the better the computational method was at predicting the absolute Gibbs free experimental energies. Generally, the strongest correlations (highest R^2 values) were found in non-polar solvents. For example, an R^2 value of 0.998 was observed in benzene employing PCM, this was a marginally stronger correlation than that found in the gas phase ($R^2 = 0.995$).

Graphs of experimental energies plotted against computationally derived values

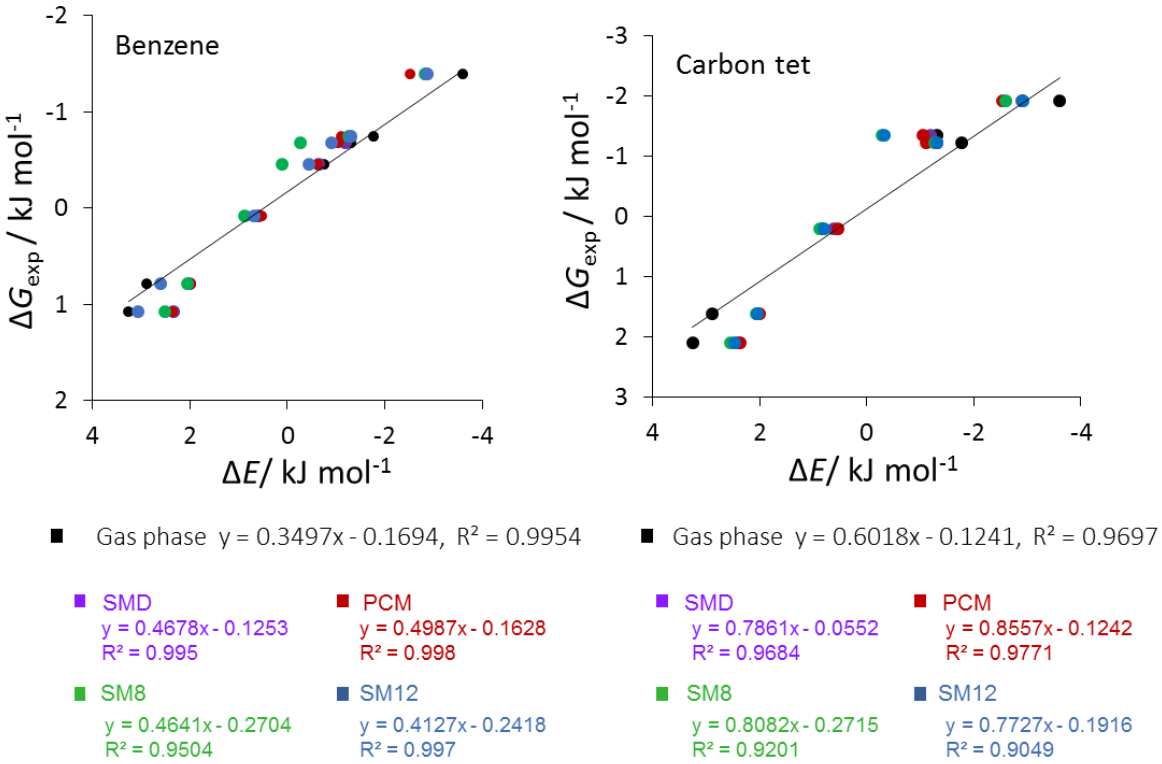

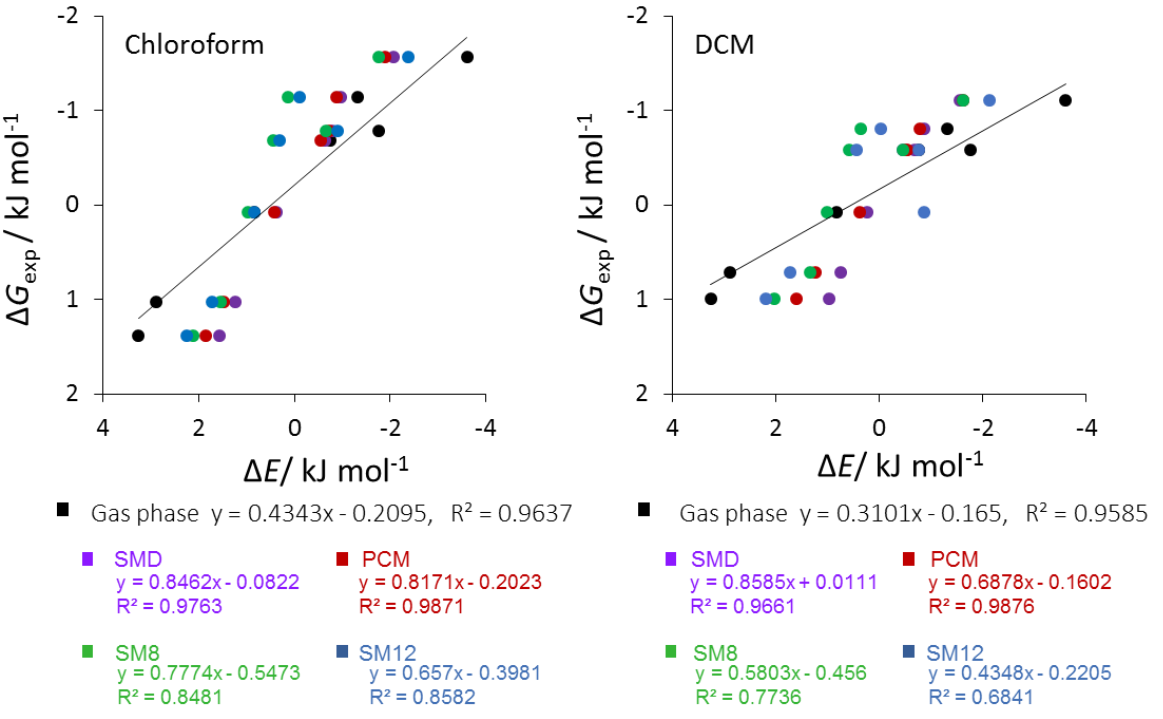

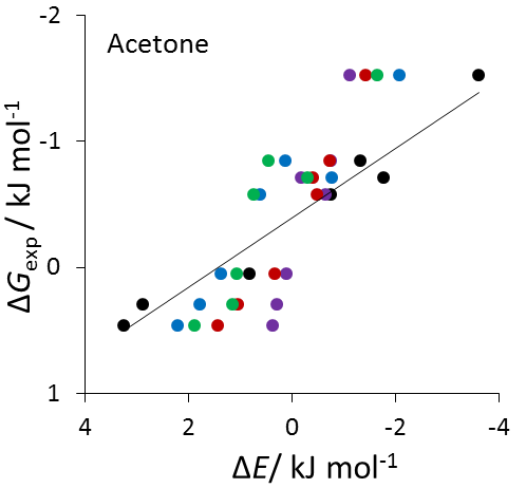

Gas phase y = 0.2766x - 0.3915, R^2 = 0.9606

SMD y = 1.1724x - 0.0884 R^2 = 0.9099

PCM y = 0.6838x - 0.3867 R^2 = 0.9631

SM8 y = 0.5701x - 0.6828 R^2 = 0.8557

SM12 y = 0.4528x - 0.6222 R^2 = 0.9261

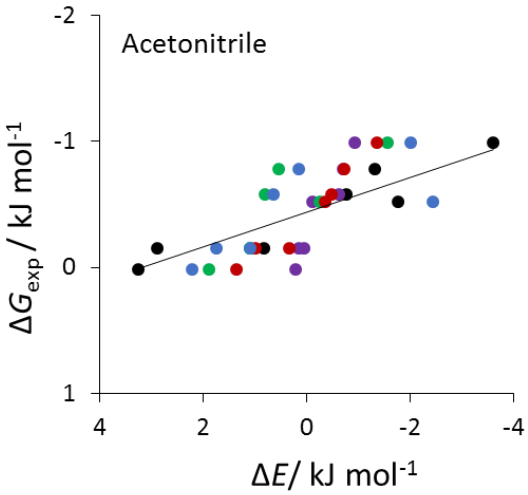

Gas phase y = 0.1381x - 0.4408, R^2 = 0.8803

SMD y = 0.7585x - 0.235 R^2 = 0.9095

PCM y = 0.3689x - 0.4378 R^2 = 0.9411

SM8 y = 0.2813x - 0.5943 R^2 = 0.7265

SM12 y = 0.1563x - 0.4804 R^2 = 0.5722

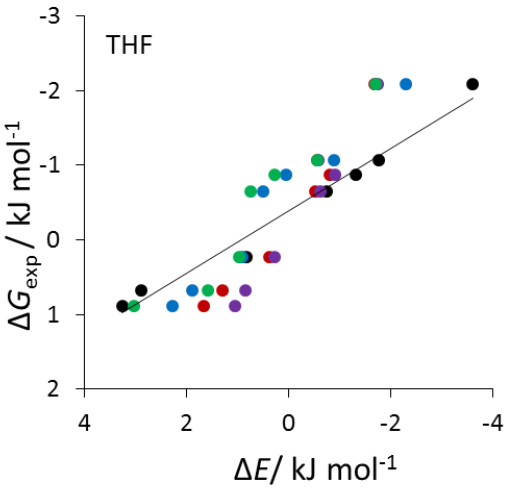

Gas phase y = 0.4184x - 0.3863, R^2 = 0.9782

SMD y = 1.0419x - 0.1594 R^2 = 0.9696

PCM y = 0.8693x - 0.3808 R^2 = 0.9575

SM8 y = 0.6678x - 0.8274 R^2 = 0.9026

SM12 y = 0.6565x - 0.6412 R^2 = 0.9558

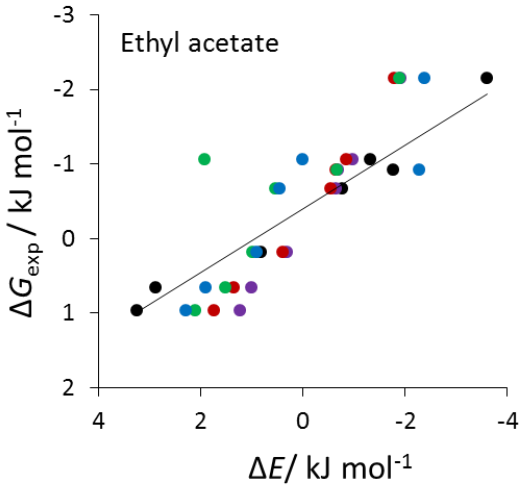

Gas phase y = 0.4275x - 0.4042, R^2 = 0.9723

SMD y = 0.9589x - 0.2098 R^2 = 0.9924

PCM y = 0.8523x - 0.398 R^2 = 0.975

SM8 y = 0.5774x - 0.8082 R^2 = 0.6003

SM12 y = 0.5286x - 0.5031 R^2 = 0.8029

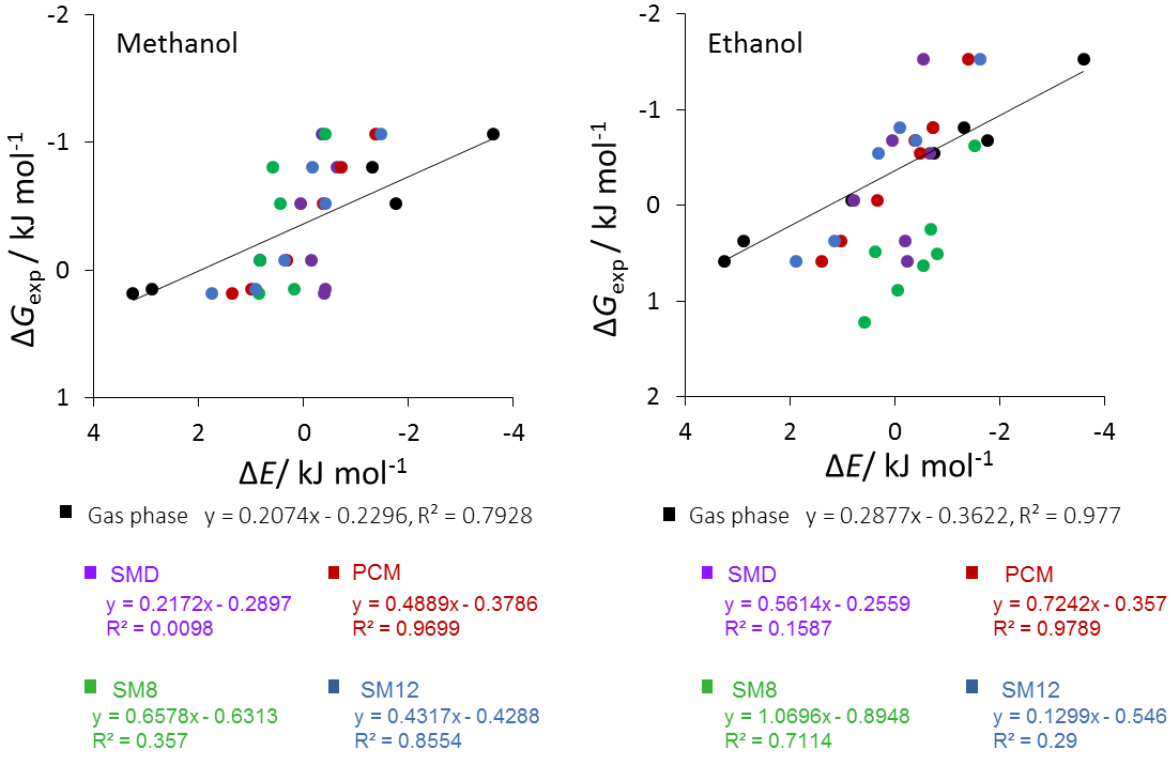

Figure 2.5: Graphs of experimentally determined Gibbs free energies plotted against computationally derived values calculated using DFT/B3LYP/6-31G* in the gas phase (black) and also employing implicit solvation models: SMD (purple), PCM (red), SM8 (green) and SM12 (blue) for ten different solvents.

The R^2 values were found to be weaker when moving to polar solvents such as ethanol and methanol. SM8 and SMD gave very poor R^2 values of 0.36 and 0.01 respectively. However, PCM still showed strong linear correlations in polar solvents with R^2 values of 0.97 and 0.98 in methanol and ethanol respectively. The R^2 values from the graphs above of the calculations performed in the gas phase and employing the implicit solvation models were plotted for every solvent investigated (Figure 2.6). Here, it can be clearly observed that PCM was the best implicit solvation model for predicting the general trends across all the solvents investigated.

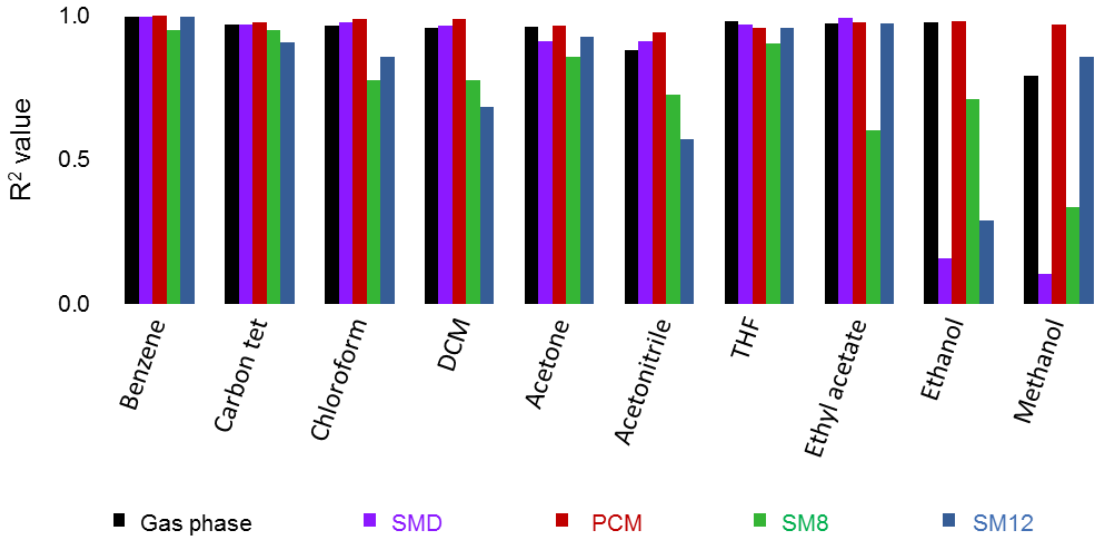

Figure 2.6: Plots of R^2 values determined by plotting the computationally derived energies in the gas (black) and solution phase calculated using DFT/B3LYP/6-31G* and employing implicit solvation models SMD (purple), PCM (red), SM8 (green) and SM12 (blue) against the experimentally determined Gibbs free energies in the ten solvents investigated.

On analysis of the gradients, the results were more varied (Figure 2.7). In general, the Gibbs free energies determined using the implicit solvation models were underpredicted ($m < 1$) compared to the experimental data. The only exception was SMD in acetonitrile, which over predicted the experimental results ($m = 1.2$). The most ideal gradients were found for ethyl acetate and THF using SMD ($m = 1.04$) and PCM ($m = 0.87$). In ethyl acetate, a gradient of 0.96 was obtained for the SMD data, while 0.85 was determined using PCM. It is unclear why these solvents gave the most ideal gradient values, though this presumably arises from better parameterisation of these solvents in the respective models. Surprisingly, even in polar solvent ethanol, a reasonably high gradient value of 0.72 was obtained when the PCM implicit solvation model was employed. To observe these trends more clearly, bar graphs were plotted of the gradient values determined in the gas phase and solution phase using each implicit solvation model (Figure 2.7).

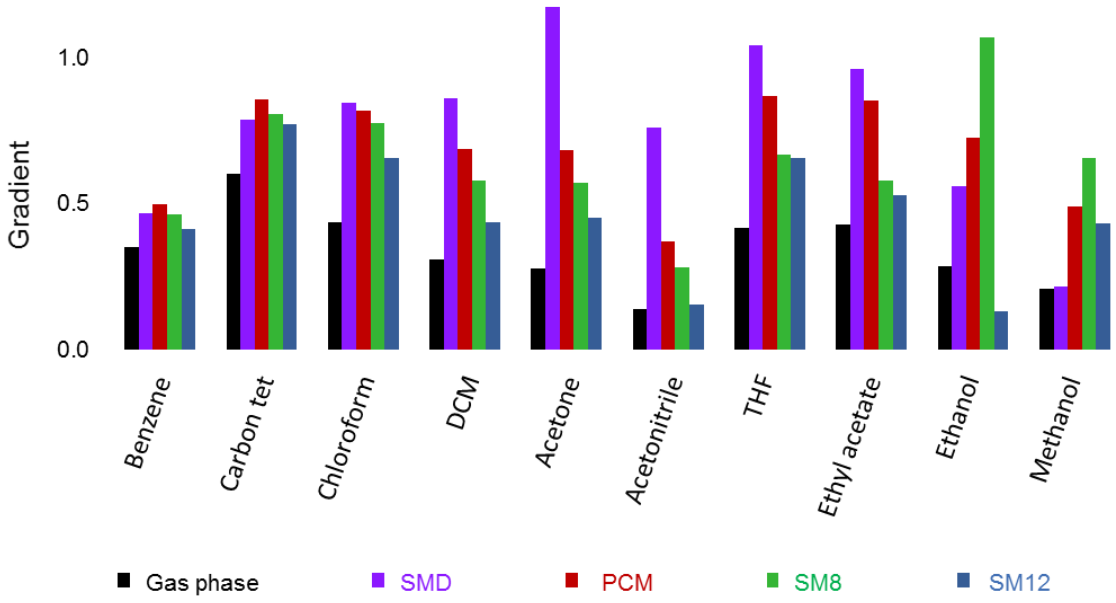

Figure 2.7: Plots of gradients determined by plotting the computationally derived energies in the gas (black) and solution phase calculated using DFT/B3LYP/6-31G* and employing implicit solvation models SMD (purple), PCM (red), SM8 (green) and SM12 (blue) against the experimentally determined Gibbs free energies in the ten solvents investigated.

Taking into account the R^2 and gradient values, it was therefore concluded that the PCM implicit solvation model was the most effective implicit solvation method at modelling solvent effects on conformational equilibria. This study also highlighted the limitations of implicit solvation models: SMD, SM8 and SM12 when investigating polar solvent effects on conformational equilibria. It is important to note that these calculations were carried out on a very simple system, this highlighted the importance of carrying out further investigations experimentally on more complex systems in order to understand fundamental non-covalent interactions in solution.

2.4 Conclusion

To conclude, solvent effects on conformational equilibria were investigated computationally using a simple *para*-substituted molecular balance series. Calculations were performed at the DFT/B3LYP/6-31G* level of theory in the gas phase in combination with the implicit solvation models PCM, SMD, SM8 and SM12. The derived Gibbs free energies were then plotted against previously determined

experimental values. In general, strong R^2 values were found in all solvents with the exception of methanol and ethanol using the SMD implicit solvation model. This meant these computational methods were good at predicting the general trends of solvent effects on conformational equilibria. The gradients of the data across the compound series indicated that the absolute magnitudes of the energy predictions were often much less reliable. The PCM solvation model was consistently the most accurate method at predicting experimental behaviour, even in polar solvents. SMD was shown to be the poorest model for predicting the absolute values in ethanol and methanol. If implicit solvation models were to be used in biomolecular simulations, water would need to be modelled, therefore the above study highlighted the limitations of implicit solvation models for understanding behaviour in polar protic solvents. Therefore, more experiments are needed to fully understand solvent effects on conformational equilibria, which might contribute to the development of improved solvent models in the future.

2.5 References

1. Mati, I. K.; Adam, C.; Cockroft, S. L. Seeing through solvent effects using molecular balances. *Chemical Science.* **2013**, *4* (10), 3965-3972.

2. Muchowska, K. B.; Adam, C.; Mati, I. K.; Cockroft, S. L. Electrostatic Modulation of Aromatic Rings via Explicit Solvation of Substituents. *Journal of the American Chemical Society.* **2013**, *135* (27), 9976-9979.

3. Verdonk, M. L.; Chessari, G.; Cole, J. C.; Hartshorn, M. J.; Murray, C. W.; Nissink, J. W. M.; Taylor, R. D.; Taylor, R. Modeling Water Molecules in Protein−Ligand Docking Using GOLD. *Journal of Medicinal Chemistry.* **2005**, *48* (20), 6504-6515.

4. Araujo, E.; Lima, A. H.; Lameira, J. Catalysis by solvation rather than the desolvation effect: exploring the catalytic efficiency of SAM-dependent chlorinase. *Physical Chemistry Chemical Physics.* **2017**, *19* (32), 21350-21356.

5. Bagchi, B.; Jana, B. Solvation dynamics in dipolar liquids. *Chemical Society Reviews.* **2010**, *39* (6), 1936-1954.

6. Otto, R.; Brox, J.; Trippel, S.; Stei, M.; Best, T.; Wester, R. Single solvent molecules can affect the dynamics of substitution reactions. *Nat Chem.* **2012**, *4* (7), 534-538.

7. Gronert, S.; Pratt, L. M.; Mogali, S. Substituent Effects in Gas-Phase Substitutions and Eliminations: β-Halo Substituents. Solvation Reverses S_N2 Substituent Effects. *Journal of the American Chemical Society.* **2001**, *123* (13), 3081-3091.

8. Mati, I. K.; Cockroft, S. L. Molecular balances for quantifying non-covalent interactions. *Chemical Society Reviews.* **2010**, *39* (11), 4195-4205.

9. Gung, B. W.; Patel, M.; Xue, X. A Threshold for Charge Transfer in Aromatic Interactions? A Quantitative Study of π-Stacking Interactions. *The Journal of Organic Chemistry.* **2005**, *70* (25), 10532-10537.

10. Cozzi, F.; Cinquini, M.; Annuziata, R.; Siegel, J. S. Dominance of polar/.pi. over charge-transfer effects in stacked phenyl interactions. *Journal of the American Chemical Society.* **1993**, *115* (12), 5330-5331.

11. Zhang, J.; Zhang, H.; Wu, T.; Wang, Q.; van der Spoel, D. Comparison of Implicit and Explicit Solvent Models for the Calculation of Solvation Free Energy in Organic Solvents. *Journal of Chemical Theory and Computation.* **2017**, *13* (3), 1034-1043.

12. Steinmann, S. N.; Sautet, P.; Michel, C. Solvation free energies for periodic surfaces: comparison of implicit and explicit solvation models. *Physical Chemistry Chemical Physics.* **2016**, *18* (46), 31850-31861.

13. Thapa, B.; Schlegel, H. B. Density Functional Theory Calculation of pKa's of Thiols in Aqueous Solution Using Explicit Water Molecules and the Polarizable Continuum Model. *The Journal of Physical Chemistry A.* **2016**, *120* (28), 5726-5735.

14. Thapa, B.; Schlegel, H. B. Theoretical Calculation of pKa's of Selenols in Aqueous Solution Using an Implicit Solvation Model and Explicit Water Molecules. *The Journal of Physical Chemistry A.* **2016**, *120* (44), 8916-8922.

15. Khuntawee, W.; Kunaseth, M.; Rungnim, C.; Intagorn, S.; Wolschann, P.; Kungwan, N.; Rungrotmongkol, T.; Hannongbua, S. Comparison of Implicit and Explicit Solvation Models for Iota-Cyclodextrin Conformation Analysis from Replica Exchange Molecular Dynamics. *Journal of Chemical Information and Modeling.* **2017**, *57* (4), 778-786.

16. White, R. P.; Meirovitch, H. Minimalist explicit solvation models for surface loops in proteins. *Journal of chemical theory and computation.* **2006**, *2* (4), 1135-1151.

17. Zhang, L. Y.; Gallicchio, E.; Friesner, R. A.; Levy, R. M. Solvent models for protein–ligand binding: Comparison of implicit solvent poisson and surface generalized born models with explicit solvent simulations. *Journal of Computational Chemistry.* **2001**, *22* (6), 591-607.

18. Cramer, C. J.; Truhlar, D. G. Implicit Solvation Models: Equilibria, Structure, Spectra, and Dynamics. *Chemical Reviews.* **1999**, *99* (8), 2161-2200.

19. Skyner, R. E.; McDonagh, J. L.; Groom, C. R.; van Mourik, T.; Mitchell, J. B. O. A review of methods for the calculation of solution free energies and the modelling of systems in solution. *Physical Chemistry Chemical Physics.* **2015**, *17* (9), 6174-6191.

20. Kleinjung, J.; Fraternali, F. Design and application of implicit solvent models in biomolecular simulations. *Current Opinion in Structural Biology.* **2014**, *25* (100), 126-134.

21. Chocholoušová, J.; Feig, M. Implicit Solvent Simulations of DNA and DNA−Protein Complexes: Agreement with Explicit Solvent vs Experiment. *The Journal of Physical Chemistry B.* **2006**, *110* (34), 17240-17251.

22. Sun, Y.; Latour, R. A. Comparison of implicit solvent models for the simulation of protein–surface interactions. *Journal of Computational Chemistry.* **2006**, *27* (16), 1908-1922.

23. Brieg, M.; Setzler, J.; Albert, S.; Wenzel, W. Generalized Born implicit solvent models for small molecule hydration free energies. *Physical Chemistry Chemical Physics.* **2017**, *19* (2), 1677-1685.

24. Tomasi, J.; Mennucci, B.; Cammi, R. Quantum Mechanical Continuum Solvation Models. *Chemical Reviews.* **2005**, *105* (8), 2999-3094.

25. Cramer, C. J.; Truhlar, D. G. A Universal Approach to Solvation Modeling. *Accounts of Chemical Research.* **2008**, *41* (6), 760-768.

26. Marenich, A. V.; Cramer, C. J.; Truhlar, D. G. Generalized Born Solvation Model SM12. *Journal of Chemical Theory and Computation.* **2013**, *9* (1), 609-620.

27. Marenich, A. V.; Cramer, C. J.; Truhlar, D. G. Universal Solvation Model Based on Solute Electron Density and on a Continuum Model of the Solvent Defined by the Bulk Dielectric Constant and Atomic Surface Tensions. *The Journal of Physical Chemistry B.* **2009**, *113* (18), 6378-6396.

28. Miertuš, S.; Scrocco, E.; Tomasi, J. Electrostatic interaction of a solute with a continuum. A direct utilizaion of AB initio molecular potentials for the prevision of solvent effects. *Chemical Physics.* **1981**, *55* (1), 117-129.

29. Cossi, M.; Rega, N.; Scalmani, G.; Barone, V. Polarizable dielectric model of solvation with inclusion of charge penetration effects. *The Journal of Chemical Physics.* **2001**, *114* (13), 5691-5701.

30. Cossi, M.; Rega, N.; Scalmani, G.; Barone, V. Energies, structures, and electronic properties of molecules in solution with the C-PCM solvation model. *Journal of Computational Chemistry.* **2003**, *24* (6), 669-681.

31. Takano, Y.; Houk, K. N. Benchmarking the Conductor-like Polarizable Continuum Model (CPCM) for Aqueous Solvation Free Energies of Neutral and Ionic Organic Molecules. *Journal of Chemical Theory and Computation.* **2005**, *1* (1), 70-77.

32. Thompson, J. D.; Cramer, C. J.; Truhlar, D. G. New Universal Solvation Model and Comparison of the Accuracy of the SM5.42R, SM5.43R, C-PCM, D-PCM, and IEF-PCM Continuum Solvation Models for Aqueous and Organic Solvation Free Energies and for Vapor Pressures. *The Journal of Physical Chemistry A.* **2004**, *108* (31), 6532-6542.

33. Mennucci, B.; Tomasi, J.; Cammi, R.; Cheeseman, J. R.; Frisch, M. J.; Devlin, F. J.; Gabriel, S.; Stephens, P. J. Polarizable Continuum Model (PCM) Calculations of Solvent Effects on Optical Rotations of Chiral Molecules. *The Journal of Physical Chemistry A.* **2002**, *106* (25), 6102-6113.

34. Yu, X.-f.; Yamazaki, S.; Taketsugu, T. Solvent effects on the excited-state double proton transfer mechanism in the 7-azaindole dimer: a TDDFT study with the

polarizable continuum model. *Physical Chemistry Chemical Physics.* **2017**, *19* (34), 23289-23301.

35. Guerard, J. J.; Arey, J. S. Critical Evaluation of Implicit Solvent Models for Predicting Aqueous Oxidation Potentials of Neutral Organic Compounds. *Journal of Chemical Theory and Computation.* **2013**, *9* (11), 5046-5058.

36. Gupta, M.; da Silva, E. F.; Svendsen, H. F. Explicit Solvation Shell Model and Continuum Solvation Models for Solvation Energy and pKa Determination of Amino Acids. *Journal of Chemical Theory and Computation.* **2013**, *9* (11), 5021-5037.

37. da Silva, E. F.; Svendsen, H. F.; Merz, K. M. Explicitly Representing the Solvation Shell in Continuum Solvent Calculations. *The Journal of Physical Chemistry A.* **2009**, *113* (22), 6404-6409.

Chapter 3

Examining Solvent and Geometric Effects on H-Bonding

Abstract

Hydrogen bonding is ubiquitous in nature where it plays key roles in DNA base pairing[1] and molecular recognition in protein-ligand interactions.[2] Here, we have used three series of synthetic molecular balances to measure solvent and substituent effects on the positions of conformational equilibria in both organic and aqueous solvents. Initially, plots of computational conformational energies against experimental results revealed that solute-solvent interactions dominated the energetic trends. Therefore, Hunter's solvent model was used to dissect away the solvent effects and provide insight on the individual intramolecular interactions and solute-solvent interactions. Following energetic dissection using the solvation model, a strong correlation was found between a constant solvent independent term and the calculated electrostatic potential over the H-bond donor. The finding confirmed that it is possible to reveal H-bond energies even in the presence of strong competing solvent effects.

Full experimental, computational and supplementary details are given in Supporting Information B, pages 137-250.

Contributions: The experimental, and computational results presented in this chapter were obtained by Nicole Yvette Meredith (NYM).

3.1 Introduction

H-bonds are fundamental non-covalent interactions. In biological systems, water competes strongly with H-bonds therefore the extent to which H-bonds regulate molecular interactions is difficult to quantify. Solvation is a complex phenomenon, where computational efforts to model it remain at a limited level as was illustrated in Chapter 2. Therefore, more experiments are necessary to further our understanding of solvent effects on non-covalent interactions such as H-bonding. Hydrogen bonding between solutes is favoured in non-polar solvents, and disfavoured in polar solvents that contain competing H-bonding donor and acceptor groups. Therefore, the majority of intermolecular H-bond studies have taken place in non-polar solvents. Abraham[3,4] and Hunter quantified various donor and acceptor groups in CCl_4, and defined H-bonding donor and acceptor coefficients, α and β of different functional groups. In solution phase, Hunter proposed that H-bonding energies could be predicted using Equation 3.1.[5]

$$\Delta G_{H\text{-}bond} = -(\alpha - \alpha_s)(\beta - \beta_s) + 6 \text{ kJ mol}^{-1} \quad (3.1)$$

Binding constants were also obtained in more competitive solvents such as DMSO and methanol, however, these studies required an exceptionally strong H-bond donor, perfluoro-*tert*-butanol (α = 4.9), with a strong acceptor, *tri*-*n*-butylphosphine oxide (β = 9.9).[6]

H-Bonding in Aqueous Solution

In nature, biomolecules contain H-bonds that interact in aqueous solution. Studying H-bonds in aqueous solution is important for optimising the activity of agrochemicals and pharmaceuticals, however, quantifying the strength of H-bonds in aqueous solution is difficult due to strong competing solvent effects. Experimental H-bond binding energies in aqueous solution have been investigated by supramolecular chemists. Davis and co-workers synthesised artificial amphiphilic macropolicyclic receptors for carbohydrate recognition (Figure 3.1).[7,8,9] The sugar OH groups from the substrate molecule formed H-bonds with the amide linkages on the pillars of the structure. The substrate molecules also bound to the receptor through hydrophobic CH-π interactions. Binding of the disaccharide cellobiose to the receptor in water was determined to be 650 M^{-1}, dominated by an enthalpic change of ΔH = –13 kJ mol^{-1} and an entropic disadvantage of $-T\Delta S$ = –2.5 kJ mol^{-1}. The binding strength was found to be due to the interactions between the axial cellobiose C-H bonds and the arene sidewalls and also due to hydrophobic forces.

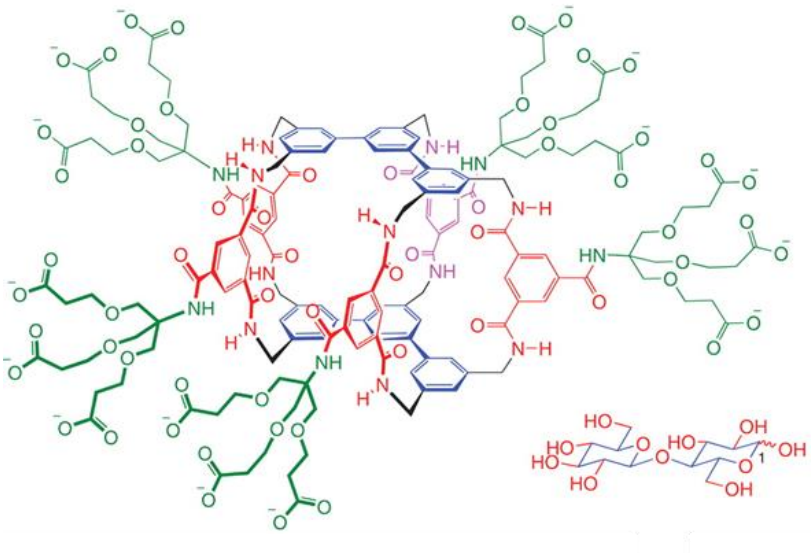

Figure 3.1: Carbohydrate receptor synthesised by Davis and coworkers[7] for binding cellobiose substrate in water.

K. Kim *et al* also found high affinity binding of amino sugars to non-charged cucurbit[7]uril hosts (K up to 10^4 M^{-1}) in water (Figure 3.2**A**).[10] These receptors did not contain C−H--π bonds and ion pairs, however, the observed binding enthalpy of −14 kJ mol^{-1} was strikingly close to the binding of cellobiose to Davis' receptor. This value was unusually small for typical CB[7] receptor-binding interactions. The main driving forces for amino sugars binding to Kim's CB[7] receptor were ion-dipole interactions between ammonium-carbonyl groups and high-energy cavity water. The latter may also occur in Davis' receptor (Figure 3.1), where there was a hydrophobic cavity. The binding of sugars to the CB7 receptor and the amphiphilic macropolicyclic receptor were strongly entropically favoured ($-T\Delta S$ from −2.8 to −10 kJ mol^{-1}), and it was therefore deduced that the desolvation of the sugar contributed a favourable entropic component to binding, but also reduced the enthalpy in water.

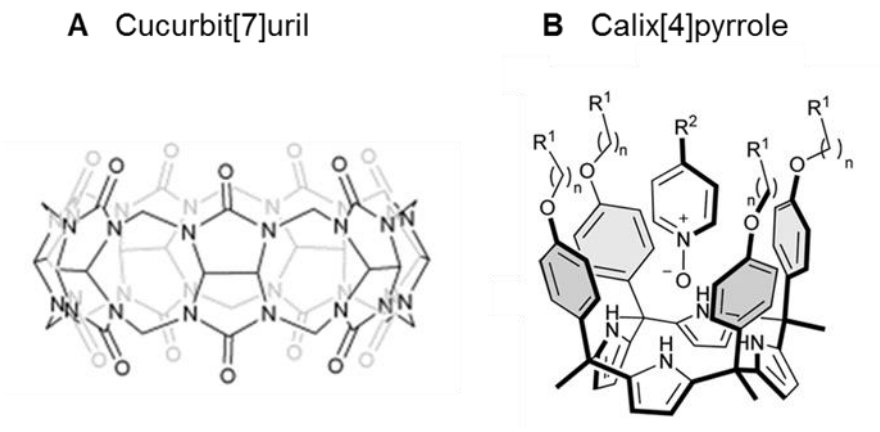

Figure 3.2: A Calix[4]pyrrole synthesised by P. Ballester *et al*[11] to investigate binding with sugars in water. **B** Molecular structures of cucurbit[7]uril (CB[7]) synthesised by K.Kim[10] for encapsulation of amino saccharides in water.

P. Ballester and co-workers[11] studied H-bonding in aqueous solution by synthesising water soluble aryl extended calix[4]pyrroles (Figure 3.2B). The hosts contained deep aromatic cavities which protected strong donor sites from the competing water interactions and therefore allowed hydrogen bonding between the four pyrrole NHs and a series of pyridine *N*-oxides. Isothermal titration calorimetry experiments were used to calculate the Gibbs free energy range between ΔG = –25 to 35 kJ mol^{-1}.

Molecular Balances Used to Investigate H-bonding in Amides

As was highlighted in the above section, H-bond energies in water have frequently been measured within cavities (analogous to protein-receptors), rather than in truly solvent-exposed systems due to the strong competing effects of water. Molecular balances offer an alternative method of studying H-bond interactions in solution.[12] The positions of conformational equilibria are determined by intramolecular interactions and solvent effects. Previous examples of molecular balances designed to study H-bonding in amides are outlined below.

Wilcox *et al* designed a molecular balance to investigate intramolecular H-bonding between amino acids in an antiparallel *β*–sheet motif (Figure 3.3).[13] Slow rotation about an *N*-aryl bond resulted in two distinct conformer peaks visible on the NMR spectra. The design was used to investigate H-bond stability in bioinspired systems as was described in full detail in Chapter 1.

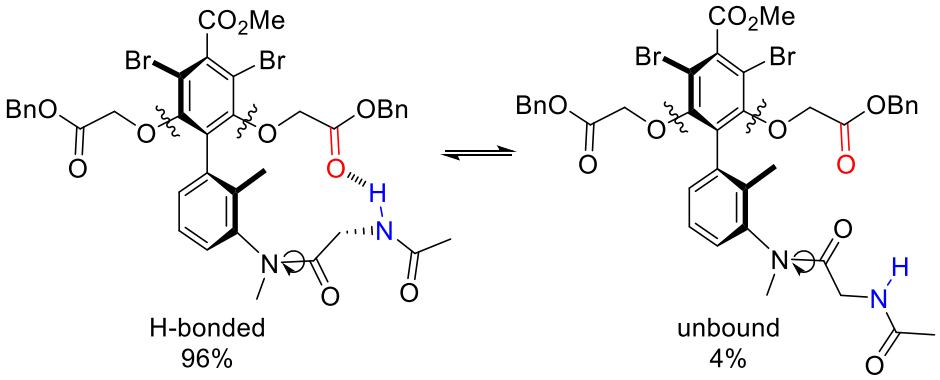

Figure 3.3: Molecular torsion balance designed by Wilcox[13] to investigate H-bonding between amides.

A. D. Hamilton and S. Thompson used synthetic diphenylacetylene molecular balances to investigate the H-bond strength between variously functionalized amides (Figure 3.4).[14] This design was introduced in Chapter 1 and it was found that the study was limited to non-polar organic solvents.

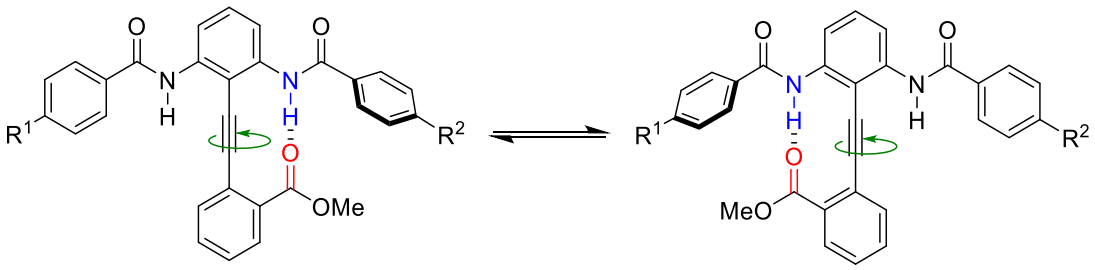

Figure 3.4: Molecular balance used by A. D. Hamiliton and S. Thompson[14] to investigate the relative H-bond strength between amides.

The Cockroft group have previously used simple molecular torsion balances to study solvent and substituent effects on intramolecular interactions (Figure 3.5).[15] The molecular balance design incorporated a formyl group which rotated slowly enough on the NMR timescale that two conformers were observed on the ^{19}F NMR spectra. Experimental energies were therefore determined in various solvents, and application of Hunter's solvation model allowed the authors to see through solvent effects to gain further insight into the behavior of the system. More recently, the same molecular balance design was used to directly measure the strength of an intramolecular H-bond and to study cooperativity in H-bond chains in an organic solvent.[16]

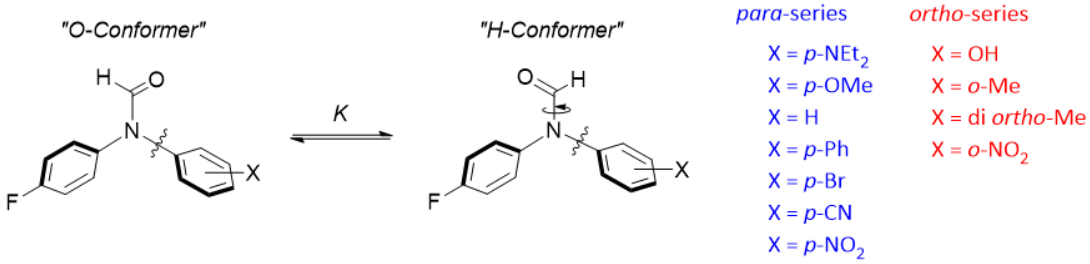

Figure 3.5: Simple molecular torsion balances used by Cockroft[15] to study solvent and substituent effects on the position of conformational equilibria.

3.2 Aims and scope of this investigation

Herein, intramolecular H-bonding between biologically relevant amides/amines was investigated in various non-competitive and competitive solvents using molecular torsion balances based on the previous designs outlined above. The effects of varying the H-bond donors along with the conformational flexibility and distance of the system were studied. The systems described below were identified as useful models as they

allowed the quantifiable examination of H-bond interactions that would not be possible using intermolecular techniques due to the entropic penalty of bringing two molecules together.

New designs of H-bonding formamide molecular balances were proposed that were based on previous designs (Figure 3.6). The molecular balances adopted distinct folded and unfolded states due to restricted rotation about the formyl group. Methylene and ethylene linkers were incorporated into the molecular balances to allow for H-bonds to form between the donor and acceptor groups in the folded conformations. In the unfolded conformations, the H-bonds were broken, and the H-bond donor and acceptor groups were exposed to the solvent. Thus, the formation of an intramolecular H-bond was in competition with the formation of H-bonds from the molecular balance with the solvent. Therefore, these designs allowed the quantification of weaker H-bonds in competitive solvents to be determined.

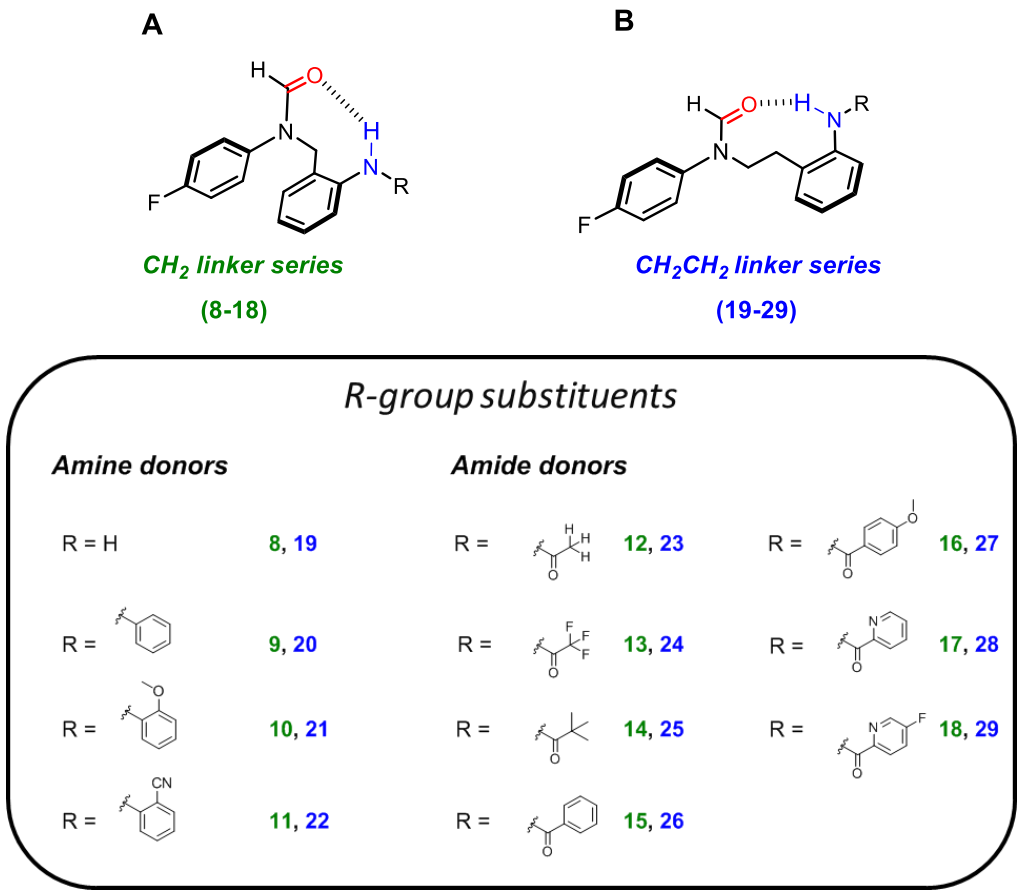

Figure 3.6: A Methylene linker molecular balance series (compounds **8-18,** green) substituted with amine and amide hydrogen bond donors. **B** Ethylene linker molecular balance series (compounds **19-29**, blue) substituted with amine and amide hydrogen bond donors.

In addition, the incorporation of a fluorine tag allowed the analysis to be carried out using ^{19}F NMR spectroscopy. This offered the following practical advantages:

1) Clear separation of the folded and unfolded peaks.
2) Simple spectra, with the absence of additional solvent peaks.
3) The use of non-deuterated solvents, this was advantageous as it allowed an extension of the number of solvent and solvent mixtures used. Non-deuterated solvents were also cheaper relative to deuterated solvents.

3.3 Synthesis of molecular torsion balances

Molecular balances were synthesised according to the schemes outlined below (full synthetic details are provided in Supporting Information B).

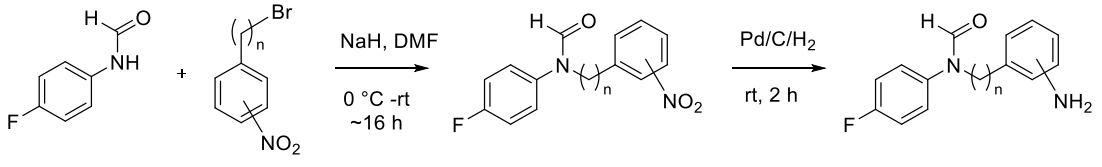

36 R = *o*-NO_2, n = 1 50%
37 R = *p*-NO_2, n = 1 50%
38 R = *o*-NO_2, n = 2 66%
41 R = *p*-NO_2, n = 2 87%

8 R = *o*-NH_2, n = 1 79%
34 R = *p*-NH_2, n = 1 74%
19 R = *o*-NH_2, n = 2 86%
35 R = *p*-NH_2, n = 2 74%

Figure 3.7: Synthesis of aniline molecular balances **8**, **19**, **34** and **35**. Full details of the synthesis can be found in Supporting Information B.

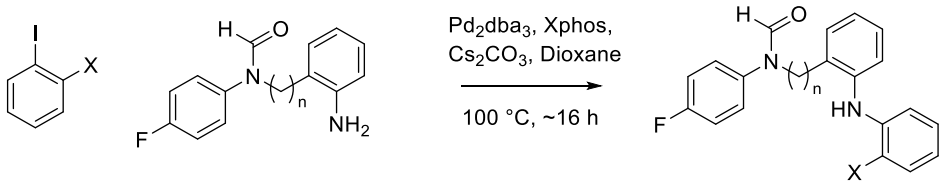

9 n = 1, X = H 62%
10 n = 1, X = OMe 76%
11 n = 1, X = CN 73%

20 n = 2, X = H 23%
21 n = 2, X = OMe 81%
22 n = 2, X = CN 26%

Figure 3.8: Synthesis of amine donor molecular torsion balances for both the methylene and ethylene series.

A

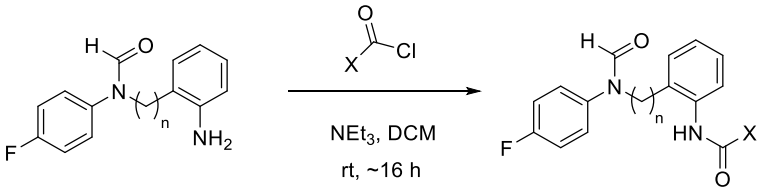

12	n = 1, X = Me	62%
13	n = 1, X = CF_3	55%
14	n = 1, X = *t*-Bu	90%
15	n = 1, X = Ph	57%
16	n = 1, X = *p*-PhOMe	74%

23	n = 2, X = Me	69%
25	n = 2, X = *t*-Bu	82%

B

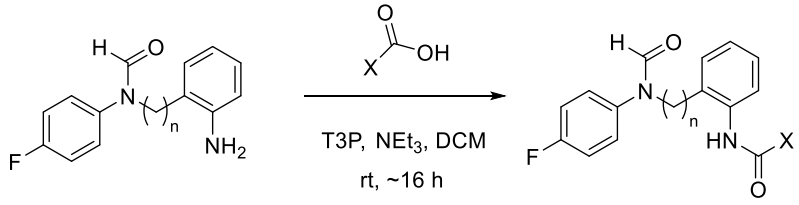

17	n = 1, X = 2-Py	17%
18	n = 1, X = 2-(5-F-Py)	21%

24	n = 2, X = CF_3	71%
26	n = 2, X = Ph	73%
27	n = 2, X = *p*-PhOMe	51%
28	n = 2, X = 2-Py	37%
29	n = 2, X = 2-(5-F-Py)	34%

Figure 3.9: Synthesis of amide donor molecular torsion balances for the methylene and ethylene series. **A** Coupling with acid chloride **B** Coupling with acids.

The syntheses of the nitro-substituted balances, **36** and **38**, were achieved via a nucleophilic substitution (S_N2) reaction between *N*-(4-fluorophenyl)formamide and 2-nitrobenzyl bromide. Balances **36** and **38** were then reduced using palladium on carbon under a hydrogen environment to yield the aniline molecular balance **8** and **19** in good yield. Balances **8** and **19** were then either coupled with an aryl halide in a Buchwald-Hartwig amination to yield the aniline donor molecular balances **9-11** and **20-22**, or alternatively coupled with the corresponding acid or acid chloride to yield the amide donor molecular balances **12-18** and **23-29**.

3.4 Conformational characterisation of the molecular balances

The equilibrium geometries of the folded and unfolded conformations of the molecular balances were calculated by running conformer distribution searches at the DFT/B3LYP/6-31G* level of theory (Figure 3.11 and Supporting Information B, Figure S3.10). The folded conformers of molecular balances **8**–**18** were found to contain intramolecular H-bonds (Figure 3.11 and Supporting Information B, S3.10). The difference in energy between the folded and unfolded conformers gave the computational conformational equilibrium energies in the absence of solvent, ΔE_{calc} (see Supporting Information B, Table 3.32 and Table S3.33), which were later compared against experimental values obtained in solution (see Supporting Information B, Figure S3.11).

An X-ray crystal structure was obtained for balance **12** (Figure 3.10 and Supporting Information B, Tables S3.35-S3.41). The balances crystallised in the folded conformation and the geometry and distance of the intramolecular H-bond compared well with the calculated structure, using DFT/B3LYP/6-31G*, which confirmed the suitability of the balance to form and measure H-bonds. It also confirmed that DFT/B3LYP/6-31G* was an appropriate level of theory to model the compounds. The H-bond in the crystallised structure measured 2.0 Å, with an angle of 162.2°. Whereas the calculated structure the H-bond had a distance of 1.9 Å, and an angle of 164.1° (Figure 3.10).

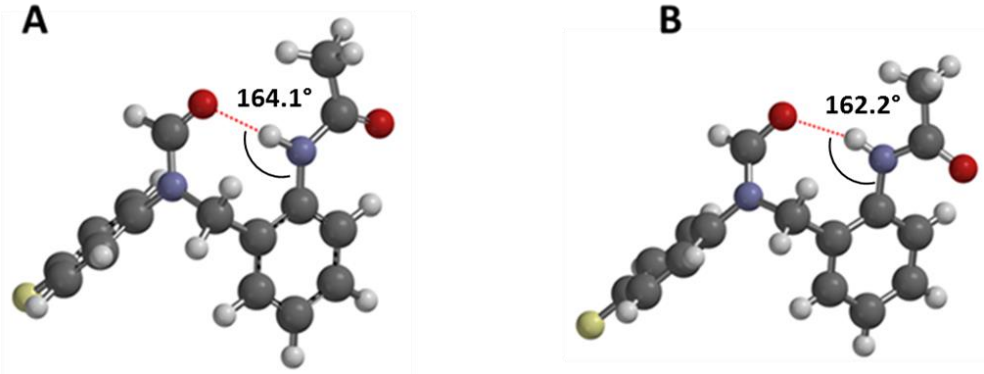

Figure 3.10: A Calculated structure of folded conformer of molecular balance **12** (DFT/B3LYP/6-31G*). **B** Obtained crystal structure of compound **12**.

8

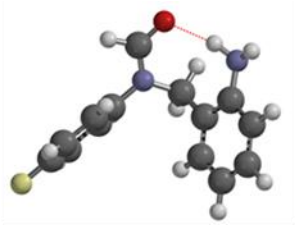

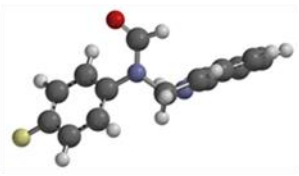

9

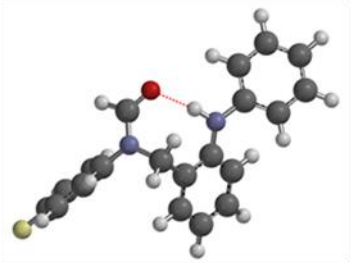

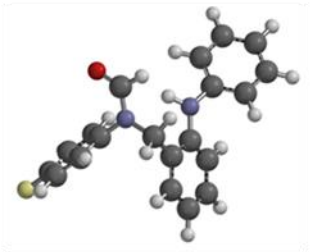

10

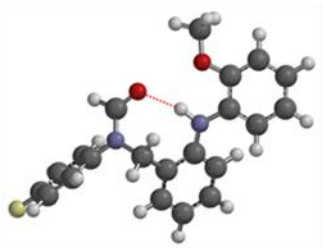

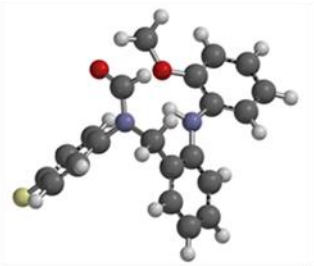

11

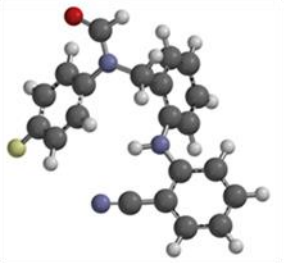

12

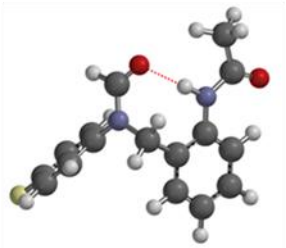

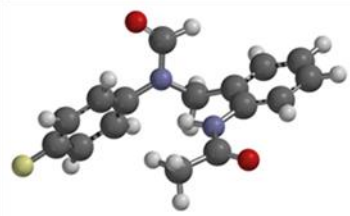

13

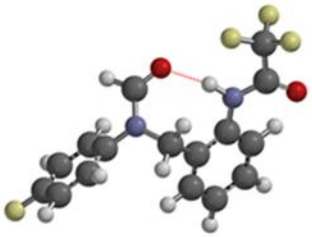

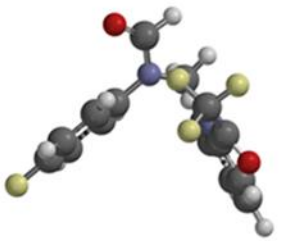

14

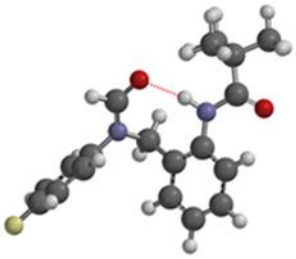

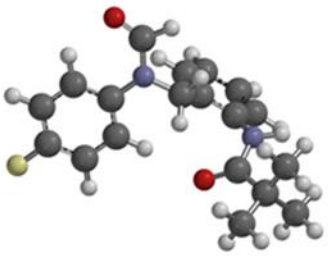

15

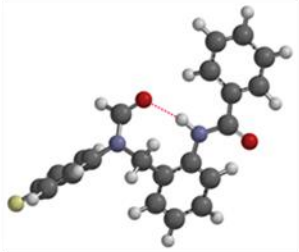

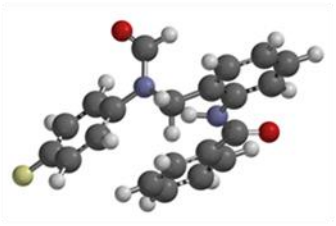

16

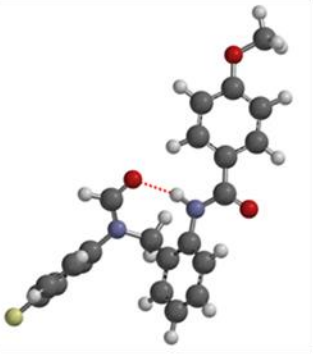

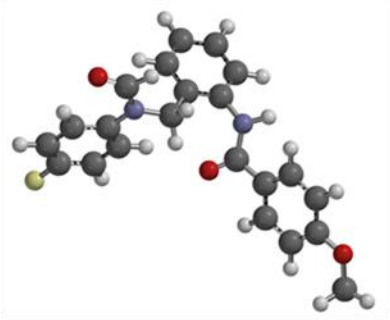

17

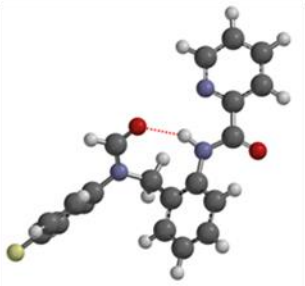

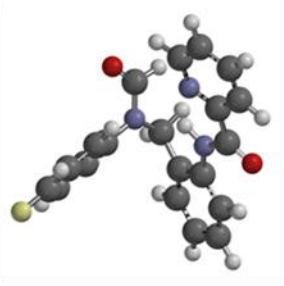

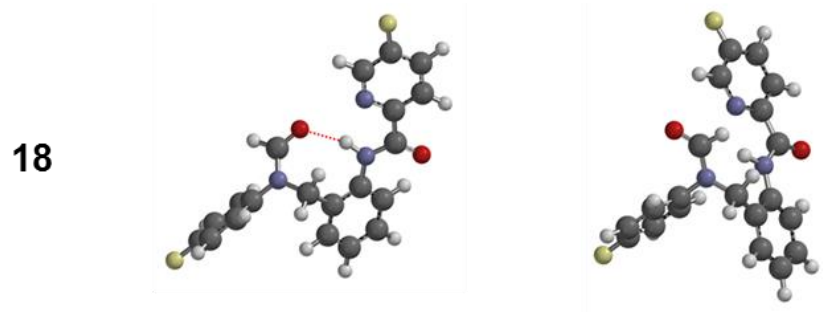

Figure 3.11: Calculated structures of the folded and unfolded conformers of the methylene molecular balance series using DFT/B3LYP/6-31G*. The calculated structures of the ethylene molecular balance series can be found in Supporting Information B, Figure S3.10.

An energy profile calculation was performed on molecular balance **8**, using the DFT/B3LYP/6-31G* level of theory, to determine the energy of the rotation barrier between the folded and unfolded states (Figure 3.12). The barrier to rotation was calculated at 91 kJ mol^{-1}.

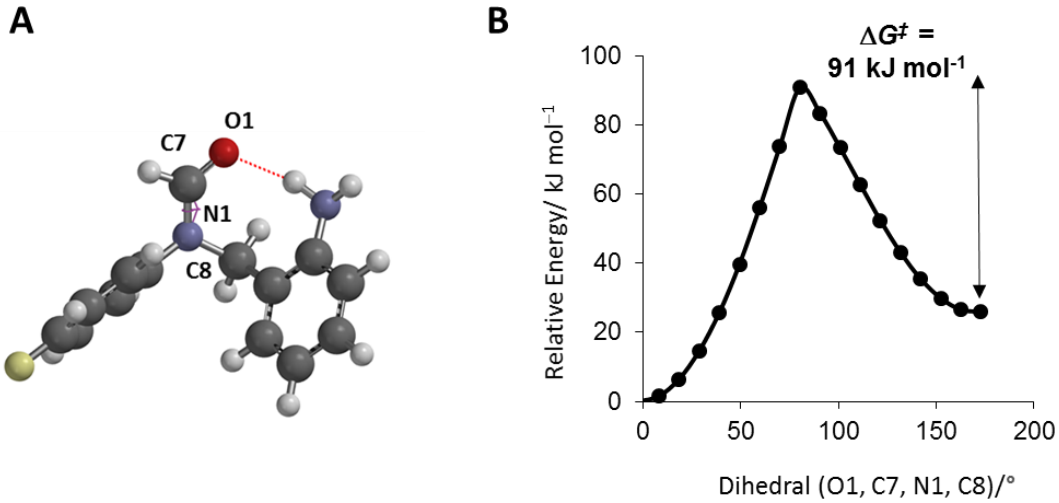

Figure 3.12: Determination of the barrier to rotation by performing an energy profile calculation at the DFT/B3LYP/6-31G* level of theory for molecular balance **8** (See supporting Information B, Table S3.34).

Consistent with this calculation, exchange between the formyl conformers was found to be slow enough on the NMR timescale that two peaks were observed on the ^{19}F spectra, corresponding to the folded and unfolded states. The equilibrium constants, $K_{fold,}$ were determined by integration of the ^{19}F NMR peaks corresponding

to each conformer (Figure 3.13). Conformational free energy differences were then calculated using the equation, $\Delta G_{\text{H-bond}} = -RT\ln K_{\text{fold}}$.

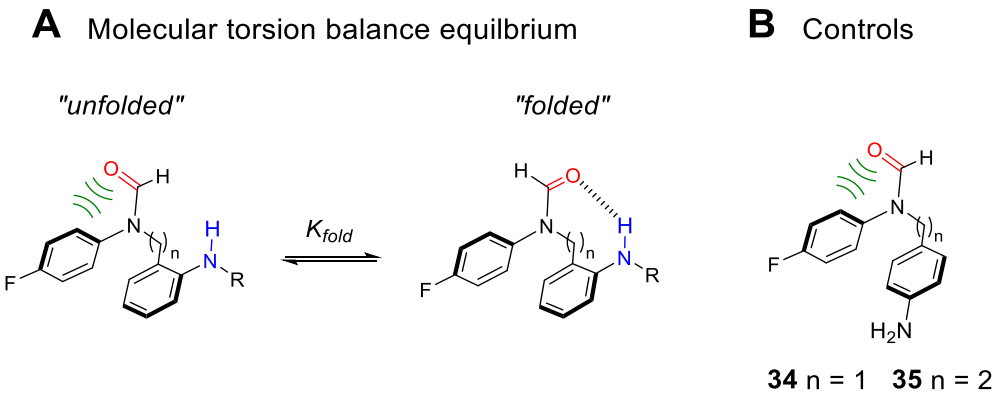

Figure 3.13: A Molecular torsion balance conformational equilibrium used to determine $\Delta G_{\text{H-bond}}$. **B** Control *para*-aniline molecular balances used to determine $\Delta G_{\text{control}}$. The H-bond strength ($\Delta\Delta G_{\text{H-bond}}$) was then estimated using Equation 3.2.

From a comparison of the 2D NMR spectra (full details are provided in Supporting Information B, S3.5-S3.9), it was determined that every molecular balance favoured the H-bonded conformation in every solvent studied. To determine whether the bias towards the 'folded' conformer was due to differences in repulsion between the carbonyl and aryl groups, balances **34** and **35** were synthesised with the NH_2 group in the *para* position (Figure 3.13). The NH_2 groups in the *para* positions in balances **34** and **35** did not form intramolecular H-bonds, however the experimental free energies in every solvent indicated a conformational preference towards the 'folded' conformer (Table 3.1).

The dissection of the H-bond strengths were calculated using Equation 3.2. Where $\Delta G_{\text{H-bond}}$ is the equilibrium energy of the *ortho* substituted molecular balances **8** and **19** that formed H-bonds, and $\Delta G_{\text{control}}$ is the Gibbs free energy of the *para* substituted control molecular balances that do not form H-bonds.

$$\text{H-bond strength} = \Delta\Delta G_{\text{H-bond}} = \Delta G_{\text{H-bond}} - \Delta G_{\text{control}} \quad (3.2)$$

Table 3.1: Dissection of H-bond strengths for the aniline molecular torsion balances. Experimental energies for molecular balances **8**, **34**, **19** and **35** can be found in Supporting Information B. Errors in $\Delta\Delta G_{\text{H-bond}}$ were calculated using $\delta\Delta\Delta G_{H-bond} = \sqrt{(\delta\Delta G_{H-bond})^2 + (\delta\Delta G_{control})^2}$. Full details of error analysis can be found in Supporting Information B.

	$\Delta G_{\text{H-bond}}$/ kJ mol^{-1}		$\Delta\Delta G_{\text{H-bond}}$ / kJ mol^{-1}	$\Delta G_{\text{control}}$/ kJ mol^{-1}		$\Delta\Delta G_{\text{H-bond}}$ / kJ mol^{-1}
	8	**34**		**19**	**35**	
Chloroform-*d*	–[a]	–5.1	<–5 (+0.5, –0.7)	–7.4	–4.5	–2.9 (+1.2, –2.3)
Acetone-d_6	–7.4	–4.3	–3.2 (+1.2, –2.3)	–5.4	–3.6	–1.8 (+0.7, –0.9)
CD_3CN	–7.0	–3.9	–3.2 (+1.0, –1.8)	–4.7	–3.0	–1.7 (+0.5, –0.6)
Ethyl acetate	n.d.[b]	–5.1	n.d.[b]	–6.6	–4.4	–2.2 (+1.0, –1.5)
THF	–9.7	–5.1	–4.6 (+0.5, –0.7)	–6.6	–4.7	–1.9 (+1.0, –1.5)
DCM	-[a]	–5.5	<–5 (+0.6, –0.8)	–7.0	–4.0	–3.0 (+1.1, –1.8)
Ethanol	–7.0	–4.3	–2.7 (+1.1, –1.8)	–4.5	–3.5	–1.0 (+0.5, –0.6)
Methanol-d_4	–6.6	–4.0	–2.6 (+1.0, –1.4)	–4.1	–3.1	–1.1 (+0.4, –0.5)
DMSO-d_6	–5.5	–3.6	–1.9 (+0.7, –0.9)	–3.5	–2.8	–0.7 (+0.4, –0.4)

[a]Only one peak observed in NMR spectrum that was assigned to the folded conformer.

[b]Not determined due to peak overlap in the NMR spectrum.

The observation of only a single conformer for the H-bonded balances in chloroform and DCM confirmed that the strongest H-bonds were formed in these solvents ($\Delta\Delta G_{\text{H-bond}}$ <–5 kJ mol^{-1}), while the next strongest H-bond was formed in THF ($\Delta\Delta G_{\text{H-bond}}$ = –4.6 kJ mol^{-1}) and the weakest in DMSO-d_6 ($\Delta\Delta G$ = –1.9 kJ mol^{-1}), which followed the expected trend. For the ethylene molecular balance **19**, a similar expected trend of H-bond strength was found on increasing the polarity of the solvent.

The H-bond strengths for the ethylene series were found to be lower by 1.3–2.8 kJ mol^{-1} relative to the methylene series, indicating weaker intramolecular H-bonds between the aniline/amide donor and the carbonyl acceptor group. To further investigate the energetic influence of flexibility, a comparative van't Hoff analysis was carried out on molecular balances **15** and **26** in DMSO to dissect the entropic and enthalpic contributions on going from a methylene to a more flexible ethylene linker (Supporting Information B, Tables 3.28 and 3.29 and Figures S3.3 and S3.4). The analyses revealed that the observed trends in behaviour had an enthalpic origin, with negligible entropic effects. This was evident as both the dissected enthalpic term (ΔH)

and the experimental Gibbs free energies decreased with increasing linker length, whilst the entropic term was similar in both compounds.

Table 3.2 Dissection of ΔH and $T\Delta S$ at 300 *K*.

Balance	$-T\Delta S$/ kJ mol^{-1}	ΔH/ kJ mol^{-1}	ΔG/ kJ mol^{-1}
15	−1.5 (+1.1, −1.2)	−3.1 ± 1.0	−4.6 (+0.4, −0.5)
26	−2.1 ± 0.3	−1.0 ± 0.1	−3.2 ± 0.3

3.5 Dissecting solvent and substituent effects on H-bonded molecular balances

Having gained a basic understanding of the conformational characteristics of these H-bonding molecular balances, the experimental conformational energies were measured for a more diverse range of balances in nine solvents ($CDCl_3$, CH_2Cl_2, THF, ethyl acetate, CD_3CN, acetone-d_6, DMSO-d_6, EtOH, and MeOD, Figure 3.14). The conformer ratios were determined at molecular balance concentrations of 3.5 mM and were found to be independent of concentration in the range of 1–4 mM, indicating that intermolecular H-bonding between the molecular balances did not perturb the data (Supporting Information B, Table S3.1).

The experimental results were then plotted against the computationally derived folding energies (Supporting Information B, Figure S3.11), determined using Equation 3.3:

$$\Delta E_{\text{calc}} = E_{\text{folded conformer}} - E_{\text{unfolded conformer}} \quad (3.3)$$

The computationally optimised energies of the folded and unfolded conformers were determined by carrying out conformer distribution searches in the gas phase at the DFT/B3LYP/6-31G* level of theory (Figure 3.11). The plots revealed good correlations between the experimental and computed gas-phase data in non-polar solvents such as THF for the methylene series ($R^2 = 0.85$), but poorer correlations for the ethylene series ($R^2 = 0.58$). The poorer correlation for the longer series, throughout the solvents investigated, was attributed to the increase in conformational flexibility on increasing the linker length. In contrast, the correlations were weak to non-existent

in polar solvents such as methanol (R^2 = 0.52 and 0.23) for the methylene and ethylene linker series respectively. These findings were unsurprising given that the calculated conformational free energies did not include solvent effects. Calculations performed in the solution phase employing implicit solvation models, on a simpler molecular balance series, were also shown to reveal poor correlations (Chapter 2).

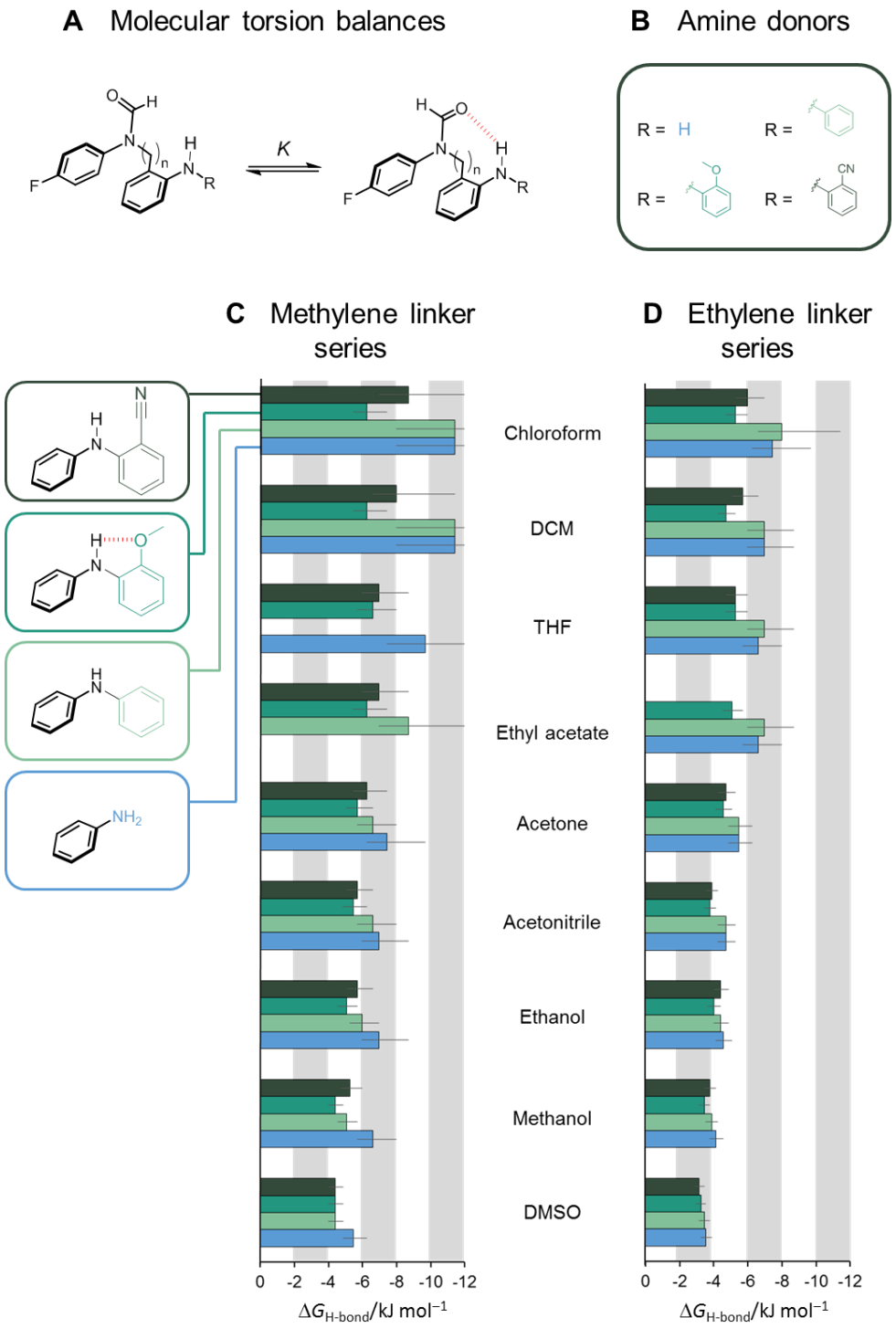

Figure 3.14: A Molecular torsion balance equilibrium. **B** Amine donor R groups. Experimental energies for **C** Methylene linker series and **D** Ethylene linker series. Colours in **C** and **D** correspond to the amine donor R groups. Secondary intramolecular H-bonds are highlighted in red. The absence of an experimental energy for molecular balance **9** in THF was due to overlapping conformer peaks. Where the conformational equilibrium constant, K > 20, conformational energies are plotted at –9.7 kJ mol^{-1} with error bars truncated beyond –10.0 kJ mol^{-1}. All data and errors are tabulated in Supporting Information B.

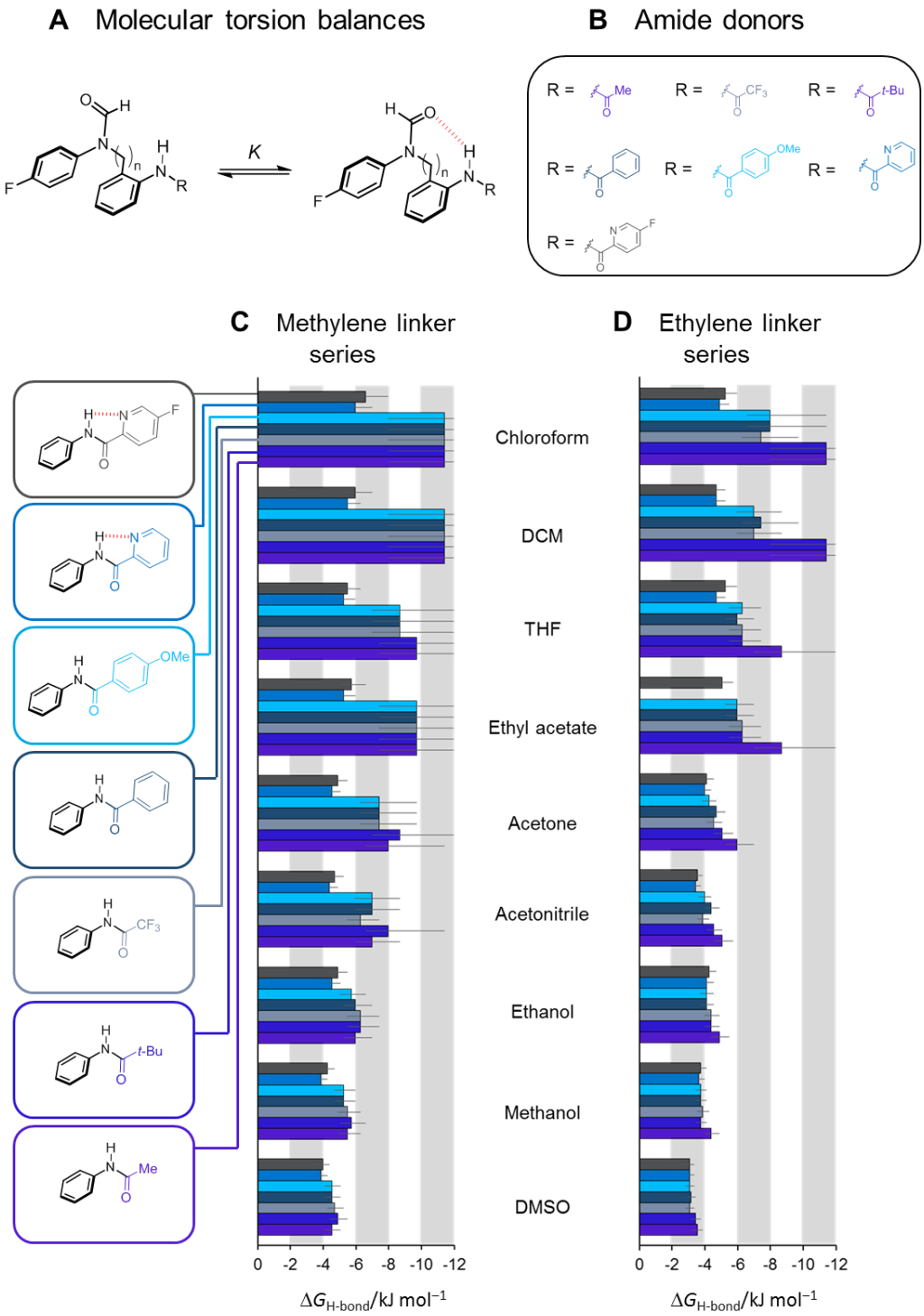

Figure 3.15: A Molecular torsion balance equilibrium. **B** Amine donor R groups. Experimental energies for **C** Methylene linker series and **D** Ethylene linker series. Colours in C and D correspond to the amide donor R groups. Secondary intramolecular H-bonds are highlighted in red. The absence of an experimental energy for molecular balance **29** in ethyl acetate was due to overlapping conformer peaks. Where the conformational equilibrium constant, K > 20, conformational energies are plotted at -9.7 kJ mol^{-1} with error bars truncated beyond –10.0 kJ mol^{-1}. All data and errors are tabulated in Supporting Information B.

A preliminary analysis of the data found that the experimental folding energies decreased with increasing solvent polarity, as measured using the empirical $E_T(30)$ polarity scale (See Supporting Information B, Figure S3.2). This finding could be rationalised as arising from the more polar solvents competing with the intramolecular H-bond, resulting in an increased population of the unfolded conformer.

To gain further insight into the system, a simple solvation model was applied to dissect away the solvent effects. Hunter's solvation model was previously adapted and to study solvent effects on simple molecular balances.[3] Two parameters were used to describe solvent polarity (α_s and β_s, which were the H-bond donor and acceptor constants of the solvent respectively). Due to the small size of the balances, the solvent-solvent interaction contributions to the equilibrium (i.e. the solvophobic term) was omitted. The same adapted solvation model was applied to the present data to model the folding energies of molecular balances **8-29** as a function of the solvents α_s and β_s parameters with ΔE, $\Delta\beta$ and $\Delta\alpha$ being determined as fitting coefficients. ΔE is a solvent independent term describing the contribution of intramolecular interactions to the position of the conformational equilibrium, whereas the $\Delta\alpha$ and $\Delta\beta$ coefficients encode the changes in solvation energies of the H-bond donor and acceptors within each balance (Figure 3.16).

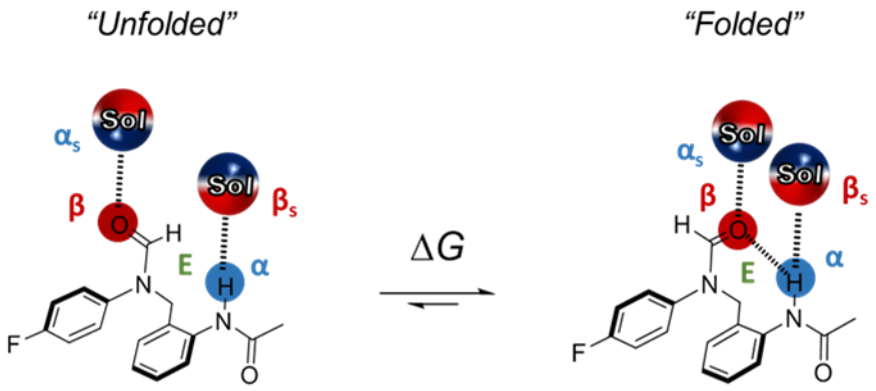

$$\Delta G = E_{fold} - E_{unfold} + \alpha_s\beta_{unfold} + \beta_s\alpha_{unfold} - \beta_s\alpha_{fold} - \alpha_s\beta_{fold}$$
$$= E_{fold} - E_{unfold} + \alpha_s(\beta_{unfold} - \beta_{fold}) + \beta_s(\alpha_{unfold} - \alpha_{fold})$$
$$= \Delta E + \beta_s\Delta\alpha + \alpha_s\Delta\beta$$

Figure 3.16: Hunter's solvation model adapted for this molecular balance series. E_{Fold} and E_{unfold} correspond to the intramolecular steric and electronic effects in the folded and unfolded conformers respectively. α and β are the H-bond donor and acceptor constants of the molecular balance and α_s and β_s are the H-bond donor and acceptor constants of the solvent respectively.

The iterative linear regression fitting of coefficients ΔE, $\Delta\beta$ and $\Delta\alpha$ gave strong linear correlations between the experimental energies ($\Delta G_{H\text{-}bond}$) and the modelled energies determined using Hunter's solvation model ($\Delta G_{\alpha/\beta\ model}$) for both molecular balance series (R^2 = 0.89 and 0.84 for the methylene and ethylene series, respectively) with a gradient of y = x (Figure 3.17). These high-quality correlations proved the excellent overall applicability of the α/β solvation model to dissecting solvent effects in these molecular balances. More scatter was observed for the most extreme conformational energies, which is due to higher errors associated with the measurement of equilibrium constants with the most extreme conformational populations. The fitting provided values of ΔE_{exp}, $\Delta\alpha$ and $\Delta\beta$ for each molecular balance, which gave additional information on the individual interactions contributing to the experimental conformational free energies (Table 3.3).

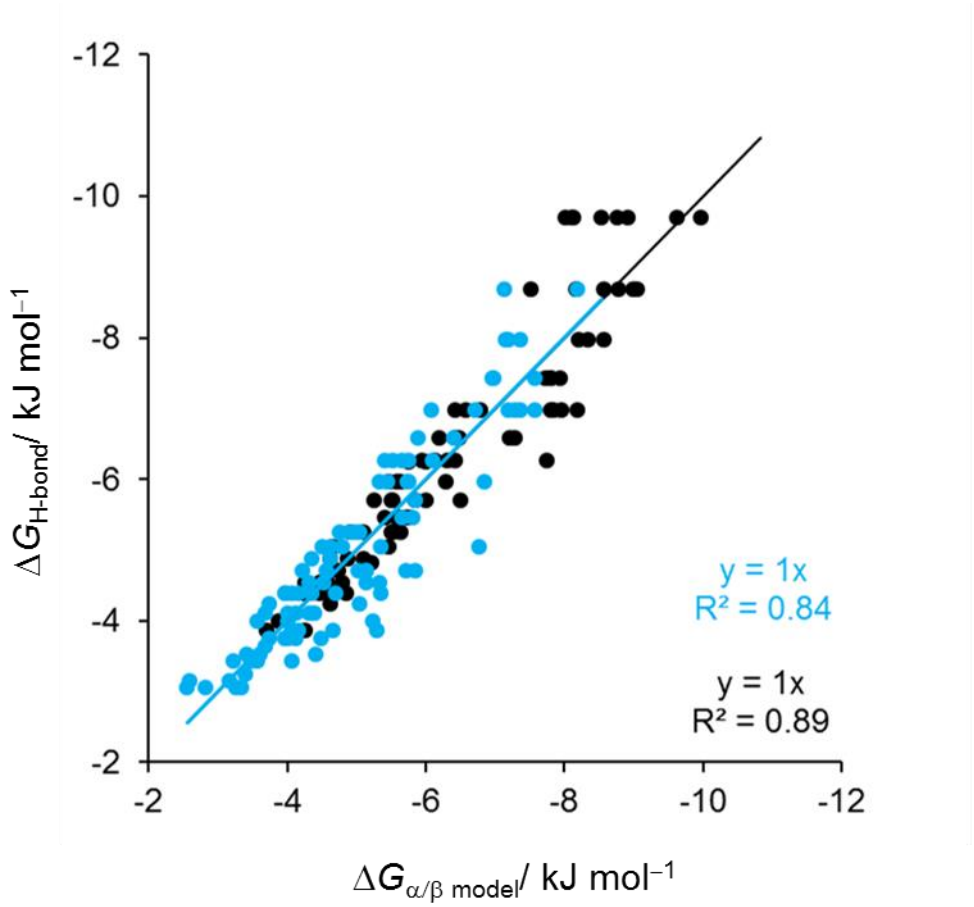

Figure 3.17: Correlation between experimentally determined conformational free energies ($\Delta G_{\text{H-bond}}$) and the values predicted from the α/β model ($\Delta G_{\alpha/\beta\ \text{model}}$) for methylene and ethylene molecular balances series in nine different solvents. Black and blue data points represent the methylene and ethylene linker series, respectively. Error bars have been omitted for clarity (see SI for full error analysis and data tables).

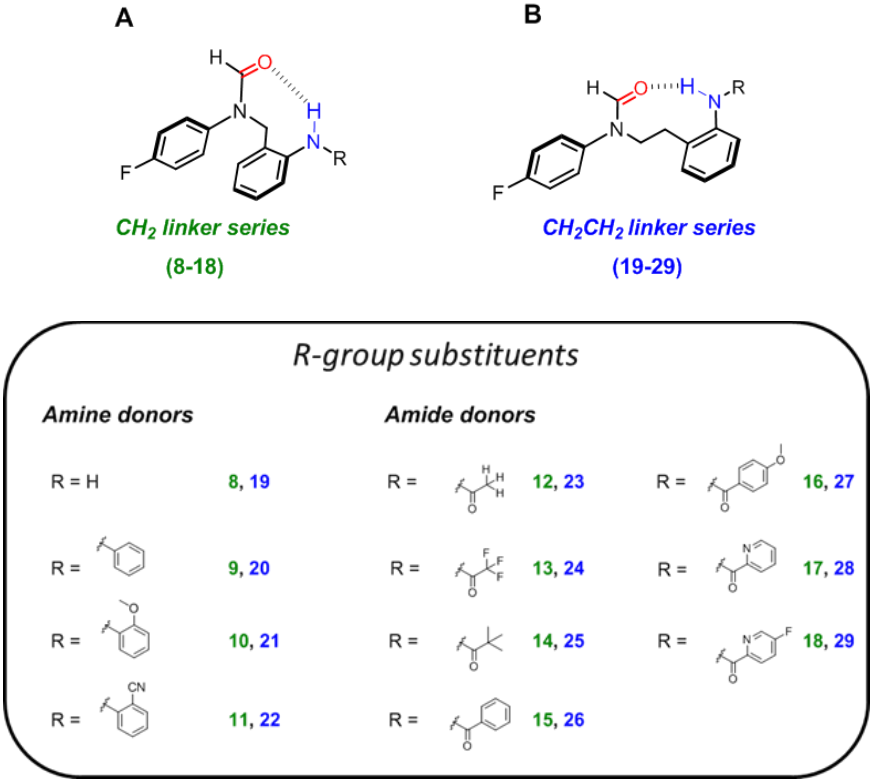

Table 3.3: ΔE, $\Delta\alpha$ and $\Delta\beta$ determined for molecular balances by fitting experimental conformational free energies to the model shown in Figure 3.16.

Compound	ΔE/ kJ mol^{-1}	$\Delta\alpha$	$\Delta\beta$
8	−12.7 ± 2.1	0.4 ± 0.3	1.4 ± 0.6
9	−13.1 ± 2.3	0.6 ± 0.3	1.7 ± 0.8
10	−8.7 ± 0.4	0.2 ± 0.0	1.1 ± 0.2
11	−10.6 ± 0.7	0.5 ± 0.1	0.9 ± 0.3
12	−15.7 ± 1.9	0.7 ± 0.3	2.5 ± 0.5
13	−16.2 ± 1.2	0.7 ± 0.2	2.4 ± 0.3
14	−13.9 ± 2.6	0.6 ± 0.4	1.9 ± 0.7
15	−14.7 ± 2.1	0.6 ± 0.3	2.1 ± 0.6
16	−14.7 ± 2.1	0.6 ± 0.3	2.2 ± 0.6
17	−7.0 ± 0.5	0.2 ± 0.1	0.6 ± 0.2
18	−7.6 ± 0.6	0.3 ± 0.1	0.5 ± 0.2
19	−10.3 ± 0.8	0.5 ± 0.1	1.3 ± 0.3
20	−11.1 ± 1.1	0.5 ± 0.1	1.6 ± 0.5
21	−6.9 ± 0.6	0.2 ± 0.1	0.9 ± 0.3
22	−7.4 ± 0.7	0.3 ± 0.1	0.6 ± 0.3
23	−13.6 ± 2.9	0.6 ± 0.4	2.3 ± 0.8
24	−9.3 ± 1.4	0.3 ± 0.2	1.3 ± 0.4
25	−9.9 ± 1.1	0.5 ± 0.1	1.1 ± 0.5
26	−10.4 ± 0.9	0.6 ± 0.1	1.1 ± 0.4
27	−10.1 ± 1.2	0.6 ± 0.1	1.1 ± 0.5
28	−5.6 ± 0.7	0.2 ± 0.1	0.4 ± 0.3
29	−6.6 ± 0.8	0.2 ± 0.1	0.6 ± 0.3

The ΔE coefficient is a solvent independent term describing the intramolecular interactions of the equilibrium. A strong correlation was found for the methylene linker series (R^2 = 0.95) on plotting the determined ΔE values against the calculated electrostatic surface potential ($ESP_{N\text{-}H}$) along the N-H of simple molecules corresponding to the donors of balances **8-29** (Figure 3.18). This finding confirmed that when the solvent was dissected away, the conformational equilibrium energy was dependent on the H-bond donor ability of the balance. A weaker correlation was found for the ethylene linker molecular balance series (R^2 = 0.75), this was attributed to the influence of the increased conformational flexibility on the intramolecular H-bonds.

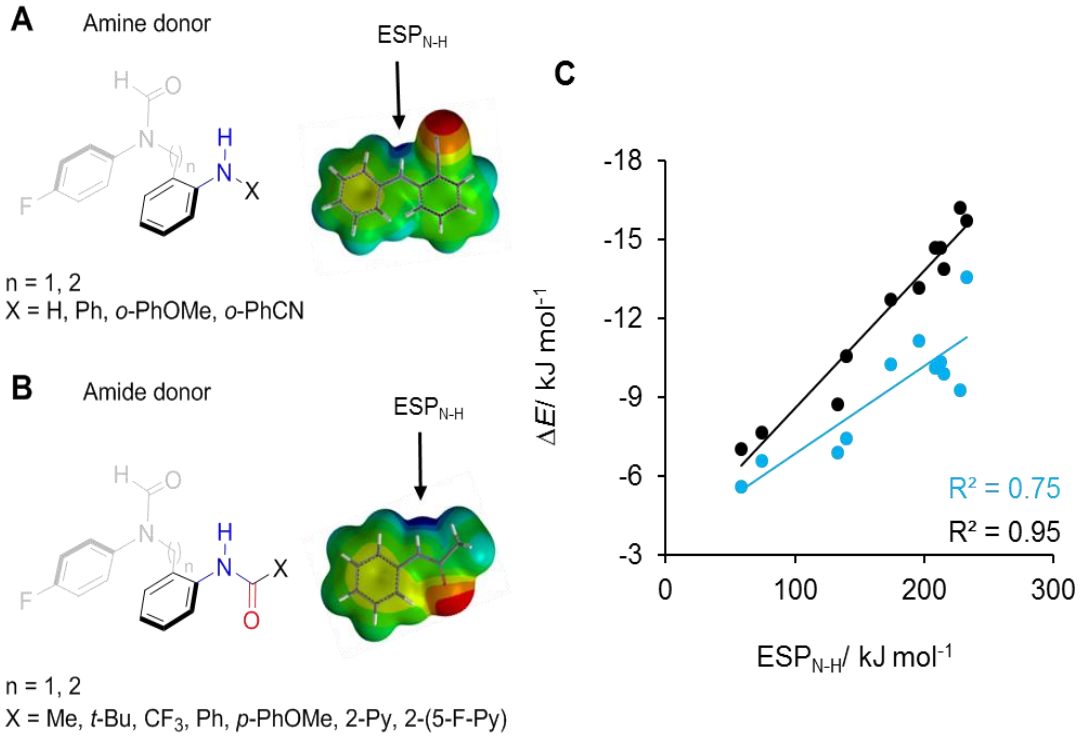

Figure 3.18: A Calculated electrostatic surface potential along the N-H bond of amine donors. **B** Calculated electrostatic surface potential along the N-H bond of amide donors **C** Correlation between the solvent independent ΔE term dissected using the model in Figure 3.16 against the calculated electrostatic surface potential ($ESP_{N\text{-}H}$) along the N-H bond of simple molecules corresponding to the H-bond amine and amide donors. Black data points represent methylene linker series. Blue data points represent ethylene linker series.

The calculated $\Delta\alpha$ and $\Delta\beta$ coefficients derived from Equation 3.4 (Table 3.3) provide insight into solvent effects on the molecular balances and the strength of the

intramolecular H-bonds. The $\Delta\alpha$ term corresponds to the change in H-bond donor ability of the unfolded conformation relative to the folded conformation, while the $\Delta\beta$ value corresponds to the accompanying change in the acceptor constant of the balance. The $\Delta\alpha$ and $\Delta\beta$ values for all molecular balances are positive, since the balance-solvent interactions favoured the unfolded conformer, which were strongest in the unfolded conformation where the H-bond donor and acceptor sites were most exposed to the solvent. It was harder for the solvent to access these sites in the folded conformation in which intramolecular H-bond interactions were formed between the major amine/amide donor and the formyl oxygen sites. Accordingly, the $\Delta\alpha$ and $\Delta\beta$ values were most positive for balances **8**, **9**, **11**, **12**, **13**, **14**, **15**, **16** in the methylene linker series and **19**, **20, 22, 23**, **24**, **25**, **26**, **27** in the ethylene linker series, in which there are no competing additional secondary interactions (Figure 3.19A).

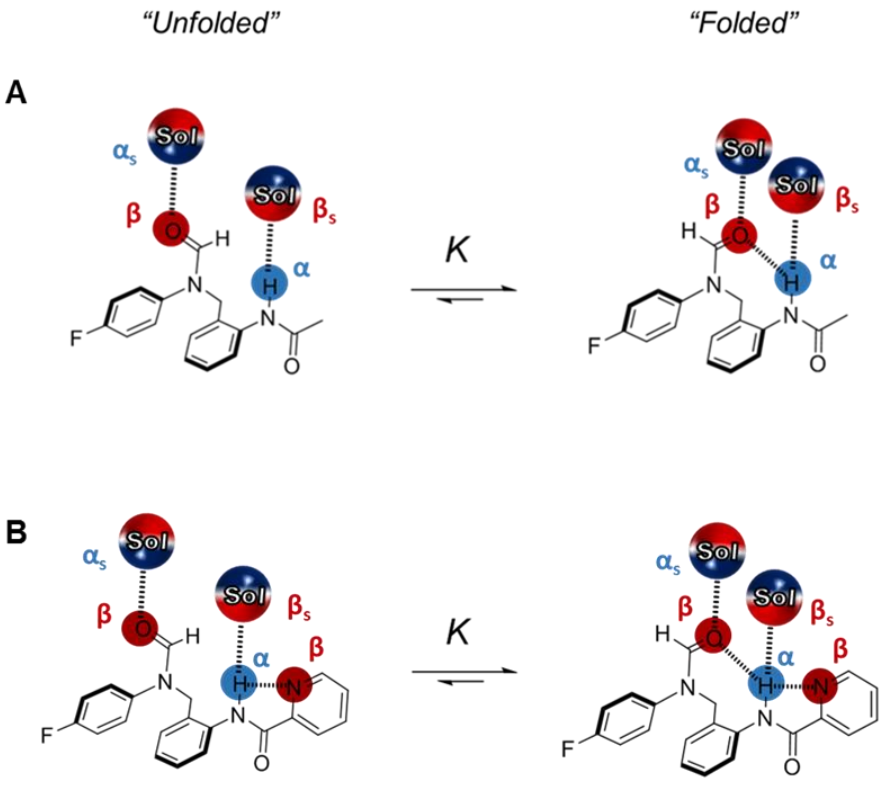

Figure 3.19: Proposed H-bond interactions contributing to the change in solvation of the molecular balances. **A** Solvation on molecular balance **12** in the folded and unfolded states without a competing acceptor group. **B** Solvation on molecular balance **17** in the folded and unfolded states with a competing acceptor group.

In contrast, the $\Delta\alpha$ and $\Delta\beta$ terms were found to be lower for molecular balances **10**, **17** and **18** in the methylene linker series and **21**, **28** and **29** for the ethylene linker series. This was consistent with the presence of additional H-bond acceptors competing with the intramolecular H-bond between the amine/amide donor and the formyl oxygen acceptor (Figure 3.20). Thus, the solvation of the donor and acceptor is similar in both the folded and unfolded conformers for molecular balances **10**, **17**, **18**, **21**, **28** and **29** due to the secondary, competing interactions that are present in both the open and closed conformers (Figure 3.20).

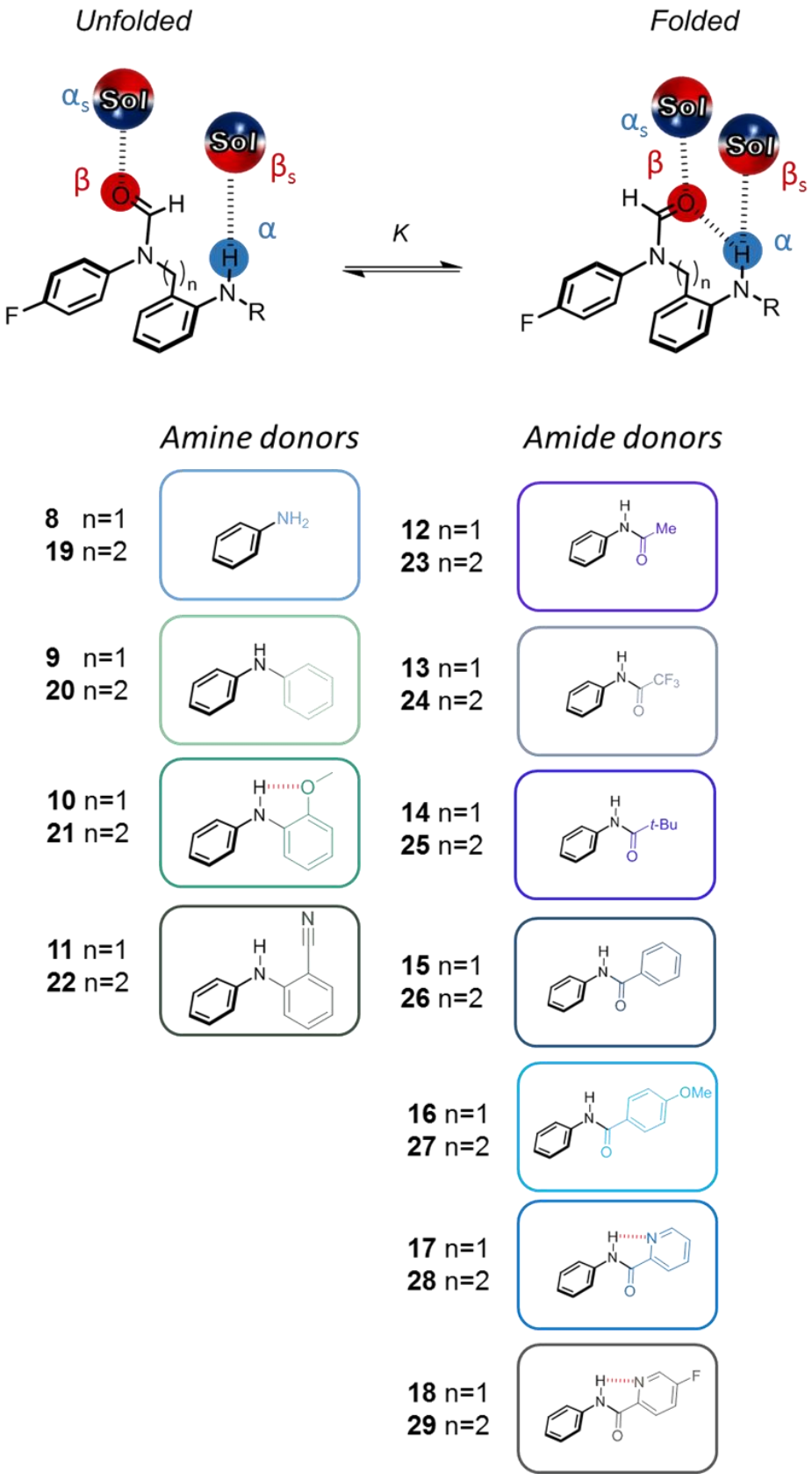

Figure 3.20: Methylene and ethylene molecular torsion balance substituents showing the secondary intramolecular H-bond interactions.

3.6 Determining H-bond energies in aqueous media

The above sections investigated electronic and distance effects on the strength of hydrogen bonds between amide acceptors and amide/aniline hydrogen bond donors in organic solvents. However, biomolecules within cellular environments interact in water solutions containing ions, proteins, lipids and sugars. Water is important in mediating protein-ligand interactions, protein-folding stability as well as catalytic processes. Therefore, carrying out investigations in water is important to understand the fundamental nature of these processes. In this section, experimental energies were determined in 16 different biologically relevant (aqueous) solvents mixtures for water-soluble molecular balances.

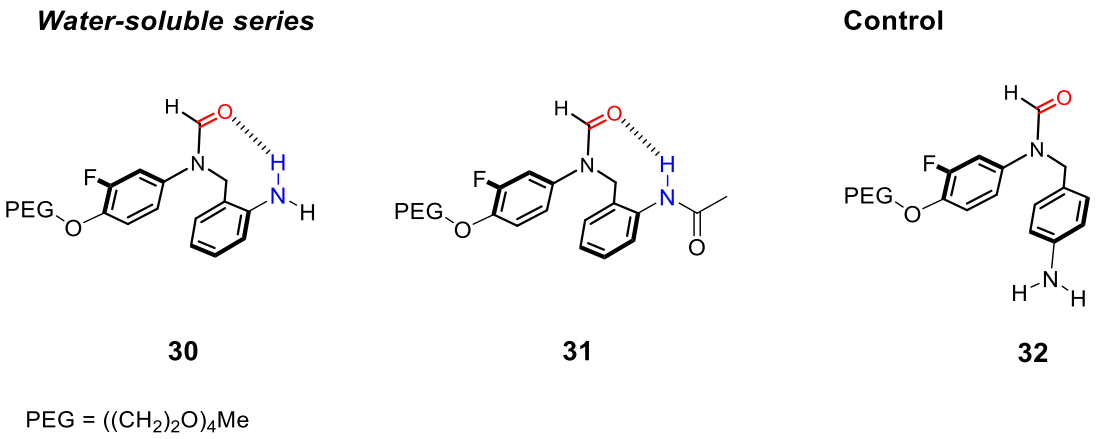

Figure 3.21: PEGylated water soluble molecular balance series (compounds **30-32**).

Synthesis of water-soluble balances

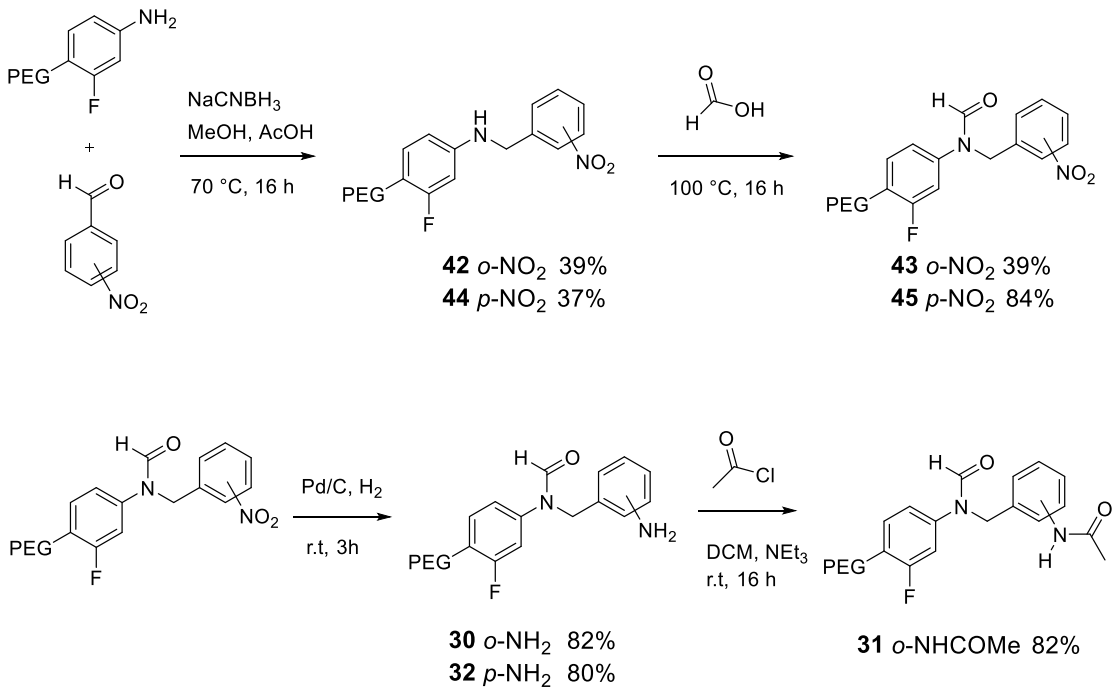

Figure 3.22: Synthesis of molecular balances **30**, **32** and **31**.

The first synthetic step involved a reductive amination reaction between the PEGylated aniline and the appropriately substituted nitro functionalised aldehyde to yield the amine compounds **42** and **44**. Formylation was subsequently performed by refluxing overnight in neat formic acid. The resulting nitro molecular balances **43** and **45** were reduced using palladium on carbon under a hydrogen environment to synthesise molecular balances **30** and **32**. Finally, the *ortho*-substituted aniline molecular balance **30** was then used to synthesise a water-soluble amide molecular balance, **31** (Figure 3.22). The aniline compound was reacted with acetyl chloride using trimethylamine as the base to yield molecular balance **31** in good yield.

^{19}F NMR spectra were obtained for molecular balances **30-32** in organic solvents, D_2O, saline solutions and buffer solutions to investigate the effect of organic and biologically relevant solvents on the conformational Gibbs free energies (Figure 3.23). Molecular balances **30-32** were found to favour the 'folded' conformations in every solvent studied (See Supporting Information B, Figures S3.5-S3.9, for full 2D assignment). The experimental conformational free energies were found to be most negative in organic solvents, and weakest in aqueous solvents, due to strong competing

effects from the water molecules. The *ortho*-substituted molecular balances **30** and **31** had the strongest preference for the folded conformation, due to H-bond formation (analogous to the methylene linker molecular balances described above). Molecular balance **30** was found to have the strongest preference for the folded conformer in every organic and aqueous solution studied relative to the amide **31** H-bond donor.

To estimate the strength of the H-bond energy, the experimental Gibbs free energy ($\Delta G_{control}$) of the *para*-substituted control molecular balance **32** was subtracted from the experimental Gibbs free energies of molecular balances **30** and **31** that formed H-bonds (Equation 3.5).

$$\Delta\Delta G_{\text{H-bond}} = \Delta G_{\text{H-bond}} - \Delta G_{\text{control}} \quad (3.5)$$

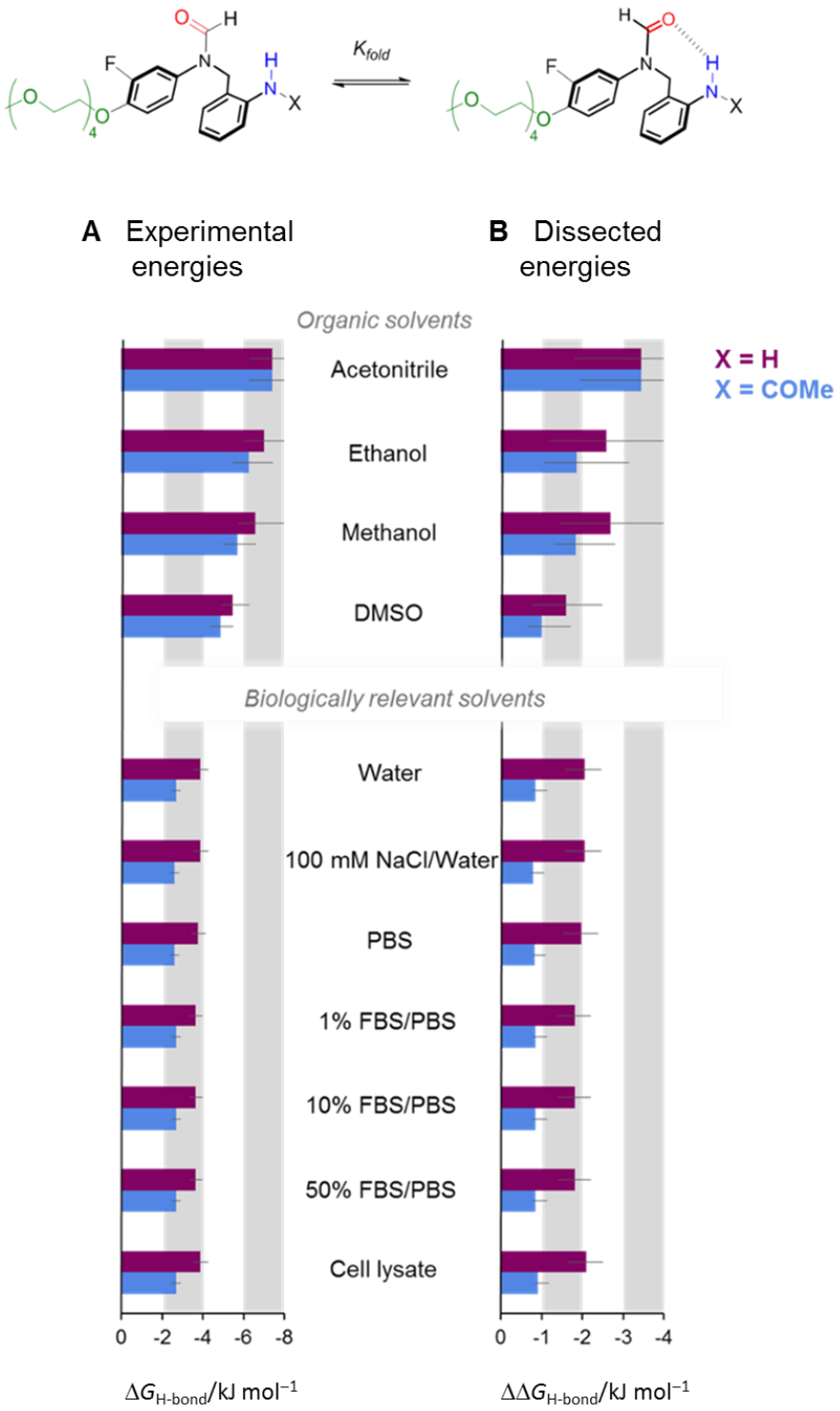

Figure 3.23: Molecular torsion balance equilibrium between the folded and unfolded conformers of the water soluble molecular balances. **A** Bar graph showing the experimental Gibbs free energies measured in solution at 298 K for molecular torsion balances **30** and **31.** **B** Dissected energies estimated using H-bond strength = $\Delta G_{H\text{-}bond} - \Delta G_{control}$. Solvent mixtures are quoted in % v/v. FBS is an abbreviation of fetal bovine serum. PBS is an abbreviation of phosphate-buffered solution. The cell lysate was HeLa cells in 5 mL of deionised water.

The estimated H-bond strengths for the aniline and amide H-bond donor molecular balances are plotted together with the experimental Gibbs free energies in Figure 3.23. It was found that the aniline molecular balance, **30**, had the most favourable H-bond interactions in every solvent. For example, in aqueous solution, the estimated dissected H-bond strength in aqueous solution for aniline donor molecular balance **30** was determined to be –1.8 kJ mol^{-1} whereas the H-bond strength was found to be –0.5 kJ mol^{-1} for amide donor molecular balance **31**. Previous research suggested that amides (α = 2.9, β = 8.3) were stronger H-bond donor and acceptors than anilines (α = 2.1, β = 5.3).[5] It was proposed here that the enhanced stability of the aniline H-bond, in this system, was due to a polarisation effect from the solvent.

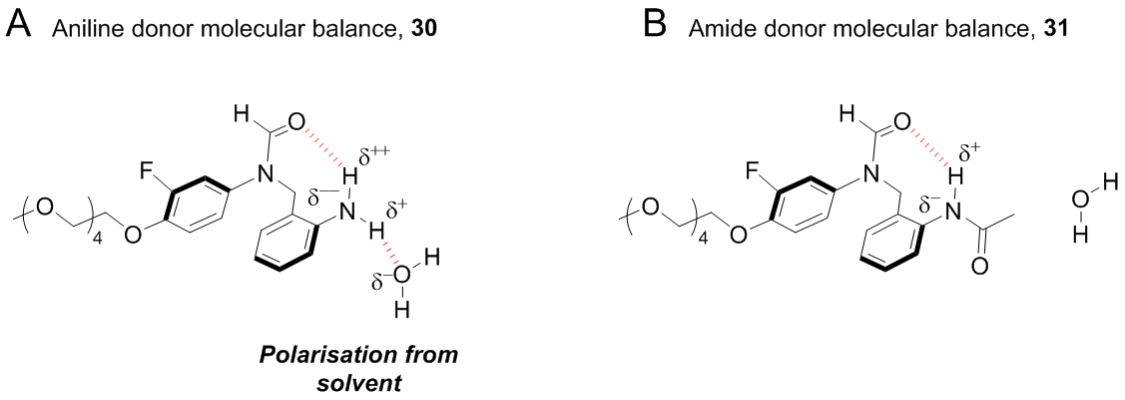

Figure 3.24: A H-bonded folded conformer of aniline donor water soluble molecular balance, **30**, interacting with water. **B** H-bonded folded conformer of amide donor molecular balance, **31,** interacting with water.

The gas phase calculations (DFT/B3LYP/6-311G*) performed on structurally analogous organic soluble molecular balances **8** and **12** (aniline and amide donors respectively) revealed that the *amide* donor molecular balance, **12**, had the strongest H-bond interaction (ΔE_{calc} for amide molecular balance **12** = –33.7 kJ mol^{-1}, and ΔE_{calc} for aniline molecular balance **8** = –25.7 kJ mol^{-1}.) This finding supported the hypothesis proposed above that the additional stability seen for the water soluble *aniline* donor molecular balance, **30**, was due to a solvation effect.

The experimental Gibbs free energies for molecular balances **30** and **31** in the different aqueous solutions were determined to be the same value (Figure 3.23). An energy of –3.9 kJ mol^{-1} was found for molecular balance **30** and –2.7 kJ mol^{-1} for

compound **31**. This was unsurprising considering the ions were in bulk water solutions, however, it did show that ions and proteins did not interfere with the intramolecular H-bonds.

3.7 Conclusion

In summary, H-bonding between anilines and amides has been investigated in competitive solvents using molecular torsion balances. Using control molecular balances, H-bond strengths were dissected out in various organic solvents. The solvent effects were further analysed and understood by applying Hunter's solvation model, where a strong linear correlation was found between a solvent independent term and the electrostatic potential of the H-bond donor of the methylene linker molecular balances. Weaker correlations were found for the ethylene linker molecular balance series, this was attributed to the increased conformational flexibility. The application of this solvation model showed that it was possible to dissect out H-bond energies against a background of strongly competing polar solvents, to correlate against gas-phase physiochemical properties. Before application of the solvation model, the raw experimental data in polar solvents was poorly predicted by computational methods. A water soluble molecular balance series was also synthesised and allowed the determination of H-bond strengths in biologically relevant solvents. These results have implications for the fundamental understanding of H-bonds between biologically relevant amides in molecular recognition, and these experimental results could be used to test theoretical models of solvation.

3.8 References

1. Watson, J. D.; Crick, F. H. C. Molecular Structure of Nucleic Acids: A Structure for Deoxyribose Nucleic Acid. Nature. 1953, 171, 737.

2. Chen, D.; Oezguen, N.; Urvil, P.; Ferguson, C.; Dann, S. M.; Savidge, T. C. Regulation of protein-ligand binding affinity by hydrogen bond pairing. Science Advances. 2016, 2 (3).

3. Abraham, M. H.; Grellier, P. L.; Prior, D. V.; Morris, J. J.; Taylor, P. J. Hydrogen bonding. Part 10. A scale of solute hydrogen-bond basicity using log K values for complexation in tetrachloromethane. Journal of the Chemical Society, Perkin Transactions 2. 1990, (4), 521-529.

4. Abraham, M. H.; Grellier, P. L.; Prior, D. V.; Duce, P. P.; Morris, J. J.; Taylor, P. J. Hydrogen bonding. Part 7. A scale of solute hydrogen-bond acidity based on log K values for complexation in tetrachloromethane. Journal of the Chemical Society, Perkin Transactions 2. 1989, (6), 699-711.

5. Hunter, C. A. Quantifying Intermolecular Interactions: Guidelines for the Molecular Recognition Toolbox. Angewandte Chemie International Edition. 2004, 43 (40), 5310-5324.

6. Cook, J. L.; Hunter, C. A.; Low, C. M. R.; Perez-Velasco, A.; Vinter, J. G. Solvent Effects on Hydrogen Bonding. Angewandte Chemie International Edition. 2007, 46 (20), 3706-3709.

7. Ferrand, Y.; Crump, M. P.; Davis, A. P. A Synthetic Lectin Analog for Biomimetic Disaccharide Recognition. Science. 2007, 318 (5850), 619-622.

8. Destecroix, H.; Renney, C. M.; Mooibroek, T. J.; Carter, T. S.; Stewart, P. F. N.; Crump, M. P.; Davis, A. P. Affinity Enhancement by Dendritic Side Chains in Synthetic Carbohydrate Receptors. Angewandte Chemie International Edition. 2015, 54 (7), 2057-2061.

9. Ke, C.; Destecroix, H.; Crump, M. P.; Davis, A. P. A simple and accessible synthetic lectin for glucose recognition and sensing. Nat Chem. 2012, 4 (9), 718-723.

10. Jang, Y.; Natarajan, R.; Ko, Y. H.; Kim, K. Cucurbit[7]uril: A High-Affinity Host for Encapsulation of Amino Saccharides and Supramolecular Stabilization of

Their α-Anomers in Water. Angewandte Chemie International Edition. 2014, 53 (4), 1003-1007.

11. Hernandez-Alonso, D.; Zankowski, S.; Adriaenssens, L.; Ballester, P. Water-soluble aryl-extended calix[4]pyrroles with unperturbed aromatic cavities: synthesis and binding studies. Organic & Biomolecular Chemistry. 2015, 13 (4), 1022-1029.

12. Mati, I. K.; Cockroft, S. L. Molecular balances for quantifying non-covalent interactions. Chemical Society Reviews. 2010, 39 (11), 4195-4205.

13. Lypson, A. B.; Wilcox, C. S. Synthesis and NMR Analysis of a Conformationally Controlled β-Turn Mimetic Torsion Balance. The Journal of Organic Chemistry. 2017, 82 (2), 898-909.

14. Luccarelli, J.; Jones, I. M.; Thompson, S.; Hamilton, A. D. Unpicking the determinants of amide NH···O=C hydrogen bond strength with diphenylacetylene molecular balances. Organic & Biomolecular Chemistry. 2017, (15), 9156-9163

15. Mati, I. K.; Adam, C.; Cockroft, S. L. Seeing through solvent effects using molecular balances. Chemical Science. 2013, 4 (10), 3965-3972.

16. Dominelli-Whiteley, N.; Brown, J. J.; Muchowska, K. B.; Mati, I. K.; Adam, C.; Hubbard, T. A.; Elmi, A.; Brown, A. J.; Bell, I. A. W.; Cockroft, S. L. Strong Short-Range Cooperativity in Hydrogen-Bond Chains. Angewandte Chemie International Edition. 2017, 56 (26), 7658-7662.

Chapter 4

Solvent Effects on Cooperativity in H-Bond Chains

Abstract

The energetics of cooperativity in hydrogen bonding are complicated by solvent effects. Here, we have used a series of synthetic molecular balances to investigate H-bond cooperativity in 19 different solvent and solvent mixtures. The trend in the experimental folding energies on adding a second and third H-bond donor to form chains revealed three different classes of cooperative behaviour. A positive cooperative effect was found in solvents with weak H-bond acceptor properties, mirroring gas phase computations. In solvents with stronger H-bond acceptor properties, negative cooperativity was observed. Protic solvents showed an intermediate behaviour in which a catechol molecular balance formed the strongest intermolecular interactions. These results have implications for the fundamental understanding of H-bond chain cooperativity in molecular recognition.

Full computational and supplementary details are given in Supporting Information C, pages 252-297

Contributions: The experimental and computational results presented in this chapter were obtained by NYM. Molecular balances **1H**, **2H** and **3H** were synthesised previously[1] but experimental free energies were determined by Nicole Yvette Meredith (NYM).

4.1 Introduction

Hydrogen bonding is a fundamental interaction in biology and chemistry. It is responsible for the unique properties of water, and it has key roles in understanding molecular recognition and supramolecular self-assembly. Hydrogen bonds exhibit non-additive character, where two hydrogen bonds may either strengthen or weaken each other. These two phenomena are commonly referred to as positive cooperativity and negative, or anti-cooperativity, respectively. Many theoretical and experimental attempts have been made to study H-bond cooperativity and anti-cooperativity in water clusters.[2-3] H-bond cooperativity has been shown to be important in catalysis[4] and it has also been studied in a wide range of supramolecular[5-6] and biomolecular systems.[7,8] H-bond interactions are typically thought to be primarily electrostatic in nature, however, the role of quantum mechanical phenomena such as covalency, charge transfer and electron resonance have also been investigated in H-bond formation.[9,10] Studies have extended into the origin of cooperativity in H-bonding, where research has suggested cooperativity arises from mutual polarisation of groups,[11] charge flow through π bonds, or from many body interactions.[12] In the solution phase, the energetics of H-bond cooperativity are complicated by solvent effects, particularly in polar solvents that strongly compete for the intramolecular H-bonds.

Solvent effects on H-bonding were studied by Hunter as shown by the desolvation equilibrium (Figure 4.1).[13-14-15] The H-bond interaction between solute molecules is in direct competition with solute-solvent interactions. If the solute-solute interactions are favoured, the equilibrium lies to the right. If the solute-solvent interactions are favoured the equilibrium lies to the left. Hunter proposed that H-bonding energies in solution could be predicted using Equation 4.1 where α and β are the H-bond coefficients of the H-bond donor and acceptor solutes, and α_S and β_S are the H-bond donor and acceptor coefficients of the solvent which relate to the relative H-bond donor and acceptor abilities defined previously by Hunter.[16-17-18]

$$\Delta G_{\text{H-bond}} = -(\alpha - \alpha_s)(\beta - \beta_s) + 6 \text{ kJ mol}^{-1} \quad (4.1)$$

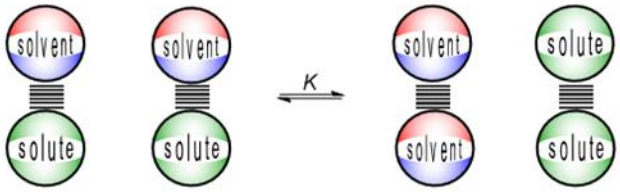

Figure 4.1: H-bonding equilibrium in solution.

Cooperativity in H-bond chains

Dannenberg and coworkers studied cooperativity in linear chains computationally;[8,19,20] Hartree-Fock (HF), density functional theory (DFT) and second order Møller-Plesset perturbation theory (MP2) calculations were performed to reveal a strong cooperative effect in formamide chains, with lower cooperative effects found for urea chains. The large cooperative effect in formamide chains was rationalised by considering pairwise electrostatic interactions, non-pairwise short-range polarisation and resonance assisted hydrogen bonding. For the two latter electronic effects, the strength of the hydrogen bonds increases as the electron density is redistributed along the chain. It was found that the contribution of these non-pairwise electronic interactions made up 75% of the total hydrogen-bond cooperativity. Similarly, Baker performed DFT calculations to study cooperativity of hydrogen-bond interactions in model systems for α helix formation, it was found that non-pairwise electronic effects accounted for half of the total cooperativity of these model systems.[21] Pidko and Greef carried out DFT calculations on H-bonded supramolecular polymers and showed that the cooperative growth of the polymers was caused by electrostatic interactions and non-additive effects brought about by redistribution of the electron density with aggregate length.[22] More recently, Ireta *et al* investigated cooperativity in H-bonded hydrogen cyanide, 4-pyridone and formamide linear chains. DFT calculations were performed to assess cooperativity in infinitely long H-bonded chains, and compared against the strengthening of the dipole-dipole interaction upon the formation of an infinite chain of effective point dipoles. The magnitude of H-bond cooperativity could be estimated by a pairwise addition of effective point dipoles, and was therefore concluded to be primarily electrostatic in origin.[23]

Karplus *et al* used Hartree-Fock calculations at the 6-31G and 6-31G* levels of theory to investigate solvent effects on H-bond cooperativity between amides.[24] The effects of trifluoroethanol, ethylene glycol, ethanol and water were investigated. It was found that addition of an H-bond donor solvent substantially increased the strength of interaction between the amides due to induced polarisation of the molecule, with ethylene glycol and trifluoroethanol having larger stabilising effects than water.

Cockroft[1] studied H-bonding cooperativity in H-bond chains experimentally using *N*,*N*-di-arylformamide molecular balances. Phenol, catechol and pyrogallol molecular balances were synthesised and used to study cooperative H-bonding (Figure 4.2).

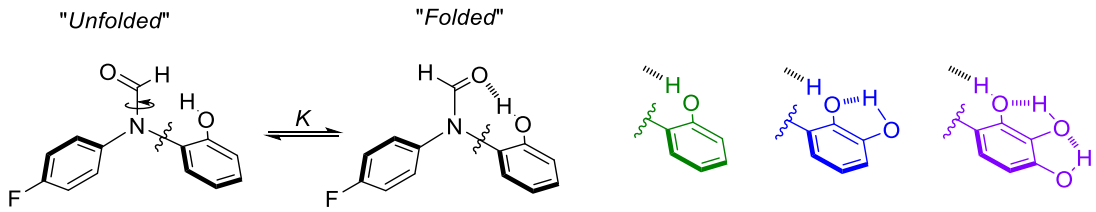

Figure 4.2: Molecular balances synthesised to study cooperative H-bonding.

The position of the conformational equilibrium in these phenol balances enabled the measurement of the energy of the H-bond at the end of a linear chain of one, two or three H-bonds. The phenol balance was found to have a strong preference for the folded conformer in $CDCl_3$, ΔG = –4.2 kJ mol^{-1}. The strength of the H-bond approximately doubled in magnitude for the catechol molecular balance, ΔG = –8.1 kJ mol^{-1}. However, on addition of a third H-bond to the system, the strength of the H-bond slightly decreased. These trends persisted in solvent mixtures of $CDCl_3$ with small amounts of CD_3CN. Experimental controls and computations confirmed that the observed binary energetic behaviour depended entirely on whether a chain of (two or more) H-bonds was present, and ruled out significant through-bond substituent effects.

4.2 Preliminary findings and new balance design

Previously, we reported the synthesis and study of molecular balances that directly measured the effect of H-bond chain length on the strength of H-bonding interactions in $CDCl_3$ solution. It was found that adding a second H-bond donor to a

form a chain doubled the strength of the terminal H bond but that further extension of the chain had little effect. These studies were limited to non-polar solvents chloroform and chloroform/acetonitrile solvent mixtures. In the present work, solvent effects on these molecular balances were expanded to include a wider range of solvents (Figure 4.3). Conformational energies measured in dichloromethane showed a similar trend to that reported previously in chloroform and chloroform/acetonitrile mixtures. However, as more polar solvents were investigated, this system proved not to be suitable for examining H-bond cooperativity due to the very small conformational free energies observed. All of the experimental energies determined in various polar solvents can be found in Supporting Information C.

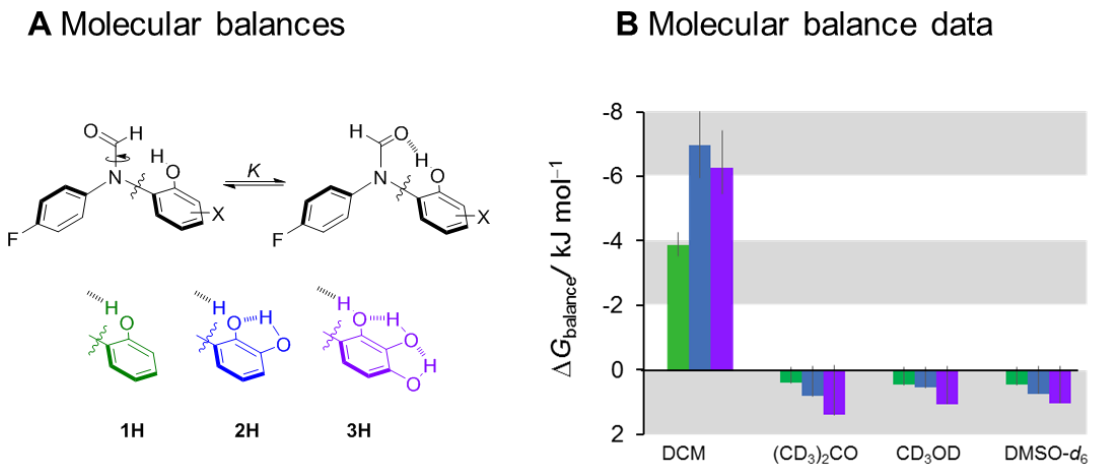

Figure 4.3: A Molecular balances used in the present investigation. **B** Experimental energies determined for molecular balances **1H**, **2H** and **3H** in DCM, acetone, methanol and DMSO.

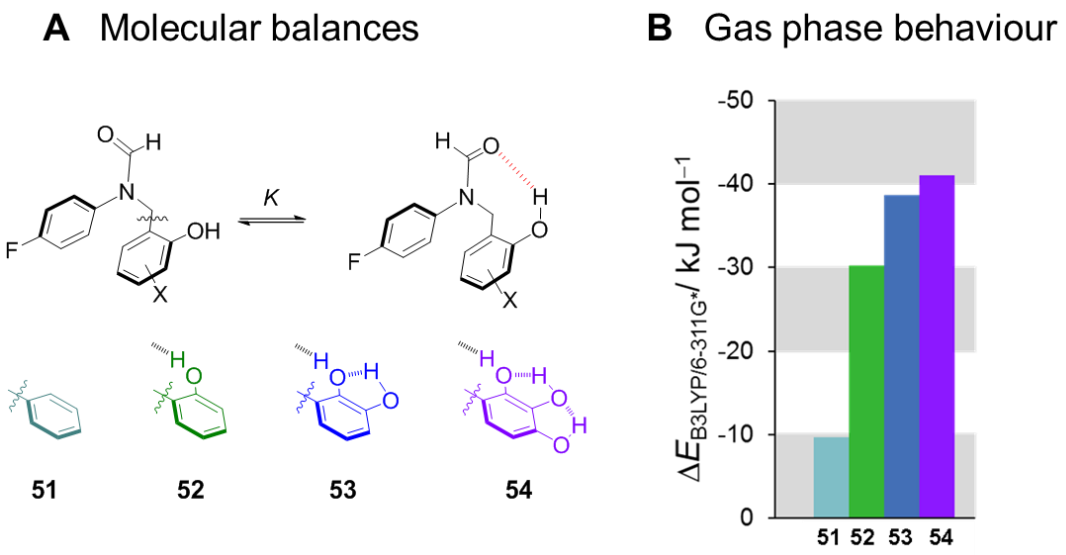

Figure 4.4: A Synthetic molecular balances **51**, **52**, **53**, **54** employed in the front investigation **B** Calculated conformational energies determined using DFT/B3LYP/6-311G*.

Due to the small conformational energies found in polar solvents using the molecular balances shown in Figure 4.3, an alternative molecular torsion balance series was proposed to examine cooperative effects in polar solvents (Figure 4.4). This new series of H-bonding formamide molecular balances were based on the design introduced in Chapter 3 that incorporated a methylene linker group. Conformer distribution searches were performed on molecular balance designs **51-54** at the B3LYP/DFT/6-311G* level of theory to determine the energetic minima for the folded and unfolded conformations of molecular balances **51-54**. The optimised structures of the folded conformations were shown to form intramolecular H-bonds for balances **51**, **52** and **53** (Supporting Information C, Figure S4.17). The energies of the optimised structures of the folded and unfolded conformers were then used to calculate the conformational equilibrium energies for molecular balances **51-54** (Equation 4.2).

$$\Delta E_{calc} = E_{\text{folded conformer}} - E_{\text{unfolded conformer}} \quad (4.2)$$

The methylene linker group increased the preference for the H-bond containing conformer, which made the system suitable for the examination of H-bond strengths in highly competitive polar solvents. The trend in the calculated conformational free energies were shown to exhibit a positive cooperative effect as the length of the H-bond was extended in the absence of any solvent (Figure 4.4). This pattern was similar

to the short-range positive cooperativity found both in the gas-phase calculations and in chloroform and chloroform/acetonitrile solvent mixtures using molecular balances **1H**, **2H**, **3H**.[1]

4.3 Synthesis of molecular torsion balances

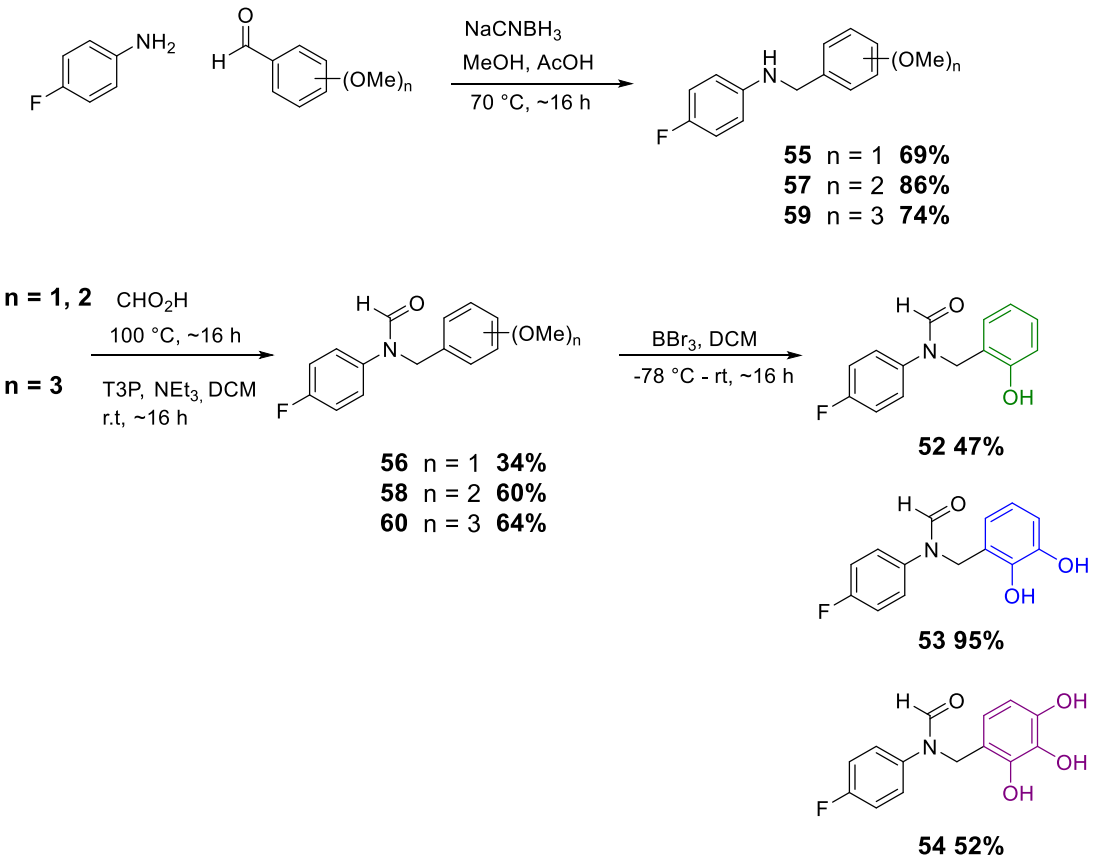

Figure 4.5: Generalised scheme showing synthesis of phenol molecular torsion balances **52**, **53** and **54**. Full details are provided in Supporting Information C.

The first step involved a reductive amination reaction between 4-fluoroaniline and the appropriately substituted methyl ether aldehyde to yield the amine products in good yield. The amine products were then formylated by refluxing overnight in neat formic acid. Finally, the methoxy products were deprotected using a solution of boron tribromide in DCM to yield the hydroxy molecular balances **52**, **53** and **54**. The initial

formylation of amine **60** where n = 3 using neat formic acid, resulted in decomposition. Therefore, gentler conditions were used where the amine was coupled with formic acid at room temperature using trimethylamine as the base and propylphosphonic anhydride solution as an activating agent to yield the product in good yield. A control molecular balance **51** that lacked the ability to form intramolecular H-bonds was synthesised in an 81% yield via the one step reaction shown below (Figure 4.6).

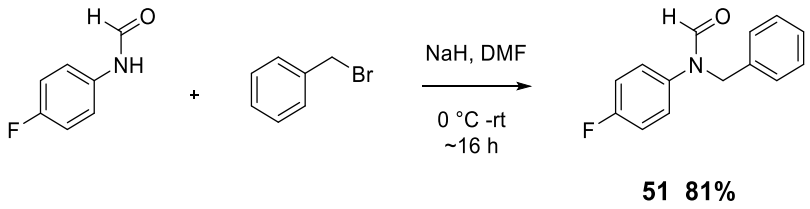

Figure 4.6: Synthesis of control molecular balance **51**. Full details are provided in Supporting Information C.

4.4 Experimental analysis

After the synthesis of molecular torsion balances, conformational free energies were determined in 19 different solvent and solvent mixtures. Experimental measurements were shown to be independent of concentration in the range 1–4 mM, discounting the influence of any intermolecular H-bonding (Supporting Information C, Table S4.2). Therefore, all energies were determined at a low concentration of 3.5 mM using ^{19}F NMR spectroscopy. Molecular balances, **51**, **52, 53** and **54,** adopted distinct folded and unfolded conformations due to restricted rotation about the C-N bond. These two distinct conformations appeared as two separate peaks on the ^{19}F NMR spectra as the restricted rotation was slow enough on the NMR timescale. In the folded conformer, an H-bond was formed between the oxygen in the formyl group and the hydrogen in the phenol group. In the unfolded state, the C=O···HO and HO···HO bonds were broken and the donor and acceptor groups were exposed to the solvent. Therefore, the formation of an intramolecular H-bond was in direct competition with H-bond interactions with the solvent. Equilibrium constants, K_{fold}, were determined by taking the integral of each peak, and the experimental conformational energies calculated using $\Delta G_{H\text{-}bond} = -RT\ln K_{fold}$. The conformer assignment of the two peaks

was performed using 2D spectroscopy (see Supporting Information C). The H-bond in balances **52-54** in chloroform (α = 2.2 and β = 0.9) and dichloromethane (α = 1.9, β = 1.1) were found to be so strong that only the H-bond folded state was observed in the ^{19}F spectrum (characterised using 2D spectroscopy). This was different to the previously synthesised molecular balances **1H**, **2H** and **3H** where the experimental energies were determined to be –4.3 kJ mol^{-1} for the phenol molecular balance, **1H**, –8.1 kJ mol^{-1} for the catechol molecular balance, **2H**, and –7.3 kJ mol^{-1} for the pyrogallol molecular balance **3H**. The methylene linker molecular balances **52-54** were asymmetrical, therefore the added stability of the balances towards the folded conformer was due to both the H-bond strength and an inherent bias towards the folded state. To account for this bias, a control molecular balance, **51**, was synthesized (Figure 4.6) that lacked the ability to form an intramolecular H-bond and experimental energies were then determined in the same 19 solvent and solvent mixtures. The estimated H-bond energy strengths were then determined using Equation 4.3.

$$\text{H-bond strength } (\Delta\Delta G_{\text{H-bond}}) = \Delta G_{\text{H-bond}} - \Delta G_{\text{control}} \quad (4.3)$$

The trend in the folding energies of molecular balances **52**, **53** and **54** in the other solvents studied revealed three different types of behaviour (Figure 4.8A). In the aprotic solvents ethyl acetate, $CDCN_3$, THF and $(CD_3)_2CO$, the experimental energies became more favourable as the number of OH groups in the chain increased. This indicated a positive cooperative effect arising from the formation of a linear intramolecular H-bond network between the OH groups. This positive cooperative pattern was consistent with the trend of experimental Gibbs free energies measured for molecular balances **1H**, **2H** and **3H** in chloroform and chloroform/acetonitrile solvent mixtures.[1] This positive cooperative effect was also observed in the gas phase for the molecular balances **1H, 2H, 3H**.[1] In addition to this, the same pattern was observed in the gas phase calculations for molecular balances **52**, **53** and **54** (Figure 4.4). It was important to note that the experimental free energies were a lot lower than the gas phase calculations due to competing solvent effects.

The H-bond energies estimated using Equation 4.3 in aprotic solvents ethyl acetate, $CDCN_3$, THF and $(CD_3)_2CO$ revealed the H-bond strengths (Figure 4.7B). The

H-bonds were found to be strongest in acetonitrile due to molecular balances **52-54** all having negative $\Delta\Delta G$ values. For ethyl acetate and acetone, the intramolecular H-bond interactions in molecular balance **52** were found to be unfavourable as the solvent outcompeted the energetics of any intermolecular H-bond cooperativity. On addition of a second OH group, the energies became favourable, resulting in stronger H-bond interactions. Molecular balance, **54**, which contained a chain of three H-bonds gave the strongest terminal H-bond energies in aprotic solvents ethyl acetate, $CDCN_3$, THF and $(CD_3)_2CO$. The H-bonds in molecular balances **52**, **53** and **54** in THF were all found to be unfavourable.

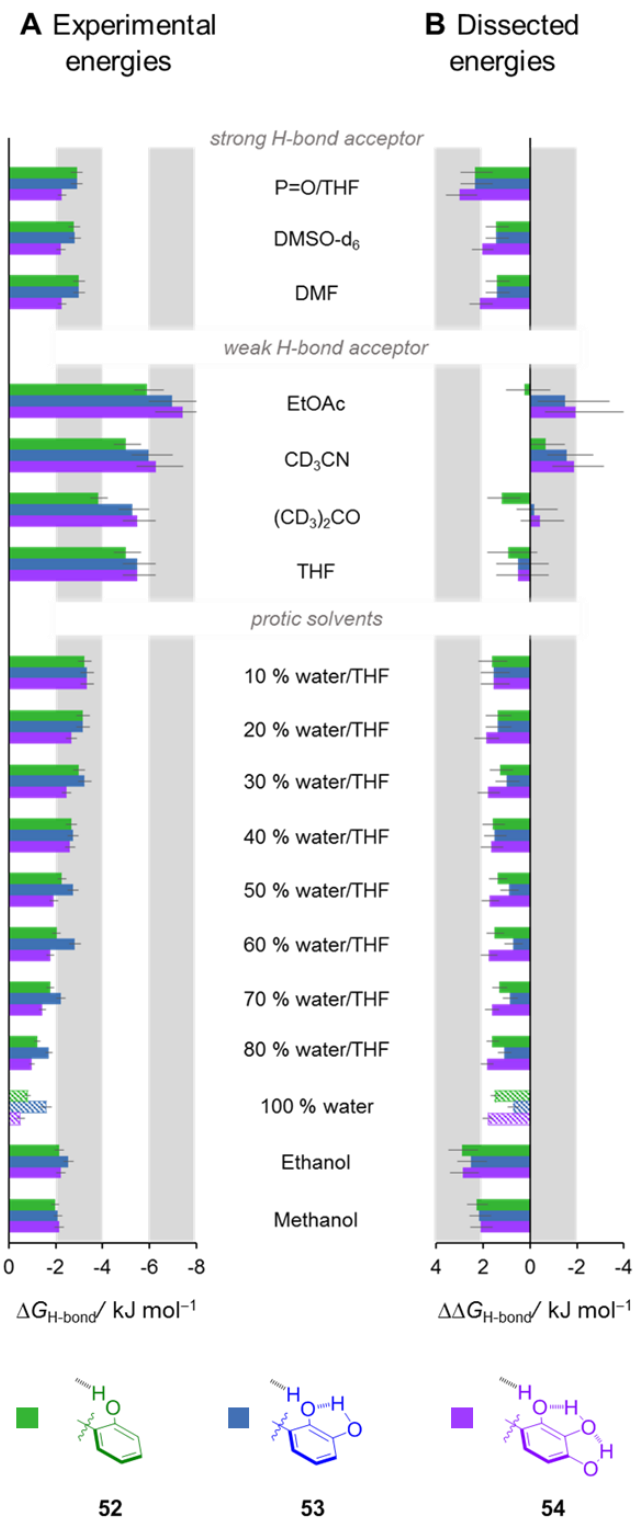

Figure 4.7: A Bar graph showing the experimental Gibbs free energies ($\Delta G_{\text{H-bond}}$) measured in solution at 298 K for molecular torsion balances **52-54**. **B** Dissected energies estimated using H-bond strength ($\Delta\Delta G_{\text{H-bond}}$) = $\Delta G_{\text{H-bond}}$– $\Delta G_{\text{Control}}$. Deuterated methanol was used. Solvent mixtures are quoted in % v/v. Dashed coloured bars represent extrapolated numbers. See Supporting Information C for full details.

In aprotic solvents DMSO-d_6, DMF and in a 0.92 M solution of tributylphosphine oxide in THF, a different trend was observed. The experimental energies were found to be similar for the phenol and catechol molecular balances, however, on addition of a third OH group the energies were found to decrease (Figure 4.7A). This was indicative of a negative cooperative effect. The H-bond energies estimated using Equation 4.3 for molecular balances **52-54** in these solvents revealed unfavourable H-bond interactions.

These two opposing classes of cooperativity in different solvent classes can be explained by considering the β values of the formamide group and the β_s values of the solvent molecules. The β values describe the H-bond acceptor properties of the formyl group on the molecular balance and the β_s values describe the H-bond acceptor properties of the solvent. The β_s and β values can either be derived from experiment or computationally, from calculated electrostatic surface potentials (ESPs).[13]

Solvents ethyl acetate ($\beta = 5.3$), $CDCN_3$ ($\beta = 5.1$), THF ($\beta = 5.9$) and $(CD_3)_2CO$ ($\beta = 5.8$) are all good H-bond acceptors with similar β values. The β value of the oxygen on the formamide on the balance ($\beta \approx 7$) is a stronger acceptor than the aforementioned solvents, and therefore the intramolecular H-bond outcompetes the solvent to form an intramolecular hydrogen bond to phenol allowing a positive cooperative effect to be manifested as the length of the H-bond chain increases. However, a different trend was observed for DMSO-d_6 ($\beta = 8.7$), DMF ($\beta = 7.7$) and phosphine oxide ($\beta = 9.9$) as they are all strong H-bond acceptors with higher β values than the formamide oxygen. Thus, these solvents outcompete the formamide group to solvate the phenol hydroxyl groups, which resulted in decreased experimental energies and a negative cooperative effect as the number of hydroxyl groups increased.

Experimental energies were also determined in more biologically relevant protic solvents: ethanol, methanol and THF/water mixtures (Figure 4.7A). As the concentration of water in THF increased, the experimental energies decreased, which was consistent with increased disruption of the H-bond networks. The catechol molecular balance **53** was shown to have the strongest H-bond interactions in the majority of solvent mixtures measured. The H-bond energies estimated using equation 4.3 revealed that the unfolded conformer was favoured and that the intramolecular H-

bonds were switched off in these competitive, protic solvents. The observation that catechol had the strongest interactions in water solutions relative to analogous phenol and pyrogallol compounds was consistent with the finding that catechols (not pyrogallols) are predominately found in nature in proteins with adhesive properties.[25,26]

The percentage of water in THF was plotted against the experimentally determined free energies for molecular balances **52-54** (see Supporting Information C, Figure 4.2) and used to extrapolate the experimental free energies in 100% water (Figure 4.7A). The extrapolated Gibbs free energy for molecular balance **52** was determined to be –0.8 kJ mol^{-1}, for molecular balance **53** the energy was calculated at –1.6 kJ mol^{-1} and for molecular balance **54** it was found to be –0.5 kJ mol^{-1}. The control molecular balance, **51**, had a calculated Gibbs free energy of –2.3 kJ mol^{-1}.

4.5 Dissection of thermodynamic parameters: van't Hoff analyses

Van't Hoff analyses was carried out on molecular balances **51-54** in DMSO, EtOAc, MeCN and 80% (v/v) water/THF mixtures to dissect out the entropic and enthalpic contributions to the experimental conformational free energies (See Supporting Information C, Tables S4.10-S4.14 and Figures S4.3-4.17). These solvents were chosen as they each represented a different pattern of the observed behaviour. These solvents also had high enough boiling points to enable Van't Hoff analysis to be carried out. As this series of molecular balances had more conformational flexibility to those investigated previously, it was important to determine whether any entropic effects were responsible for the observed differences in the cooperativity patterns in different solvents.

The results of the dissection are shown below in Tables 4.1-4.3 and in Figure 4.8A-C for solvents DMSO, CD_3CN and EtOAc. Unfortunately, the ^{19}F NMR peaks coalesced for balance 54 in the 80% water/THF solvent mixture. This meant that integrals were not measured at 320-330 K. Therefore, experimental Gibbs free energies were not measured at these temperatures and consequentially enthalpic and

entropic terms were not reported. See Supporting Information C, Table S4.13-S4.14, for the data that was measured for this solvent system.

Table 4.1: Dissection of ΔH and $T\Delta S$ at 300 K in DMSO-d_6.

Balance	$-T\Delta S$/ kJ mol^{-1}	ΔH/ kJ mol^{-1}	ΔG/ kJ mol^{-1}
51	−1.3	−3.0	−4.3
52	−0.9	−1.9	−2.8
53	−1.1	−1.7	−2.8
54	−1.4	−0.8	−2.2

Table 4.2: Dissection of ΔH and $T\Delta S$ at 300 K in CD_3CN.

Balance	$-T\Delta S$/ kJ mol^{-1}	ΔH/ kJ mol^{-1}	ΔG/ kJ mol^{-1}
51	+0.2	−4.7	−4.4
52	−6.3	+1.4	−4.9
53	−4.4	−1.6	−6.1
54	−4.1	−2.3	−6.4

Table 4.3: Dissection of ΔH and $T\Delta S$ at 300 K in EtOAc.

Balance	$-T\Delta S$/ kJ mol^{-1}	ΔH/ kJ mol^{-1}	ΔG/ kJ mol^{-1}
51	−3.7	−1.9	−5.6
52	−5.2	−0.9	−6.1
53	−5.8	−1.4	−7.2
54	−2.6	−5.0	−7.6

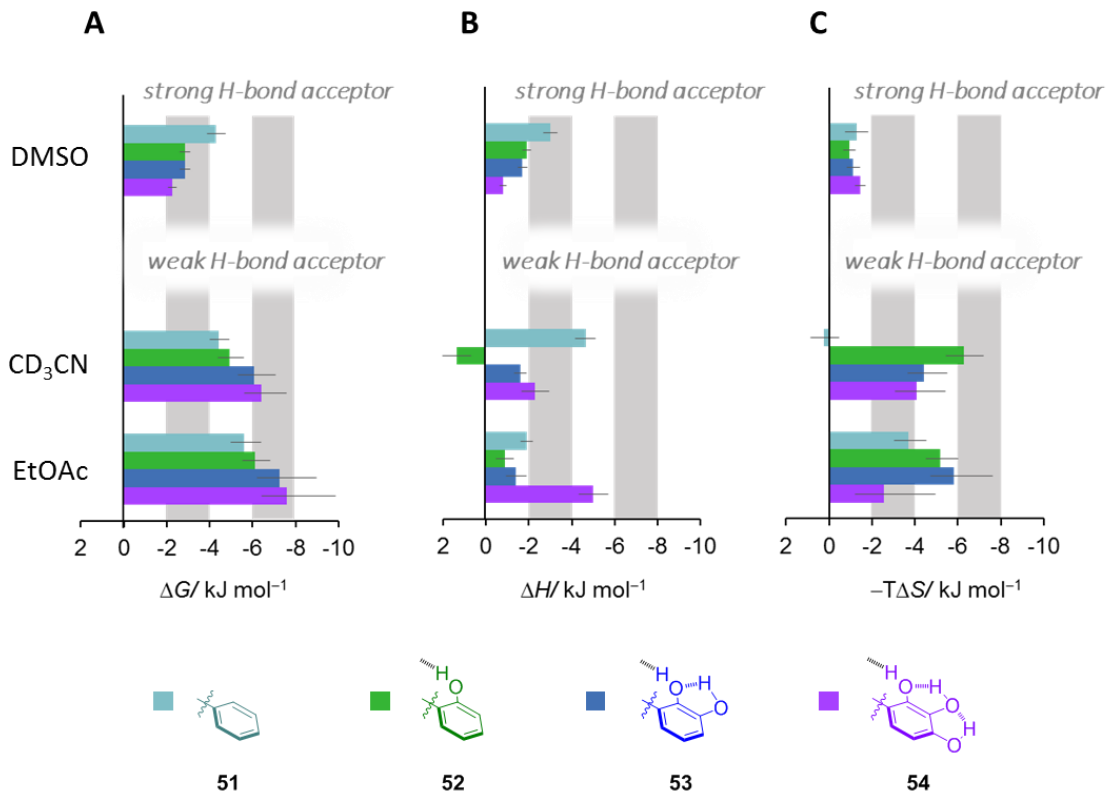

Figure 4.8: A The experimental Gibbs free energies of molecular balances **52**, **53** and **54** in different solvents measured at 300 K. **B** Enthalpic contributions to the experimental conformational energies. **C** Entropic contributions to the experimental conformational free energies. See Supporting Information C for full details of error analysis.

On analysis of the above results, it was concluded that the conformational free energies of molecular balances **52-54** were enthalpically driven in DMSO, CD_3CN and EtOAc. In DMSO, on increasing the number of phenol groups, the experimental free energies decreased, in line with the enthalpic contributions to the conformational free energies, but opposed by the entropic contributions due to enthalpy-entropy compensation.[27] However, in CD_3CN and EtOAc, the Gibbs free energies increased with increasing number of phenol groups. Again, this trend was mirrored in the dissected enthalpic terms, and opposed by entropy contributions. These findings showed that the behaviour of these systems were enthalpically driven, which might be expected due to the intramolecular nature of the H-bond formed in the molecular balances.

4.6 Implicit modelling of solvent effects

The calculated conformational energies were determined in DMSO and methanol employing the polarizable continuum model (PCM) implicit solvation model. However, the computational results did not predict the experimental behaviour (Figure 4.9). Positive cooperative effects were still predicted in DMSO and methanol, contradicting what was observed in the experiments. These findings highlighted the inability of the PCM implicit solvation model to even predict a general pattern of behaviour in a very simple intramolecular system. Improved computational approaches are required to properly model solvent effects, particularly for polar and biologically relevant aqueous solutions.

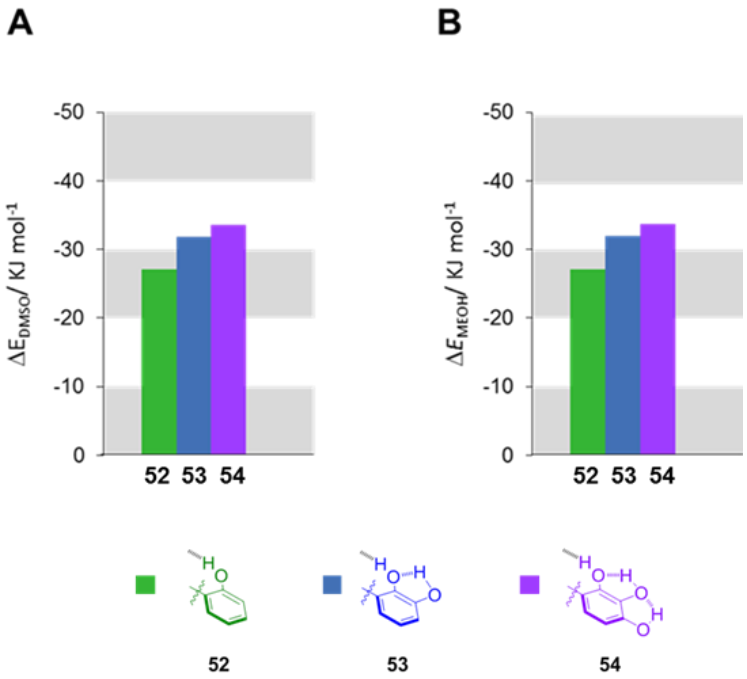

Figure 4.9: Graphs of calculated conformational energies employing the PCM solvation model using DFT/B3LYP/6-311G*. **A** calculated in DMSO **B** calculated in MeOH.

4.7 Conclusion

In summary, we have designed and synthesised a series of molecular balances to investigate solvent effects on cooperativity in H-bond chains. Experimental energies were determined in a range of different solvents with varying properties and three different types of behaviour were found. Solvents with weak β values were shown to exhibit positive cooperativity on increasing the length of the H-bond chain. In contrast solvents with high H-bond acceptor β abilities strongly disrupted the H-bond chains, resulting in negative cooperativity as the H-bond chain length was increased. Folding energies obtained in protic solvent and solvent mixtures showed that the catechol-containing molecular balance, **53**, was able to form the most favorable terminal H-bond interactions, perhaps providing an explanation of why such groups have evolved as the active components in the biological adhesives that mussels secrete to cling to surfaces.[25-26] Simple implicit solvent modelling performed using PCM failed to reproduce the experimental trends, highlighting the limitations of current computational solvent models. These results have implications for the fundamental understanding of H-bonds in molecular recognition, and these experimental results could be used to help develop and benchmark new theoretical models of solvation.

4.8 References

1. Dominelli-Whiteley, N.; Brown, J. J.; Muchowska, K. B.; Mati, I. K.; Adam, C.; Hubbard, T. A.; Elmi, A.; Brown, A. J.; Bell, I. A. W.; Cockroft, S. L. Strong Short-Range Cooperativity in Hydrogen-Bond Chains. *Angewandte Chemie International Edition.* **2017**, *56* (26), 7658-7662.

2. Gibb, B. C. Weird and wonderful water. *Nature Chemistry.* **2016**, *8*, 733.

3. Guevara-Vela, J. M.; Romero-Montalvo, E.; Mora Gomez, V. A.; Chavez-Calvillo, R.; Garcia-Revilla, M.; Francisco, E.; Pendas, A. M.; Rocha-Rinza, T. Hydrogen bond cooperativity and anticooperativity within the water hexamer. *Physical Chemistry Chemical Physics.* **2016**, *18* (29), 19557-19566.

4. Chen, H.-Y.; Gou, M.; Wang, J.-B. De novo endo-functionalized organic cages as cooperative multi-hydrogen-bond-donating catalysts. *Chemical Communications*, **2017**, *53* (25), 3524-3526.

5. Badjić, J. D.; Nelson, A.; Cantrill, S. J.; Turnbull, W. B.; Stoddart, J. F. Multivalency and Cooperativity in Supramolecular Chemistry. *Accounts of Chemical Research.* **2005**, *38* (9), 723-732.

6. Sijbesma, R. P.; Beijer, F. H.; Brunsveld, L.; Folmer, B. J. B.; Hirschberg, J. H. K. K.; Lange, R. F. M.; Lowe, J. K. L.; Meijer, E. W. Reversible Polymers Formed from Self-Complementary Monomers Using Quadruple Hydrogen Bonding. *Science.* **1997**, *278* (5343), 1601-1604.

7. Kobko, N.; Dannenberg, J. J. Cooperativity in Amide Hydrogen Bonding Chains. Relation between Energy, Position, and H-Bond Chain Length in Peptide and Protein Folding Models. *The Journal of Physical Chemistry A.* **2003**, *107* (48), 10389-10395.

8. Kobko, N.; Paraskevas, L.; del Rio, E.; Dannenberg, J. J. Cooperativity in Amide Hydrogen Bonding Chains: Implications for Protein-Folding Models. *Journal of the American Chemical Society.* **2001**, *123* (18), 4348-4349.

9. Martín Pendás, A.; A Blanco, M.; Francisco, E. *The nature of the hydrogen bond: A synthesis from the interacting quantum atoms picture*. 2006; Vol. 125, p 184112.

10. Grabowski, S. J. What Is the Covalency of Hydrogen Bonding? *Chemical Reviews.* **2011**, *111* (4), 2597-2625.

11. Steiner, T. The Hydrogen Bond in the Solid State. *Angewandte Chemie International Edition.* **2002**, *41* (1), 48-76.

12. Cisneros, G. A.; Wikfeldt, K. T.; Ojamäe, L.; Lu, J.; Xu, Y.; Torabifard, H.; Bartók, A. P.; Csányi, G.; Molinero, V.; Paesani, F. Modeling Molecular Interactions in Water: From Pairwise to Many-Body Potential Energy Functions. *Chemical Reviews.* **2016**, *116* (13), 7501-7528.

13. Hunter, C. A. Quantifying Intermolecular Interactions: Guidelines for the Molecular Recognition Toolbox. *Angewandte Chemie International Edition.* **2004**, *43* (40), 5310-5324.

14. Cook, J. L.; Hunter, C. A.; Low, C. M. R.; Perez-Velasco, A.; Vinter, J. G. Solvent Effects on Hydrogen Bonding. *Angewandte Chemie International Edition* **2007**, *46* (20), 3706-3709.

15. Cook, J. L.; Hunter, C. A.; Low, C. M. R.; Perez-Velasco, A.; Vinter, J. G. Preferential Solvation and Hydrogen Bonding in Mixed Solvents. *Angewandte Chemie International Edition.* **2008,** *47* (33), 6275-6277.

16. Abraham, M. H.; Platts, J. A. Hydrogen Bond Structural Group Constants. *The Journal of Organic Chemistry.* **2001**, *66* (10), 3484-3491.

17. Abraham, M. H.; Grellier, P. L.; Prior, D. V.; Duce, P. P.; Morris, J. J.; Taylor, P. J. Hydrogen bonding. Part 7. A scale of solute hydrogen-bond acidity based on log K values for complexation in tetrachloromethane. *Journal of the Chemical Society, Perkin Transactions 2.* **1989**, (6), 699-711.

18. Abraham, M. H. Scales of solute hydrogen-bonding: their construction and application to physicochemical and biochemical processes. *Chemical Society Reviews.* **1993**, *22* (2), 73-83.

19. Chen, Y.-f.; Dannenberg, J. J. Cooperative 4-Pyridone H-Bonds with Extraordinary Stability. A DFT Molecular Orbital Study. *Journal of the American Chemical Society.* **2006**, *128* (25), 8100-8101.

20. Wieczorek, R.; Dannenberg, J. J. H-Bonding Cooperativity and Energetics of α-Helix Formation of Five 17-Amino Acid Peptides. *Journal of the American Chemical Society.* **2003**, *125* (27), 8124-8129.

21. Morozov, A. V.; Tsemekhman, K.; Baker, D. Electron Density Redistribution Accounts for Half the Cooperativity of α Helix Formation. *The Journal of Physical Chemistry B.* **2006**, *110* (10), 4503-4505.

22. Filot, I. A. W.; Palmans, A. R. A.; Hilbers, P. A. J.; van Santen, R. A.; Pidko, E. A.; de Greef, T. F. A. Understanding Cooperativity in Hydrogen-Bond-Induced Supramolecular Polymerization: A Density Functional Theory Study. *The Journal of Physical Chemistry B.* **2010**, *114* (43), 13667-13674.

23. Nochebuena, J.; Cuautli, C.; Ireta, J. Origin of cooperativity in hydrogen bonding. *Physical Chemistry Chemical Physics.* **2017**, *19* (23), 15256-15263.

24. Guo, H.; Karplus, M. Solvent Influence on the Stability of the Peptide Hydrogen Bond: A Supramolecular Cooperative Effect. *The Journal of Physical Chemistry.* **1994**, *98* (29), 7104-7105.

25. Lee, H.; Dellatore, S. M.; Miller, W. M.; Messersmith, P. B. Mussel-Inspired Surface Chemistry for Multifunctional Coatings. *Science.* **2007**, *318* (5849), 426-430.

26. Lee, H.; Lee, B. P.; Messersmith, P. B. A reversible wet/dry adhesive inspired by mussels and geckos. *Nature.* **2007**, *448*, 338.

27. Liu, L.; Guo, Q.-X. Isokinetic Relationship, Isoequilibrium Relationship, and Enthalpy−Entropy Compensation. *Chemical Reviews.* **2001**, *101* (3), 673-696.

Final Remarks

Overall conclusions and future work

Many molecular balance designs have been used to study intramolecular interactions in solution. Wilcox,[1] A.D Hamilton,[2] and Cockroft[3,4] have all designed molecular torsion balances to specifically study hydrogen bonds in solution. The research in this thesis involves the design of systems that were used to measure the strength of H-bonds in competitive solvents. The focus was to investigate solvation computationally, to study the strength of H-bonds between amides and anilines (H-bonds that are ubiquitous in nature: in amino acids, and in the secondary and tertiary structures of proteins) and to investigate H-bond co-cooperativity between phenol groups. The motivation was to quantify H-bond energies in biologically relevant environments, to therefore gain a deeper understanding of fundamental interactions and phenomena.

More specifically, in chapter two, work was carried out to determine how effective current implicit solvation models (SMD, PCM, SM8 and SM12) are at predicting the experimental conformational free energies of a simple molecular balance design. Experimental conformational energies were plotted against the computationally calculated energies to show poor correlations for polar solvents and improved correlations for non-polar solvents. PCM was shown to give the best correlations throughout this study, even in polar solvents. These results highlighted the limitations of using implicit solvation models to model solvation on conformational equilibria.

In chapter three, the rational design and synthesis of H-bond molecular balance systems were studied to measure the strength of H-bonds in competitive solvents, where previous research had focused on the measurement of H-bonds in non-polar solvents. The electronics of the hydrogen bond donors were systematically varied to incorporate both electron donating/withdrawing groups into the model systems, therefore varying the H-bond donor ability of the model systems. The H-bond distance and conformational flexibility of the systems were also probed, through incorporation

of different linker groups. Experimental energies were determined on these systems to measure the strength of H-bonds in solution and, on analysis of the results, it was shown that the solvent-solute interactions dominated over solute-solute interactions. A solvation model was applied to these data to gain further information on the system; a solvent-independent coefficient showed a linear relationship with the hydrogen bond donor ability of the balances, whereas the other coefficients gave insight into the changes of solvation on the donor and acceptor parts of the balance. Energies were also determined for a water soluble molecular balance series and energies determined using ^{19}F NMR spectroscopy in aqueous solvents.

In chapter four, molecular balances incorporating a methylene linker were designed to investigate cooperative H-bonds between phenol, catechol and pyrogallol groups. Experimental energies were determined in organic and aqueous/organic solvent mixtures and three different classes of behaviour were observed in the solvents tested. In solvents with good H-bond acceptor ability, a negative cooperative effect was observed, whereas in solvents with poor H-bond acceptor ability, a positive cooperative effect was observed. An intermediate behaviour was found for the aqueous solvent mixtures.

Future work could involve using IR spectroscopy, to characterise the molecular balances and to investigate the shifts in the N-H and O-H peaks. The methylene linker molecular balance design principle could be used to investigate the effect of systematically varying the acceptor on the H-bond strength. Other synthetic future work could involve incorporating amino acids into the molecular balance designs, to investigate the strength of H-bonds in systems that more closely resemble H-bonds in biology. Further computational work could involve modelling the methylene linker molecular balance using the implicit solvation models (SMD, PCM, SM8 and SM12) described in Chapter two. The computational results could then be correlated against the experimental determined Gibbs free energies, to assess how accurately the H-bond strengths are predicted computationally. Computationally, NBO analysis could also be carried out to further analyse the nature of the H-bonds.

References

1. Lypson, A. B.; Wilcox, C. S. Synthesis and NMR Analysis of a Conformationally Controlled β-Turn Mimetic Torsion Balance. *The Journal of Organic Chemistry.* **2017**, *82* (2), 898-909.

2. Luccarelli, J.; Jones, I. M.; Thompson, S.; Hamilton, A. D. Unpicking the determinants of amide NH···O=C hydrogen bond strength with diphenylacetylene molecular balances. *Organic & Biomolecular Chemistry.* **2017**, (15), 9156-9163.

3. Dominelli-Whiteley, N.; Brown, J. J.; Muchowska, K. B.; Mati, I. K.; Adam, C.; Hubbard, T. A.; Elmi, A.; Brown, A. J.; Bell, I. A. W.; Cockroft, S. L. Strong Short-Range Cooperativity in Hydrogen-Bond Chains. *Angewandte Chemie International Edition.* **2017**, *56* (26), 7658-7662.

4. Mati, I. K.; Adam, C.; Cockroft, S. L. Seeing through solvent effects using molecular balances. Chemical Science. 2013, 4 (10), 3965-3972.

Supporting Information A

Chapter 2: Limitations of Implicit Solvation Models

Table of Contents

Molecular torsion balances studied

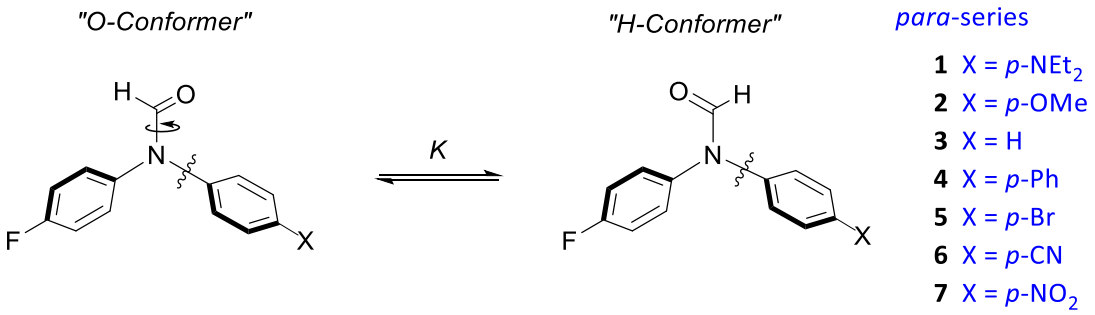

Figure S2.1: Structures of molecular torsion balances used in the present study**.**

Experimental thermodynamic data

All molecular balances were characterised in $CDCl_3$ by ^{1}H and ^{13}C-NMR, and the O and H conformers were identified using 2D NMR methods.[1,2]

The ratios of the ^{19}F-NMR peak integrations were used to calculate the free energy difference between the two conformers, ΔG_{exp} in the 11 solvents below, at 298 K. The conformational ratios were shown not to vary with the changes of the concentrations within the range used for the NMR study.[1,2]

$$\Delta G_{exp} = -RTlnK = -RTln\frac{["\text{H conformer}"]}{["\text{O conformer}"]}$$

The error in the experimental energies were previously determined to be 0.12 kJ mol^{-1}.[1,2]

Table S2.1: Conformational free energies, ΔG_{exp}, measured in 11 solvents (values given in kJ mol^{-1}). Blanks in the data were due to solubility issues.

	ΔG_{exp}/ kJ mol^{-1}						
Solvents	**(1) p-NEt2**	**(2) *p*-OMe**	**(3) H**	**(4) Ph**	**(5) Br**	**(6) CN**	**(7) NO_2**
Benzene	–1.39	–0.75	–0.68	–0.46	0.08	0.78	1.07
Carbontet	–1.92	–1.22	–1.35	n.d.[a]	0.21	1.62	2.09
Chloroform	–1.57	–0.78	–1.14	–0.68	0.08	1.03	1.39
DCM	–1.11	–0.58	–0.81	–0.58	0.08	0.71	0.99
Diethylether	–2.4	–1.27	–1.11	n.d.[a]	0.37	1.27	1.98
Ethylacetate	–2.15	–0.92	–1.07	–0.68	0.18	0.65	0.96
THF	–2.09	–1.07	–0.88	–0.65	0.23	0.68	0.88
Acetone	–1.53	–0.71	–0.85	–0.58	0.05	0.29	0.46
Acetonitrile	–0.99	–0.52	–0.78	–0.58	–0.15	–0.15	0.02
Ethanol	–1.53	–0.68	–0.81	–0.55	–0.05	0.37	0.58
Methanol	–1.07	–0.52	–0.81	n.d.[a]	–0.08	0.15	0.18

[a]Not determined as insoluble

Computational methods and data

Calculations were performed in Spartan ’14, Spartan ‘16 and Gaussian 09. The geometries were fully optimised at the DFT/B3LYP level of theory using the 6-31G* basis set in the gas phase.

Structures were also optimised in the solution phase. Calculations were ran employing the polarizable continuum model (PCM) and the solvation model on density (SMD) as implemented in Gaussian 09 using DFT/B3LYP/6-31G*.

Structures were also optimised employing the SM8 and SM12 continuum solvation models in Spartan ’14 and Spartan ’16 respectively, using DFT/B3LYP/6-31G*. Frequencies were obtained for all optimised structures to ensure the absence of imaginary frequencies in the minima.

Gas Phase

Table S2.2: Calculated energies determined for 7 molecular balances in the gas phase using DFT/B3LYP/6-31G*.

		Gas phase	
Balance	**H conformer**	**O conformer**	**ΔE/ kJ mol^{-1}**
(1) p-NEt$_2$	–2478464.47	–2478460.86	–3.60
(2) p-OMe	–2220917.08	–2220915.32	–1.76
(3) H	–1920181.02	–1920179.71	–1.31
(4) Ph	–2526937.99	–2526937.23	–0.76
(5) Br	–8671898.95	–8671899.78	0.83
(6) CN	–2162408.19	–2162411.07	2.89
(7) NO$_2$	–2457198.53	–2457201.78	3.26

		Gas phase	
Balance	**H conformer**	**O conformer**	**ΔE/ kJ mol^{-1}**
(1) p-NEt$_2$	–2478464.47	–2478460.86	–3.60
(2) p-OMe	–2220917.08	–2220915.32	–1.76
(3) H	–1920181.02	–1920179.71	–1.31
(4) Ph	–2526937.99	–2526937.23	–0.76
(5) Br	–8671898.95	–8671899.78	0.83
(6) CN	–2162408.19	–2162411.07	2.89
(7) NO$_2$	–2457198.53	–2457201.78	3.26

PCM

Table S2.3: Calculated energies determined for 7 molecular balances in 10 different solvents employing the PCM implicit solvation model using DFT/B3LYP/6-31G*.

	Benzene			Carbon tetrachloride		
Balance	**H conformer**	**O conformer**	**ΔE/ kJ mol^{-1}**	**H conformer**	**O conformer**	**ΔE/ kJ mol^{-1}**
(1) *p*-NEt$_2$	–2478478.97	–2478476.45	–2.52	–2478478.73	–2478476.19	–2.54
(2) *p*-OMe	–2220931.69	–2220930.59	–1.10	–2220931.45	–2220930.34	–1.11
(3) H	–1920193.38	–1920192.33	–1.05	–1920193.17	–1920192.12	–1.05
(4) Ph	–2526952.57	–2526951.94	–0.63	–2526952.33	–2526951.70	–0.63
(5) Br	–8671912.09	–8671912.62	0.53	–8671911.87	–8671912.41	0.54
(6) CN	–2162427.64	–2162429.63	1.99	–2162427.32	–2162429.32	2.00
(7) NO$_2$	–2457217.30	–2457219.65	2.35	–2457216.99	–2457219.36	2.36

	Chloroform			DCM		
Balance	**H conformer**	**O conformer**	**ΔE/ kJ mol^{-1}**	**H conformer**	**O conformer**	**ΔE/ kJ mol^{-1}**
(1) *p*-NEt$_2$	–2478485.74	–2478483.83	–1.90	–2478488.92	–2478487.31	–1.61
(2) *p*-OMe	–2220938.49	–2220937.77	–0.72	–2220941.66	–2220941.13	–0.53
(3) H	–1920199.14	–1920198.26	–0.88	–1920201.83	–1920201.04	–0.79
(4) Ph	–2526959.31	–2526958.76	–0.56	–2526962.45	–2526961.93	–0.52
(5) Br	–8671918.21	–8671918.63	0.42	–8671921.07	–8671921.44	0.37
(6) CN	–2162436.83	–2162438.31	1.48	–2162441.15	–2162442.38	1.23
(7) NO$_2$	–2457226.12	–2457227.97	1.85	–2457230.27	–2457231.86	1.60

	Acetone			Acetonitrile		
Balance	**H conformer**	**O conformer**	**ΔE/ kJ mol^{-1}**	**H conformer**	**O conformer**	**ΔE/ kJ mol^{-1}**
(1) *p*-NEt$_2$	–2478491.01	–2478489.58	–1.43	–2478491.71	–2478490.35	–1.36
(2) *p*-OMe	–2220943.73	–2220943.32	–0.41	–2220944.42	–2220944.06	–0.36
(3) H	–1920203.59	–1920202.85	–0.74	–1920204.18	–1920203.46	–0.72
(4) Ph	–2526964.49	–2526964.00	–0.49	–2526965.17	–2526964.69	–0.48
(5) Br	–8671922.92	–8671923.26	0.34	–8671923.55	–8671923.88	0.33
(6) CN	–2162443.97	–2162445.02	1.06	–2162444.91	–2162445.91	1.00
(7) NO$_2$	–2457232.97	–2457234.40	1.42	–2457233.88	–2457235.25	1.37

	THF			Ethyl acetate		
Balance	**H conformer**	**O conformer**	**ΔE/ kJ mol^{-1}**	**H conformer**	**O conformer**	**ΔE/ kJ mol^{-1}**
(1) *p*-NEt$_2$	–2478488.19	–2478486.51	–1.68	–2478487.15	–2478485.38	–1.77
(2) *p*-OMe	–2220940.93	–2220940.36	–0.58	–2220939.90	–2220939.27	–0.64
(3) H	–1920201.21	–1920200.40	–0.81	–1920200.34	–1920199.50	–0.84
(4) Ph	–2526961.73	–2526961.20	–0.53	–2526960.71	–2526960.17	–0.54
(5) Br	–8671920.41	–8671920.79	0.38	–8671919.48	–8671919.88	0.40
(6) CN	–2162440.16	–2162441.44	1.29	–2162438.76	–2162440.12	1.37
(7) NO$_2$	–2457229.32	–2457230.97	1.65	–2457227.97	–2457229.71	1.74

	Ethanol			Methanol		
Balance	H conformer	O conformer	ΔE/ kJ mol^{-1}	H conformer	O conformer	ΔE/ kJ mol^{-1}
(1) *p*-NEt_2	–2478491.30	–2478489.90	–1.40	–2478491.62	–2478490.25	–1.37
(2) *p*-OMe	–2220944.01	–2220943.62	–0.39	–2220944.33	–2220943.96	–0.37
(3) H	–1920203.83	–1920203.10	–0.73	–1920204.10	–1920203.38	–0.72
(4) Ph	–2526964.77	–2526964.28	–0.49	–2526965.08	–2526964.60	–0.48
(5) Br	–8671923.18	–8671923.52	0.34	–8671923.47	–8671923.80	0.33
(6) CN	–2162444.35	–2162445.39	1.03	–2162444.79	–2162445.79	1.00
(7) NO_2	–2457233.35	–2457234.75	1.40	–2457233.77	–2457235.14	1.37

SMD

Table S2.4: Calculated energies determined for 7 molecular balances in 10 different solvents employing the SMD implicit solvation model using DFT/B3LYP/6-31G*.

	Benzene			Carbon tetrachloride		
Balance	H conformer	O conformer	ΔE/ kJ mol^{-1}	H conformer	O conformer	ΔE/ kJ mol^{-1}
(1) *p*-NEt_2	–2478515.41	–2478512.56	–2.85	–2478517.27	–2478514.37	–2.90
(2) *p*-OMe	–2220958.83	–2220957.56	–1.28	–2220960.18	–2220958.88	–1.30
(3) H	–1920221.89	–1920220.71	–1.18	–1920223.38	–1920222.19	–1.19
(4) Ph	–2526994.21	–2526993.58	–0.63	–2526996.47	–2526995.84	–0.62
(5) Br	–8671945.85	–8671946.45	0.60	–8671947.12	–8671947.74	0.62
(6) CN	–2162453.69	–2162455.68	1.99	–2162455.38	–2162457.43	2.05
(7) NO_2	–2457246.09	–2457248.43	2.34	–2457247.46	–2457249.87	2.41

	Chloroform			DCM		
Balance	H conformer	O conformer	ΔE/ kJ mol^{-1}	H conformer	O conformer	ΔE/ kJ mol^{-1}
(1) *p*-NEt_2	–2478521.89	–2478519.83	–2.06	–2478527.57	–2478526.02	–1.55
(2) *p*-OMe	–2220964.08	–2220963.29	–0.79	–2220970.01	–2220969.55	–0.46
(3) H	–1920226.78	–1920225.80	–0.98	–1920231.79	–1920230.92	–0.87
(4) Ph	–2527000.62	–2526999.98	–0.64	–2527006.86	–2527006.19	–0.67
(5) Br	–8671950.80	–8671951.18	0.38	–8671955.74	–8671955.97	0.23
(6) CN	–2162463.00	–2162464.23	1.23	–2162471.05	–2162471.80	0.75
(7) NO_2	–2457250.39	–2457251.96	1.57	–2457258.36	–2457259.33	0.97

	Acetone			Acetonitrile		
Balance	**H conformer**	**O conformer**	**ΔE/ kJ mol^{-1}**	**H conformer**	**O conformer**	**ΔE/ kJ mol^{-1}**
(1) *p*-NEt$_2$	–2478524.13	–2478523.01	–1.12	–2478522.59	–2478521.65	–0.94
(2) *p*-OMe	–2220968.86	–2220968.67	–0.19	–2220967.29	–2220967.19	–0.11
(3) H	–1920229.24	–1920228.48	–0.76	–1920228.30	–1920227.59	–0.71
(4) Ph	–2527002.02	–2527001.38	–0.64	–2527001.20	–2527000.57	–0.63
(5) Br	–8671953.26	–8671953.37	0.11	–8671951.90	–8671951.94	0.05
(6) CN	–2162470.38	–2162470.68	0.30	–2162469.81	–2162469.96	0.15
(7) NO$_2$	–2457258.39	–2457258.77	0.38	–2457256.88	–2457257.09	0.21

	THF			Ethyl acetate		
Balance	**H conformer**	**O conformer**	**ΔE/ kJ mol^{-1}**	**H conformer**	**O conformer**	**ΔE/ kJ mol^{-1}**
(1) *p*-NEt$_2$	–2478517.93	–2478516.18	–1.74	–2478518.41	–2478516.50	–1.91
(2) *p*-OMe	–2220963.38	–2220962.80	–0.58	–2220963.59	–2220962.90	–0.68
(3) H	–1920224.50	–1920223.58	–0.92	–1920224.69	–1920223.72	–0.97
(4) Ph	–2526995.94	–2526995.31	–0.63	–2526996.21	–2526995.57	–0.63
(5) Br	–8671948.31	–8671948.59	0.28	–8671948.47	–8671948.80	0.33
(6) CN	–2162463.12	–2162463.96	0.84	–2162462.73	–2162463.73	1.00
(7) NO$_2$	–2457252.70	–2457253.75	1.04	–2457252.51	–2457253.75	1.24

	Ethanol			Methanol		
Balance	**H conformer**	**O conformer**	**ΔE/ kJ mol^{-1}**	**H conformer**	**O conformer**	**ΔE/ kJ mol^{-1}**
(1) *p*-NEt$_2$	–2478518.73	–2478518.18	–0.55	–2478517.77	–2478517.42	–0.35
(2) *p*-OMe	–2220963.50	–2220963.54	0.04	–2220962.89	–2220962.93	0.05
(3) H	–1920224.27	–1920223.54	–0.73	–1920223.51	–1920222.87	–0.64
(4) Ph	–2526994.26	–2526993.59	–0.67	–2526992.75	–2526992.10	–0.66
(5) Br	–8671948.47	–8671948.39	–0.08	–8671947.61	–8671947.47	–0.14
(6) CN	–2162462.54	–2162462.34	–0.20	–2162461.53	–2162461.11	–0.42
(7) NO$_2$	–2457248.18	–2457247.93	–0.24	–2457246.34	–2457245.94	–0.40

SM8

Table S2.5: Calculated energies determined for 7 molecular balances in 10 different solvents employing the SM8 implicit solvation model using DFT/B3LYP/6-31G*.

	Benzene			Carbon tetrachloride		
Balance	**H conformer**	**O conformer**	**ΔE/ kJ mol⁻¹**	**H conformer**	**O conformer**	**ΔE/ kJ mol⁻¹**
(1) *p*-NEt₂	–2478043.43	–2478040.61	–2.82	–2478046.5	–2478043.9	–2.60
(2) *p*-OMe	–2220536.98	–2220535.72	–1.26	–2220538.97	–2220537.69	–1.28
(3) H	–1919855.99	–1919855.72	–0.27	–1919857.95	–1919857.66	–0.29
(4) Ph	–2526514.06	–2526514.17	0.11	–2526516.41	–2526516.68	0.27
(5) Br	–8676014.11	–8676014.98	0.87	–8676016.15	–8676017.02	0.87
(6) CN	–2162040.68	–2162042.72	2.04	–2162044.2	–2162046.27	2.07
(7) NO₂	–2456781.58	–2456784.08	2.50	–2456783.55	–2456786.09	2.54

	Chloroform			DCM		
Balance	**H conformer**	**O conformer**	**ΔE/ kJ mol⁻¹**	**H conformer**	**O conformer**	**ΔE/ kJ mol⁻¹**
(1) *p*-NEt₂	–2478047.11	–2478045.35	–1.76	–2478048.03	–2478046.41	–1.62
(2) *p*-OMe	–2220540.42	–2220539.77	–0.65	–2220541.83	–2220541.37	–0.46
(3) H	–1919858.75	–1919858.88	0.13	–1919859.63	–1919859.99	0.36
(4) Ph	–2526516.98	–2526517.41	0.43	–2526517.82	–2526518.41	0.59
(5) Br	–8676017.04	–8676018	0.96	–8676017.78	–8676018.8	1.02
(6) CN	–2162052.29	–2162053.84	1.55	–2162056.66	–2162058	1.34
(7) NO₂	–2456786.99	–2456789.11	2.12	–2456789.87	–2456791.9	2.03

	Acetone			Acetonitrile		
Balance	**H conformer**	**O conformer**	**ΔE/ kJ mol⁻¹**	**H conformer**	**O conformer**	**ΔE/ kJ mol⁻¹**
(1) *p*-NEt₂	–2478047.91	–2478046.27	–1.64	–2478041.70	–2478040.13	–1.57
(2) *p*-OMe	–2220544.31	–2220544.00	–0.31	–2220538.43	–2220538.18	–0.25
(3) H	–1919860.60	–1919861.05	0.45	–1919855.60	–1919856.13	0.53
(4) Ph	–2526518.68	–2526519.43	0.75	–2526512.01	–2526512.82	0.81
(5) Br	–8676018.40	–8676019.46	1.06	–8676013.05	–8676014.14	1.09
(6) CN	–2162056.78	–2162057.93	1.15	–2162053.89	–2162054.99	1.10
(7) NO₂	–2456792.64	–2456794.53	1.89	–2456787.33	–2456789.21	1.88
	THF			**Ethyl acetate**		
Balance	**H conformer**	**O conformer**	**ΔE/ kJ mol⁻¹**	**H conformer**	**O conformer**	**ΔE/ kJ mol⁻¹**
(1) *p*-NEt₂	–2478042.96	–2478041.25	–1.71	–2478042.84	–2478040.95	–1.89
(2) *p*-OMe	–2220539.79	–2220539.23	–0.56	–2220539.47	–2220538.80	–0.67
(3) H	–1919857.00	–1919857.28	0.28	–1919856.67	–1919858.59	1.92
(4) Ph	–2526514.23	–2526514.98	0.75	–2526513.90	–2526514.45	0.55
(5) Br	–8675968.06	–8675969.03	0.97	–8676014.22	–8676015.22	1.00
(6) CN	–2162049.29	–2162050.87	1.58	–2162048.37	–2162049.89	1.52
(7) NO₂	–2456732.83	–2456735.85	3.02	–2456786.50	–2456788.62	2.12

Balance	Ethanol			Methanol		
	H conformer	O conformer	ΔE/ kJ mol^{-1}	H conformer	O conformer	ΔE/ kJ mol^{-1}
(1) *p*-NEt_2	–2478043.23	–2478042.61	–0.62	–2478046.62	–2478046.21	–0.41
(2) *p*-OMe	–2220541.27	–2220541.52	0.25	–2220544.41	–2220544.85	0.44
(3) H	–1919858.08	–1919858.59	0.51	–1919860.95	–1919861.54	0.59
(4) Ph	–2526513.71	–2526514.34	0.63	–2526516.56	–2526517.25	0.69
(5) Br	–8676015.72	–8676016.61	0.89	–8676018.53	–8676019.36	0.83
(6) CN	–2162053.38	–2162053.86	0.48	–2162056.78	–2162056.97	0.19
(7) NO_2	–2456789.88	–2456791.1	1.22	–2456793.63	–2456794.48	0.85

SM12

Table S2.6: Calculated energies determined for 7 molecular balances in 10 different solvents employing the SM12 implicit solvation model using DFT/B3LYP/6-31G*.

Balance	Benzene			Carbon tetrachloride		
	H conformer	O conformer	ΔE/ kJ mol^{-1}	H conformer	O conformer	ΔE/ kJ mol^{-1}
(1) *p*-NEt_2	–2478042.14	–2478039.28	–2.86	–2478044.21	–2478041.29	–2.92
(2) *p*-OMe	–2220536.05	–2220534.75	–1.30	–2220537.83	–2220536.52	–1.31
(3) H	–1919817.03	–1919816.13	–0.90	–1919856.59	–1919856.26	–0.33
(4) Ph	–2526459.38	–2526458.93	–0.45	–2526514.96	–2526515.01	0.05
(5) Br	–8675968.24	–8675968.93	0.69	–8676013.37	–8676014.16	0.79
(6) CN	–2161998.43	–2162001.03	2.60	–2162041.61	–2162043.66	2.05
(7) NO_2	–2456733.15	–2456736.20	3.05	–2456779.05	–2456781.52	2.47

Balance	Chloroform			DCM		
	H conformer	O conformer	ΔE/ kJ mol^{-1}	H conformer	O conformer	ΔE/ kJ mol^{-1}
(1) *p*-NEt_2	–2478046.88	–2478044.51	–2.37	–2478047.70	–2478045.57	–2.13
(2) *p*-OMe	–2220541.68	–2220540.78	–0.90	–2220542.55	–2220541.78	–0.77
(3) H	–1919859.13	–1919859.01	–0.12	–1919860.02	–1919860.00	–0.02
(4) Ph	–2526517.39	–2526517.69	0.30	–2526518.41	–2526518.85	0.44
(5) Br	–8676015.68	–8676016.51	0.83	–8676016.10	–8676015.23	–0.87
(6) CN	–2162049.49	–2162051.21	1.72	–2162052.00	–2162053.72	1.72
(7) NO_2	–2456783.11	–2456785.35	2.24	–2456785.09	–2456787.28	2.19

Balance	Acetone			Acetonitrile		
	H conformer	O conformer	ΔE/ kJ mol^{-1}	H conformer	O conformer	ΔE/ kJ mol^{-1}
(1) *p*-NEt_2	–2478047.35	–2478045.28	–2.07	–2478042.81	–2478040.79	–2.02
(2) *p*-OMe	–2220541.88	–2220541.12	–0.76	–2220538.67	–2220536.23	–2.44
(3) H	–1919859.70	–1919859.83	0.13	–1919856.35	–1919856.50	0.15
(4) Ph	–2526518.04	–2526518.65	0.61	–2526513.48	–2526514.12	0.64
(5) Br	–8676014.39	–8676015.77	1.38	–8676011.06	–8676012.14	1.08
(6) CN	–2162049.15	–2162050.94	1.79	–2162047.83	–2162049.57	1.74
(7) NO_2	–2456786.55	–2456788.75	2.20	–2456782.67	–2456784.88	2.21

Balance	THF			Ethyl acetate		
	H conformer	O conformer	ΔE/ kJ mol^{-1}	H conformer	O conformer	ΔE/ kJ mol^{-1}
(1) *p*-NEt$_2$	–2478043.04	–2478040.74	–2.30	–2478042.72	–2478040.35	–2.37
(2) *p*-OMe	–2220537.71	–2220536.81	–0.90	–2220537.38	–2220535.11	–2.27
(3) H	–1919856.39	–1919856.44	0.05	–1919856.03	–1919856.05	0.02
(4) Ph	–2526514.12	–2526514.62	0.50	–2526513.60	–2526514.06	0.46
(5) Br	–8676011.77	–8676012.68	0.91	–8676011.40	–8676012.30	0.90
(6) CN	–2162043.40	–2162045.28	1.88	–2162042.87	–2162044.77	1.90
(7) NO$_2$	–2456782.21	–2456784.49	2.28	–2456781.56	–2456783.85	2.29

Balance	Ethanol			Methanol		
	H conformer	O conformer	ΔE/ kJ mol^{-1}	H conformer	O conformer	ΔE/ kJ mol^{-1}
(1) *p*-NEt$_2$	–2478044.33	–2478042.70	–1.63	–2478046.58	–2478045.11	–1.47
(2) *p*-OMe	–2220541.65	–2220541.24	–0.41	–2220544.20	–2220543.79	–0.41
(3) H	–1919858.30	–1919858.20	–0.10	–1919860.22	–1919860.05	–0.17
(4) Ph	–2526514.09	–2526514.41	0.32	–2526515.92	–2526516.20	0.28
(5) Br	–8676006.69	–8676014.36	7.67	–8676015.95	–8676016.31	0.36
(6) CN	–2162048.40	–2162049.54	1.14	–2162050.93	–2162051.84	0.91
(7) NO$_2$	–2456784.56	–2456786.44	1.88	–2456786.82	–2456788.58	1.76

Table of R^2 values

Table S2.7: R^2 values determined from plots of the experimental Gibbs free energies against the calculated conformational free energies in the gas phase and also in the solution phase employing implicit solvation models SMD, PCM, SM8 and SM12 using DFT/B3LYP/6-31G*.

Solvent	R^2 Values				
	Gas phase	SMD	PCM	SM8	SM12
Benzene	0.995	0.995	0.998	0.950	0.997
Carbon tetrachloride	0.970	0.968	0.977	0.950	0.905
Chloroform	0.964	0.976	0.987	0.777	0.858
DCM	0.959	0.966	0.988	0.774	0.684
Acetone	0.961	0.910	0.963	0.856	0.926
Acetonitrile	0.880	0.910	0.941	0.727	0.572
THF	0.978	0.970	0.958	0.903	0.956
Ethylacetate	0.972	0.992	0.975	0.600	0.972
Ethanol	0.977	0.159	0.979	0.711	0.290
Methanol	0.793	0.106	0.970	0.337	0.855

Table of gradient values

Table S2.8: Gradient values determined from plots of the experimental Gibbs free energies against the calculated conformational free energies in the gas phase and also in the solution phase employing implicit solvation models SMD, PCM, SM8 and SM12 using DFT/B3LYP/6-31G*.

Solvent	Gradient				
	Gas phase	SMD	PCM	SM8	SM12
Benzene	0.350	0.468	0.499	0.464	0.413
Carbon tetrachloride	0.602	0.786	0.856	0.808	0.773
Chloroform	0.434	0.846	0.817	0.777	0.657
DCM	0.310	0.859	0.688	0.580	0.435
Acetone	0.277	1.172	0.684	0.570	0.453
Acetonitrile	0.138	0.759	0.369	0.281	0.156
THF	0.418	1.042	0.869	0.668	0.657
Ethylacetate	0.428	0.959	0.852	0.577	0.529
Ethanol	0.288	0.561	0.724	1.070	0.130
Methanol	0.207	0.217	0.489	0.658	0.432

References

1. Mati, I. K.; Adam, C.; Cockroft, S. L. Seeing through solvent effects using molecular balances. *Chemical Science.* **2013**, *4* (10), 3965-3972.

2. Muchowska, K. B.; Adam, C.; Mati, I. K.; Cockroft, S. L. Electrostatic Modulation of Aromatic Rings via Explicit Solvation of Substituents. *Journal of the American Chemical Society.* **2013**, *135* (27), 9976-9979.

Supporting Information B

Chapter 3: Geometric and solvent effects on H-bonding

Table of Contents

Molecular torsion balances studied

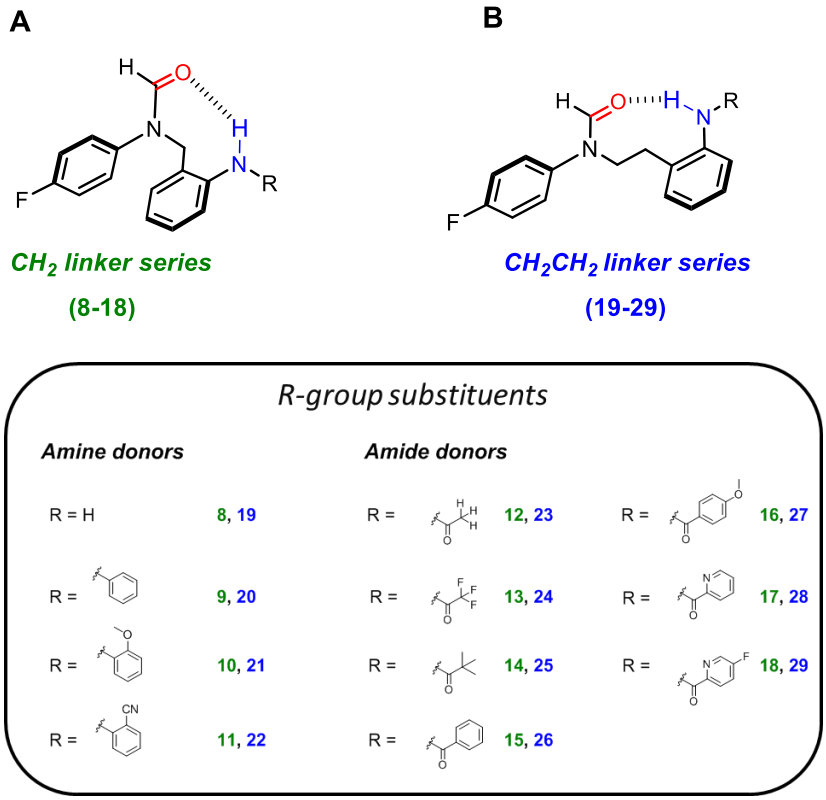

Figure S3.1: A Methylene linker molecular balance series (compounds **8-18,** green) substituted with amine and amide hydrogen bond donors. **B** Ethylene linker molecular balance series (compounds **19-29**, blue) substituted with amine and amide hydrogen bond donors.

Determination of experimental conformational free energies, ΔG_{EXP}

All molecular torsion balances were fully characterized in DMSO-d_6 by ^{1}H and ^{13}C-NMR, prior to the determination of experimental conformational free energies (see Conformer Characterisation section below). The NMR peaks corresponding to the folded and unfolded conformers were assigned using 2D NMR methods as detailed in the conformer assignment section below. NMR spectra used for conformational free energy calculation were determined by ^{19}F NMR spectroscopy using a Bruker Ultrashield 500 MHz, heteronuclear (512 scans). Conformer ratios were determined at

balance concentrations of 3.5 mM and were found to be independent of concentration in a range of 1 – 4 mM (Table S3.1) The conformational free energy differences measured in a range of solvents are provided in Tables S3.2-S3.26.

$$\Delta G_{EXP} = -RTlnK = -RTln\frac{[\text{Folded}]}{[\text{Unfolded}]}$$

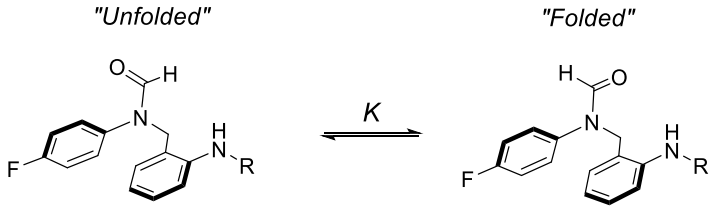

A conservative 3% estimate of the error in the integral of the minor conformer NMR peak was applied (e.g. the integration ratio was [∫major conformer = 1] / [∫minor conformer ± 0.03]), resulting in asymmetric ΔG_{EXP} error margins as listed in Tables S3.2-S3.26. All ^{19}F NMR measurements were carried out once to determine the integration ratio and therefore the Gibb's free energies.

Table S3.1: Concentration study of molecular balances **10, 12, 18**.

Compound	c/ mM	MeOD ΔG_{exp}/ kJ mol^{-1}	$CDCl_3$ ΔG_{exp}/ kJ mol^{-1}
10	1	–4.4	–6.3
	2	–4.4	–6.3
	4	–4.4	–6.3
12	1	–5.3	< – 10
	2	–5.3	< – 10
	4	–5.5	< – 10
18	1	–4.4	–6.6
	2	–4.4	–6.6
	4	–4.4	–6.6

Methylene linker series

Table S3.2: Experimental conformational free energy differences of molecular balance **8**, ΔG_{EXP} measured in various solvents at 298 K.

8			
		Error	
	ΔG / kJ mol^{-1}	–	+
Chloroform-d	< – 10[a]	–	–
Acetone	–7.4	2.3	1.2
Acetonitrile-d3	–7.0	1.7	1.0
Ethyl acetate	n.d.[b]	n.d.[b]	n.d.[b]
Tetrahydrofuran	–9.7	7.4	2.3
Dichloromethane	< – 10[a]	–	–
Ethanol	–7.0	1.7	1.0
Methanol-d4	–6.6	1.4	0.9
DMSO-d6	–5.5	0.8	0.6

[a]Only one peak observed in NMR spectrum that was assigned to the folded conformer.

[b]Not determined due to peak overlap in the NMR spectrum.

Table S3.3: Experimental conformational free energy differences of molecular balance **9,** ΔG_{EXP} measured in various solvents at 298 K.

9			
		Error	
	ΔG / kJ mol^{-1}	–	+
Chloroform-d	< – 10[a]	–	–
Acetone	–6.6	1.4	0.9
Acetonitrile-d3	–6.6	1.4	0.9
Ethyl acetate	–8.7	8.4	1.7
Tetrahydrofuran	n.d.[b]	n.d.[b]	n.d.[b]
Dichloromethane	< – 10[a]	–	–
Ethanol	–6.0	1.0	0.7
Methanol-d4	–5.1	0.7	0.5
DMSO-d6	–4.4	0.5	0.4

[a]Only one peak observed in NMR spectrum that was assigned to the folded conformer.

[b]Not determined due to peak overlap in the NMR spectrum.

Table S3.4: Experimental conformational free energy differences of molecular balance **10**, ΔG_{EXP} measured in various solvents at 298 K.

10			
		Error	
	ΔG / kJ mol^{-1}	–	+
Chloroform-d	–6.3	1.2	0.8
Acetone	–5.7	0.9	0.7
Acetonitrile-d3	–5.5	0.8	0.6
Ethyl acetate	–6.3	1.2	0.8
Tetrahydrofuran	–6.6	1.4	0.9
Dichloromethane	–6.3	1.2	0.8
Ethanol	–5.1	0.7	0.5
Methanol-d4	–.4	0.5	0.4
DMSO-d6	–4.4	0.5	0.4

[a]Only one peak observed in NMR spectrum that was assigned to the folded conformer.

[b]Not determined due to peak overlap in the NMR spectrum.

Table S3.5: Experimental conformational free energy differences of molecular balance **11**, ΔG_{EXP} measured in various solvents at 298 K.

11			
		Error	
	ΔG / kJ mol^{-1}	–	+
Chloroform-d	–8.7	8.4	1.7
Acetone	–6.3	1.2	0.8
Acetonitrile-d3	–5.7	0.9	0.7
Ethyl acetate	–7.0	1.7	1.0
Tetrahydrofuran	–7.0	1.7	1.0
Dichloromethane	–8.0	3.4	1.4
Ethanol	–5.7	0.9	0.7
Methanol-d4	–5.3	0.7	0.6
DMSO-d6	–4.4	0.5	0.4

[a]Only one peak observed in NMR spectrum that was assigned to the folded conformer.

[b]Not determined due to peak overlap in the NMR spectrum.

Table S3.6: Experimental conformational free energy differences of molecular balance **12**, ΔG_{EXP} measured in various solvents at 298 K

12			
		Error	
	ΔG / kJ mol^{-1}	–	+
Chloroform-d	< – 10[a]	–	–
Acetone	–8.0	3.4	1.4
Acetonitrile-d3	–7.0	1.7	1.0
Ethyl acetate	–9.7	7.4	2.3
Tetrahydrofuran	–9.7	7.4	2.3
Dichloromethane	< – 10[a]	–	–
Ethanol	–6.0	1.0	0.7
Methanol-d4	–5.5	0.8	0.6
DMSO-d6	–4.5	0.5	0.4

[a]Only one peak observed in NMR spectrum that was assigned to the folded conformer.

Table S3.7: Experimental conformational free energy differences of molecular balance **13**, ΔG_{EXP} measured in various solvents at 298 K

13			
		Error	
	ΔG / kJ mol^{-1}	–	+
Chloroform-d	< – 10[a]	–	–
Acetone	–8.7	8.4	1.7
Acetonitrile-d3	–8.0	3.4	1.4
Ethyl acetate	–9.7	7.4	2.3
Tetrahydrofuran	–9.7	7.4	2.3
Dichloromethane	< – 10[a]	–	–
Ethanol	–6.3	1.2	0.8
Methanol-d4	–5.7	0.9	0.7
DMSO-d6	–4.9	0.6	0.5

[a]Only one peak observed in NMR spectrum that was assigned to the folded conformer.

Table S3.8: Experimental conformational free energy differences of molecular balance **14**, ΔG_{EXP} measured in various solvents at 298 K.

14			
		Error	
	ΔG / kJ mol^{-1}	–	+
Chloroform-d	< – 10[a]	–	–
Acetone	–7.4	2.3	1.2
Acetonitrile-d3	–6.3	1.2	0.8
Ethyl acetate	–9.7	7.4	2.3
Tetrahydrofuran	–8.7	8.4	1.7
Dichloromethane	< – 10[a]	–	–
Ethanol	–6.3	1.2	0.8
Methanol-d4	–5.5	0.8	0.6
DMSO-d6	–4.7	0.6	0.5

[a]Only one peak observed in NMR spectrum that was assigned to the folded conformer.

Table S3.9: Experimental conformational free energy differences of molecular balance **15**, ΔG_{EXP} measured in various solvents at 298 K.

15			
		Error	
	ΔG / kJ mol^{-1}	–	+
Chloroform-d	< – 10[a]	–	–
Acetone	–7.4	2.3	1.2
Acetonitrile-d3	–7.0	1.7	1.0
Ethyl acetate	n.d.[b]	n.d.[b]	n.d.[b]
Tetrahydrofuran	–8.7	8.4	1.7
Dichloromethane	< – 10[a]	–	–
Ethanol	–6.0	1.0	0.7
Methanol-d4	–5.3	0.7	0.6
DMSO-d6	–4.5	0.5	0.4

[a]Only one peak observed in NMR spectrum that was assigned to the folded conformer.

[b]Not determined due to peak overlap in the NMR spectrum.

Table S3.10: Experimental conformational free energy differences of molecular balance **16,** ΔG_{EXP} measured in various solvents at 298 K.

16			
		Error	
	ΔG / kJ mol^{-1}	–	+
Chloroform-d	< – 10[a]	–	–
Acetone	–7.4	2.3	1.2
Acetonitrile-d3	–7.0	1.7	1.0
Ethyl acetate	n.d.[b]	n.d.[b]	n.d.[b]
Tetrahydrofuran	–8.7	8.4	1.7
Dichloromethane	< – 10[a]	–	–
Ethanol	–5.7	0.9	0.7
Methanol-d4	–5.3	0.7	0.6
DMSO-d6	–4.5	0.5	0.4

[a]Only one peak observed in NMR spectrum that was assigned to the folded conformer.
[b]Not determined due to peak overlap in the NMR spectrum.

Table S3.11: Experimental conformational free energy differences of molecular balance **17**, ΔG_{EXP} measured in various solvents at 298 K.

17			
		Error	
	ΔG / kJ mol^{-1}	–	+
Chloroform-d	–6.0	1.0	0.7
Acetone	–4.5	0.5	0.4
Acetonitrile-d3	–4.4	0.5	0.4
Ethyl acetate	–5.3	0.7	0.6
Tetrahydrofuran	–5.3	0.7	0.6
Dichloromethane	–5.5	0.8	0.6
Ethanol	n.d.[a]	n.d.[a]	n.d.[a]
Methanol-d4	–3.9	0.4	0.3
DMSO-d6	–4.1	0.4	0.4

[a]Not determined due to peak overlap in the NMR spectrum.

Table S3.12: Experimental conformational free energy differences of molecular balance **18,** ΔG_{EXP} measured in various solvents at 298 K.

18			
		Error	
	ΔG / kJ mol^{-1}	–	+
Chloroform-d	–6.6	1.4	0.9
Acetone	–4.9	0.6	0.5
Acetonitrile-d3	–4.7	0.6	0.5
Ethyl acetate	–5.7	0.9	0.7
Tetrahydrofuran	–5.5	0.8	0.6
Dichloromethane	–6.0	1.0	0.7
Ethanol	–4.9	0.6	0.5
Methanol-d4	–4.2	0.5	0.4
DMSO-d6	–4.0	0.4	0.4

Ethylene linker series

Table S3.13: Experimental conformational free energy differences of molecular balance **19**, ΔG_{EXP} measured in various solvents at 298 K.

19			
		Error	
	ΔG / kJ mol^{-1}	-	+
Chloroform-d	–7.4	2.3	1.2
Acetone	–5.5	0.8	0.6
Acetonitrile-d3	–4.7	0.6	0.5
Ethyl acetate	–6.6	1.4	0.9
Tetrahydrofuran	–6.6	1.4	0.9
Dichloromethane	–7.0	1.7	1.0
Ethanol	–4.5	0.5	0.4
Methanol-d4	–4.1	0.4	0.4
DMSO-d6	–3.5	0.3	0.3

Table S3.14: Experimental conformational free energy differences of molecular balance **20**, ΔG_{EXP} measured in various solvents at 298 K.

20			
		Error	
	ΔG / kJ mol^{-1}	–	+
Chloroform-d	–8.0	3.4	1.4
Acetone	–5.5	0.8	0.6
Acetonitrile-d3	–4.7	0.6	0.5
Ethyl acetate	–7.0	1.7	1.0
Tetrahydrofuran	–7.0	1.7	1.0
Dichloromethane	–7.0	1.7	1.0
Ethanol	–4.4	0.5	0.4
Methanol-d4	–3.9	0.4	0.3
DMSO-d6	–3.4	0.3	0.3

Table S3.15: Experimental conformational free energy differences of molecular balance **21**, ΔG_{EXP} measured in various solvents at 298 K.

21			
		Error	
	ΔG / kJ mol^{-1}	-	+
Chloroform-d	–5.1	0.7	0.5
Acetone	–4.5	0.6	0.5
Acetonitrile-d3	–3.8	0.5	0.4
Ethyl acetate	–5.1	1.0	0.7
Tetrahydrofuran	–5.3	0.7	0.6
Dichloromethane	–4.7	2.3	1.1
Ethanol	–4.0	0.4	0.4
Methanol-d4	–3.4	0.4	0.3
DMSO-d6	–3.2	0.3	0.3

Table S3.16: Experimental conformational free energy differences of molecular balance **22**, ΔG_{EXP} measured in various solvents at 298 K.

22			
		Error	
	ΔG / kJ mol^{-1}	–	+
Chloroform-d	−6.0	1.0	0.7
Acetone	−4.7	0.6	0.5
Acetonitrile-d3	−3.9	0.4	0.3
Ethyl acetate	n.d.[a]	n.d.[a]	n.d.[a]
Tetrahydrofuran	−5.3	0.7	0.6
Dichloromethane	−5.7	0.9	0.7
Ethanol	−4.4	0.5	0.4
Methanol-d4	−3.8	0.4	0.3
DMSO-d6	−3.2	0.3	0.3

[a]Not determined due to peak overlap in the NMR spectrum.

Table S3.17: Experimental conformational free energy differences of molecular balance **23**, ΔG_{EXP} measured in various solvents at 298 K.

23			
		Error	
	ΔG / kJ mol^{-1}	–	+
Chloroform-d	< – 10[a]	–	–
Acetone	−6.0	1.0	0.7
Acetonitrile-d3	−5.1	0.7	0.5
Ethyl acetate	−8.7	8.4	1.7
Tetrahydrofuran	−8.7	8.4	1.7
Dichloromethane	< – 10[a]	–	–
Ethanol	−4.9	0.6	0.5
Methanol-d4	−4.4	0.5	0.4
DMSO-d6	−3.5	0.3	0.3

[a]Only one peak observed in NMR spectrum that was assigned to the folded conformer.

Table S3.18: Experimental conformational free energy differences of molecular balance **24,** ΔG_{EXP} measured in various solvents at 298 K.

24			
		Error	
	ΔG / kJ mol^{-1}	–	+
Chloroform-d	< – 10[a]	–	–
Acetone	–5.1	0.7	0.5
Acetonitrile-d3	–4.5	0.5	0.4
Ethyl acetate	–6.3	1.2	0.8
Tetrahydrofuran	–6.3	1.2	0.8
Dichloromethane	< – 10[a]	–	–
Ethanol	–4.4	0.5	0.4
Methanol-d4	–3.8	0.4	0.3
DMSO-d6	–3.4	0.3	0.3

[a]Only one peak observed in NMR spectrum that was assigned to the folded conformer.

Table S3.19: Experimental conformational free energy differences of molecular balance **25,** ΔG_{EXP} measured in various solvents at 298 K.

25			
		Error	
	ΔG / kJ mol^{-1}	-	+
Chloroform-d	–7.4	2.3	1.2
Acetone	–4.5	0.5	0.4
Acetonitrile-d3	–3.9	0.4	0.3
Ethyl acetate	–6.3	1.2	0.8
Tetrahydrofuran	–6.3	1.2	0.8
Dichloromethane	–7.0	1.7	1.0
Ethanol	–4.4	0.5	0.4
Methanol-d4	–3.9	0.4	0.3
DMSO-d6	–3.1	0.3	0.2

Table S3.20: Experimental conformational free energy differences of molecular balance **26,** ΔG_{EXP} measured in various solvents at 298 K.

26			
		Error	
	ΔG / kJ mol^{-1}	–	+
Chloroform-d	–8.0	3.4	1.4
Acetone	–4.7	0.6	0.5
Acetonitrile-d3	–4.4	0.5	0.4
Ethyl acetate	–6.0	1.0	0.7
Tetrahydrofuran	–6.0	1.0	0.7
Dichloromethane	–7.4	2.3	1.2
Ethanol	–4.1	0.4	0.4
Methanol-d4	–4.7	0.6	0.5
DMSO-d6	–3.2	0.3	0.3

Table S3.21: Experimental conformational free energy differences of molecular balance **27,** ΔG_{EXP} measured in various solvents at 298 K.

27			
		Error	
	ΔG / kJ mol^{-1}	-	+
Chloroform-d	–8.0	3.4	1.4
Acetone	–4.7	0.6	0.5
Acetonitrile-d3	–4.4	0.5	0.4
Ethyl acetate	–6.0	1.0	0.7
Tetrahydrofuran	–6.0	1.0	0.7
Dichloromethane	–7.4	2.3	1.2
Ethanol	–4.1	0.4	0.4
Methanol-d4	–3.8	0.4	0.3
DMSO-d6	–3.2	0.3	0.3

Table S3.22: Experimental conformational free energy differences of molecular balance **28,** ΔG_{EXP} measured in various solvents at 298 K.

28			
		Error	
	ΔG / kJ mol^{-1}	–	+
Chloroform-d	–4.9	0.6	0.5
Acetone	–4.0	0.4	0.4
Acetonitrile-d3	–3.4	0.3	0.3
Ethyl acetate	n.d.[a]	n.d.[a]	n.d.[a]
Tetrahydrofuran	–4.7	0.6	0.5
Dichloromethane	–4.4	0.5	0.4
Ethanol	–4.1	0.4	0.4
Methanol-d4	–3.6	0.4	0.3
DMSO-d6	–3.1	0.3	0.2

[a]Not determined due to peak overlap in the NMR spectrum.

Table S3.23: Experimental conformational free energy differences of molecular balance **29,** ΔG_{EXP} measured in various solvents at 298 K.

29			
		Error	
	ΔG / kJ mol^{-1}	-	+
Chloroform-d	–5.3	0.7	0.6
Acetone	–4.1	0.4	0.4
Acetonitrile-d3	–3.5	0.3	0.3
Ethyl acetate	–5.1	0.7	0.5
Tetrahydrofuran	–5.3	0.7	0.6
Dichloromethane	–4.7	0.6	0.5
Ethanol	–4.2	0.5	0.4
Methanol-d4	–3.8	0.4	0.3
DMSO-d6	–3.1	0.3	0.2

Water soluble series

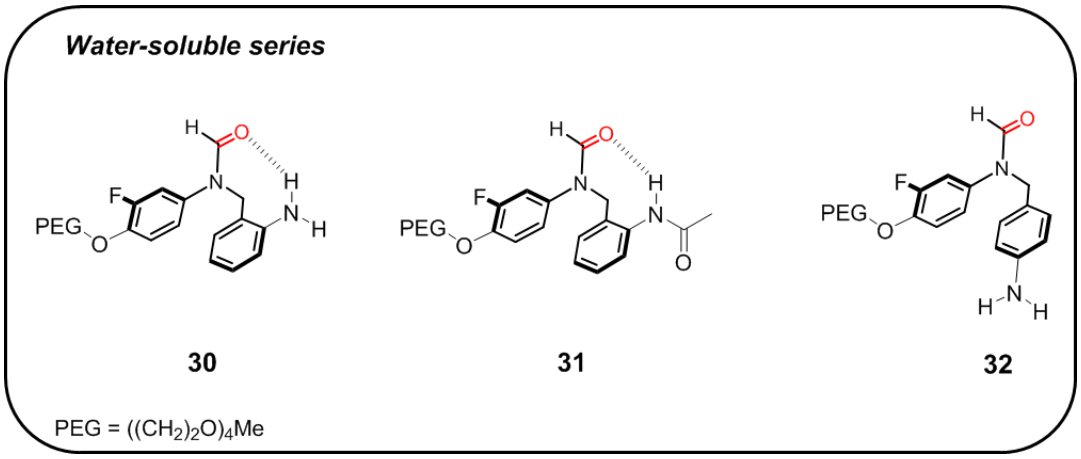

Table S3.24: Experimental conformational free energy differences of molecular balance **30**, ΔG_{EXP} measured in various solvents at 298 K.

30			
		Error	
	ΔG/ kJ mol^{-1}	–	+
Chloroform	< – 10[a]	–	–
Ethyl acetate	< – 10[a]	–	–
Tetrahydrofuran	< – 10[a]	–	–
Dichloromethane	< – 10[a]	–	–
Ethanol	–7.0	1.7	1.0
Acetone	< – 10[a]	–	–
Methanol	–6.6	1.4	0.9
Acetonitrile	–7.4	2.3	1.2
DMSO	–5.5	0.8	0.6
Water	–3.9	0.4	0.3
100 mM NaCl	–3.9	0.4	0.3
PBS pH 7.4	–3.8	0.4	0.3
1 % FBS/PBS pH 7.4	–3.6	0.4	0.3
10 % FBS/PBS pH 7.4	–3.6	0.4	0.3
50 % FBS/PBS pH 7.4	–3.6	0.4	0.3
Cell Lysate	–3.9	0.4	0.3

[a]Only one peak observed in NMR spectrum that was assigned to the folded conformer.

Table S3.25: Experimental conformational free energy differences of molecular balance **31**, ΔG_{EXP} measured in various solvents at 298 K.

	31		
		Error	
	ΔG/ kJ mol^{-1}	–	+
Chloroform	< – 10[a]	–	–
Ethyl acetate	< – 10[a]	–	–
Tetrahydrofuran	< – 10[a]	–	–
Dichloromethane	< – 10[a]	–	–
Ethanol	–6.3	1.2	0.8
Acetone	–8.0	3.4	1.4
Methanol	–5.7	0.9	0.7
Acetonitrile	–7.4	2.3	1.2
DMSO	–4.9	0.6	0.5
Water	–2.7	0.2	0.2
100 mM NaCl	–2.6	0.2	0.2
PBS pH 7.4	–2.6	0.2	0.2
1 % FBS/PBS pH 7.4	–2.7	0.2	0.2
10 % FBS/PBS pH 7.4	–2.7	0.2	0.2
50 % FBS/PBS pH 7.4	–2.7	0.2	0.2
Cell Lysate	–2.7	0.2	0.2

[a]Only one peak observed in NMR spectrum that was assigned to the folded conformer.

Table S3.26: Experimental conformational free energy differences of molecular balance **32**, ΔG_{EXP} measured in various solvents at 298 K.

32			
		Error	
	ΔG/ kJ mol^{-1}	–	+
Chloroform	–5.1	0.7	0.5
Ethyl acetate	–5.3	0.7	0.6
Tetrahydrofuran	–5.1	0.7	0.5
Dichloromethane	–4.7	0.6	0.5
Ethanol	–4.4	0.5	0.4
Acetone	–4.5	0.5	0.4
Methanol	–3.9	0.4	0.3
Acetonitrile	–4.0	0.4	0.4
DMSO	–3.9	0.4	0.3
Water	–1.8	0.2	0.2
100 mM NaCl	–1.8	0.2	0.2
PBS pH 7.4	–1.8	0.2	0.2
1 % FBS/PBS pH 7.4	–1.8	0.2	0.2
10 % FBS/PBS pH 7.4	–1.8	0.2	0.2
50 % FBS/PBS pH 7.4	–1.8	0.2	0.2
Cell Lysate	–1.8	0.2	0.2

Experimental energies plotted against solvent polarity parameter

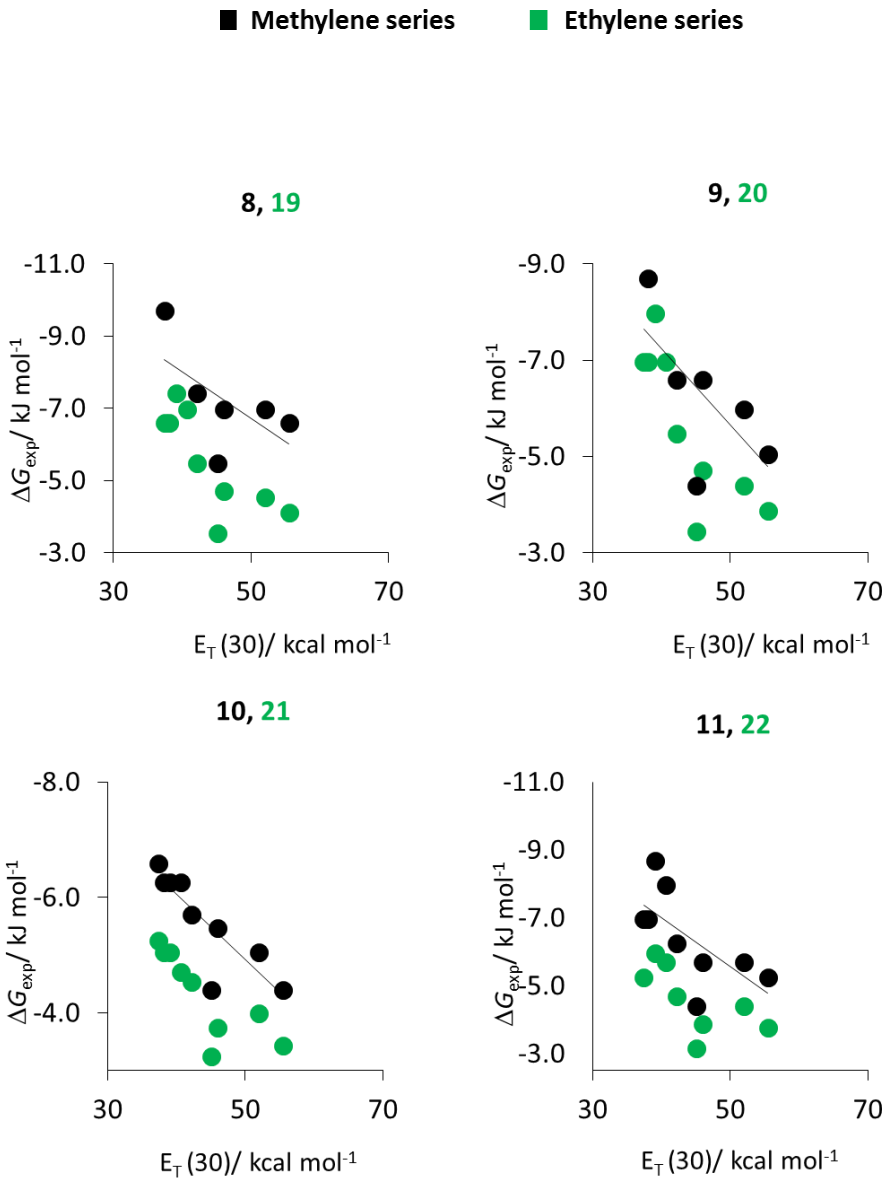

Figure S3.2: Correlation of ΔG_{exp} vs $E_T(30)$.

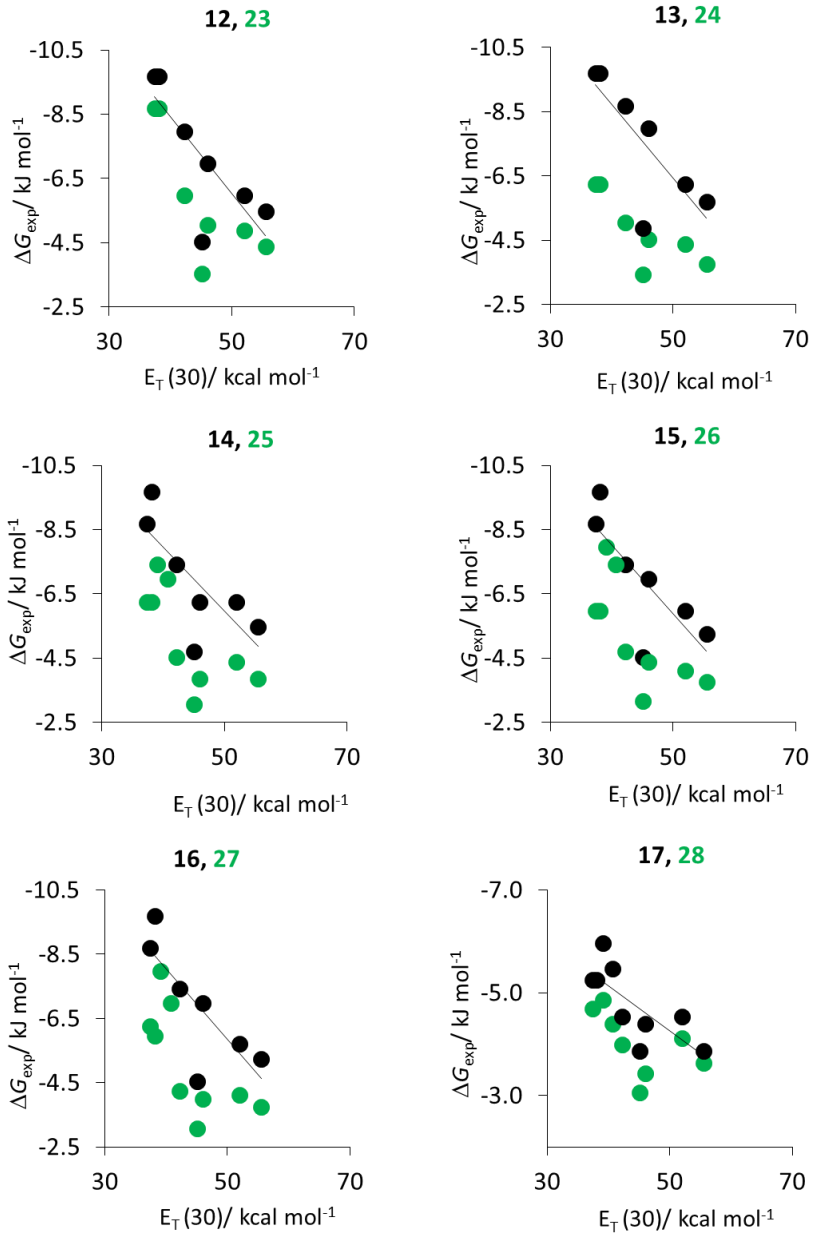

Figure S3.2(cont): Correlation of ΔG_{exp} vs $E_T(30)$.

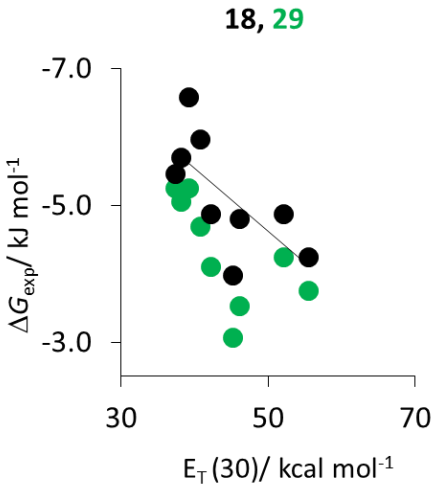

Figure S3.2 (cont): Correlation of ΔG_{exp} vs $E_T(30)$.

Van't Hoff analyses of compounds 15 and 26

Van't Hoff analysis was carried out on ~3.5 mM samples of compounds **15** and **26** in DMSO. Samples were prepared and placed in an air-tight Wilmad-cap NMR tube. Spectra were obtained at a minimum of seven temperatures, beginning with the coldest. Samples were equilibrated at each temperature for 30 minutes within the spectrometer. Results are shown in Table S3.28-S3.29 and Figures S3.3-3.4 showing the derivation of thermodynamic parameters from the gradient and intercept according to the equation $\Delta G = \Delta H - T\Delta S$.

Table S3.28: Van't Hoff analysis (**15** and **26**).

T/ K	1/*T*	15	26
300	0.00333	1.845	1.277
305	0.00328	1.808	1.273
310	0.00323	1.766	1.266
315	0.00317	1.760	1.259
320	0.00313	1.772	1.248
325	0.00308	one peak	1.241
330	0.00303	one peak	1.245

Table S3.29: Dissection of ΔH and TΔS at 300 K

Balance	$-T\Delta S$/ kJ mol^{-1}	ΔH/ kJ mol^{-1}	ΔG/ kJ mol^{-1}
15	−1.5 (+1.1, −1.2)	−3.1 ± 1.0	−4.6 (+0.4, −0.5)
26	−2.1 ± 0.3	−1.0 ± 0.1	−3.2 ± 0.3

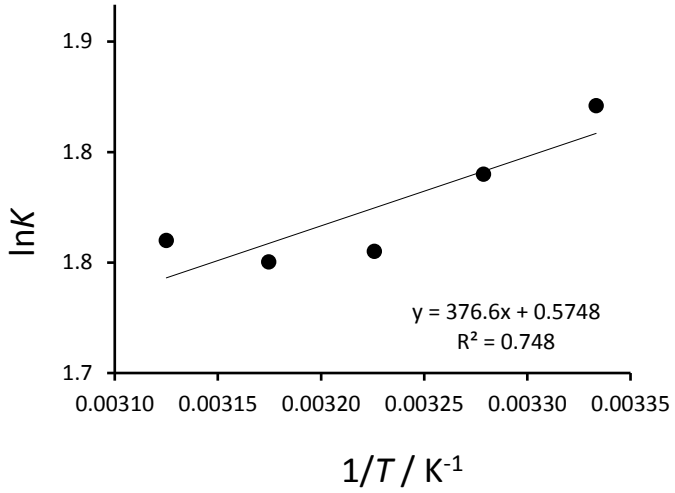

Figure S3.3: van't Hoff analysis for compound **15**.

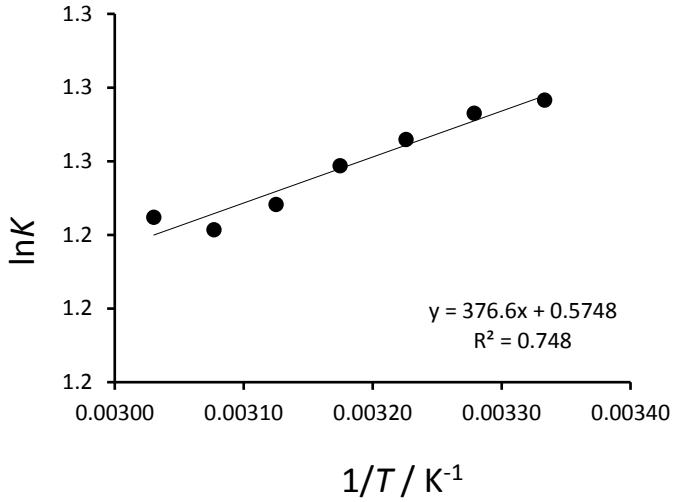

Figure S3.4: Van't Hoff analysis for compound **26**.

Linear regression to obtain modelled free energies ($\Delta G_{\alpha\beta\,\text{model}}$)

Multiple linear regression was performed in *Origin v8.5.1* for each data set for each balance in all solvents (using the constants listed in Table S30) to obtain the values of ΔE, $\Delta\alpha$ and $\Delta\beta$ quoted in the main text. Errors in $\Delta G_{\alpha\beta\ \text{model}}$ ($\delta\Delta G$) were calculated as follows:

$$\delta\Delta G = \sqrt{(\delta\Delta E)^2 + (\delta\Delta\alpha)^2 + (\delta\Delta\beta)^2}$$

where $\delta\Delta E$, $\delta\Delta\alpha$ and $\delta\Delta\beta$ are the fitting errors in ΔE, $\Delta\alpha$ and $\Delta\beta$ as output by *Origin*. $\Delta G_{\alpha\beta\ \text{model}}$ values are reported in Table S3.31.

Table S3.30: α_s and β_s values used in linear regressions

Solvent	α_s	β_s
Chloroform	2.2	0.9
Acetone	1.5	5.8
Acetonitrile	1.7	5.1
Ethyl acetate	1.5	5.3
THF	0.9	5.9
DCM	1.9	1.1
Ethanol	2.7	5.3
Methanol	2.7	5.3
DMSO	2.2	8.7

Table S3.31: Predicted energies of methylene (**8-18**) and ethylene (**19-29**) molecular balances series, with error analysis.

Compound	Solvent	ΔG_{exp}/kJ mol-1	$\Delta G_{\alpha/\beta\ \text{model}}$ /kJ mol-1	$\delta\Delta G$/kJ mol-1
8	**Chloroform-d**	< – 10[a]	–	–
	Acetone	–7.4	–7.9	2.6
	Acetonitrile-d3	–7.0	–8.0	2.6
	Ethyl acetate	n.d.[b]	n.d.[b]	n.d.[b]
	Tetrahydrofuran	–9.7	–8.8	2.6
	Dichloromethane	< – 10[a]	–	–
	Ethanol	–7.0	–6.4	2.6
	Methanol-d4	–6.6	–6.4	2.6
	DMSO-d6	–5.5	–5.6	2.6
9	**Chloroform-d**	< – 10[a]	–	–
	Acetone	–6.6	–7.2	3.0
	Acetonitrile-d3	–6.6	–7.3	3.0
	Ethyl acetate	–8.7	–7.5	3.0
	Tetrahydrofuran	< – 10[a]	–	–

	Dichloromethane	< – 10[a]	–	–
	Ethanol	–6.0	–5.5	3.0
	Methanol-d4	–5.1	–5.5	3.0
	DMSO-d6	–4.4	–4.3	3.0
10	**Chloroform-d**	–6.3	–6.1	0.5
	Acetone	–5.7	–5.8	0.5
	Acetonitrile-d3	–5.5	–5.8	0.5
	Ethyl acetate	–6.3	–6.0	0.5
	Tetrahydrofuran	–6.6	–6.5	0.5
	Dichloromethane	–6.3	–6.4	0.5
	Ethanol	–5.1	–4.7	0.5
	Methanol-d4	–4.4	–4.7	0.5
	DMSO-d6	–4.4	–4.5	0.5
11	**Chloroform-d**	–8.7	–8.2	0.8
	Acetone	–6.3	–6.3	0.8
	Acetonitrile-d3	–5.7	–6.5	0.8
	Ethyl acetate	–7.0	–6.6	0.8
	Tetrahydrofuran	–7.0	–6.8	0.8
	Dichloromethane	–8.0	–8.3	0.8
	Ethanol	–5.7	–5.5	0.8
	Methanol-d4	–5.3	–5.5	0.8
	DMSO-d6	–4.4	–4.2	0.8
12	**Chloroform-d**	< – 10[a]	–	–
	Acetone	–8.0	–8.2	2.3
	Acetonitrile-d3	–7.0	–8.2	2.3
	Ethyl acetate	–9.7	–8.5	2.3
	Tetrahydrofuran	–9.7	–9.6	2.3
	Dichloromethane	< – 10[a]	–	–
	Ethanol	–6.0	–5.6	2.3
	Methanol-d4	–5.5	–5.6	2.3
	DMSO-d6	–4.5	–4.6	2.3
13	**Chloroform-d**	< – 10[a]	–	–
	Acetone	–8.7	–8.6	1.3
	Acetonitrile-d3	–8.0	–8.6	1.3
	Ethyl acetate	–9.7	–8.9	1.3
	Tetrahydrofuran	–9.7	–10.0	1.3
	Dichloromethane	< – 10[a]	–	–
	Ethanol	–6.3	–6.0	1.3
	Methanol-d4	–5.7	–6.0	1.3
	DMSO-d6	–4.9	–4.9	1.3
14	**Chloroform-d**	< – 10[a]	–	–
	Acetone	–7.4	–7.7	3.2
	Acetonitrile-d3	–6.3	–7.7	3.2
	Ethyl acetate	–9.7	–8.0	3.2

	Tetrahydrofuran	−8.7	−8.8	3.2
	Dichloromethane	< − 10[a]	–	–
	Ethanol	−6.3	−5.8	3.2
	Methanol-d4	−5.5	−5.8	3.2
	DMSO-d6	−4.7	−4.7	3.2
15	**Chloroform-d**	< − 10[a]	–	–
	Acetone	−7.4	−7.8	2.6
	Acetonitrile-d3	−7.0	−7.8	2.6
	Ethyl acetate	n.d.[b]	n.d.[b]	n.d.[b]
	Tetrahydrofuran	−8.7	−9.0	2.6
	Dichloromethane	< − 10[a]	–	–
	Ethanol	−6.0	−5.6	2.6
	Methanol-d4	−5.3	−5.6	2.6
	DMSO-d6	−4.5	−4.5	2.6
16	**Chloroform-d**	< − 10[a]	–	–
	Acetone	−7.4	−7.8	2.5
	Acetonitrile-d3	−7.0	−7.8	2.5
	Ethyl acetate	n.d.[b]	n.d.[b]	n.d.[b]
	Tetrahydrofuran	−8.7	−9.0	2.5
	Dichloromethane	< − 10[a]	–	–
	Ethanol	−5.7	−5.5	2.5
	Methanol-d4	−5.3	−5.5	2.5
	DMSO-d6	−4.5	−4.5	2.5
17	**Chloroform-d**	−6.0	−5.6	0.6
	Acetone	−4.5	−4.8	0.6
	Acetonitrile-d3	−4.4	−4.9	0.6
	Ethyl acetate	−5.3	−4.9	0.6
	Tetrahydrofuran	−5.3	−5.1	0.6
	Dichloromethane	−5.5	−5.7	0.6
	Ethanol	n.d.[b]	n.d.[b]	n.d.[b]
	Methanol-d4	−3.9	−4.2	0.6
	DMSO-d6	−4.1	−3.7	0.6
18	**Chloroform-d**	−6.6	−6.2	0.6
	Acetone	−4.9	−5.1	0.6
	Acetonitrile-d3	−4.7	−5.2	0.6
	Ethyl acetate	−5.7	−5.3	0.6
	Tetrahydrofuran	−5.5	−5.4	0.6
	Dichloromethane	−6.0	−6.3	0.6
	Ethanol	−4.9	−4.6	0.6
	Methanol-d4	−4.2	−4.6	0.6
	DMSO-d6	−4.0	−3.9	0.6
19	**Chloroform-d**	−7.4	−7.0	1.0
	Acetone	−5.5	−5.7	1.0
	Acetonitrile-d3	−4.7	−5.7	1.0
	Ethyl acetate	−6.6	−5.9	1.0

	Tetrahydrofuran	–6.6	–6.4	1.0
	Dichloromethane	–7.0	–7.3	1.0
	Ethanol	–4.5	–4.3	1.0
	Methanol-d4	–4.1	–4.3	1.0
	DMSO-d6	–3.5	–3.4	1.0
20	**Chloroform-d**	–8.0	–7.2	1.3
	Acetone	–5.5	–5.8	1.3
	Acetonitrile-d3	–4.7	–5.9	1.3
	Ethyl acetate	–7.0	–6.1	1.3
	Tetrahydrofuran	–7.0	–6.7	1.3
	Dichloromethane	–7.0	–7.6	1.3
	Ethanol	–4.4	–4.2	1.3
	Methanol-d4	–3.9	–4.2	1.3
	DMSO-d6	–3.4	–3.2	1.3
21	**Chloroform-d**	–5.1	–4.8	0.7
	Acetone	–4.5	–4.5	0.7
	Acetonitrile-d3	–3.8	–4.5	0.7
	Ethyl acetate	–5.1	–4.6	0.7
	Tetrahydrofuran	–5.3	–5.0	0.7
	Dichloromethane	–4.7	–5.0	0.7
	Ethanol	–4.0	–3.6	0.7
	Methanol-d4	–3.4	–3.6	0.7
	DMSO-d6	–3.2	–3.4	0.7
22	**Chloroform-d**	–6.0	–5.7	0.8
	Acetone	–4.7	–4.6	0.8
	Acetonitrile-d3	–3.9	–4.7	0.8
	Ethyl acetate	n.d.[b]	n.d.[b]	n.d.[b]
	Tetrahydrofuran	–5.3	–4.9	0.8
	Dichloromethane	–5.7	–5.9	0.8
	Ethanol	–4.4	–4.0	0.8
	Methanol-d4	–3.8	–4.0	0.8
	DMSO-d6	–3.2	–3.2	0.8
23	**Chloroform-d**	< – 10[a]	–	–
	Acetone	–6.0	–6.8	3.6
	Acetonitrile-d3	–5.1	–6.8	3.6
	Ethyl acetate	–8.7	–7.1	3.6
	Tetrahydrofuran	–8.7	–8.2	3.6
	Dichloromethane	< – 10[a]	–	–
	Ethanol	–4.9	–4.3	3.6
	Methanol-d4	–4.4	–4.3	3.6
	DMSO-d6	–3.5	–3.6	3.6
24	**Chloroform-d**	< – 10[a]	–	–
	Acetone	–5.1	–5.4	1.5
	Acetonitrile-d3	–4.5	–5.3	1.5
	Ethyl acetate	–6.3	–5.5	1.5
	Tetrahydrofuran	–6.3	–6.1	1.5
	Dichloromethane	< – 10[a]	–	–
	Ethanol	–4.4	–4.0	1.5
	Methanol-d4	–3.8	–4.0	1.5
	DMSO-d6	–3.4	–3.5	1.5
25	**Chloroform-d**	–7.4	–7.0	1.4

	Acetone	–4.5	–5.1	1.4
	Acetonitrile-d3	–3.9	–5.3	1.4
	Ethyl acetate	–6.3	–5.4	1.4
	Tetrahydrofuran	–6.3	–5.8	1.4
	Dichloromethane	–7.0	–7.2	1.4
	Ethanol	–4.4	–4.1	1.4
	Methanol-d4	–3.9	–4.1	1.4
	DMSO-d6	–3.1	–2.8	1.4
26	**Chloroform-d**	–8.0	–7.4	1.0
	Acetone	–4.7	–5.1	1.0
	Acetonitrile-d3	–4.4	–5.3	1.0
	Ethyl acetate	–6.0	–5.4	1.0
	Tetrahydrofuran	–6.0	–5.7	1.0
	Dichloromethane	–7.4	–7.6	1.0
	Ethanol	–4.1	–4.1	1.0
	Methanol-d4	–4.7	–4.1	1.0
	DMSO-d6	–3.2	–2.6	1.0
27	**Chloroform-d**	–8.0	–7.2	1.5
	Acetone	–4.7	–5.0	1.5
	Acetonitrile-d3	–4.4	–5.2	1.5
	Ethyl acetate	–6.0	–5.3	1.5
	Tetrahydrofuran	–6.0	–5.7	1.5
	Dichloromethane	–7.4	–7.4	1.5
	Ethanol	–4.1	–4.0	1.5
	Methanol-d4	–3.8	–4.0	1.5
	DMSO-d6	–3.2	–2.6	1.5
28	**Chloroform-d**	–4.9	–4.6	0.8
	Acetone	–4.0	–4.0	0.8
	Acetonitrile-d3	–3.4	–4.1	0.8
	Ethyl acetate	n.d.[b]	n.d.[b]	n.d.[b]
	Tetrahydrofuran	–4.7	–4.2	0.8
	Dichloromethane	–4.4	–4.7	0.8
	Ethanol	–4.1	–3.7	0.8
	Methanol-d4	–3.6	–3.7	0.8
	DMSO-d6	–3.1	–3.3	0.8
29	**Chloroform-d**	–5.3	–5.0	1.0
	Acetone	–4.1	–4.4	1.0
	Acetonitrile-d3	–3.5	–4.4	1.0
	Ethyl acetate	–5.1	–4.5	1.0
	Tetrahydrofuran	–5.3	–4.8	1.0
	Dichloromethane	–4.7	–5.1	1.0
	Ethanol	–4.2	–3.7	1.0
	Methanol-d4	–3.8	–3.7	1.0
	DMSO-d6	–3.1	–3.3	1.0

[a]Only one peak observed in NMR spectrum that was assigned to the folded conformer.

[b]Not determined due to peak overlap in the NMR spectrum.

Conformer assignment by NMR spectroscopy

The following figures present the NMR spectra (^{1}H, ^{13}C, HSQC, COSY, NOESY and HMBC) of N-[2-[(4-fluoro-N-formyl-anilino)methyl]phenyl]-2,2-dimethyl-propanamide (compound **14**) in DMSO-d_6, showing the full spectral assignment for both conformers. The proton resonances have been labelled numerically and carbon resonances alphabetically. Red peaks with prime notation (') denotes a minor conformer, while blue indicates the major conformer.

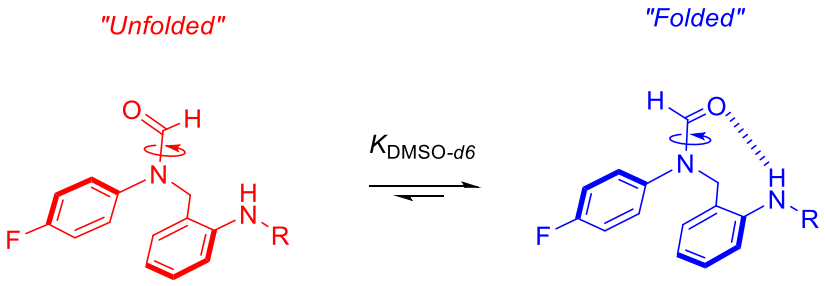

The major and minor conformers were unambiguously distinguished by analysing the HMBC spectra (Figure S3.7); H-C correlation through multiple bonds. The formyl proton has a cross peak with the *trans*-CH_2 carbon in the H-bonded conformer, whereas in the unbound conformer the formyl proton has a *trans*-cross peak with trans-quaternary aromatic carbon.

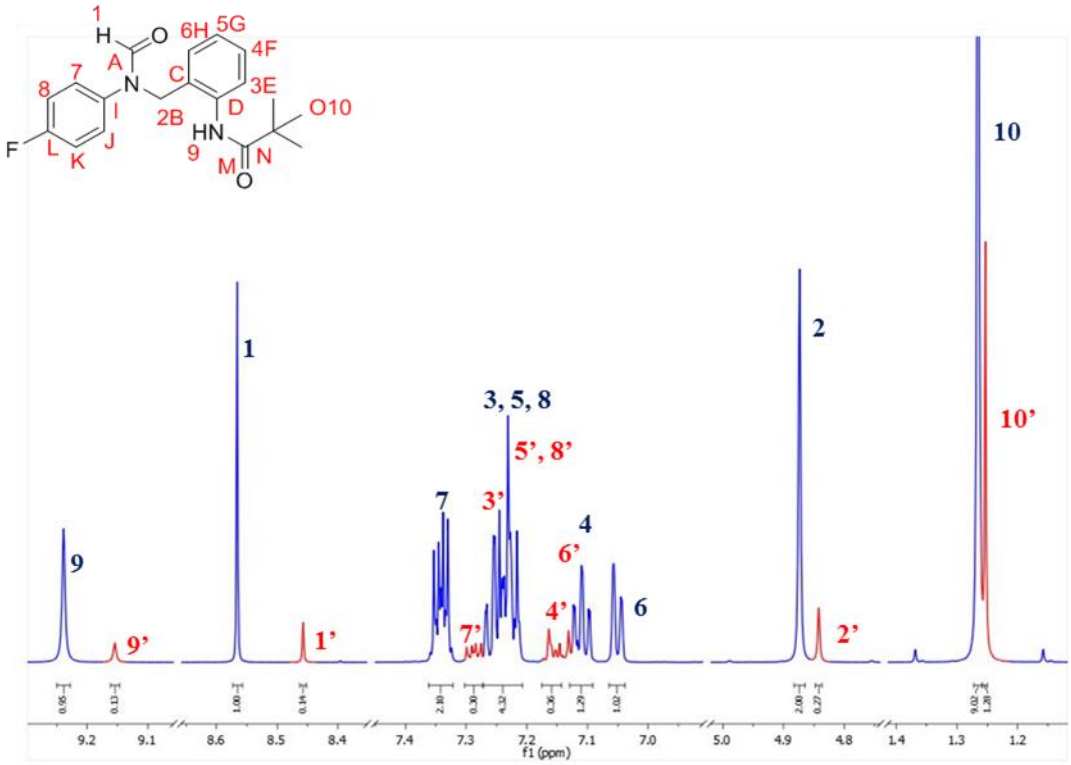

Figure S3.5: ^{1}H NMR spectrum of compound **14** in DMSO-d_6.

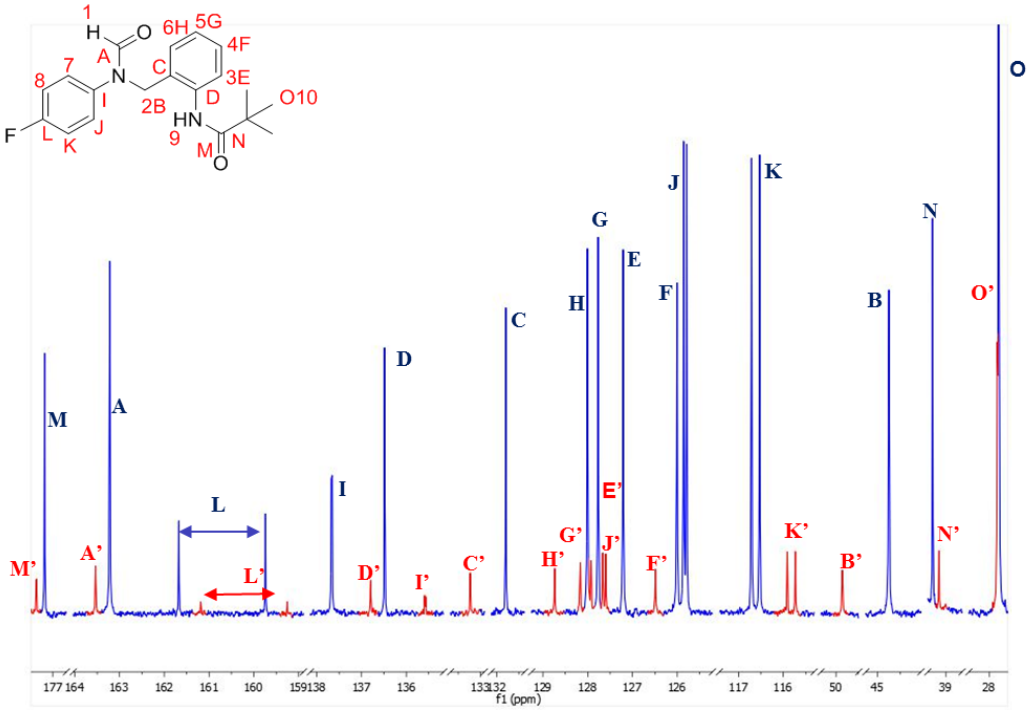

Figure S3.6: ^{13}C NMR spectrum of compound **14** in DMSO-d_6.

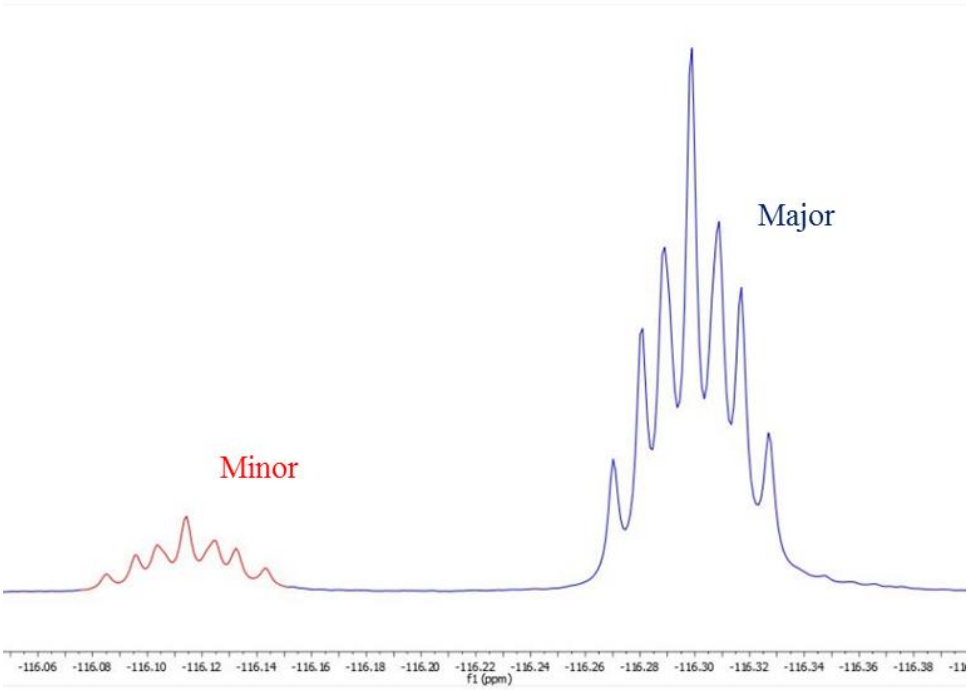

Figure S3.7: ^{19}F NMR spectrum of compound **14** in DMSO-d_6.

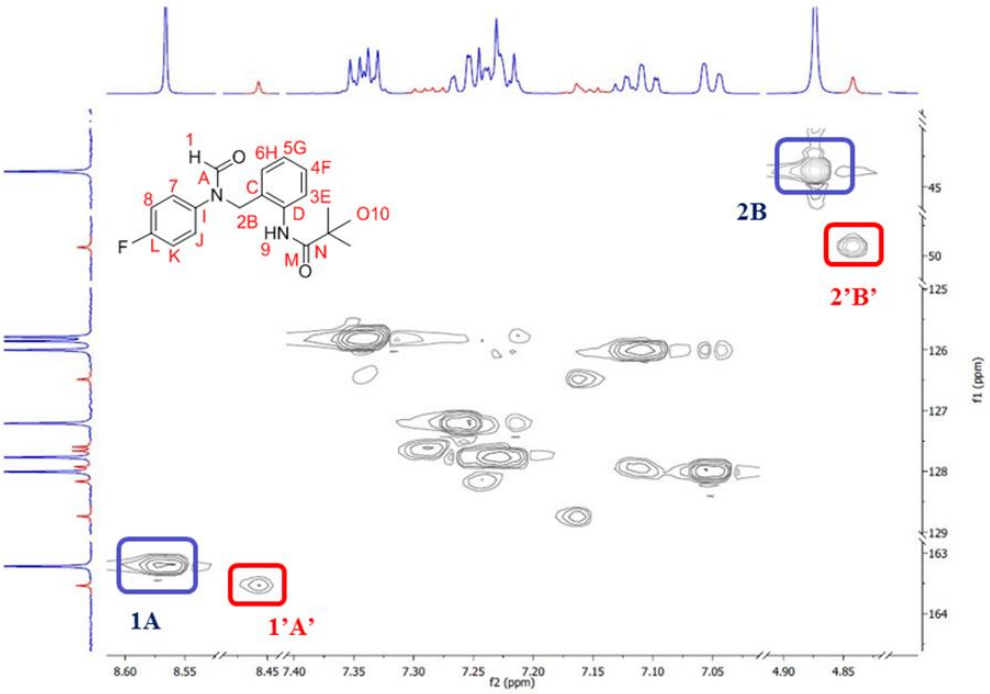

Figure S3.8: HSQC spectrum compound **14** in DMSO-d_6.

In the example depicted in Figure S7, the major formyl proton 1 couples to carbon B, and the minor formyl proton 1' couples with I'.

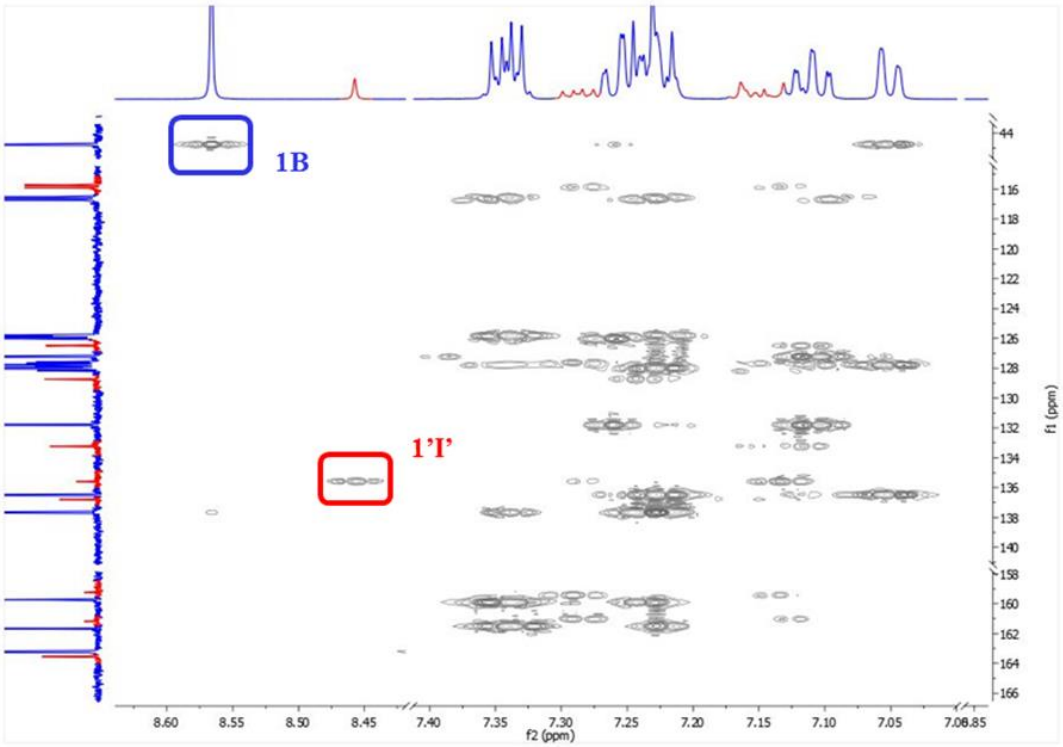

Figure S3.9: HMBC NMR spectrum compound **14** in DMSO-d_6.

Computational methods and data

Geometry minimization and calculated conformational energies

Conformer distribution searches were performed on full molecular balances using Spartan ’14 with DFT/B3LYP/6-31G* to obtain the minimised geometries of the unfolded and folded conformers. The resulting gas phase energies and corresponding energy differences, ΔG_{DFT} in each conformer are reported in Tables **S3.32** and Table **S3.33**. The minimized B3LYP/6-31G* geometries of the folded and unfolded are presented in Figures **S3.11**.

Table S3.32: Calculated energies of methylene molecular balance series using DFT/B3LYP/6-31G*.

Compound	Energy folded conformer/ kJ mol^{-1}	Energy unfolded conformer/ kJ mol^{-1}	ΔG_{DFT}/ kJ mol^{-1}	ESP_{N-H}/kJ mol^{-1}
8	–2168382.72	–2168357.04	–25.68	212.80
9	–2775006.32	–2774975.31	–31.01	208.80
10	–3075676.88	–3075665.46	–11.42	58.30
11	–3017187.93	–3017170.65	–17.28	74.30
12	–2569202.53	–2569168.79	–33.74	173.80
13	–3350833.51	–3350803.96	–29.55	133.00
14	–2878852.66	–2878820.25	–32.41	139.70
15	–3072608.36	–3072576.89	–31.47	196.10
16	–3373291.82	–3373263.77	–28.05	232.40
17	–3114720.65	–3114712.84	–7.81	215.40
18	–3375251.93	–3375239.88	–12.05	227.80

Table S3.33: Calculated energies of ethylene molecular balance series using DFT/B3LYP/6-31G*.

Compound	Energy folded conformer/ kJ mol^{-1}	Energy unfolded conformer/ kJ mol^{-1}	ΔG_{DFT}/ kJ mol^{-1}	ESP_{N-H}/kJ mol^{-1}
19	–2271602.61	–2271581.46	–21.15	212.80
20	–2878225.95	–2878200.78	–25.17	208.80
21	–3373338.26	–3373313.30	–24.96	58.30
22	–3120409.74	–3120395.91	–13.83	74.30
23	–2672423.69	–2672391.95	–31.74	173.80
24	–3454051.86	–3454031.22	–20.64	133.00
25	–2982069.38	–2982042.84	–26.54	139.70
26	–3175823.57	–3175801.70	–21.87	196.10
27	–3476505.30	–3476489.23	–16.07	232.40
28	–3217944.33	–3217934.66	–9.67	215.40
29	–3478472.28	–3478465.21	–7.07	227.80

Optimised geometries of ethylene molecular balance series (19-29).

19

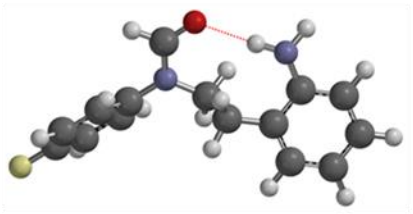

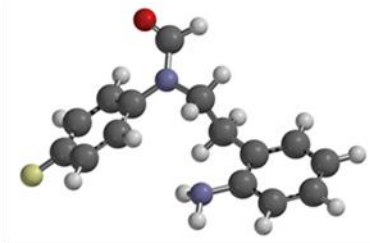

20

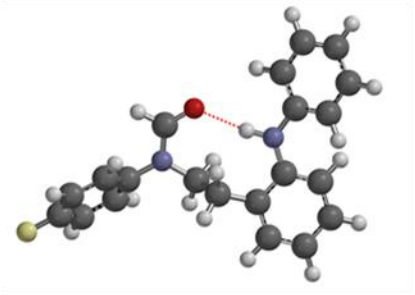

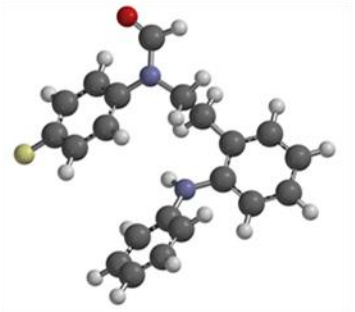

21

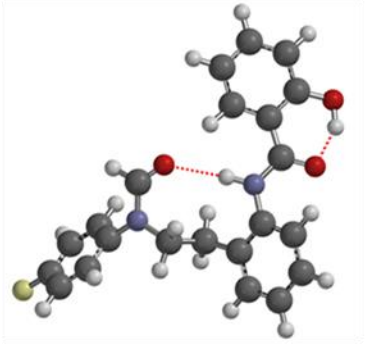

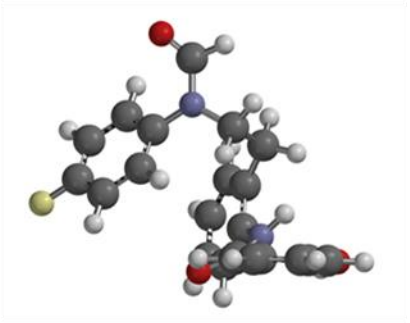

22

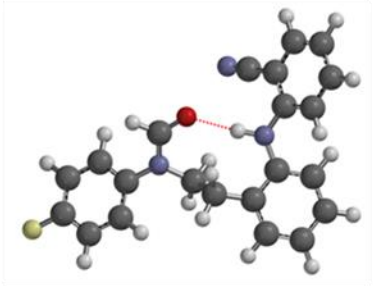

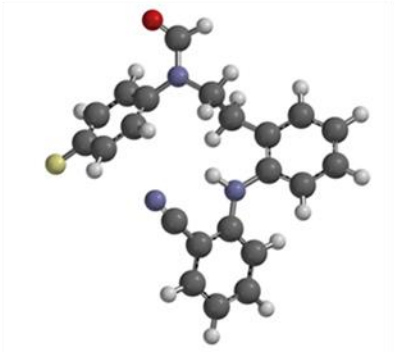

23

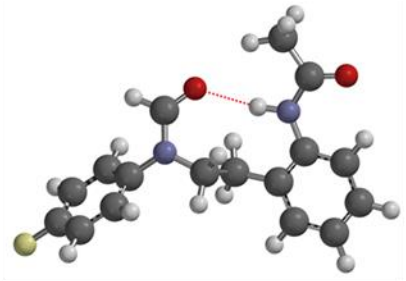

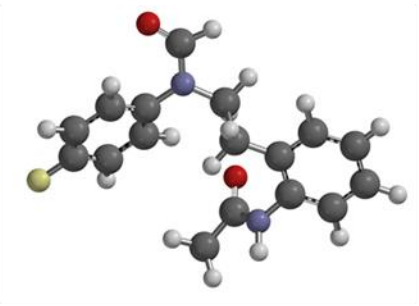

24

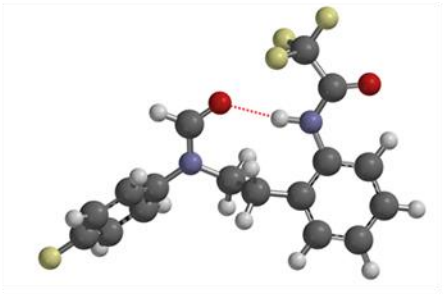

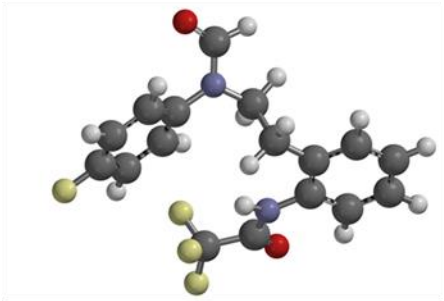

25

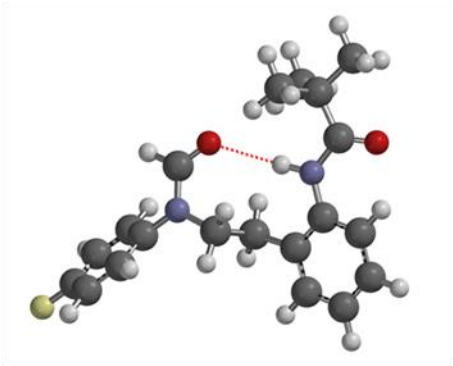

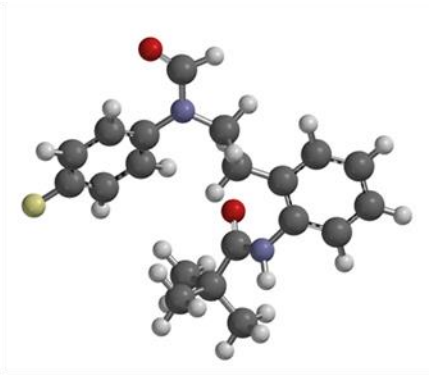

26

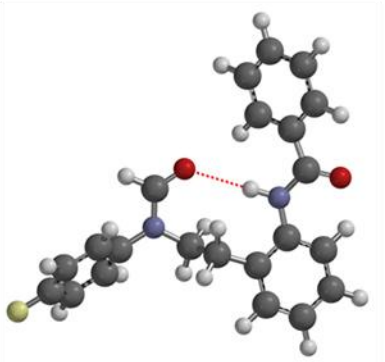

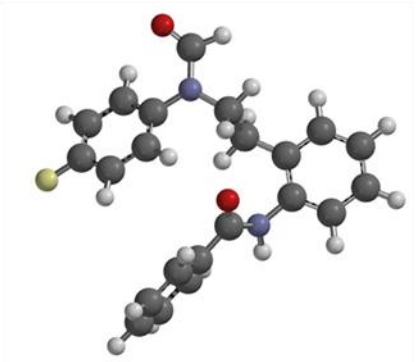

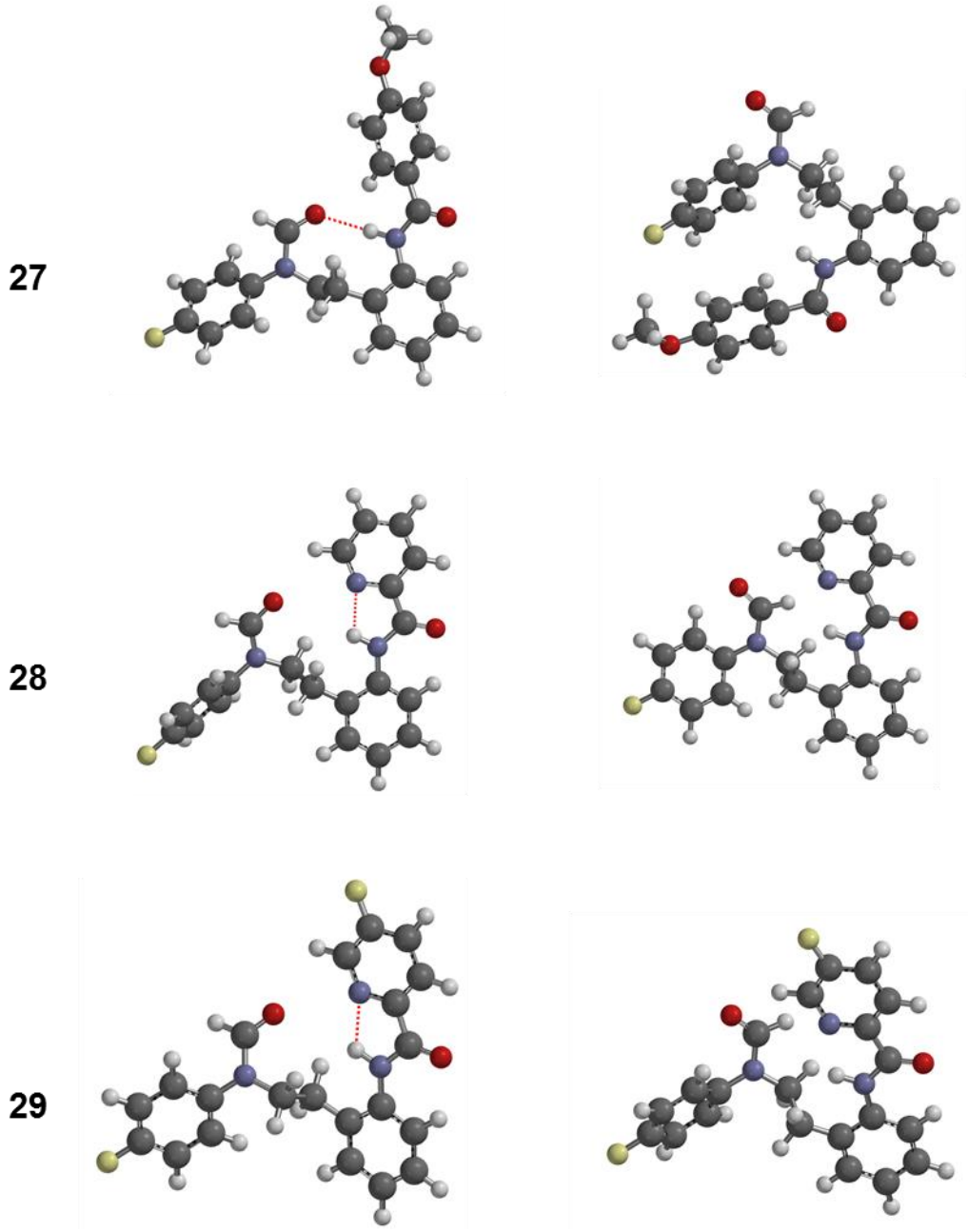

Figure S3.10: DFT/B3LYP/6-31G* minimised structures of balances (**19-29**) both the folded and unfolded conformers.

Barrier to rotation calculation

Table 3.34: Energy profile calculation performed for molecular balance **8** at the DFT/B3LYP/6-31G* level of theory.

Relative energy/ kJ mol^{-1}	Dihedral/°
0.0	-2.0
1.5	8.3
6.5	18.6
14.6	28.9
25.7	39.2
39.8	49.5
56.1	59.8
73.7	70.1
90.8	80.3
105.8	90.6
116.9	100.9
123.4	111.2
67.1	121.5
57.7	131.8
49.5	142.1
43.0	152.3
39.0	162.6
36.3	172.9
25.9	-176.8
26.6	-166.5
29.9	-156.2
35.5	-146.0
43.1	-135.7
52.4	-125.4
62.8	-115.1
73.4	-104.8
83.5	-94.5
92.0	-84.2
98.0	-74.0
99.6	-63.7
57.0	-53.4
43.9	-43.1
33.1	-32.8
25.3	-22.5
20.1	-12.2
18.3	-2.0

Experimental energies plotted against computational energies

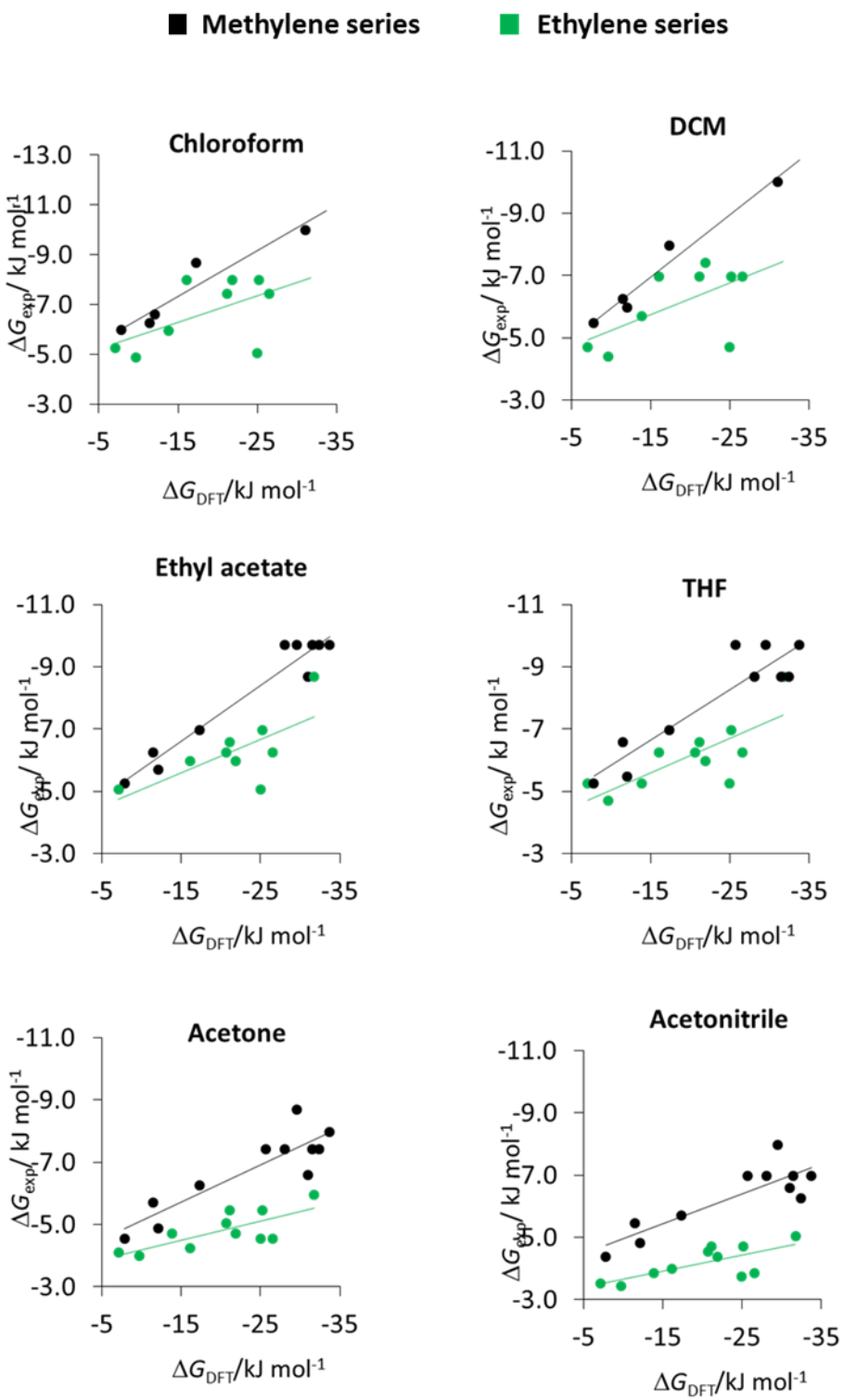

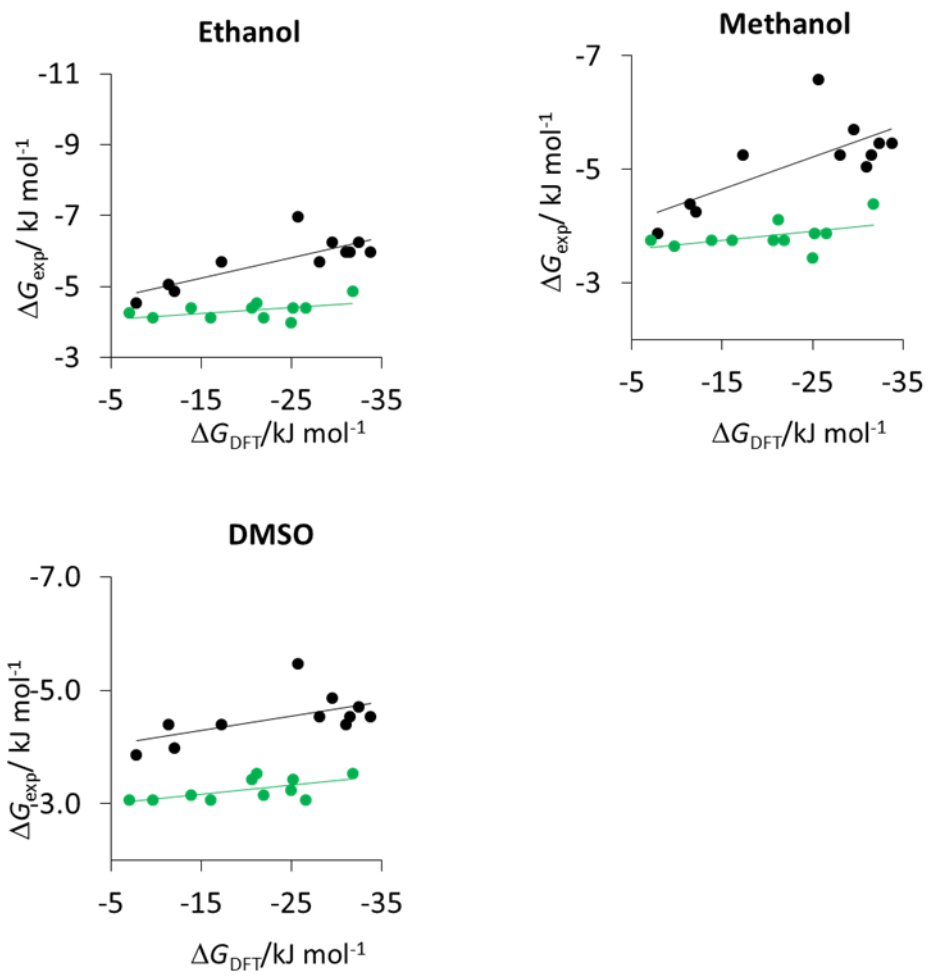

Figure S3.11. Experimental energies of molecular balances **8-29** in nine different solvents plotted against computationally derived equilibrium energies.

Crystallographic data

Experimental. Single colourless block-shaped crystals of (**Compound 12**) were recrystallised from DCM by slow evaporation. A suitable crystal (0.34×0.16×0.05) mm^3 was selected and mounted on a MITIGEN holder in Paratone oil on a Rigaku Oxford Diffraction SuperNova diffractometer. The crystal was kept at T = 120.0 K during data collection. Using **Olex2** (Dolomanov et al., 2009), the structure was solved with the **ShelXS** (Sheldrick, 2008) structure solution program, using the Direct Methods solution method. The model was refined with version 2016/6 of **ShelXL** (Sheldrick, 2015) using Least Squares minimisation.

Crystal Data. $C_{16}H_{15}FN_2O_2$, M_r = 286.30, triclinic, P-1 (No. 2), a = 7.7752(4) Å, b = 9.3986(5) Å, c = 10.6511(7) Å, α = 101.842(5)°, β = 102.717(5)°, γ = 108.474(5)°, V = 687.59(8) $Å^3$, T = 120.0 K, Z = 2, Z' = 1, μ(MoK$_\alpha$) = 0.102, 12391 reflections measured, 3454 unique (R_{int} = 0.0392) which were used in all calculations. The final wR_2 was 0.1079 (all data) and R_1 was 0.0516 (I > 2(I)).

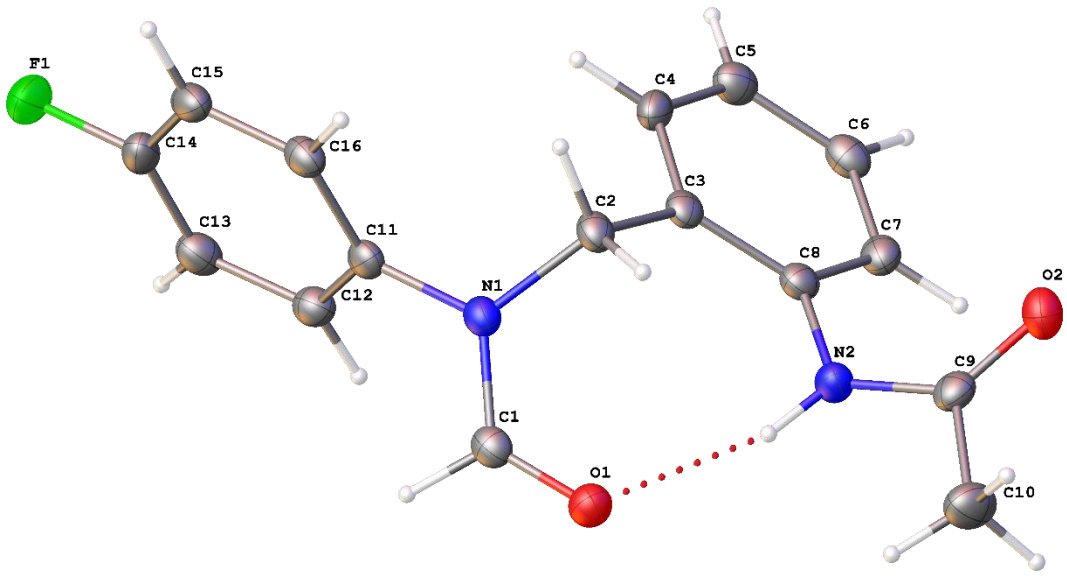

Figure S3.12: The molecular structure of compound **12**. Displacement ellipsoids are at the 50% probability level.

Table 3.35: Crystallographic data for molecular balance **12**.

Compound	**12**
Formula	$C_{16}H_{15}FN_2O_2$
$D_{calc.}$/ g cm^{-3}	1.383
μ/mm^{-1}	0.102
Formula Weight	286.30
Colour	colourless
Shape	block
Size/mm^3	0.34×0.16×0.05
T/K	120.0
Crystal System	triclinic
Space Group	P-1
a/Å	7.7752(4)
b/Å	9.3986(5)
c/Å	10.6511(7)
α/°	101.842(5)
β/°	102.717(5)
γ/°	108.474(5)
V/Å^3	687.59(8)
Z	2
Z'	1
Wavelength/Å	0.71073
Radiation type	MoK_α
Θ_{min}/°	3.516
Θ_{max}/°	29.678
Measured Refl.	12391
Independent Refl.	3454
Reflections Used	2726
R_{int}	0.0392
Parameters	195
Restraints	0
Largest Peak	0.246
Deepest Hole	-0.253
GooF	1.064
wR_2 (all data)	0.1079
wR_2	0.0992
R_1 (all data)	0.0695
R_1	0.0516

Table S3.36: Fractional Atomic Coordinates (×10⁴) and Equivalent Isotropic Displacement Parameters (Å²×10³) for **12**. U_{eq} is defined as 1/3 of the trace of the orthogonalised U_{ij}.

Atom	x	y	z	U_{eq}
F1	9355.9(16)	-152.6(13)	6221.0(11)	35.0(3)
O1	2905.5(17)	4353.0(14)	5526.4(12)	23.5(3)
O2	3266.6(17)	8213.2(14)	9718.9(12)	26.3(3)
N1	4699.6(19)	3201.4(15)	6616.7(13)	18.4(3)
N2	3862(2)	6734.3(17)	8016.7(15)	21.2(3)
C1	3879(2)	3543.5(18)	5532.0(16)	19.0(3)
C2	4428(2)	3788.0(19)	7929.3(16)	19.3(3)
C3	5928(2)	5378.3(18)	8763.6(15)	17.4(3)
C4	7666(2)	5469(2)	9563.9(16)	20.2(3)
C5	9068(2)	6896(2)	10372.9(17)	22.4(4)
C6	8747(2)	8267(2)	10393.3(17)	21.7(4)
C7	7032(2)	8216.1(19)	9618.2(16)	20.7(3)
C8	5622(2)	6777.4(19)	8805.4(15)	18.3(3)
C9	2796(2)	7461.2(19)	8535.8(17)	20.5(3)
C10	975(3)	7262(2)	7521.7(19)	30.6(4)
C11	5927(2)	2352.0(18)	6528.8(15)	17.9(3)
C12	7403(2)	2832.3(19)	5984.9(16)	20.7(3)
C13	8559(2)	1980(2)	5864.0(17)	23.8(4)
C14	8218(3)	681(2)	6318.1(17)	24.2(4)
C15	6795(3)	195(2)	6886.3(16)	23.3(4)
C16	5631(2)	1036.0(19)	6986.9(16)	20.7(3)

Table S3.37: Anisotropic Displacement Parameters (×10⁴) **12**. The anisotropic displacement factor exponent takes the form: $-2\pi^2[h^2a^{*2} \times U_{11} + \ldots + 2hka^* \times b^* \times U_{12}]$

Atom	U_{11}	U_{22}	U_{33}	U_{23}	U_{13}	U_{12}
F1	45.9(7)	42.9(7)	32.3(6)	14.2(5)	15.4(5)	33.4(6)
O1	25.0(6)	24.2(6)	21.9(6)	6.0(5)	5.2(5)	12.0(5)
O2	28.7(7)	24.2(6)	26.3(7)	3.6(5)	10.2(5)	11.9(6)
N1	22.0(7)	16.6(6)	16.8(7)	4.3(5)	7.0(6)	7.3(6)
N2	24.7(8)	21.7(7)	17.5(7)	3.9(6)	3.9(6)	12.2(6)
C1	19.8(8)	17.3(8)	17.1(8)	4.0(6)	6.0(6)	4.1(7)
C2	25.0(9)	18.1(8)	17.4(8)	5.7(6)	10.8(7)	8.3(7)
C3	21.4(8)	18.3(8)	15.4(8)	6.1(6)	9.9(6)	7.7(7)
C4	26.1(9)	21.7(8)	19.7(8)	7.9(7)	11.0(7)	14.4(7)
C5	20.4(8)	29.1(9)	19.8(8)	7.2(7)	7.4(7)	11.3(7)
C6	21.4(8)	22.3(8)	18.2(8)	4.6(7)	7.5(7)	3.8(7)
C7	27.4(9)	17.3(8)	20.2(8)	7.7(6)	9.7(7)	9.3(7)
C8	20.7(8)	21.4(8)	14.8(8)	6.0(6)	7.3(6)	9.0(7)
C9	24.0(9)	18.0(8)	23.5(9)	10.1(7)	8.8(7)	9.6(7)
C10	29.6(10)	40.8(11)	30.3(10)	15.2(8)	10.4(8)	20.8(9)
C11	20.0(8)	15.7(7)	13.9(8)	0.8(6)	2.4(6)	5.7(7)
C12	22.7(8)	19.5(8)	18.2(8)	5.5(6)	5.0(7)	6.6(7)
C13	23.0(9)	30.4(9)	18.2(8)	6.3(7)	6.5(7)	11.0(8)
C14	29.7(9)	27.0(9)	18.3(8)	3.5(7)	4.3(7)	18.2(8)
C15	34.1(10)	18.5(8)	16.4(8)	4.4(6)	5.3(7)	10.8(8)
C16	24.7(9)	18.3(8)	16.3(8)	3.3(6)	6.4(7)	5.5(7)

Table S3.38: Bond Lengths in Å for **12.**

Atom	Atom	Length/Å
F1	C14	1.3616(19)
O1	C1	1.2315(19)

Atom	Atom	Length/Å
O2	C9	1.220(2)
N1	C1	1.343(2)
N1	C2	1.480(2)
N1	C11	1.431(2)
N2	C8	1.423(2)
N2	C9	1.365(2)
C2	C3	1.509(2)
C3	C4	1.397(2)
C3	C8	1.402(2)
C4	C5	1.384(2)
C5	C6	1.385(2)
C6	C7	1.386(2)
C7	C8	1.393(2)
C9	C10	1.511(2)
C11	C12	1.388(2)
C11	C16	1.392(2)
C12	C13	1.390(2)
C13	C14	1.374(2)
C14	C15	1.374(3)
C15	C16	1.384(2)

Table S3.39: Bond Angles in ° for **12**.

Atom	Atom	Atom	Angle/°
C1	N1	C2	119.84(13)
C1	N1	C11	120.30(13)
C11	N1	C2	119.76(13)
C9	N2	C8	123.18(14)
O1	C1	N1	125.19(15)
N1	C2	C3	112.90(13)
C4	C3	C2	119.23(14)
C4	C3	C8	118.25(15)
C8	C3	C2	122.48(14)
C5	C4	C3	121.44(15)
C4	C5	C6	119.49(16)
C5	C6	C7	120.48(16)
C6	C7	C8	119.88(15)
C3	C8	N2	120.01(15)
C7	C8	N2	119.54(14)
C7	C8	C3	120.46(15)
O2	C9	N2	123.16(15)
O2	C9	C10	122.40(15)
N2	C9	C10	114.44(15)
C12	C11	N1	120.27(14)
C12	C11	C16	120.03(15)
C16	C11	N1	119.69(15)
C11	C12	C13	120.21(16)
C14	C13	C12	118.15(16)
F1	C14	C13	118.72(16)
F1	C14	C15	118.27(15)
C15	C14	C13	123.00(15)
C14	C15	C16	118.56(15)
C15	C16	C11	120.02(16)

Table S3.40: Torsion Angles in ° for **12**.

Atom	Atom	Atom	Atom	Angle/°
F1	C14	C15	C16	-179.94(15)
N1	C2	C3	C4	-84.22(18)
N1	C2	C3	C8	98.06(17)
N1	C11	C12	C13	-178.13(14)
N1	C11	C16	C15	179.02(14)
C1	N1	C2	C3	-89.90(18)
C1	N1	C11	C12	50.4(2)
C1	N1	C11	C16	-129.38(17)
C2	N1	C1	O1	1.3(2)
C2	N1	C11	C12	-125.91(16)
C2	N1	C11	C16	54.3(2)
C2	C3	C4	C5	-178.34(15)
C2	C3	C8	N2	-1.5(2)
C2	C3	C8	C7	178.31(14)
C3	C4	C5	C6	0.0(2)
C4	C3	C8	N2	-179.28(14)
C4	C3	C8	C7	0.6(2)
C4	C5	C6	C7	0.4(2)
C5	C6	C7	C8	-0.4(2)
C6	C7	C8	N2	179.73(15)
C6	C7	C8	C3	-0.1(2)
C8	N2	C9	O2	0.2(3)
C8	N2	C9	C10	-179.86(15)
C8	C3	C4	C5	-0.5(2)
C9	N2	C8	C3	129.03(17)
C9	N2	C8	C7	-50.8(2)
C11	N1	C1	O1	-175.00(15)
C11	N1	C2	C3	86.40(17)
C11	C12	C13	C14	-1.2(2)
C12	C11	C16	C15	-0.7(2)
C12	C13	C14	F1	-179.18(14)
C12	C13	C14	C15	-0.2(3)
C13	C14	C15	C16	1.1(3)
C14	C15	C16	C11	-0.6(2)
C16	C11	C12	C13	1.6(2)

Table S3.41: Hydrogen Fractional Atomic Coordinates (×10⁴) and Equivalent Isotropic Displacement Parameters (Å²×10³) for **12**. U_{eq} is defined as 1/3 of the trace of the orthogonalised U_{ij}.

Atom	x	y	z	U_{eq}
H2	3360(30)	6060(30)	7180(20)	36(6)
H1	4063.94	3128.05	4703.23	23
H2A	4455.66	3025.62	8443.91	23
H2B	3156.79	3856.38	7767.35	23
H4	7890.46	4530.89	9552.75	24
H5	10242.16	6934.67	10910.22	27
H6	9709.01	9249.56	10942.68	26
H7	6817.63	9160.26	9640.88	25
H10A	1057.25	8280.86	7390.44	46
H10B	-103.52	6853.63	7855.26	46
H10C	791.07	6523.09	6661.55	46
H12	7622.72	3746.52	5694.35	25
H13	9558.37	2286.81	5478.14	29
H15	6612.96	-699.37	7203.34	28
H16	4630.85	715.17	7368.73	25

Table S3.42: Hydrogen Bond information for **12**.

D	H	A	d(D-H)/Å	d(H-A)/Å	d(D-A)/Å	D-H-A/deg
N2	H2	O1	0.90(2)	2.00(2)	2.8702(19)	162.5(19)

Experimental

General procedures

All chemicals were obtained from commercial sources and used as received. All reactions were carried out under a nitrogen atmosphere. Analytical TLC was carried out on Merck aluminium sheets coated with silica gel 60F and visualised using UV light (254 nm). Flash chromatography was carried out on silica gel 60. Solvent ratios have been indicated in brackets. Mass spectrometry was performed by the University of Edinburgh technician-supported mass spectrometry service, using a ThermoElectron MAT XP spectrometer for EI-HRMS. Melting points were measured in a Gallenkamp melting point apparatus and are uncorrected. ^{1}H and ^{13}C NMR spectra were recorded on either 400 or 500 or 600 MHz Bruker Avance III spectrometer. ^{19}F NMR spectra were recorded on a 400 or 500 MHz Bruker Avance III spectrometer. NMR chemical shifts are reported in parts per million (δ) relative to trimethylsilane (δ = 0) or $CDCl_3$ (^{1}H δ = 7.26 and ^{13}C δ = 77.16) as an internal reference. Both major and minor conformer chemical shifts were recorded for all balances where unambiguous assignment was possible. Minor conformers are denoted by prime notations (‘). Coupling constants, *J*, are reported in Hertz. Signal splitting patterns in ^{1}H NMR spectra could not be determined in cases where conformer signals resulted in overlapping peaks. The chemical shifts of aromatic protons were often identified using HSQC/HMBC spectra and the signals are recorded as multiplets (m).

Methylene linker series

Scheme summary

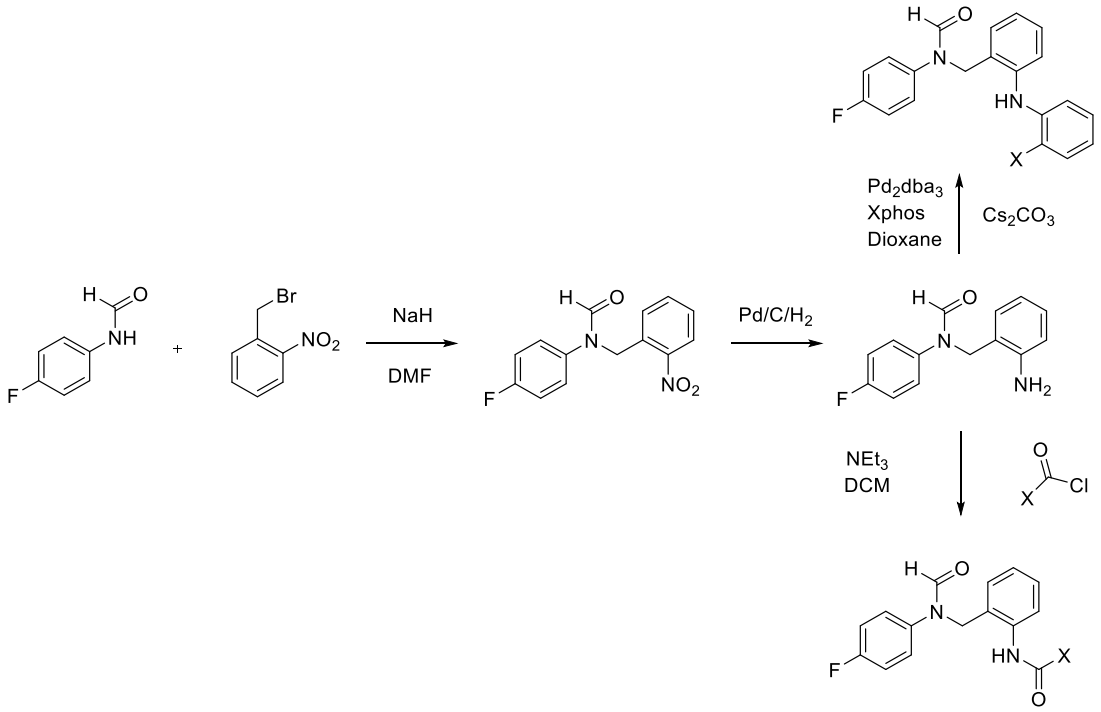

***N*-(4-fluorophenyl)-*N*-[(2-nitrophenyl)methyl]formamide (36)**

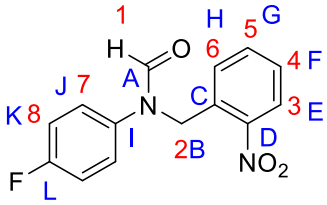

To a flask under a nitrogen atmosphere was added a solution of *N*-(4-fluorophenyl) formamide (870 mg, 6.25 mmol), in dry DMF (30 mL), 2-nitrobenzyl bromide (1.35 g, 6.25 mmol) was then added and the mixture cooled to 0 °C. Sodium hydride (300 mg, 7.50 mmol) was then carefully added and the mixture allowed to warm to room temperature. The reaction mixture was stirred overnight, diluted with DCM (10 mL) and quenched with water (10 mL). The organics were then reduced *in vacuo*, dried with $MgSO_4$ and purified using column chromatography (30 % EtOAc/*n*-Hex) to yield a white solid (800 mg, 2.91 mmol, 50 %).

^{1}H NMR (500 MHz, $CHCl_3$-*d*) δ 8.61 (1, s, 1H), 8.52 (1', s, 1H), 8.10 (3', dd, *J* = 8.2, 1.4 Hz, 1H), 8.05 (3, dt, *J* = 7.6, 1.2 Hz, 1H), 7.65 – 7.60 (5, m, 1H), 7.53 – 7.49 (4',

m, 1H), 7.48 – 7.44 (5’, 6, 4, m, 3H), 7.41 (6’, m, 1H), 7.26 – 7.22 (7’, m, 2H), 7.15 – 7.06 (7, 8, m, 4H), 7.05 – 7.01 (8’, m, 2H), 5.39 (2, s, 2H), 5.29 (2’, s, 2H).

^{13}C NMR (126 MHz, $CHCl_3$-*d*) δ 162.99 (A’, s), 162.46 (A, s), 161.41 (L, d, *J* = 247.8 Hz), 148.30 (D, s), 148.10 (D’, s), 136.75 (I, d, *J* = 3.1 Hz), 134.29 (I’, d, *J* = 3.3 Hz), 133.87 (G’, s), 133.75 (G, s), 131.97 (C’, s), 131.78 (C, s), 129.81 (H’, s), 129.22 (F’, s), 129.03 (H, s), 128.47 (F, s), 126.82 (J’, d, *J* = 8.4 Hz), 125.63 (E’, s), 125.43 (J, d, *J* = 8.5 Hz), 125.30 (E, s), 116.79 (K, d, *J* = 22.9 Hz), 116.19 (K’, d, *J* = 22.6 Hz), 51.10 (B’, s) 46.67 (B, s).

^{19}F NMR (471 MHz, $CHCl_3$-*d*) δ -114.02 (major), -114.24 (minor).

EI HRMS: obtained m/z 274.07607 M+ (expected m/z 274.07482 M+).

MP: 115 – 116 °C.

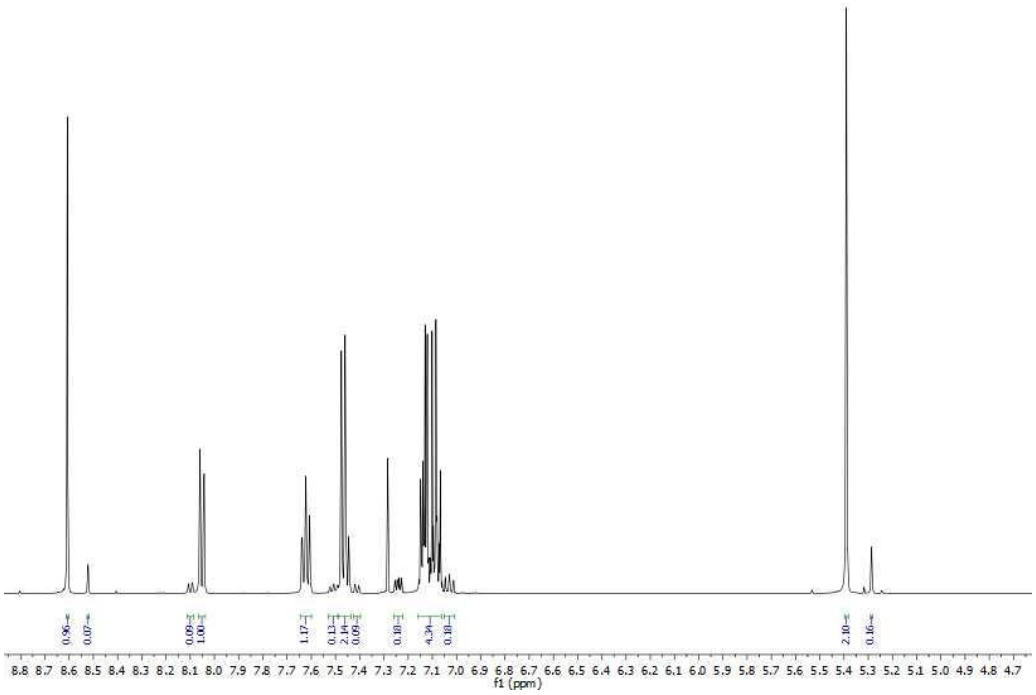

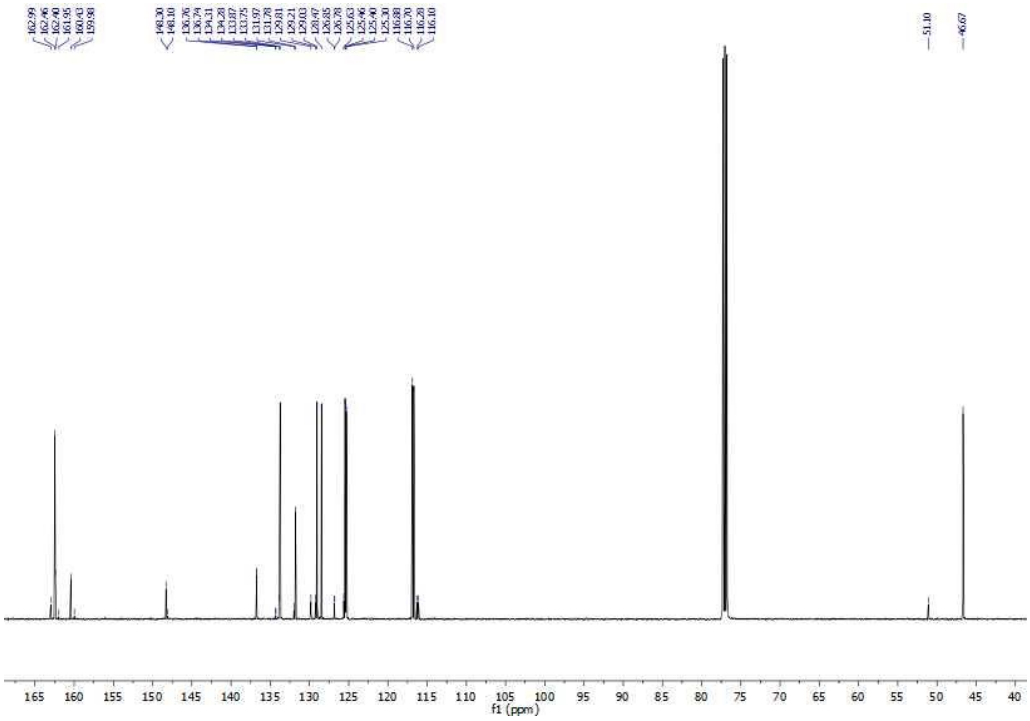

_N_-[2-(2-aminophenyl)ethyl]-_N_-(4-fluorophenyl)formamide (8)

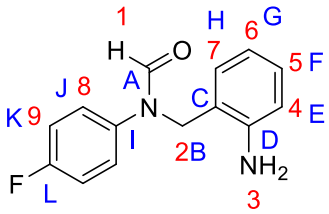

To a reaction flask under a nitrogen atmosphere was added a solution of _N_-(4-fluorophenyl)-_N_-[(2-nitrophenyl)methyl]formamide (200 mg, 0.730 mmol) in THF (10 mL) and EtOH (10 mL). Palladium on carbon (10 wt %) was then added and the reaction mixture placed under a hydrogen environment. The reaction mixture was monitored to completion via TLC and then filtered through Celite. The crude mixture was reduced under pressure and purified using column chromatography (2 % MeOH/DCM) to yield a white solid (140 mg, 79%).

^{1}H NMR (601 MHz, DMSO-d_6) δ 8.54 (1', s, 1H), 8.51 (1, s, 1H), 7.35-7.31 (8, m, 2H), 7.30-7.28 (8', m, 2H) 7.24-7.19 (9, m, 2H), 7.17-7.13 (9', m, 2H), 6.96-6.95 (6', m, 1H), 6.94-6.90 (6, m, 1H), 6.81-6.80 (7', m, 1H), 6.79-6.76 (7, m, 1H), 6.64-6.65 (4', m, 1H), 6.63-6.61 (4, m, 1H), 6.47-6.44 (5', m, 1H), 6.43-6.39 (5, m, 1H), 5.05 (3, s, 2H), 5.03 (3', s, 2H), 4.82 (2, s, 2H), 4.79 (2', s, 2H).

^{13}C NMR (151 MHz, DMSO-d_6) δ 163.66 (A', s), 163.14 (A, s), 160.75 (L, d, J = 243.2 Hz), 146.68 (D', s), 146.60 (D, s), 137.33 (I, d, J = 2.7 Hz), 135.77 (I', d, J = 3.0 Hz), 129.46 (H, s), 128.93 (H', s), 128.66 (G', s), 128.60 (G, s), 127.70 (J', d, J = 8.5 Hz), 126.24 (J, d, J = 8.5 Hz), 116.52 (K, d, J = 22.7 Hz), 116.65 (F', s), 116.46 (K', d, J = 22.7 Hz), 116.28 (F, s), 115.81 (E', s), 115.24 (E, s), 120.08 (C', s), 119.10 (C, s) 49.49 (B', s), 44.67 (B, s).

^{19}F NMR (471 MHz, DMSO-d_6) δ -116.18 (major + minor overlapping).

EI HRMS: obtained m/z 244.10012 M+ (expected m/z 244.10064 M+).

MP: 72 – 74 °C.

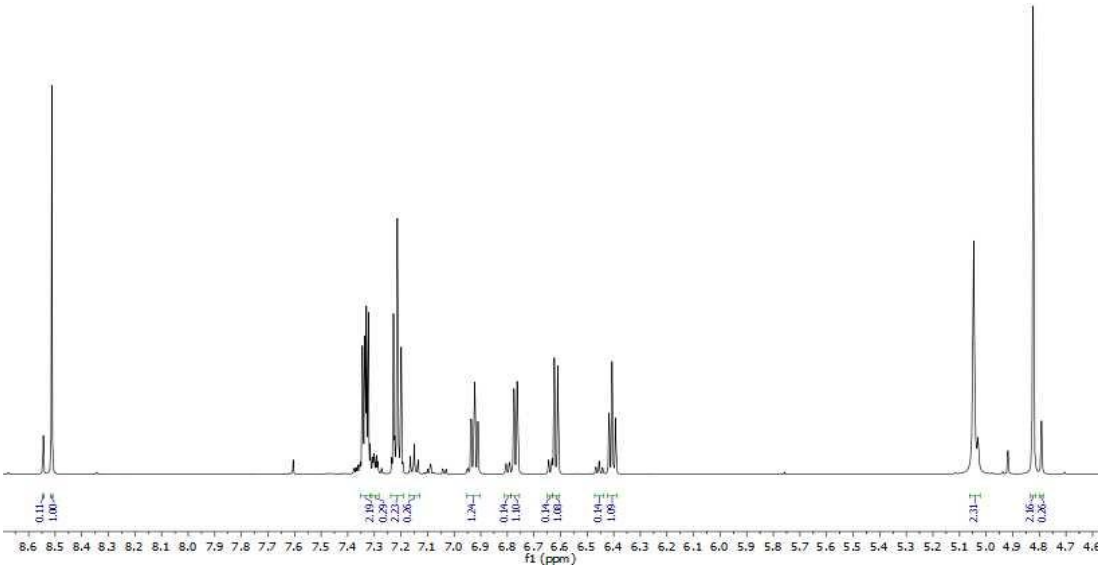

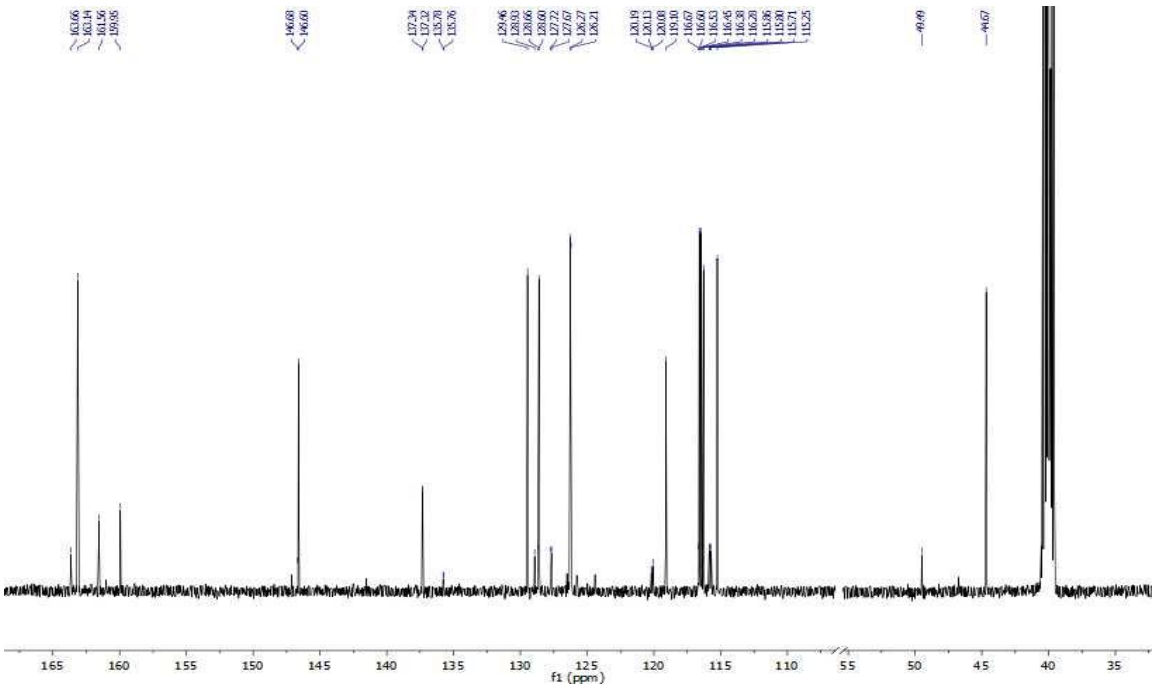

_N_-(4-fluorophenyl)-_N_-[(4-nitrophenyl)methyl]formamide (37)

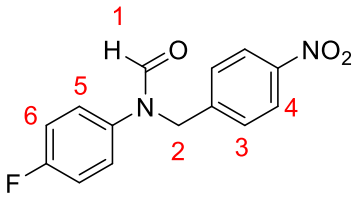

To a flask under a nitrogen atmosphere was added a solution of *N*-(4-fluorophenyl) formamide (400 mg, 2.88 mmol), in dry DMF (10 mL), 4-nitrobenzyl bromide (621 mg, 2.88 mmol) was then added and the mixture cooled to 0 °C. Sodium hydride (138 mg, 3.46 mmol) was then carefully added and the mixture allowed to warm to room temperature. The reaction mixture was stirred overnight, diluted with DCM (10 mL) and quenched with water (10 mL). The organics were then reduced *in vacuo*, dried with $MgSO_4$ and purified using column chromatography (30 % EtOAc/n-Hex) to yield a white solid (513 mg, 65%).

^{1}H NMR (500 MHz, Chloroform-*d*) δ 8.50 (1, s, 1H), 8.23 – 8.14 (4, m, 2H), 7.46 – 7.38 (3, m, 2H), 7.13 – 7.05 (5, 6, m, 4H), 5.06 (2, s, 2H).

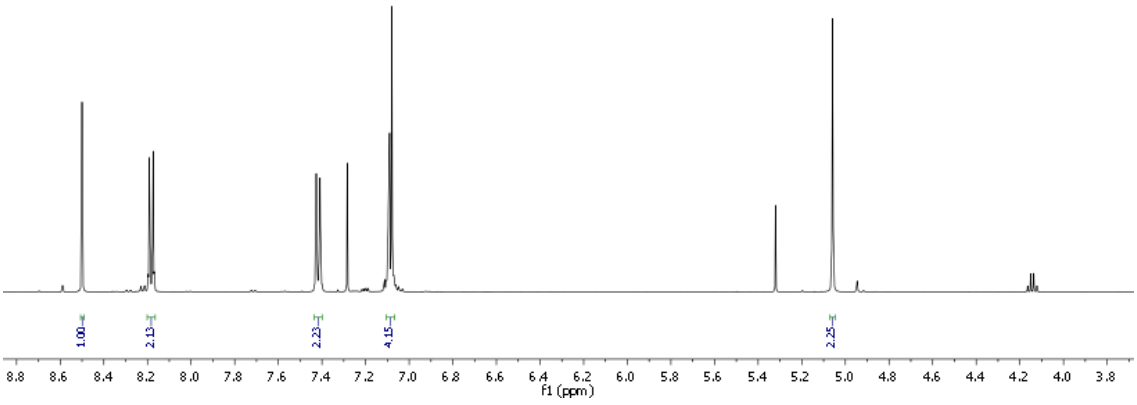

_N_-[(4-aminophenyl)methyl]-_N_-(4-fluorophenyl)formamide (34)

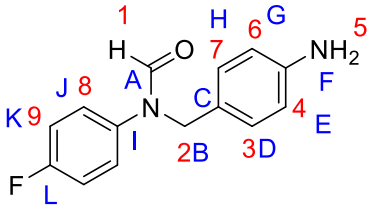

To a reaction flask under a nitrogen atmosphere was added a solution of *N*-(4-fluorophenyl)-*N*-[(2-nitrophenyl)methyl]formamide (500 mg, 1.82 mmol) in THF (5 mL) and EtOH (5 mL). Palladium on carbon (10 wt %) was then added and the reaction mixture placed under a hydrogen environment. The reaction mixture was monitored to completion via TLC and then filtered through Celite. The crude mixture was reduced under pressure and purified using column chromatography (2 % MeOH/DCM) to yield a white solid (329 mg, 74 %).

^{1}H NMR (601 MHz, DMSO) δ 8.53 (1', s, 1H), 8.47 (1, s, 1H), 7.33 – 7.28 (8, m, 2H), 7.27 – 7.24 (8', m, 2H), 7.22 – 7.17 (9, m, 2H), 7.16 – 7.12 (9', m, 2H), 6.85 (7', 3', m, 2H), 6.83 (7, 3, m, 2H), 6.46 (6', 4', m, 2H), 6.45 – 6.42 (6, 4, m, 2H), 5.01 (5', s, 2H), 4.96 (5, s, 2H), 4.79 (2, s, 2H), 4.72 (2', s, 2H).

^{13}C NMR (126 MHz, DMSO) δ 163.18 (s), 162.61 (s), 160.61 (d, *J* = 243.2 Hz) 160.26 (d, *J* = 243.2 Hz), 148.56 (s), 148.25 (s), 137.62 (d, *J* = 2.7 Hz), 135.64 (d, *J* = 2.5 Hz), 129.00 (s), 128.97 (s), 128.11 (d, *J* = 8.4 Hz), 126.22 (d, *J* = 8.5 Hz), 123.95 (s), 123.90 (s), 116.45 (d, *J* = 22.6 Hz), 115.80 (d, *J* = 22.4 Hz), 114.29 (s), 114.26 (s), 52.81 (s), 47.13 (s).

^{19}F NMR (376 MHz, DMSO) δ -116.10 – -116.19 (minor, m), -116.50 – -116.58 (major, m).

EI HRMS: obtained m/z 244.10072 M+ (expected m/z 244.10064 M+).

MP: 64-67 °C

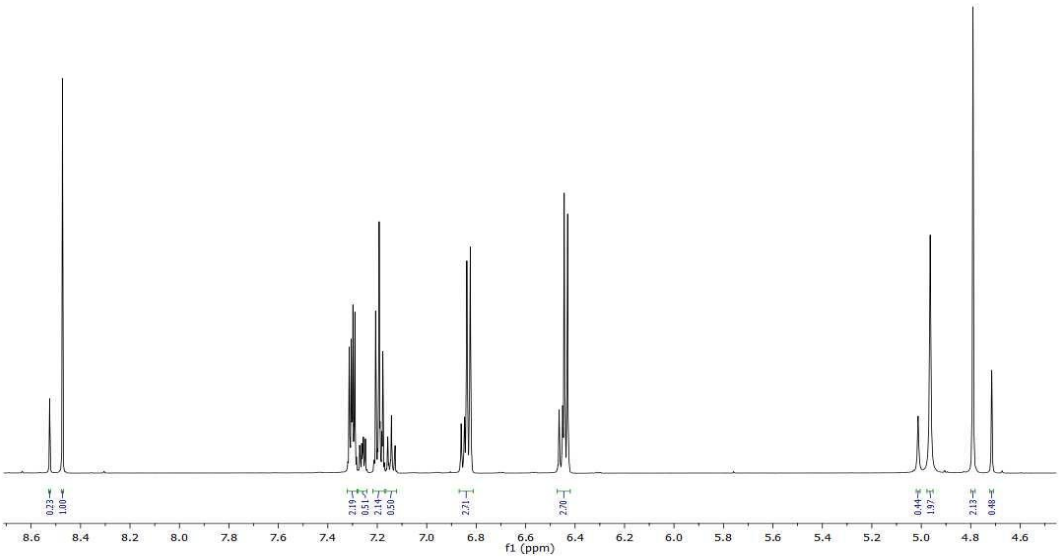
0.23
1.00
2.10
5.14
2.14
0.50
2.71
2.70
0.44
1.97
2.13
0.48
8.6
8.4
8.2
8.0
7.8
7.6
7.4
7.2
7.0
6.8
6.6
6.4
6.2
6.0
5.8
5.6
5.4
5.2
5.0
4.8
4.6
f1 (ppm)

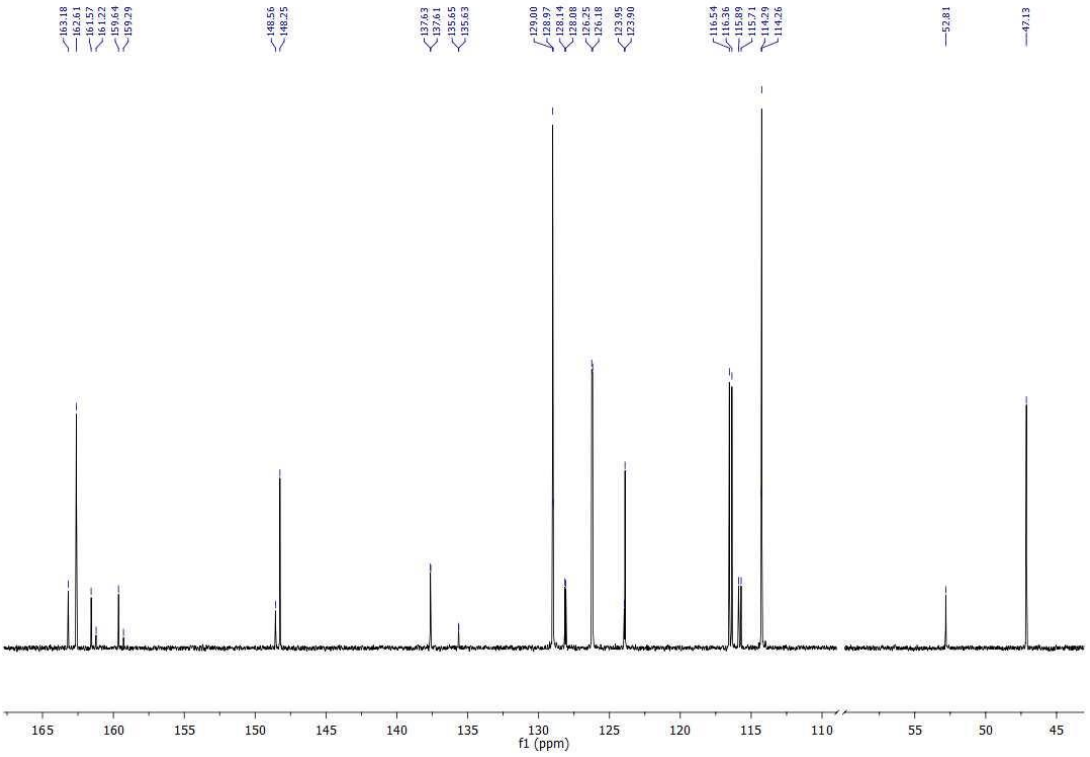
163.18
162.61
161.57
161.22
159.64
159.29
148.56
148.25
137.63
137.61
135.65
135.63
129.00
128.97
128.14
128.08
126.25
126.18
123.95
123.90
116.54
116.36
115.89
115.71
114.29
114.26
52.81
47.13
165
160
155
150
145
140
135
130
125
120
115
110
55
50
45
f1 (ppm)

Buchwald-Hartwig couplings

General Method:

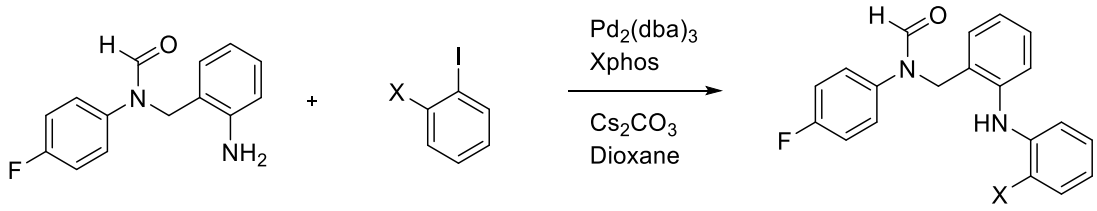

To a flask under a nitrogen atmosphere was added a solution of *N*-[2-(2-aminophenyl)ethyl]-*N*-(4-fluorophenyl)formamide in degassed dioxane (10 mL). The appropriately substituted iodobenzene was then added along with caesium carbonate, XPhos and $Pd_2(dba)_3$. The reaction mixture was then refluxed overnight, and filtered through celite. Water was added and then the reaction mixture was extracted with DCM (2 x 10 mL), dried over $MgSO_4$, concentrated under reduced pressure and purified by column chromatography.

N-[(2-anilinophenyl)methyl]-*N*-(4-fluorophenyl)formamide (9)

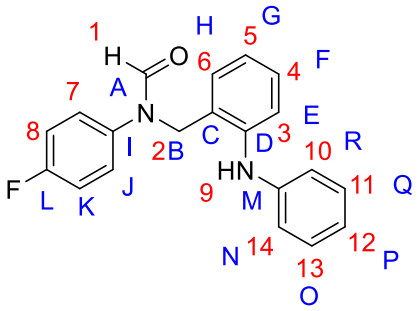

Prepared according to general method: Dioxane (10 mL), *N*-[2-(2-aminophenyl)methyl]-*N*-(4-fluorophenyl)formamide (200 mg, 0.819 mmol), iodobenzene (284 mg, 155 µL, 1.39 mmol), Cs_2CO_3 (800 mg, 2.46 mmol), XPhos (39.0 mg, 0.0820 mmol) and $Pd_2(dba)_3$ (0.0450 mg, 0.0491 mmol). Purification with column chromatography (1:1 EtOAc: *n*-Hex) yielded a yellow solid (163 mg, 62%).

^{1}H NMR (500 MHz, DMSO-d_6) δ 8.58 (1, s, 1H), 8.46 (1', s, 1H), 7.57 (9, s, 1H), 7.36 – 7.31 (7, m, 2H), 7.27 – 7.23 (7', m, 2H), 7.23 – 7.09 (8, m, 2H, 8', m, 2H, 3, m, 1H, 3', m, 1H, 14, 10, m, 2H, 14', 10', m, 2H), 7.08 – 7.04 (6, m, 1H, 6', m, 1H), 6.96 –

6.85 (5, m, 1H, 5’, m, 1H, 11, 13, m, 2H, 11’, 13’, m, 2H), 6.83 – 6.75 (12, m, 1H, 12’, m, 1H), 4.97 (2, s, 2H), 4.94 (2’, s, 2H).

^{13}C NMR (126 MHz, DMSO) δ 163.43 (s), 163.27 (s), 160.67 (d, *J* = 243.2 Hz), 145.54 (s), 145.00 (s), 141.55 (s), 141.35 (s), 137.53 (d, *J* = 2.8 Hz), 135.52 (d, *J* = 2.5 Hz), 129.81 (s), 129.61 (s), 129.42 (s), 128.96 (s), 128.89 (s), 128.44 (s), 128.27 – 128.14 (m), 127.77 (s), 127.72 (s), 125.81 (d, *J* = 8.5 Hz), 122.99 (s), 122.24 (s), 122.06 (s), 120.32 (s), 119.82 (s), 119.44 (s), 116.73 (s), 116.56 (d, *J* = 22.6 Hz), 116.11 (s), 115.77 (d, *J* = 22.3 Hz), 49.52 (s), 44.59 (s).

^{19}F NMR (471 MHz, DMSO-d_6) δ -116.11 (minor), -116.30 (major).

EI HRMS: obtained m/z 320.13189 M+ (expected m/z 320.13194 M+).

MP: 97-99 °C

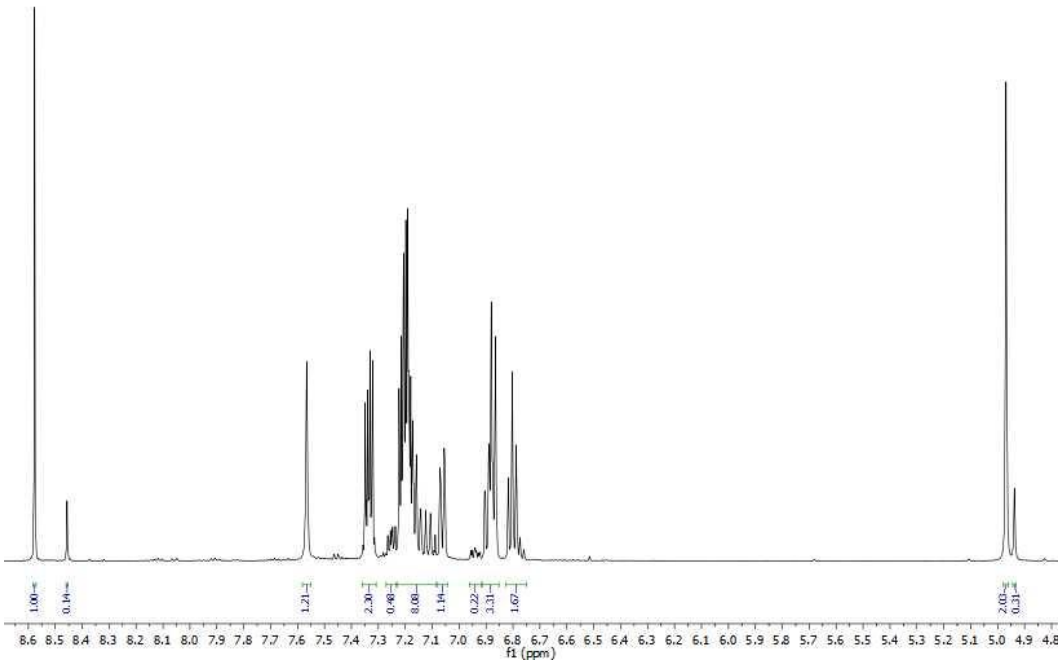

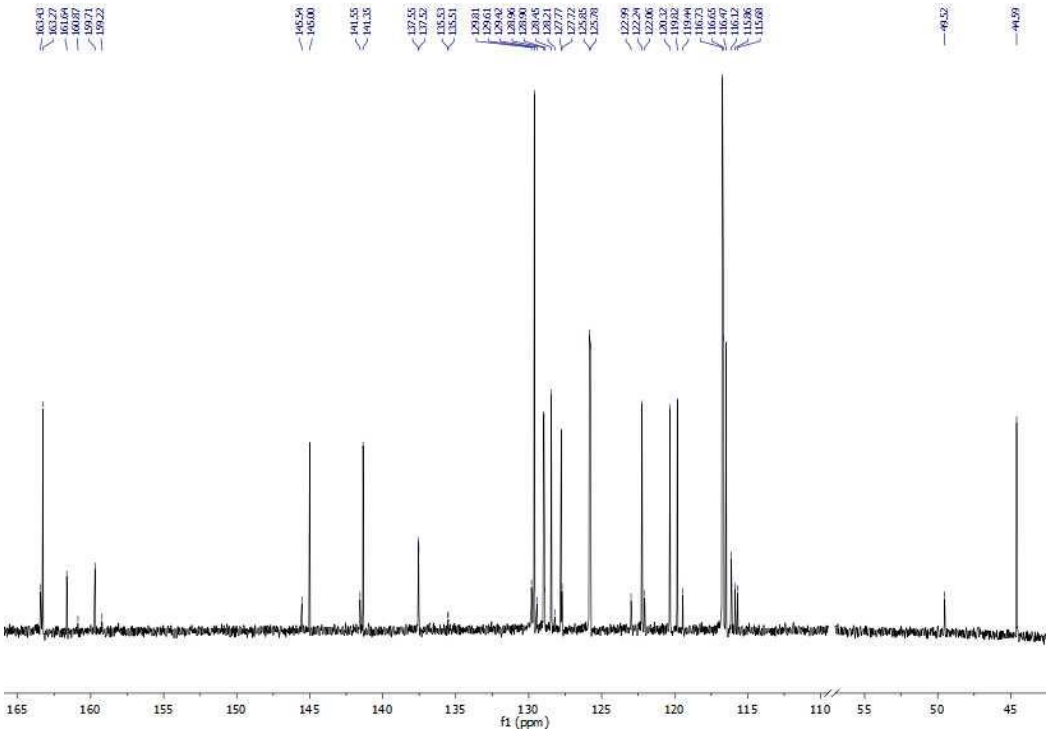

_N_-(4-fluorophenyl)-_N_-[[2-(2-methoxyanilino)phenyl]methyl]formamide (10)

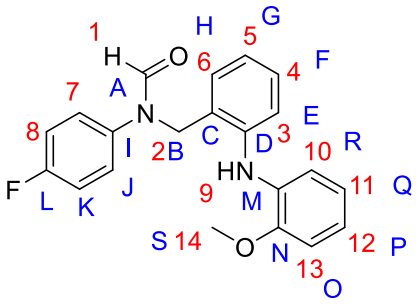

Prepared according to general method: Dioxane (10 mL), _N_-[2-(2-aminophenyl)methyl]-_N_-(4-fluorophenyl)formamide (200 mg, 0.819 mmol), 2-methoxyiodobenzene (325 mg, 182 µL, 1.39 mmol), Cs_2CO_3 (800 mg, 2.46 mmol), XPhos (39.0 mg, 0.0820 mmol) and $Pd_2(dba)_3$ (0.0450 mg, 0.0491 mmol). Purification with column chromatography (1:1 EtOAc: _n_-Hex) yielded a brown oil (278 mg, 76%)

^{1}H NMR (500 MHz, DMSO-d_6) δ 8.54 (1, s, 1H), 8.47 (1', s, 1H), 7.35 – 7.30 (7, m, 2H), 7.28 – 7.24 (7', m, 2H), 7.23 – 7.17 (8, m, 2H), 7.16 – 7.09 (8', m, 2H, 6', m, 1H, 4, m, 1H, 4', m, 1H), 7.08 – 7.04 (6, m, 1H), 7.04 – 6.98 (3, m, 1H, 3', m, 1H, 10, m, 1H, 10', m, 1H), 6.95 – 6.95 – 6.77 (5, m, 1H, 13, m, 1H, 11, m, 1H, 12, m, 1H, 5', m,

1H, 13', m, 1H, 11', m, 1H, 12', m, 1H), 6.70 - 6.67 (13', m, 1H), 4.97 (2, s, 2H), 4.96 (2,' s, 2H), 3.84 (14', s, 1H), 3.83 (14, s, 3H).

^{13}C NMR (126 MHz, DMSO) δ 163.41 (s), 163.10 (s), 160.74 (d, *J* = 243.3 Hz), 160.27 (d, *J* = 243.2 Hz), 149.70 (s), 149.01 (s), 141.84 (s), 137.34 (d, *J* = 2.8 Hz), 135.39 (d, 2.5 Hz), 134.16 (s), 133.62 (s), 130.17 (s), 129.74 (s), 128.91 (s), 128.84 (s), 128.54 (s), 127.91 (d, *J* = 8.5 Hz), 127.14 (s), 126.21 (d, *J* = 8.6 Hz), 122.67 (s), 121.85 (s), 121.77 (s), 121.15 (s), 121.10 (s), 120.97 (s), 120.32 (s), 119.91 (s), 116.81 (s), 116.54 (d, *J* = 22.6 Hz), 115.76 (d, *J* = 22.5 Hz), 115.39 (s), 111.90 (s), 111.71 (s), 56.03 (s), 49.91 (s), 44.68 (s).

^{19}F NMR (471 MHz, DMSO-d_6) δ -116.05 (minor), -116.16 (major).

EI HRMS: obtained m/z 350.14288 M+ (expected m/z 350.14251 M+).

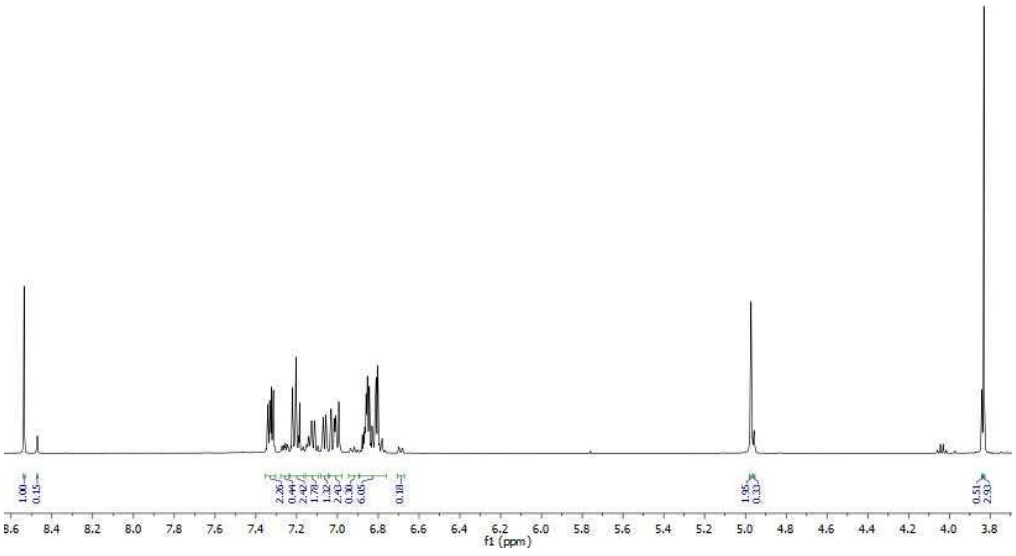

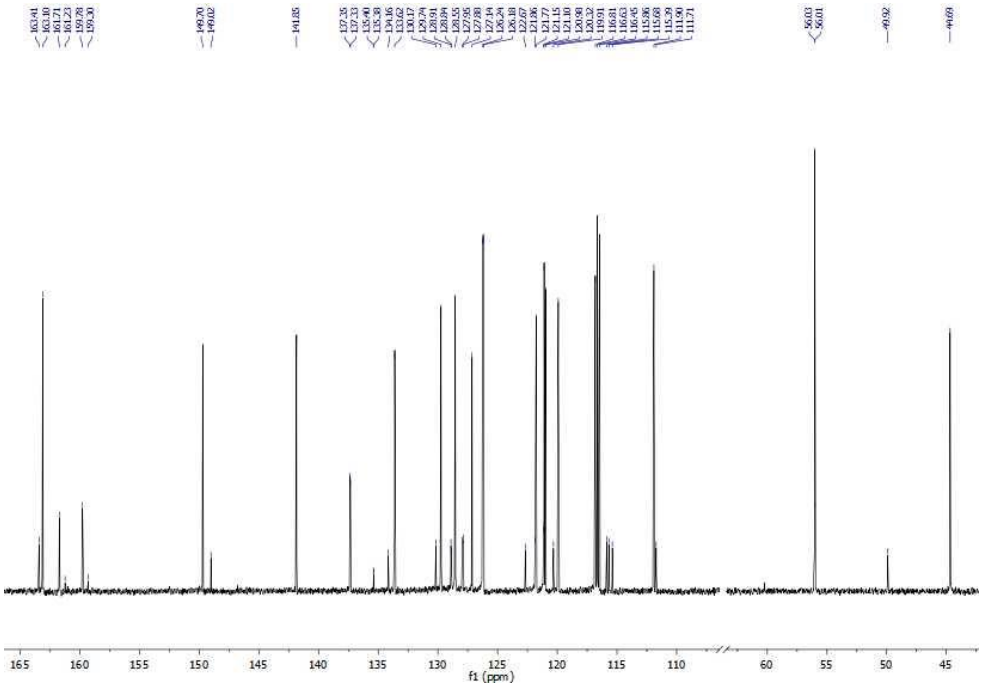

_N_-[[2-(2-cyanoanilino)phenyl]methyl]-_N_-(4-fluorophenyl)formamide (11)

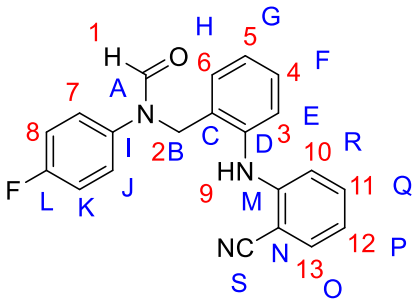

Prepared according to general method: Dioxane (10 mL), _N_-[2-(2-aminophenyl)ethyl]-_N_-(4-fluorophenyl)formamide (200 mg, 0.819 mmol), 2-iodobenzonitrile (318 mg, 1.39 mmol), Cs_2CO_3 (800 mg, 2.46 mmol), XPhos (39.0 mg, 0.0820 mmol) and $Pd_2(dba)_3$ (0.0450 mg, 0.0491 mmol). Purification with column chromatography (1:1 EtOAc: _n_-Hex) yielded a brown oil (206 mg, 73%).

^{1}H NMR (500 MHz, DMSO-d_6) δ 8.54 (1, s, 1H), 8.40 (1', s, 1H), 8.02 (9', s, 1H), 7.98 (9, s, 1H), 7.63 – 7.60 (13, m, 1H, 13', m, 1H), 7.43 – 7.35 (11, m, 1H, 11', m, 1H), 7.33 – 7.28 (7, m, 2H, 7', m, 2H), 7.28 – 7.23 (4, m, 2H, 4', m, 2H), 7.20 – 7.06 (6, m, 1H, 8, m, 2H, 5, m, 1H, 3, m, 1H, 6', m, 1H, 8', m, 2H, 5', m, 1H, 3', m, 1H), 6.91 – 6.85 (12, m, 1H, 12', m, 1H), 6.61 – 6.58 (10, m, 1H), 6.48 – 6.46 (10', s, 1H), 4.95 (2, s, 2H), 4.93 (2', s, 2H).

^{13}C NMR (126 MHz, DMSO) δ 163.21 (s), 163.09 (s), 160.62 (d, *J* = 243.2 Hz), 160.20 (d, *J* = 243.2 Hz), 149.19 (s), 148.91 (s), 139.77 (s), 139.53 (s), 137.52 (d, *J* = 2.7 Hz), 135.40 (d, 2.5 Hz), 134.66 (s), 134.26 (s), 134.23 (s), 132.47 (s), 131.34 (s), 130.10 (s), 129.26 (s), 129.21 (s), 128.78 (s), 127.73 (d, *J* = 8.5 Hz), 126.22 (s), 125.76 (s), 125.63 (d, *J* = 8.5 Hz), 125.31 (s), 125.04 (s), 119.66 (s), 119.41 (s), 118.20 (s), 118.10 (s), 116.52 (d, *J* = 22.7 Hz), 116.20 (s), 115.87 (s), 115.75 (d, *J* = 22.5 Hz), 98.93 (s), 98.31 (s), 49.43 (s), 44.44 (s).

^{19}F NMR (471 MHz, DMSO-d_6) δ -116.10 (minor), -116.42 (major).

EI HRMS: obtained m/z 345.12864 M+ (expected m/z 345.12719 M+).

MP: 90 – 92 °C.

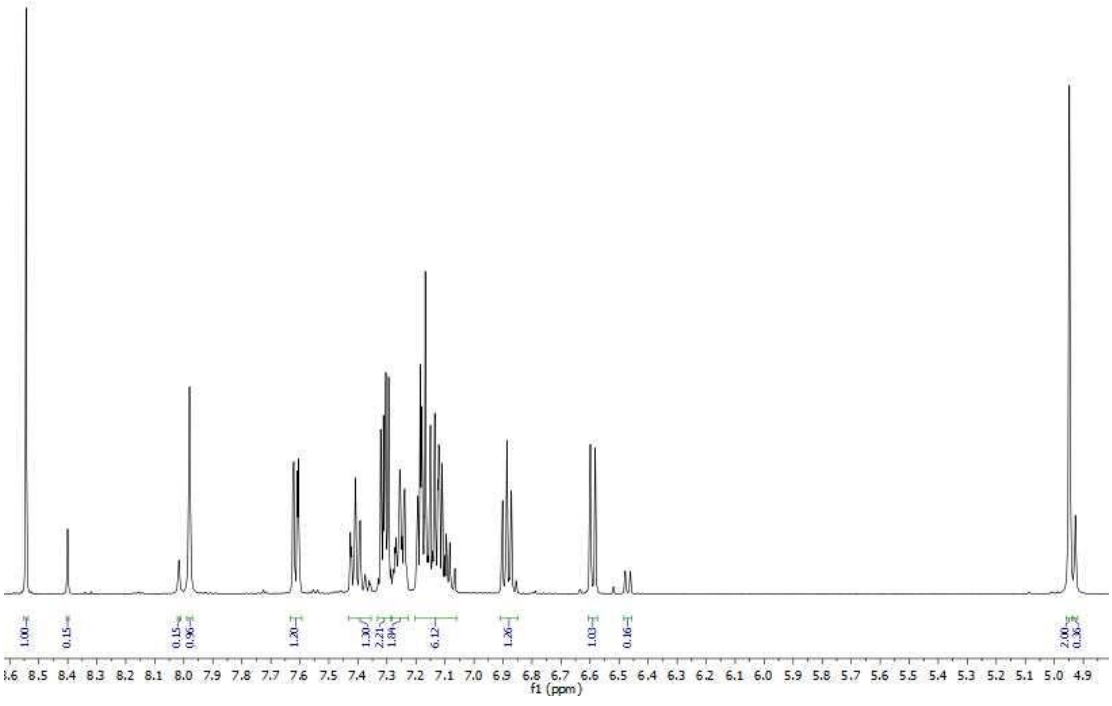

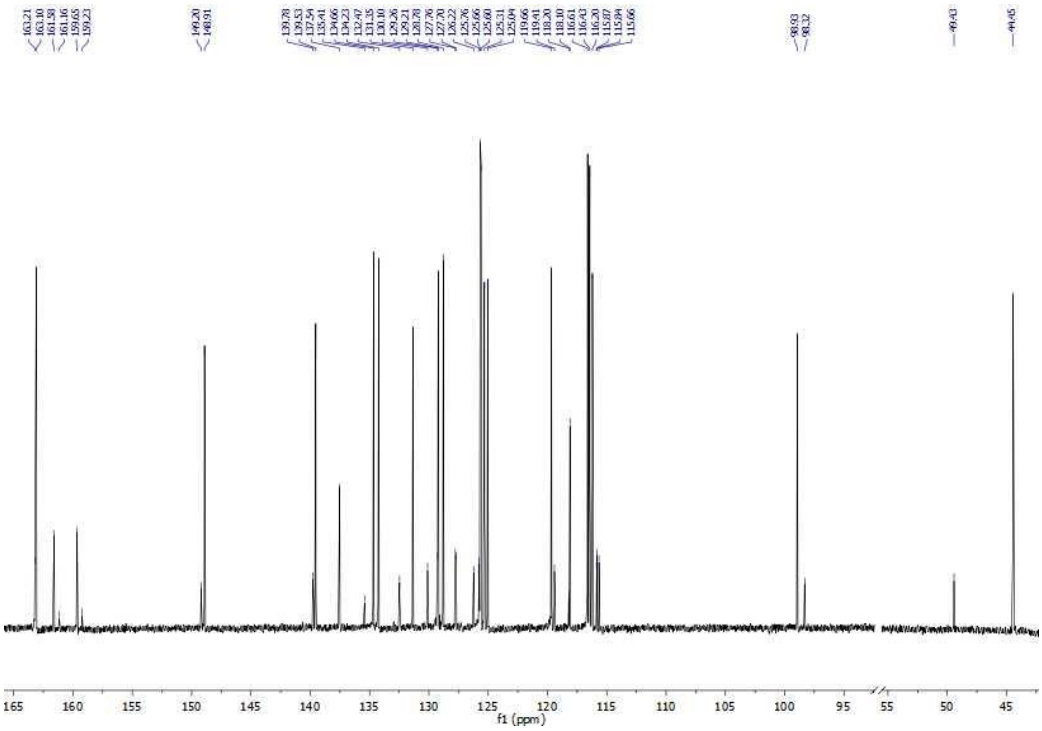

Amide Couplings

General Method:

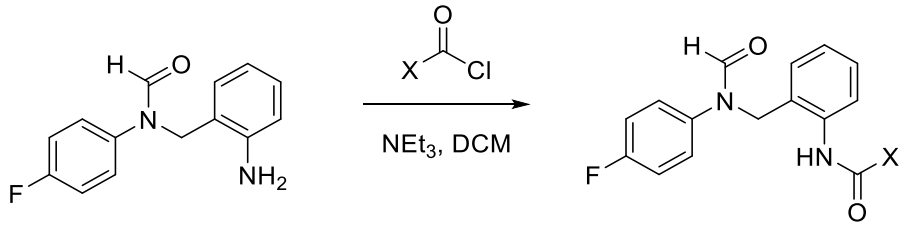

To a solution of aniline in dry DCM was added an appropriately substituted acid chloride. Triethylamine was then added and the reaction mixture heated to reflux. The reaction mixture was monitored to completion via TLC and then diluted with DCM and washed with saturated Na_2HCO_3. The aqueous phase was extracted with DCM and the combined organic phases were then washed with water and brine, dried over $MgSO_4$ and concentrated *in vacuo*. The crude product was then purified by column chromatography.

General Method:

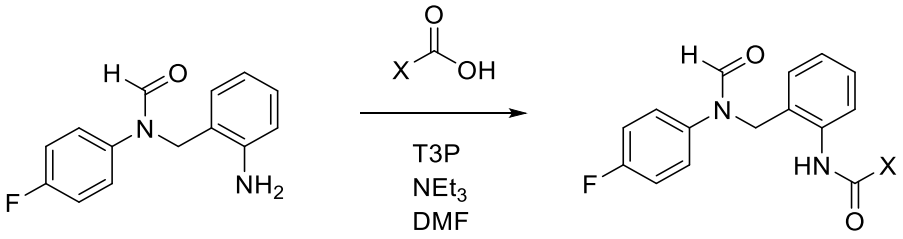

To a solution of aniline in dry DMF was added an appropriately substituted acid. Propylphosphonic anhydride solution was then added followed by triethylamine. The reaction mixture was stirred overnight at room temperature and then extracted with DCM, washed with 2M HCl, water and brine. The combined organic phases were then dried over $MgSO_4$ and concentrated *in vacuo*. The crude product was then purified by column chromatography.

***N*-[2-[(4-fluoro-*N*-formyl-anilino)methyl]phenyl]acetamide (12)**

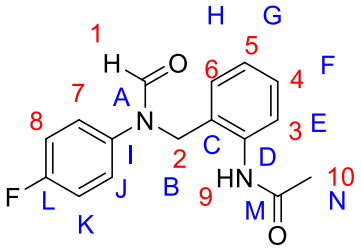

Prepared according to general method: DCM (10 mL), *N*-[2-(2-aminophenyl)ethyl]-*N*-(4-fluorophenyl)formamide (670 mg, 2.74 mmol), acetyl chloride (290 µL, 4.12 mmol) and triethylamine (770 µL, 5.49 mmol). Purification with column chromatography (1:1 EtOAc: *n*-Hex) yielded a white solid (490 mg, 62 %).

^{1}H NMR (601 MHz, DMSO-d_6) δ 9.58 (9', s, 1H) 9.49 (9, s, 1H), 8.55 (1, s, 1H), 8.49 (1', s, 1H), 7.40 (3, d, J = 7.9 Hz, 1H), 7.37 – 7.32 (7, m, 2H), 7.28 – 7.25 (7', m, 2H), 7.24 – 7.19 (8, 2H, 5, 1H, 3', 1H, 5', 1H), 7.15-7.10 (8', m, 2H, 6', m, 1H, 4', m, 1H), 7.05-7.09 (6, 1H, 4, 1H), 4.95 (s, 2, 2H), 4.90 (s, 2', 2H), 2.05 (10, s, 3H), 2.05 (10', s, 3H).

^{13}C NMR (126 MHz, DMSO-d_6) δ 168.89 (M, s), 163.42 (A’, s), 163.19 (A, s), 160.70 (L, d, J = 243.2 Hz), 160.27 (L’, d, J = 244.4 Hz), 137.48 (I, d, J = 2.9 Hz), 136.49 (D’, s), 136.45 (D, s), 135.44 (I, d, J = 2.5 Hz), 131.81 (C’, s), 130.48 (C, s), 129.16 (H’, s), 128.53 (H, s), 128.33 (G’, s), 127.97 (G, s) 127.88 (J’, d, J = 8.4 Hz), 126.95 (E’, s), 126.10 (F’, s), 125.95 (J, d, J = 8.5 Hz), 125.68 (E, s) 125.54 (F, s) 116.56 (K, d, J = 22.6 Hz) 115.80 (K’, d) 50.02 (B’, s), 44.69 (B, s), 23.78 (N, s), 23.54 (N’, s).

^{19}F NMR (471 MHz, DMSO-d_6) δ -116.02 (minor), -116.27 (major).

EI HRMS: obtained m/z 309.10150 M+ (expected m/z 309.10098 M+).

MP: 106 – 108 °C.

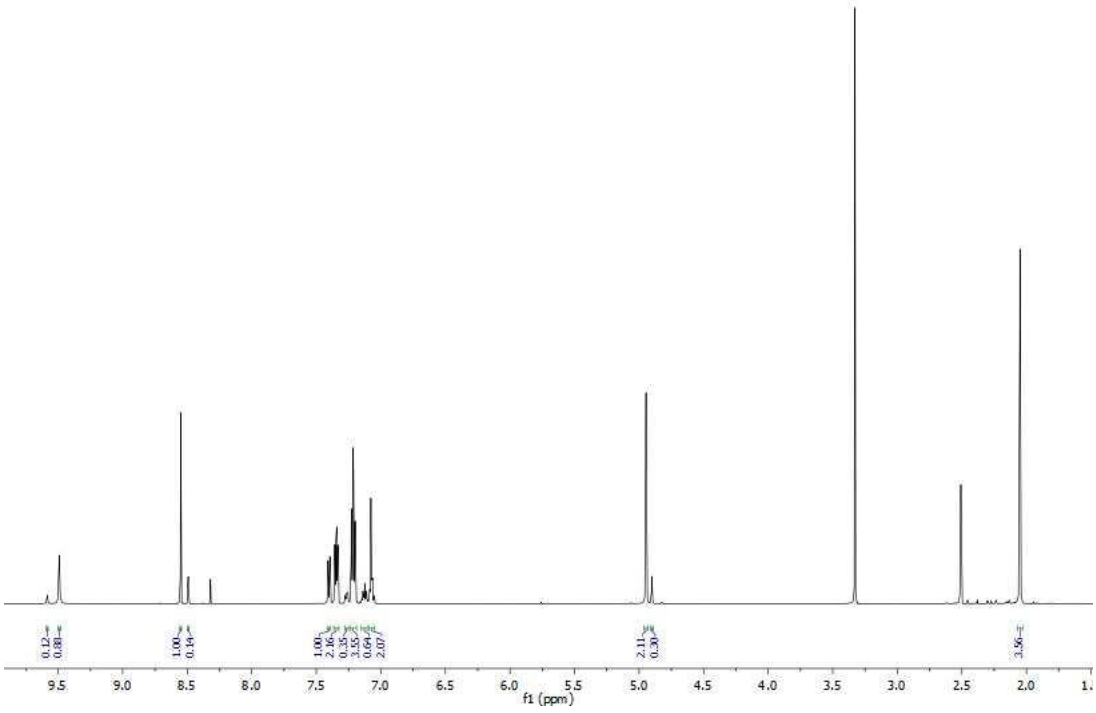

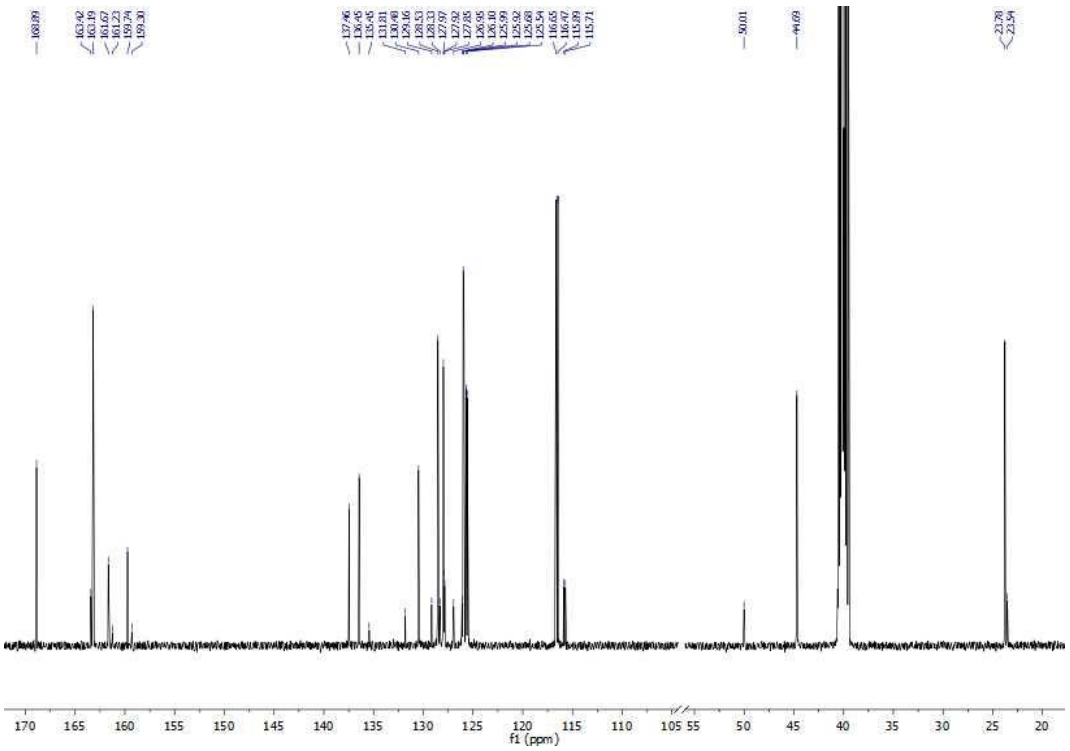

2,2,2-trifluoro-*N*-[2-[(4-fluoro-*N*-formyl-anilino)methyl]phenyl]acetamide (13)

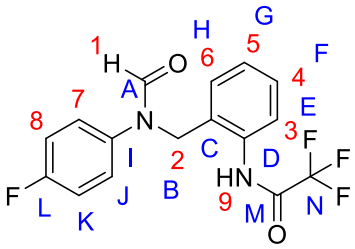

Prepared according to general method **A**: DCM (5 mL), *N*-[2-(2-aminophenyl)ethyl]-*N*-(4-fluorophenyl)formamide (240 mg, 0.982 mmol), trifluoroacetic anhydride (140 µL, 1.47 mmol) and triethylamine 140 µL, 1.94 mmol). Purification with column chromatography (1:1 EtOAc: *n*-Hex) yielded a white solid (180 mg, 55 %).

^{1}H NMR (601 MHz, DMSO-d_6) δ 11.08 (9, s, 1H), 8.50 (1, s, 1H), 8.46 (1', s, 1H), 7.36 – 7.31 (7, m, 2H, 3, m, 1H, 5, m, 1H, 3', m, 1H), 7.30 – 7.18 (8, m, 2H, 6, m, 1H, 4, m, 1H, 6', m, 1H, 4', m, 1H), 7.15-7.12 (8', m, 2H), 4.95 (2, s, 2H), 4.93 (2', s, 2H).

^{13}C NMR (126 MHz, DMSO-d_6) δ 163.23 (A', s), 163.04 (A, s), 160.80 (L, d, J = 243.4 Hz), 160.39 (L', d, J = 243.2 Hz), 155.94 (q, J = 36.8 Hz), 137.26 (I, d, J = 2.8 Hz), 135.15 (I', d, J = 3.7 Hz), 133.66 (D', s), 133.40 (D, s), 132.97 (C', s), 132.59 (C, s),

129.90 (s), 129.23 (s), 128.91 (s), 128.55 (s), 128.15 (s), 128.07 (s), 127.99 (s), 127.92 (s), 127.41 (s), 126.24 (J, d, *J* = 8.5 Hz), 119.90 (s), 117.61 (s), 116.58 (d, *J* = 22.7 Hz), 115.88 (d, *J* = 22.5 Hz), 115.31 (s), 113.02 (s), 49.60 (s), 44.38 (s).

^{19}F NMR (471 MHz, DMSO-d_6) δ -73.71 (C$\underline{F}_3$', minor), -73.87 (C$\underline{F}_3$ major), -115.84 (C$\underline{F}$ minor), -116.09 (C$\underline{F}$ major) tt, *J* = 9.1, 4.9 Hz).

EI HRMS: obtained m/z 340.08245 M+ (expected m/z 340.08294 M+).

MP: 130 – 132 °C.

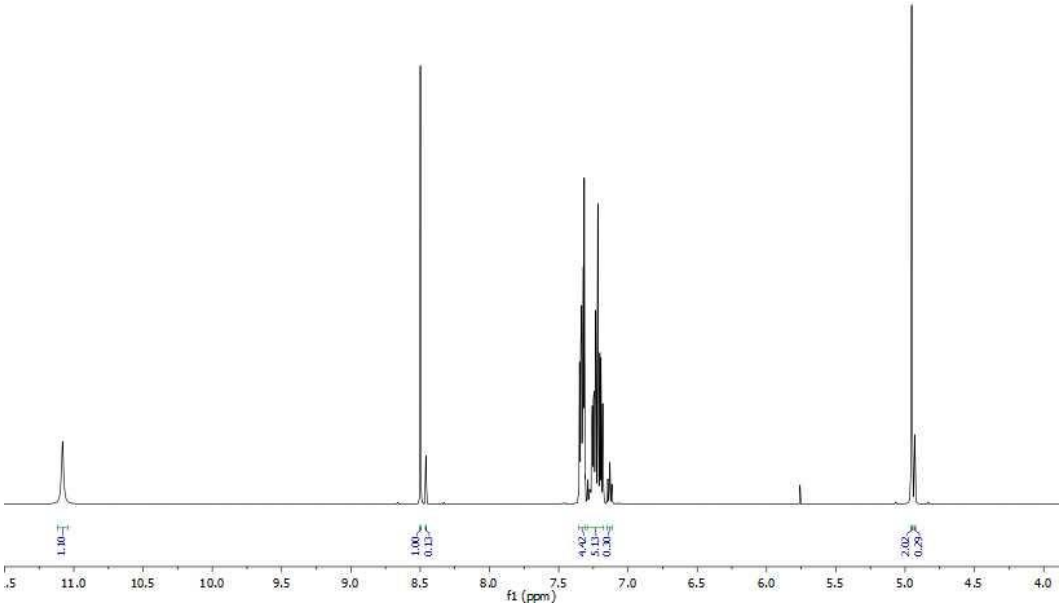

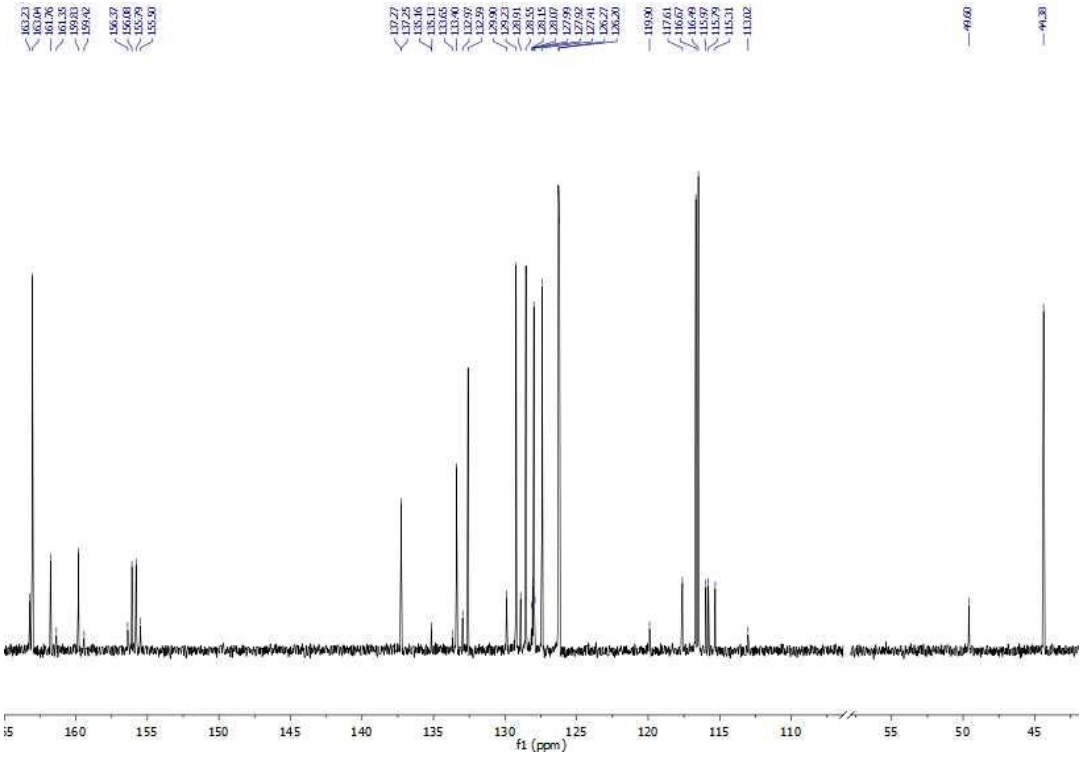

***N*-[2-[(4-fluoro-*N*-formyl-anilino)methyl]phenyl]-2,2-dimethyl-propanamide**

(14)

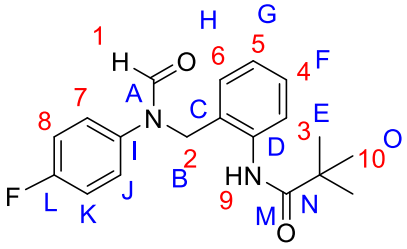

Prepared according to general method **A**: DCM (10 mL), *N*-[2-(2-aminophenyl)ethyl]-*N*-(4-fluorophenyl)formamide (700 mg, 2.87 mmol), trimethylacetyl chloride (530 µL, 4.31 mmol) and triethylamine (800 µL, 5.73 mmol). Purification with column chromatography (1:1 EtOAc: *n*-Hex) yielded a white solid (850 mg, 90 %).

^{1}H NMR (601 MHz, DMSO-d_6) δ 9.24 (9, s, 1H), 9.15 (9', s, 1H), 8.57 (1, s, 1H), 8.46 (1', s, 1H), 7.36 – 7.32 (7, m, 2H), 7.30 – 7.21 (8, m, 2H, 7', m, 2H, 3, m, 1H, 4, m,

1H, 3', m, 1H), 7.17-7.09 (8', m, 2H, 6', m, 1H, 4', m, 1H, 5, m, 1H, 5', m, 1H), 7.05-7.04 (6, m, 1H), 4.87 (2, s, 2H), 4.84 (2', s, 2H), 1.27 (10, s, 9H), 1.25 (10', s, 9H).

^{13}C NMR (126 MHz, DMSO-d_6) δ 177.37 (M', s), 177.19 (M, s), 163.54 (A', s), 163.22 (A, s), 160.71 (L, d, J = 243.2 Hz), 137.66 (I, d, J = 2.6 Hz), 136.79 (D', s), 136.48 (D, s), 135.57 (I', d, J = 2.5 Hz), 133.23 (C', s), 131.80 (C, s), 128.74 (H', s), 128.17 (E', s), 128.00 (H, s), 127.93 (G', s), 127.77 (F, s), 127.64 (J, d, J = 8.4 Hz), 127.21 (E, s), 126.49 (F', s), 126.01 (G, s), 125.82 (J, d, J = 8.5 Hz), 116.62 (K, d, J = 22.7 Hz), 115.82 (K', d, J = 22.5 Hz), 49.86 (B', s), 44.74 (B, s), 39.30 (N, s), 39.16 (N', s), 27.81 (O', s), 27.79 (O, s).

^{19}F NMR (471 MHz, DMSO-d_6) δ -116.11 (minor), -116.30 (major).

EI HRMS: obtained m/z 328.15717 M+ (expected m/z 328.15816 M+).

MP: 160 – 161 °C.

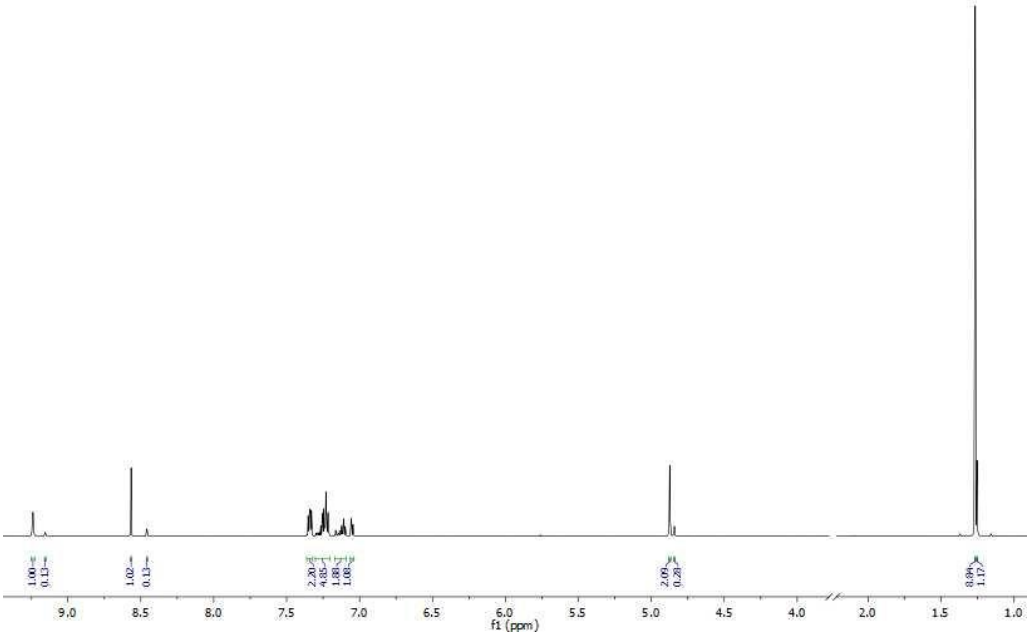

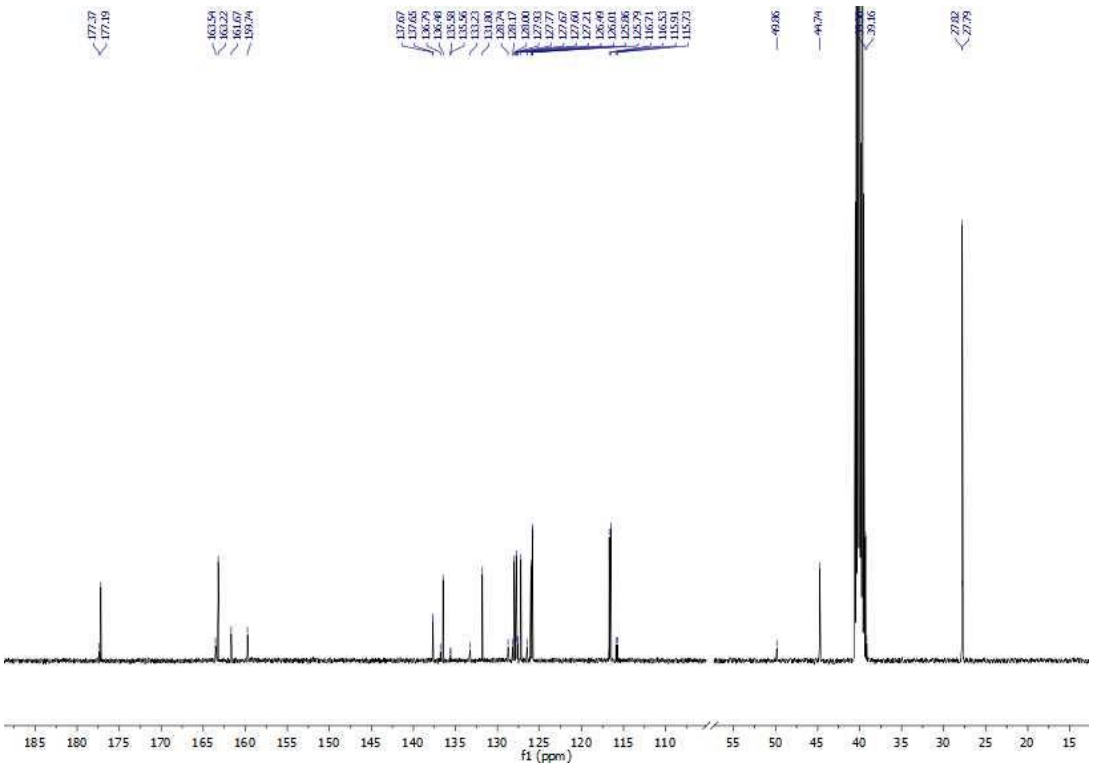

_N_-[2-[(4-fluoro-_N_-formyl-anilino)methyl]phenyl]benzamide (15)

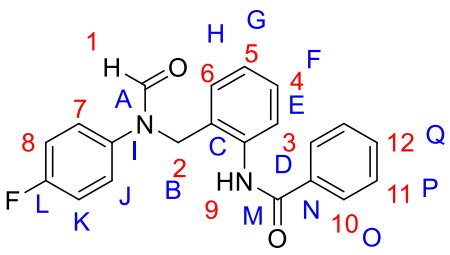

Prepared according to general method A: DCM (10 mL), *N*-[2-(2-aminophenyl)ethyl]-*N*-(4-fluorophenyl)formamide (1.03 g, 4.21 mmol), benzoyl chloride (730 µL, 6.33 mmol) and triethylamine (1.18 mL, 8.40 mmol). Purification with column chromatography (1:1 EtOAc: *n*-Hex) yielded a white solid (840 mg, 57 %).

^{1}H NMR (601 MHz, DMSO-d_6) δ 10.12 (9, s, 1H), 8.54 (1, s, 1H), 8.40 (1', s, 1H), 8.03 – 8.00 (10', m, 1H), 8.00 – 7.98 (10', m, 2H), 7.63 – 7.59 (12, m, 1H, 12', m, 1H), 7.57 – 7.52 (11, m, 2H, 11', m, 2H), 7.43 (3, m, 1H), 7.39 – 7.34 (7, m, 2H), 7.32 – 7.27 (5, m, 1H, 7', m, 2H), 7.23 – 7.10 (8, m, 2H, 4, m, 1H, 6, m, 1H, 6', m, 1H, 8', m, 2H, 4', m, 1H), 5.01 (2, s, 2H), 4.97 (2', s, 2H).

^{13}C NMR (151 MHz, DMSO-d_6) δ 166.01 (M, s), 163.31 (A’, s), 163.18 (A, s), 160.69 (L, d, J = 243.2 Hz), 137.63 (I, d, J = 2.7 Hz), 136.28 (D, s), 134.72 (N, s), 132. 10 (Q, s), 131.95 (C, s), 128.89 (s), 128.83 (P, s), 128.42 (s), 128.39 (F, s), 128.22 (O, s), 127.96 (G, s), 127.84 (J’, d, J = 8.4 Hz), 127.14 (E, s), 126.32 (H, s), 125.95 (J, d, J = 8.5 Hz), 116.57 (K, d, J = 22.6 Hz), 115.80 (K’, d, J = 22.4 Hz), 44.91 (B, s), 40.55 (B’, s).

^{19}F NMR (471 MHz, DMSO-d_6) δ -116.06 (minor), -116.30 (major).

EI HRMS: obtained m/z 348.12830 M+ (expected m/z 348.12686 M+).

MP: 183 – 185 °C.

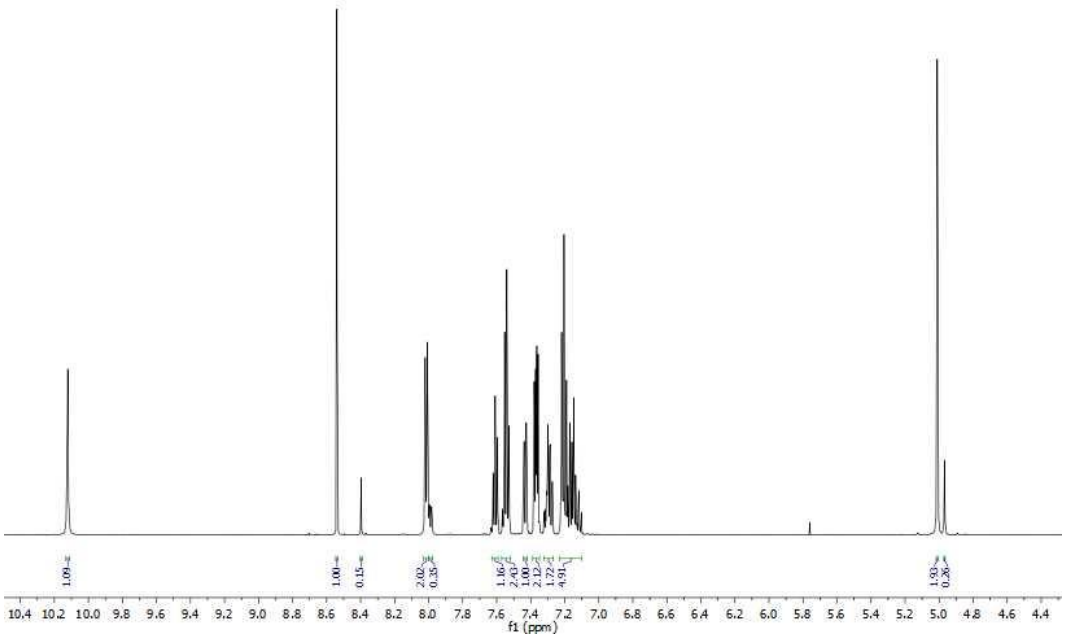

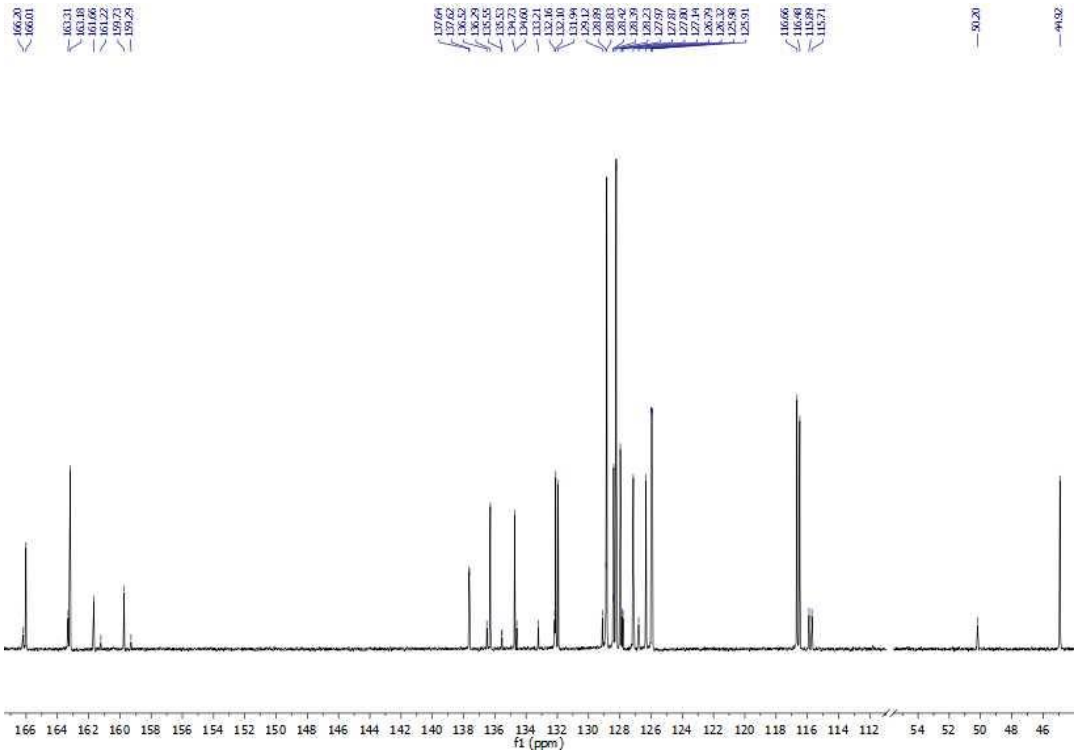

_N_-[2-[(4-fluoro-_N_-formyl-anilino)methyl]phenyl]-4-methoxy-benzamide (16)

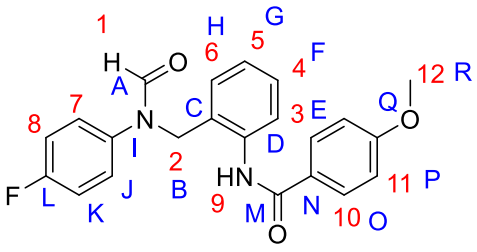

Prepared according to general method **A**: DCM (15 mL), *N*-[2-(2-aminophenyl)ethyl]-*N*-(4-fluorophenyl)formamide (700 mg, 2.87 mmol), 4-methoxybenzoyl chloride (730 g, 4.28 mmol) and triethylamine (430 µL, 3.44 mmol). Purification with column chromatography (4 % MeOH/ DCM) yielded a white solid (800 mg, 74 %).

^{1}H NMR (601 MHz, DMSO-d_6) δ 9.98 (9, s, 1H), 8.54 (1, s, 1H), 8.38 (1', s, 1H), 8.01 - 7.97 (10, m, 2H, 10', m, 2H), 7.43 – 7.42 (3, m, 1H), 7.38 – 7.34 (7, m, 2H), 7.31-7.26 (4, m, 1H, 7', m, 2H, 3', m, 1H), 7.23 – 7.18 (8, m, 2H, 6', m, 1H, 4', m, 1H), 7.17 – 7.11 (8', m, 2H, 6, m, 2H, 5, m, 1H, 5', m, 1H), 7.10 – 7.05 (11, m, 2H, 11', m, 2H), 4.99 (2, s, 1H), 4.95 (2', s, 1H), 3.86 (12', s, 3H), 3.85 (12, s, 3H).

^{13}C NMR (126 MHz, DMSO-d_6) δ 165.58 (M’, s), 165.41 (M, s), 163.27 (A’, s), 163.18 (A, s), 162.46 (Q’, s), 162.43 (Q, s), 160.69 (L, d, *J* = 243.2 Hz), 160.25 (L’, d, *J* = 243.2 Hz), 137.63 (I, d, *J* = 2.8 Hz), 136.73 (D’, s), 136.48 (D, s), 135.54 (I’, d, *J* = 2.5 Hz), 133.19 (C’, s), 131.81 (C, s), 130.14 (O, s), 129.11 (O’, s), 128.38 (H’, s), 128.36 (H, s), 127.95 (F’, s), 127.92 (F, s), 127.83 (J, d, *J* = 8.4 Hz), 127.07 (E, s), 126.84 (N, s), 126.67 (E’, s), 126.62 (G’, s), 126.10 (G, s), 125.93 (J, d, *J* = 8.5 Hz), 116.57 (K, d, *J* = 22.6 Hz), 115.78 (K’, d, *J* = 22.5 Hz), 114.11 (P’, s), 114.05 (P, s), 55.91 (R, s), 55.38 (R’, s), 50.28 (B’, s), 44.96 (B, s).

^{19}F NMR (471 MHz, DMSO-d_6) δ - 116.08 (minor), -116.30 (major)

EI HRMS: obtained m/z 378.13921 M+ (expected m/z 378.13742 M+).

MP: 176 – 177 °C.

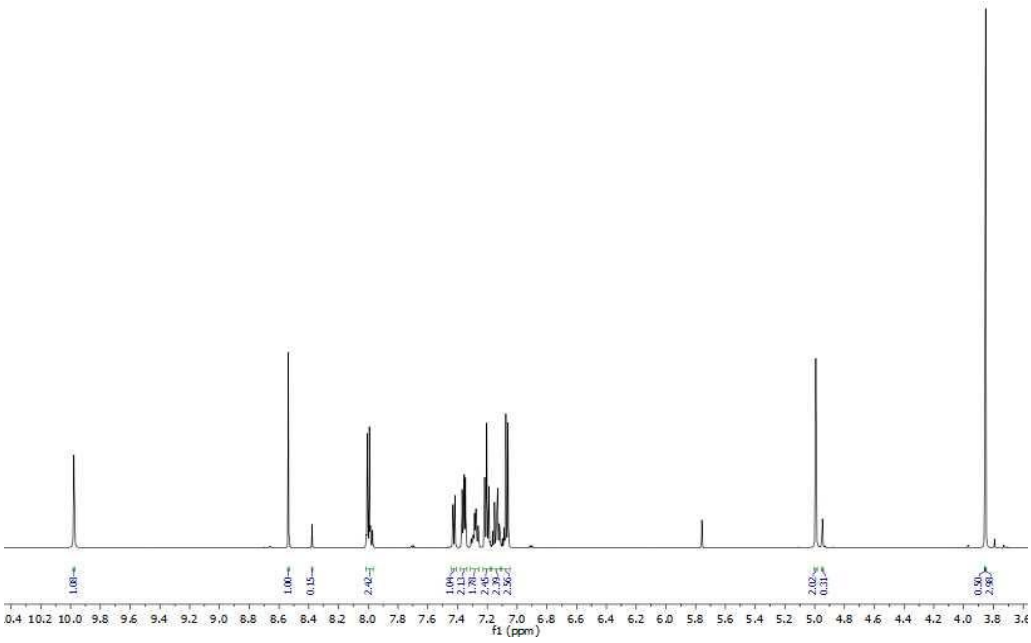

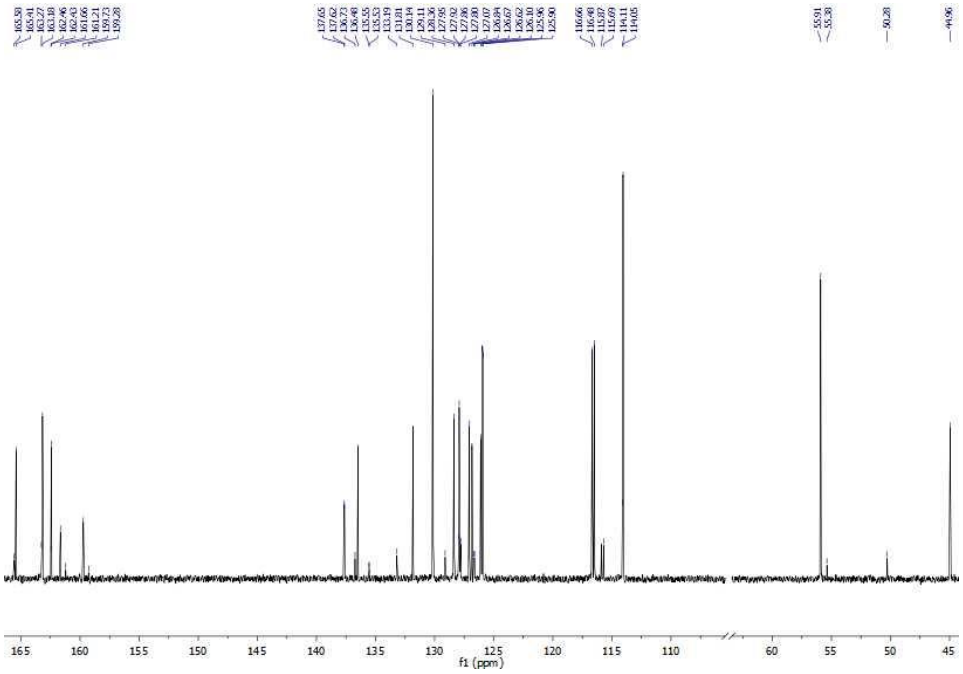

_N_-[2-[(4-fluoro-_N_-formyl-anilino)methyl]phenyl]pyridine-2-carboxamide (17)

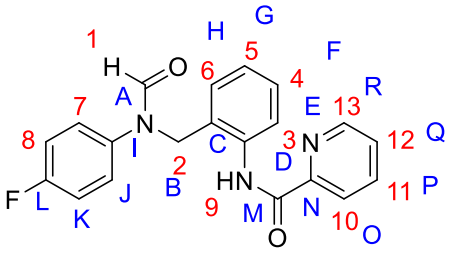

Prepared according to general method: DMF (4 mL), _N_-[2-(2-aminophenyl)ethyl]-_N_-(4-fluorophenyl)formamide (200 mg, 0.819 mmol), 2-picolinic acid (100 mg, 0.819 mmol), propylphosphonic anhydride (50 % mass) in ethyl acetate (540 µL, 0.900 mmol), triethylamine (100 mg, 140 µL, 0.983 mmol). Purification with column chromatography (1:1 EtOAc: _n_-Hex) yielded a white solid (49.0 mg, 17%).

^{1}H NMR (601 MHz, DMSO-d_6) δ 10.55 (9', s, 1H), 10.53 (9, s, 1H), 8.76 – 8.73 (10, m, 1H, 10', m, 1H), 8.56 (1, s, 1H), 8.50 (1', s, 1H), 8.17-8.13 (13, m, 1H, 13', m, 1H), 8.10-8.06 (12, m, 1H, 12', m, 1H), 7.72-7.67 (11, m, 1H, 11', m, 1H), 7.64 – 7.59 (3, m, 1H, 3', m, 1H), 7.38 – 7.34 (7, m, 2H), 7.33 - 7.25 (4, m, 1H, 7', m, 2H, 4', m, 1H), 7.22-7.20 (6, m, 1H, 6', m, 1H), 7.19 – 7.14 (8, m, 2H, 5, m, 1H, 5', m, 1H), 7.11 – 7.07 (8', m, 2H), 5.07 (2', s, 2H), 5.04 (2, s, 2H).

^{13}C NMR (151 MHz, DMSO-d_6) δ 163.39 (A’, s), 163.18 (M, s), 163.11 (A, s), 160.62 (L, d, J = 243.2 Hz), 150.11 (s), 149.94 (s),

148.94 (O, s), 138.63 (Q’, s), 138.49 (Q, s), 137.54 (I, d, J = 2.7 Hz), 136.39 (s), 135.96 (s), 130.87 (s), 128.79 (H, s), 128.05 (F, s), 127.40 (P, s), 126.08 (G’, s), 126.06 (G, s), 125.91 (E, s), 125.83 (J, d, J = 8.5 Hz), 122.81 (R’, s), 122.79 (R, s), 116.52 (K, d, J = 22.6 Hz), 115.79 (K’, d, J = 22.1 Hz), 50.29 (B’, s), 44.88 (B, s).

EI HRMS: obtained m/z 349.12148 M+ (expected m/z 349.12211 M+).

MP: 79 – 80 °C.

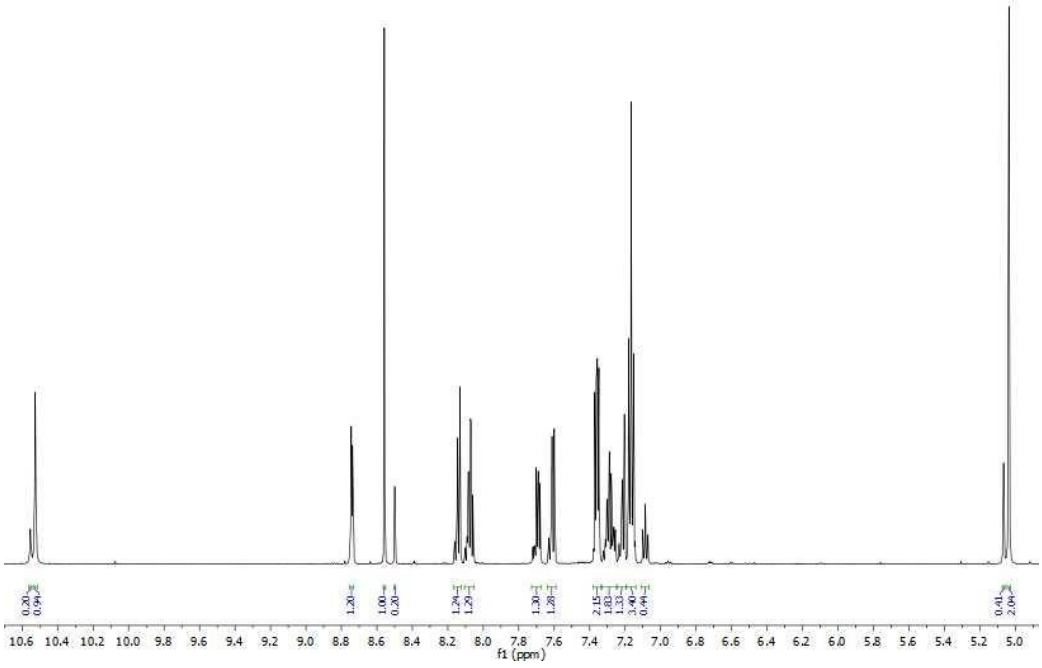

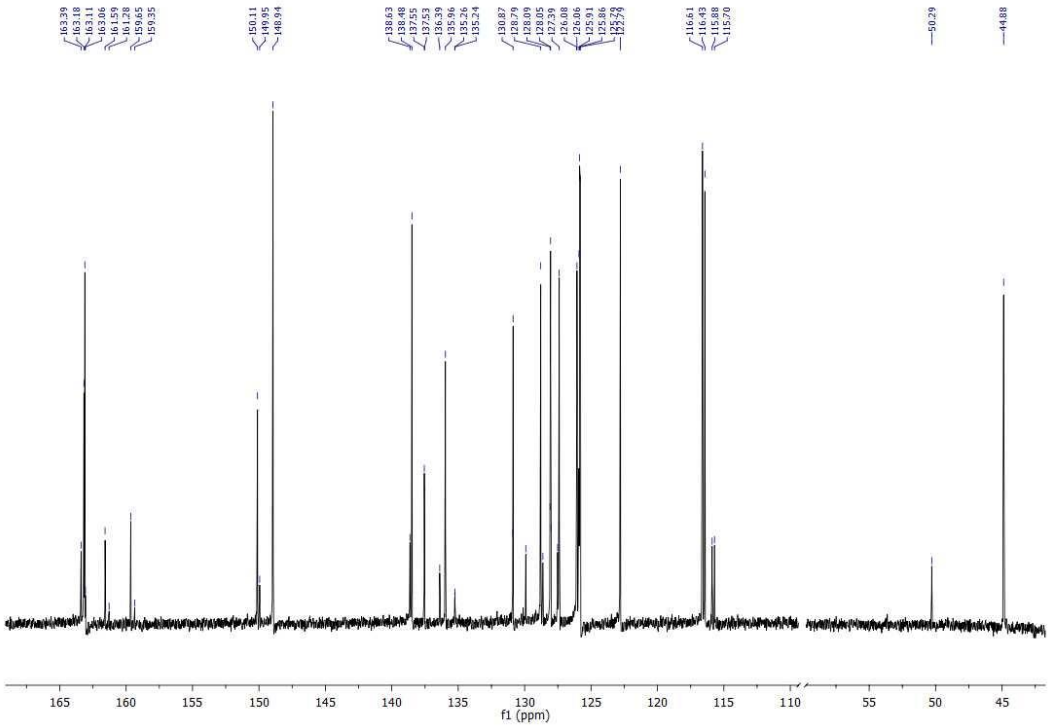

5-fluoro-*N*-[2-[(4-fluoro-*N*-formyl-anilino)methyl]phenyl]pyridine-2-carboxamide (18)

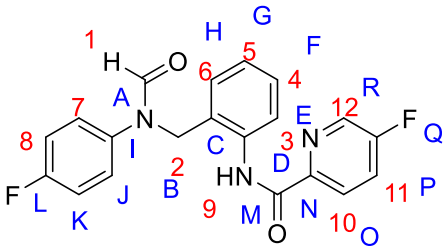

Prepared according to general method **B**: DMF (4 mL), *N*-[2-(2-aminophenyl)ethyl]-*N*-(4-fluorophenyl)formamide (200 mg, 0.819 mmol), 5-fluoro-2-pyridinecarboxylic acid (110 mg, 0.819 mmol) propylphosphonic anhydride (50 % mass) in ethyl acetate (540 µL, 0.900 mmol), triethylamine (100 mg, 140 µL, 0.983 mmol). Purification with column chromatography yielded a white solid (63.0 mg, 21 %).

^{1}H NMR (601 MHz, DMSO-d_6) δ 10.47 (9, s, 1H, 9', s, 1H), 8.74-8.73 (10, m, 1H, 10', m, 1H), 8.53 (1, s, 1H), 8.46 (1', s, 1H), 8.23-8.19 (12, m, 1H, 12', m 1H), 8.01-7.96 (11, m, 1H, 11', m, 1H), 7.55 – 7.52 (3, m, 1H, 3', m, 1H), 7.37 – 7.33 (7, m, 2H),

7.33 – 7.24 (4, m, 1H, 6, m, 1H, 7’, m, 2H), 7.24 – 7.14 (8, m, 2H, 5, m, 1H, 5’, m, 1H, 4’, m, 1H, 6’, m, 1H), 7.11 – 7.07 (8’, 2H), 5.04 (2’, s, 2H), 5.02 (2, s, 2H).

^{13}C NMR (126 MHz, DMSO-d_6) δ 163.34 (s), 163.09 (s), 162.36 (s), 162.31 (s), 161.58 (s), 160.31 (s), 159.65 (s), 146.92 (d, J = 3.6 Hz), 146.78 (d, 2.5 Hz), 137.59 (d, J = 2.8 Hz), 137.42 (s), 137.22 (s), 136.25 (s), 135.89 (s), 135.33 (d, J = 3.8 Hz), 131.60 (s), 131.30 (s), 129.75 (s), 128.82 (s), 128.57 (s), 128.06 (s), 128.04 (s), 127.99 (s), 126.74 (s), 126.32 (s), 126.24 (s) 125.85 (d, J = 8.5 Hz), 125.33 (s), 125.13 (s), 125.07 (s), 125.04 (s), 116.51 (d, J = 22.6 Hz), 115.78 (d, J = 22.5 Hz), 50.27 (s), 44.93 (s).

^{19}F NMR (471 MHz, DMSO-d_6) δ -115.97 (minor), -116.41 (major), -122.26 (minor), -122.48 (major).

EI HRMS: obtained m/z 367.11162 M+ (expected m/z 367.11268 M+).

MP: 79 – 80 °C.

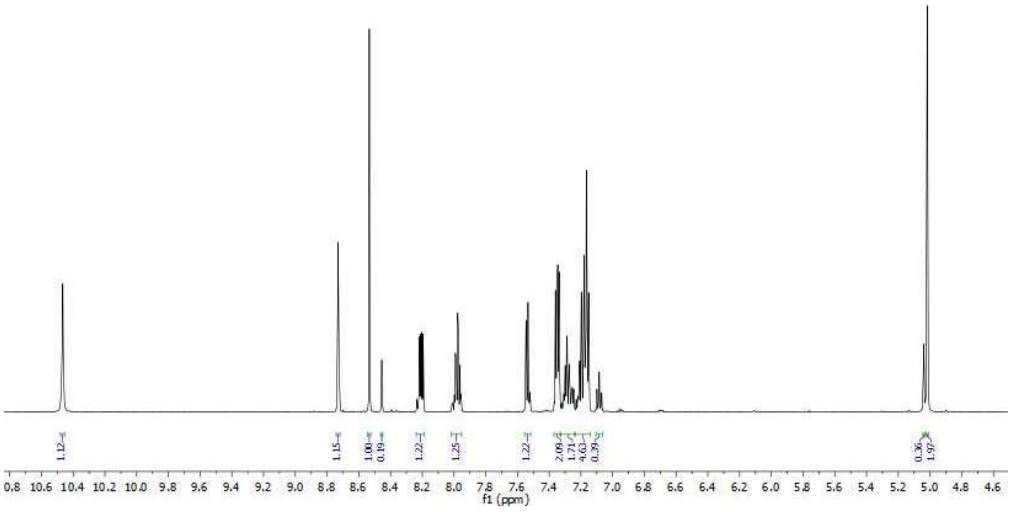

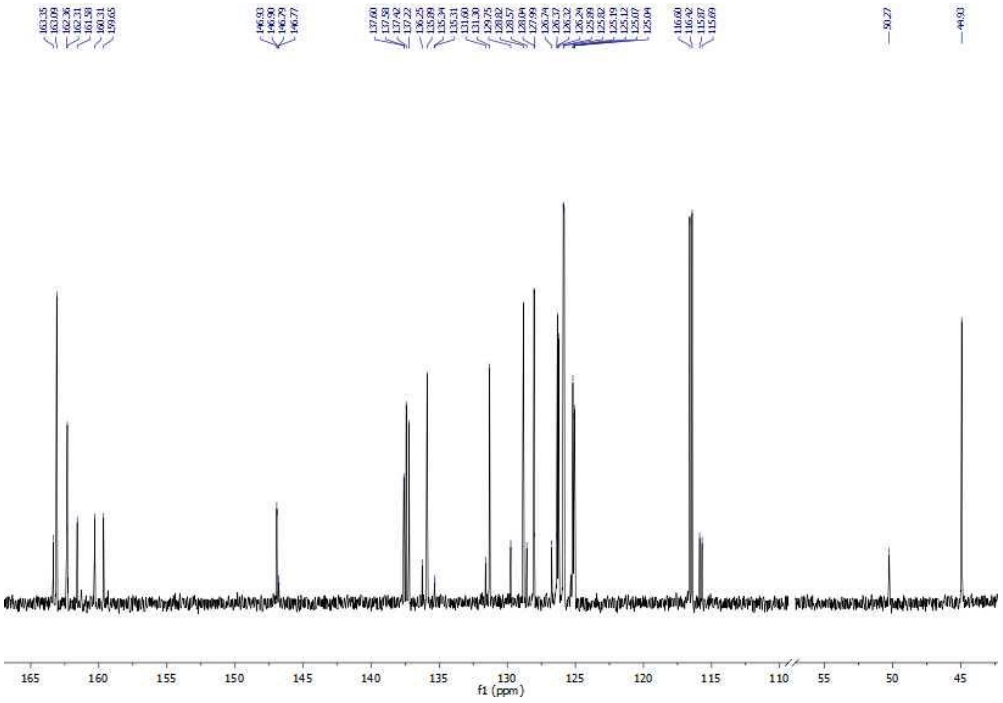

Ethylene linker series

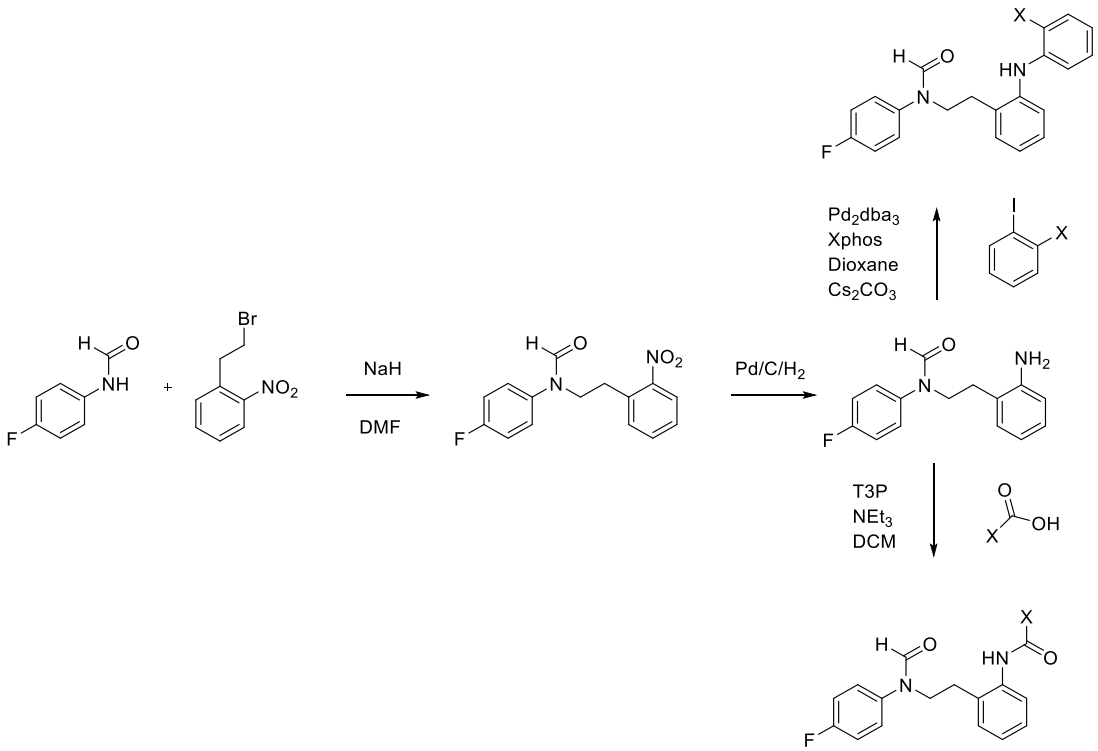

_N_-(4-fluorophenyl)-_N_-[2-(2-nitrophenyl)ethyl]formamide (38)

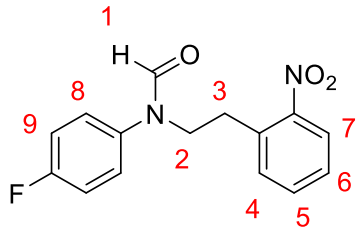

To a flask under a nitrogen atmosphere was added a solution of *N*-(4-fluorophenyl) formamide (200 mg, 1.44 mmol) in dry DMF (10 mL), 2-nitrophenethyl bromide (333 mg, 1.43 mmol) was then added and the mixture cooled to 0 °C. Sodium hydride (69.0 mg, 1.73 mmol) was then carefully added and the mixture allowed to warm to room temperature. The reaction mixture was stirred overnight, diluted in DCM (10 mL) and quenched with water (10 mL). The organics were then reduced *in vacuo*, dried with $MgSO_4$ and purified using column chromatography to yield a white solid (274 mg, 66 %).

^{1}H NMR (500 MHz, Chloroform-*d*) δ 8.34 (1, s, 1H), 8.23 (1', s, 1H), 7.99 (7', m, 1H), 7.92 (7, m, 1H), 7.55 (5, 5', m, 2H), 7.44 (4, 4', m, 2H), 7.39 (6, m, 1H), 7.35 – 7.31 (6', m, 1H), 7.15 – 7.06 (8, 9, 8', 9', m, 8H), 4.14 – 4.09 (2, m, 2H), 4.06 – 4.01 (2', m, 2H), 3.21 – 3.16 (3, m, 2H), 3.13 – 3.08 (3', m, 2H).

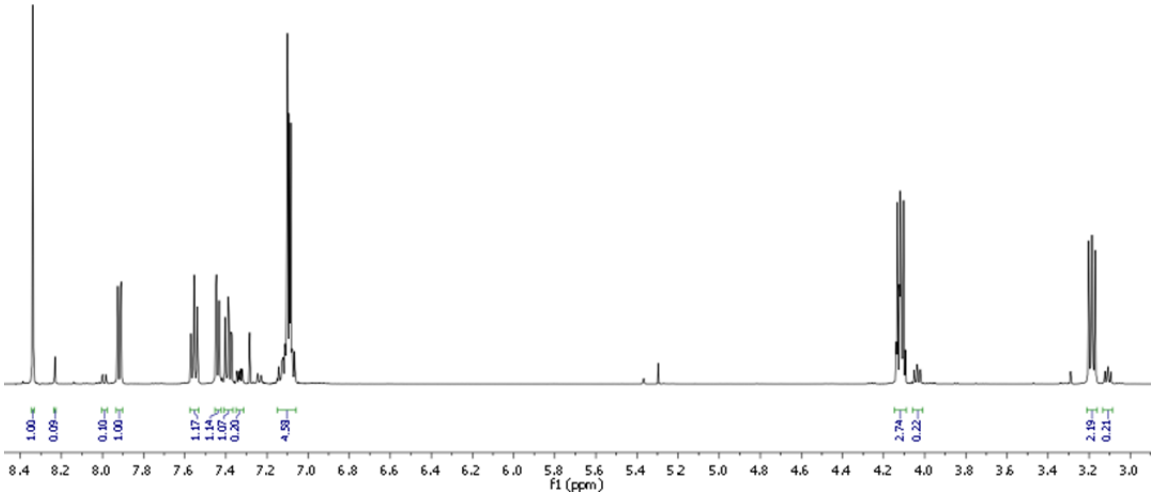

_N_-[2-(2-aminophenyl)ethyl]-_N_-(4-fluorophenyl)formamide (19)

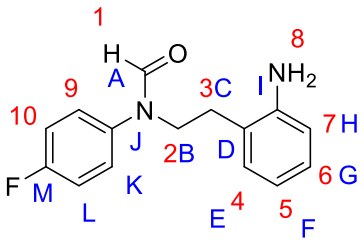

To a reaction flask under a nitrogen atmosphere was added a solution of *N*-(4-fluorophenyl)-*N*-[2-(2-nitrophenyl)ethyl]formamide (150 mg, 0.581 mmol) in EtOH (10 mL). Palladium on carbon (10 wt %) was then added and the reaction mixture placed under a hydrogen environment. The reaction mixture was monitored to completion via TLC and then filtered through Celite. The crude mixture was reduced under pressure and purified using column chromatography (1:4 EtOAc: *n*-Hex) to yield a white solid (120 mg, 86 %).

^{1}H NMR (601 MHz, DMSO-d_6) δ 8.38 (1, s, 1H), 8.10 (1', s, 1H), 7.43 – 7.40 (9', m, 1H), 7.38 – 7.34 (9, m, 2H), 7.28 – 7.24 (10, m, 2H, 10', m, 2H), 6.94 – 6.90 (6, m, 1H, 6', m, 1H), 6.87 (4, dd, J = 7.4, 1.6 Hz, 1H), 6.77 (4', dd, J = 7.5, 1.6 Hz, 1H), 6.64 – 6.60 (7, m, 1H, 7', m, 1H), 6.49 – 6.45 (5, m, 1H, 5', m, 1H), 4.97 (8, s, 2H), 4.92 (8', s, 1H), 3.89 – 3.87 (2', m, 2H), 3.86 – 3.82 (2, m, 2H), 2.72 – 2.67 (3, m, 2H), 2.63 – 2.61 (3', m, 2H).

^{13}C NMR (151 MHz, DMSO-d_6) δ 162.92 (A', s), 162.90 (A, s), 160.76 (M, d, J = 243.11 Hz), 160.39 (M', d, J = 243.11 Hz), 146.85 (I, s), 138.03 (J, d, J = 2.7 Hz), 135.60 (J', d, J = 2.8 Hz), 130.45 (E', s), 130.11 (E, s), 128.13 (K, d, J = 7.6 Hz), 127.76 (G', s), 127.71 (G, s), 126.13 (K', d, J = 8.5 Hz), 121.82 (D, s), 121.44 (D', s), 116.59 (L, d, J = 22.7 Hz), 116.65 (F, s), 116.65 (F', s), 116.07 (L', d, J = 22.5 Hz), 115.39 (H', s), 115.13 (H, s), 48.12 (B', s), 44.83 (B, s), 30.93 (C', s), 29.72 (C, s).

EI HRMS: obtained m/z 258.11552 M+ (expected m/z 258.11629 M+).

MP: 81 – 83 °C.

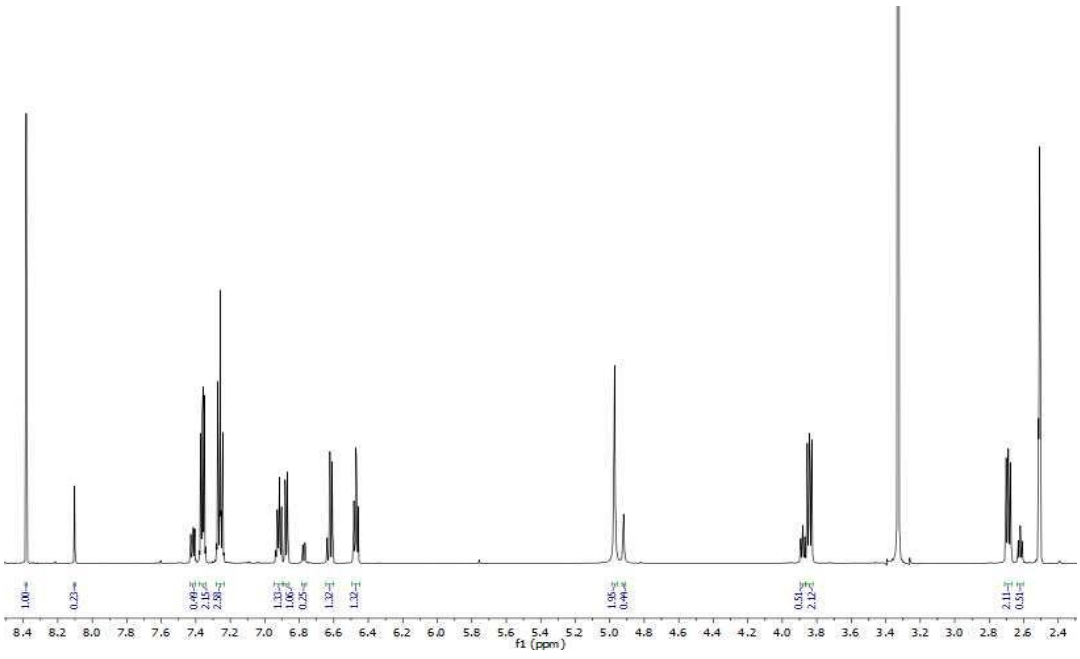
1.00
0.23
0.49
2.15
2.58
1.32
1.06
0.25
1.32
1.32
1.95
0.64
0.53
2.12
2.11
0.51
8.4 8.2 8.0 7.8 7.6 7.4 7.2 7.0 6.8 6.6 6.4 6.2 6.0 5.8 5.6 5.4 5.2 5.0 4.8 4.6 4.4 4.2 4.0 3.8 3.6 3.4 3.2 3.0 2.8 2.6 2.4
f1 (ppm)

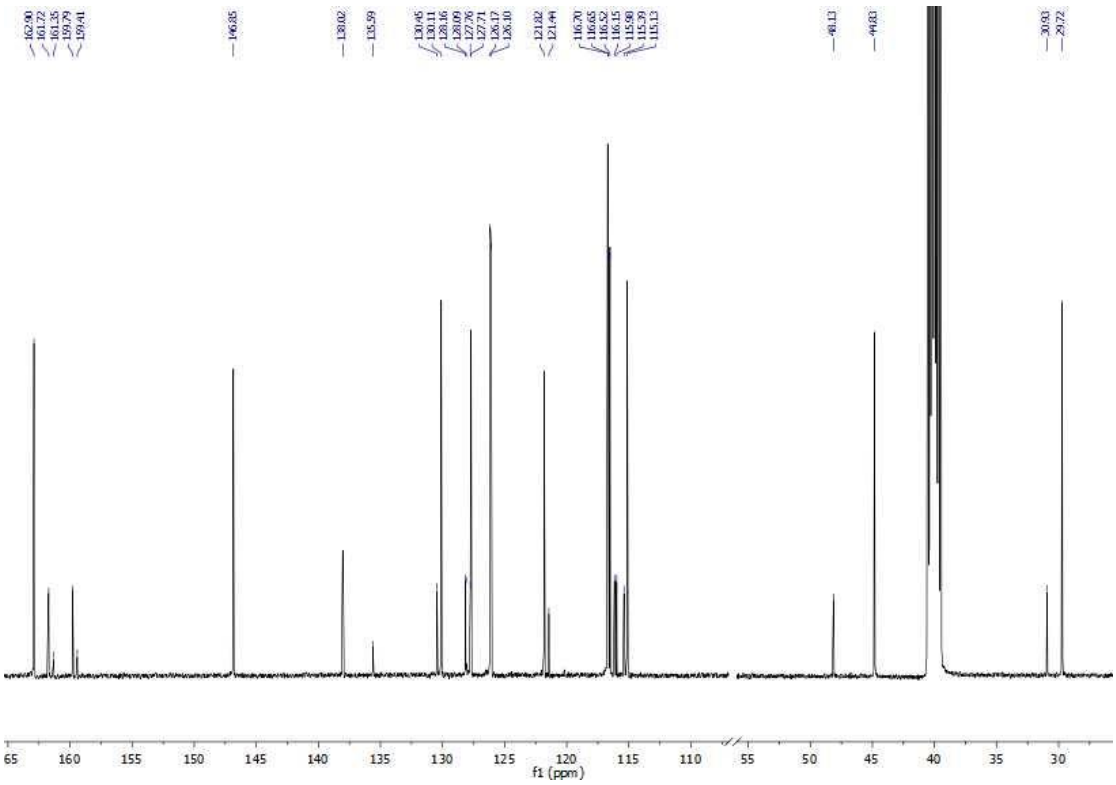

2-(4-nitrophenyl)acetaldehyde (39)

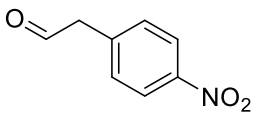

To a mixture of 2-(4-nitrophenyl)ethanol (1 g, 5.98 mmol) in acetonitrile (10 mL) was added iodoxybenzoic acid (8.4 g, 14.95 mmol). The reaction mixture was then refluxed for 2 hours. It was then filtered through Celite, washed with 1M NaOH (10 mL) and extracted with DCM (2 x 10 mL). The reaction was monitored to completion using TLC and used without further purification to yield an orange oil (612 mg, 62%).

4-fluoro-*N*-[2-(4-nitrophenyl)ethyl]aniline (40)

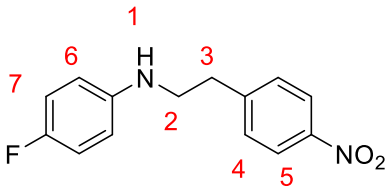

To a solution of 4-fluoroaniline (480 mg, 4.32 mmol) in dry methanol (10 mL) was added 2-(4-nitrophenyl)acetaldehyde (720 mg, 4.36 mmol) and sodium cyanoborohydride (360 mg, 5.67 mmol). Acetic acid (1.31 g, 1.31 mL, 0.022 mmol) was then added dropwise and the mixture heated to reflux overnight. The reaction mixture was then reduced under pressure and dissolved in ethyl acetate (10 mL), washed with water (10 mL) and brine (10 mL). The

reaction mixture was then concentrated, dried with $MgSO_4$ and purified using column chromatography (30 % EtOAc/n-Hex) to yield a yellow solid (866 mg, 77%).

^{1}H NMR (500 MHz, Chloroform-*d*) δ 8.23 – 8.18 (5, m, 2H), 7.42 – 7.37 (4, m, 2H), 6.96 – 6.89 (7, m, 2H), 6.60 – 6.54 (6, m, 2H), 3.55 (1, s, 1H), 3.45 (2, t, *J* = 6.9 Hz, 1H), 3.04 (3, t, *J* = 6.9 Hz, 1H).

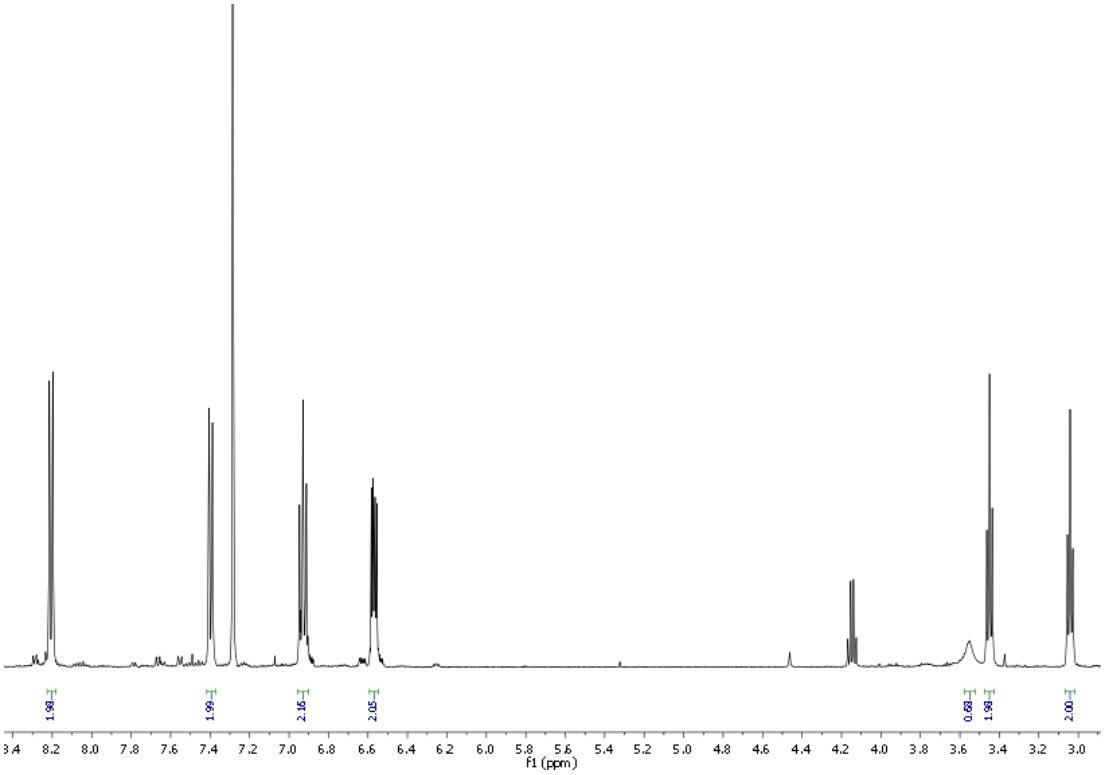

_N_-(4-fluorophenyl)-_N_-[2-(4-nitrophenyl)ethyl]formamide (41)

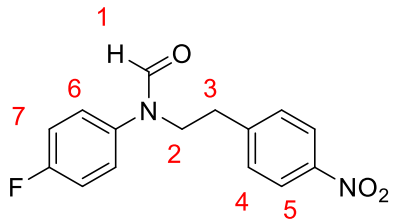

To a solution of 4-fluoro-*N*-[2-(4-nitrophenyl)ethyl]aniline (300 mg, 1.153 mmol) in dry DCM (10 mL) was added formic acid (53 mg, 43 µL, 1.153 mmol). Propylphosphonic anhydride solution (808 mg, 755 µL, 1.268 mmol) was then added followed by trimethylamine (140 mg, 0.193 µL, 1.384 mmol). The reaction

mixture was stirred overnight at room temperature and then extracted with DCM (10 mL), washed with 2M HCl (10 mL), water (10 mL) and brine (10 mL). The combined organic phases were then dried over $MgSO_4$ and concentrated in *vacuo*. The crude product was then purified using column chromatography (1:1 EtOAc: *n*-Hex) to yield a yellow solid (288 mg, 87%).

^{1}H NMR (400 MHz, Chloroform-*d*) δ 8.30 (1, s, 1H), 8.18 – 8.14 (5, m, 2H), 7.38 – 7.33 (4, m, 2H), 7.16 – 7.05 (6, 7, m, 4H), 4.13 – 4.06 (2, m, 2H), 3.03 – 2.97 (3, m, 2H).

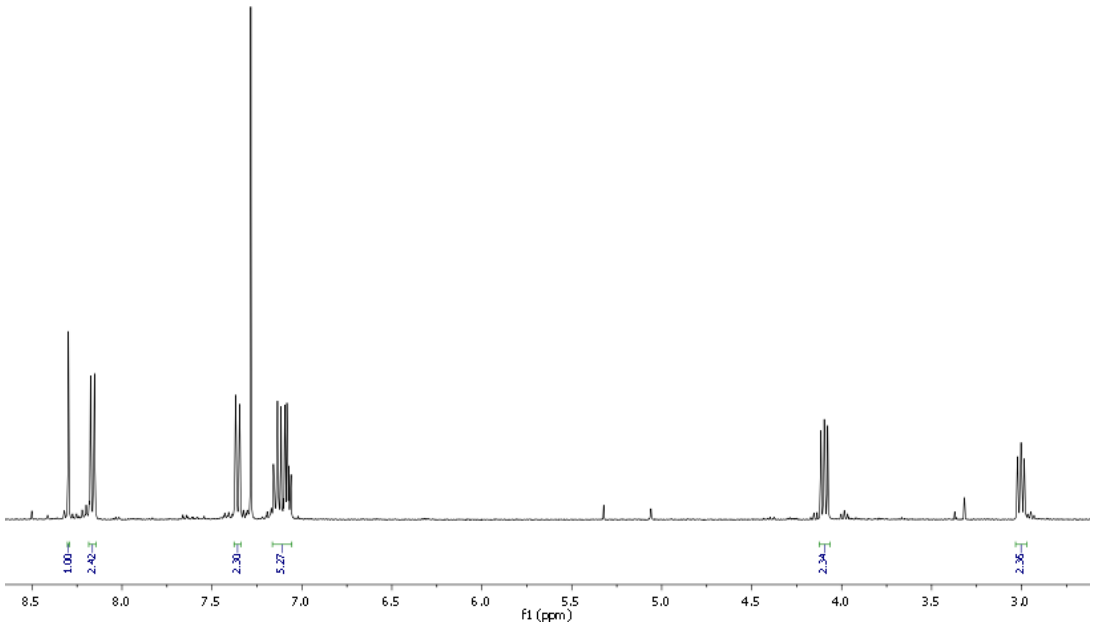

_N_-[2-(4-aminophenyl)ethyl]-_N_-(4-fluorophenyl)formamide (35)

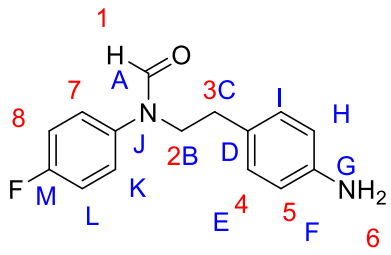

To a reaction flask under a nitrogen atmosphere was added a solution of *N*-(4-fluorophenyl)-*N*-[2-(2-nitrophenyl)ethyl]formamide (200 mg, 0.694 mmol) in EtOH (10 mL). Palladium on carbon (10% wt) was then added and the reaction mixture placed under a hydrogen environment. The reaction mixture was monitored to completion via TLC and then filtered through Celite. The crude mixture was reduced under pressure and purified using column chromatography (1:4 EtOAc: *n*-Hex) to yield a white solid (132 mg, 74%).

^{1}H NMR (500 MHz, DMSO-d_6) δ 8.32 (1, s, 1H), 8.07 (1', s, 1H), 7.40 – 7.37 (7', m, 2H), 7.36 – 7.31 (7, m, 2H), 7.29 – 7.24 (8', 8, m, 4H), 6.82-6.79 (4, 4', m, 4H), 6.52 – 6.48 (5', m, 2H), 6.48 – 6.44 (5, m, 2H), 4.90 (6', s, 2H), 4.87 (6, s, 2H), 3.91 – 3.83 (2, 2', m, 4H), 2.59 – 2.53 (3, 3', m, 4H).

^{13}C NMR (126 MHz, DMSO-d_6) δ 162.85 (s), 162.42 (s), 160.72 (d, *J* = 243.2 Hz), 160.41 (d, *J* = 244.4 Hz), 147.50, 147.42, 137.72 (d, *J* = 2.6 Hz), 135.43 (d, *J* = 2.9 Hz), 129.71, 129.48, 128.21 (d, *J* = 8.5 Hz), 126.30 (d, *J* = 8.5 Hz), 125.62, 125.11, 116.63 (d, *J* = 22.5 Hz), 116.10 (d, *J* = 22.4 Hz), 114.48, 114.44, 51.05, 46.46, 33.98, 32.80.

^{19}F NMR (471 MHz, DMSO-d6) δ -115.90 – -115.96 (minor, m), -116.39 – -116.44 (major, m).

EI HRMS: obtained m/z 258.11722 M+ (expected m/z 258.11629 M+).

MP: 84 – 86 °C.

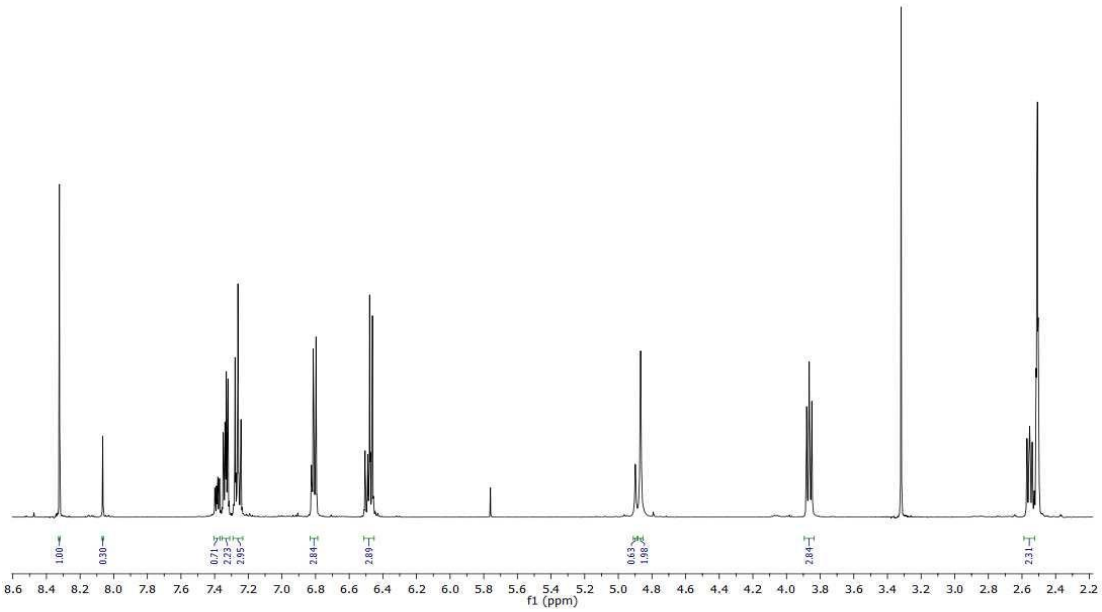
1.00
0.30
0.71
2.23
2.95
2.84
2.89
0.63
1.98
2.84
2.31
f1 (ppm)

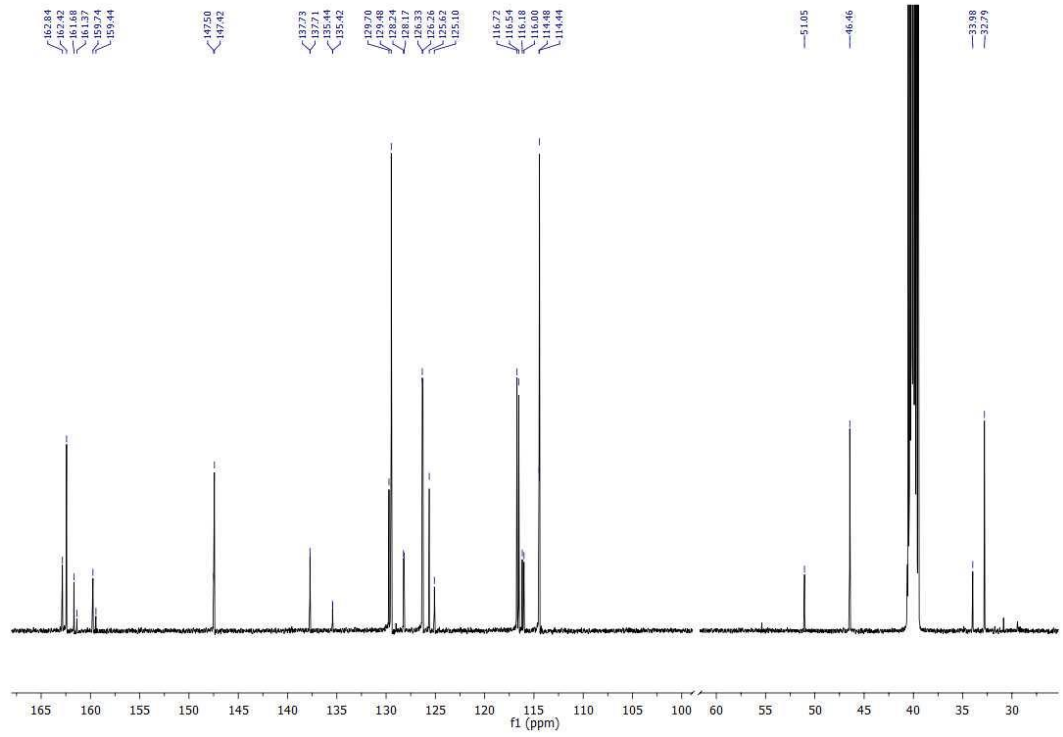
162.84
162.42
161.68
161.37
159.74
159.44
147.50
147.42
137.73
137.71
135.44
135.42
129.70
129.48
128.24
128.17
126.33
126.26
125.52
125.10
116.72
116.54
116.18
116.00
114.48
114.44
51.05
46.46
33.98
32.79
f1 (ppm)

Buchwald-Hartwig couplings

General Method:

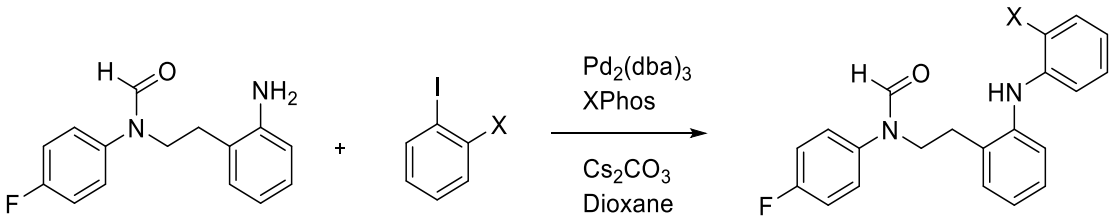

To a flask under a nitrogen atmosphere was added a solution of *N*-[2-(2-aminophenyl)ethyl]-*N*-(4-fluorophenyl)formamide in degassed dioxane (10 mL). The appropriately substituted iodobenzene was then added along with caesium carbonate, XPhos and $Pd_2(dba)_3$. The reaction mixture was then refluxed overnight, and filtered through celite. Water was added and then the reaction mixture was extracted with DCM (2 x 10 mL), dried over $MgSO_4$, concentrated under reduced pressure and purified by column chromatography.

_N_-[2-(2-anilinophenyl)ethyl]-_N_-(4-fluorophenyl)formamide (20)

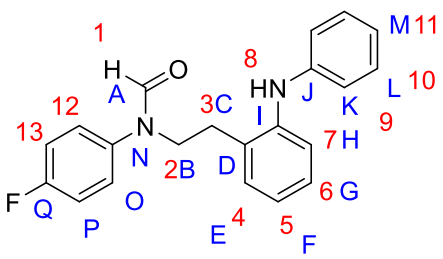

Prepared according to general method: Dioxane (10 mL), *N*-[2-(2-aminophenyl)ethyl]-*N*-(4-fluorophenyl)formamide (300 mg, 1.16 mmol), iodobenzene (400 mg, 224 µL, 1.97 mmol), Cs_2CO_3 (1.14 g, 3.48 mmol), XPhos (55.3 mg, 0.116 mmol) and $Pd_2(dba)_3$ (63.8 mg, 0.0697 mmol). Purification with column chromatography (1:1 EtOAc: *n*-Hex) yielded a yellow solid (91 mg, 23%).

^{1}H NMR (500 MHz, DMSO-d6) δ 8.36 (1, s, 1H), 8.08 (1', s, 1H), 7.47 (8, s, 1H), 7.45 (8', s, 1H), 7.35 – 7.30 (12', m, 2H), 7.27 – 7.22 (12, m, 2H), 7.21 – 7.13 (13, m, 2H, 13', m, 2H, 4, m, 1H, 4', m, 1H, 6, m, 1H, 6', m, 1H, 5, m, 1H, 5', m, 1H), 6.99 (7', m, 1H), 6.95 (7, m, 1H), 6.84 – 6.70 (9, m, 2H, 9', m, 2H, 11, m, 1H, 11', m, 1H, 10, m, 1H, 10', m, 1H), 3.91 – 3.88 (2, 2', m, 4H), 2.88 – 2.81 (3, m, 2H), 2.79 – 2.76 (3', m, 2H).

^{13}C NMR (126 MHz, DMSO-d_6) δ 162.75, 160.64 (d, *J* = 243.2 Hz), 160.30 (d, *J* = 243.2 Hz), 146.03, 145.72, 141.63, 141.58, 137.85 (d, *J* = 2.8 Hz), 135.41 (d, *J* = 3.1 Hz), 131.42, 131.39, 131.17, 131.00, 129.54, 129.48, 127.99, 127.89, 127.83, 125.82 (d, *J* = 8.5 Hz), 123.33, 122.86, 122.72, 121.50, 119.20, 119.04, 116.53 (d, *J* = 22.5 Hz), 116.13, 115.96 (d, *J* = 22.4 Hz), 115.82, 49.07, 45.18, 31.36, 29.88.

^{19}F NMR (471 MHz, DMSO-d_6) δ -116.09 (minor), -116.58 (major).

EI HRMS: obtained m/z 334.14816 M+ (expected m/z 334.14759 M+)

MP: 86-87 °C.

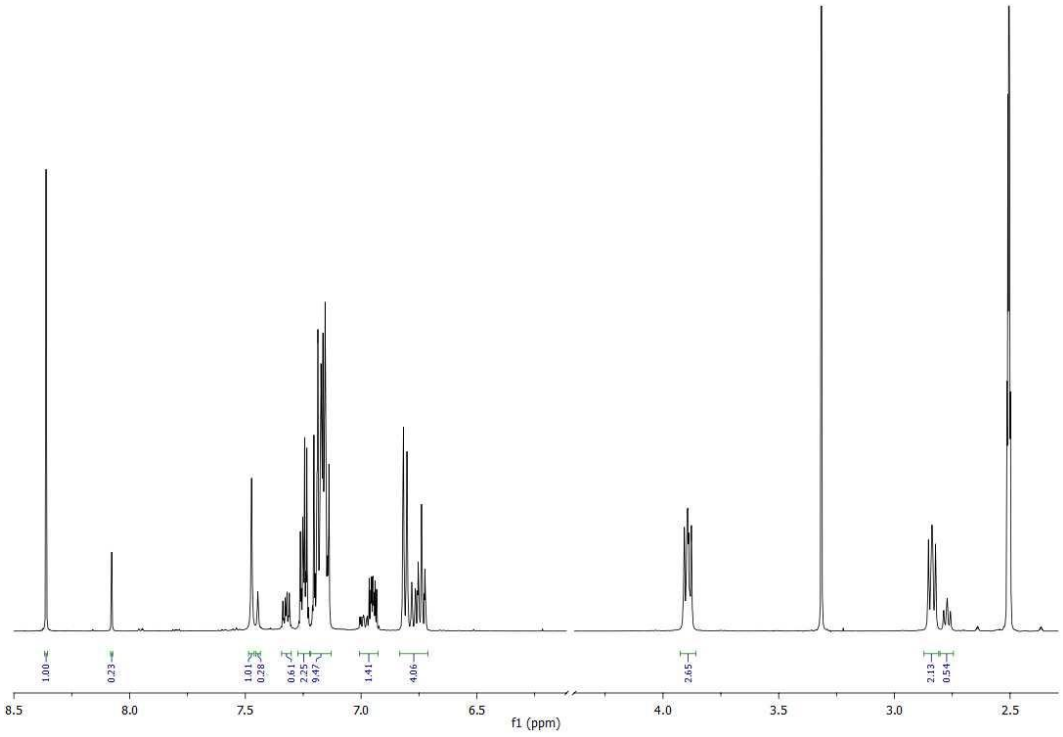

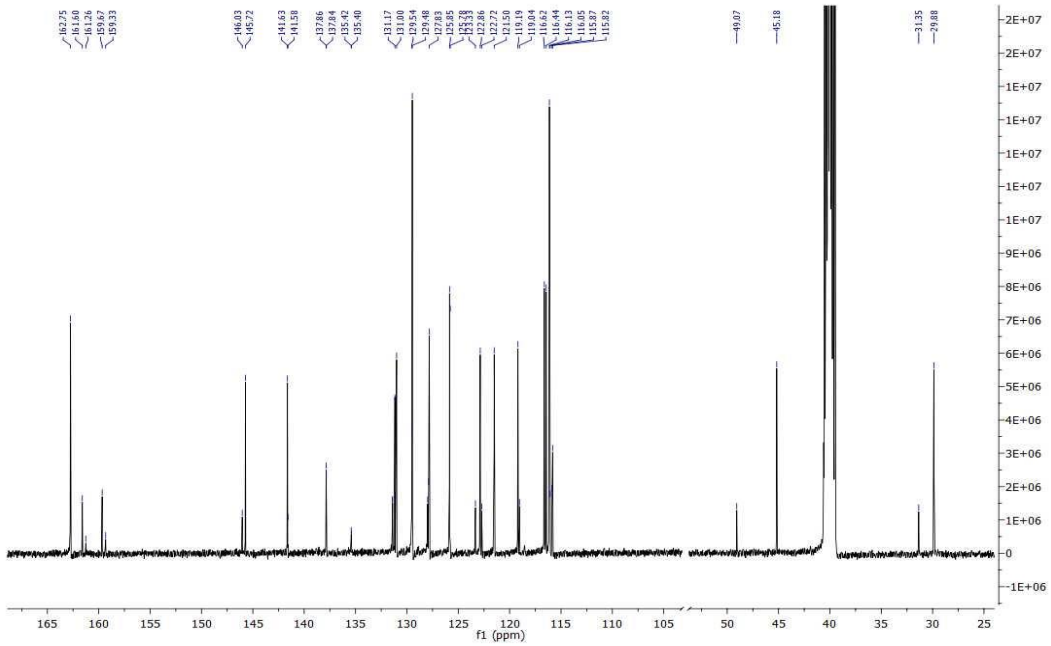

_N_-(4-fluorophenyl)-_N_-[2-[2-(2-methoxyanilino)phenyl]ethyl]formamide (21)

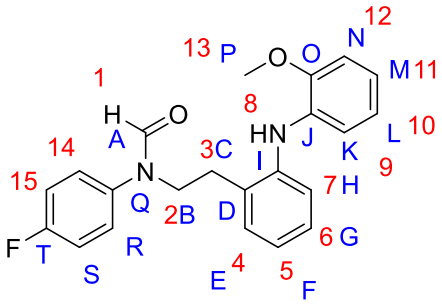

Prepared according to general method: Dioxane (10 mL), _N_-[2-(2-aminophenyl)ethyl]-_N_-(4-fluorophenyl)formamide (300 mg, 1.16 mmol), 2-iodoanisole (462 mg, 257 µL, 1.97 mmol), Cs_2CO_3 (1.14 g, 3.48 mmol), XPhos (55.3 mg, 0.116 mmol) and $Pd_2(dba)_3$ (63.8 mg, 0.0697 mmol). Purification with column chromatography (1:1 EtOAc: _n_-Hex) yielded a brown oil (110 mg, 26 %).

^{1}H NMR (500 MHz, DMSO-d_6) δ 8.35 (1, s, 1H), 8.09 (1', s, 1H), 7.35 – 7.30 (14', m, 1H), 7.27 – 7.21 (14, m, 2H, 15', m, 2H), 7.21 – 7.13 (15, m, 2H, 5, m, 1H, 5', m, 1H), 7.04 – 7.00 (7, m, 1H, 7', m, 1H), 7.00 – 6.94 (5, m, 1H, 5', m, 1H, 6, m, 1H, 6', m, 1H), 6.81 – 6.72 (9, m, 1H, 9', m, 1H, 11, m, 1H, 11', m, 1H), 6.66 – 6.58 (12, m, 1H, 12', m, 1H, 10, m, 1H, 10', m, 1H), 3.93 – 3.87 (2, m, 2H, 2', m, 2H), 3.81 (13, s, 3H, 13', s, 3H), 2.83 – 2.77 (3, m, 2H), 2.74 (3', m, 2H).

^{13}C NMR (126 MHz, DMSO-d_6) δ 162.82 (s), 162.60 (s), 160.61 (d, J = 242.9 Hz), 149.03 (s), 148.93 (s), 141.77 (s), 137.76 (d, J = 2.6 Hz), 135.38 (d, J = 3.0 Hz), 134.91

(s), 134.67 (s), 131.46 (s), 131.33 (s), 131.16 (s), 130.85 (s), 127.98 (s), 127.84 (s), 127.76 (s), 125.77 (d, *J* = 8.5 Hz), 123.31 (s), 123.08 (s), 123.00 (s), 122.01 (s), 121.17 (s), 121.10 (s), 120.03 (s), 119.94 (s), 116.51 (d, *J* = 22.5 Hz), 115.95 (d, *J* = 22.4 Hz), 115.46 (s), 115.28 (s), 111.59 (s), 111.54 (s), 55.99 (s), 55.95 (s), 48.95 (s), 45.03 (s), 31.32 (s), 29.78 (s).

^{19}F NMR (471 MHz, DMSO-d_6) δ -116.11 (minor), -116.60 (major).

EI HRMS: obtained m/z 364.15891 M+ (expected m/z 364.15816 M+).

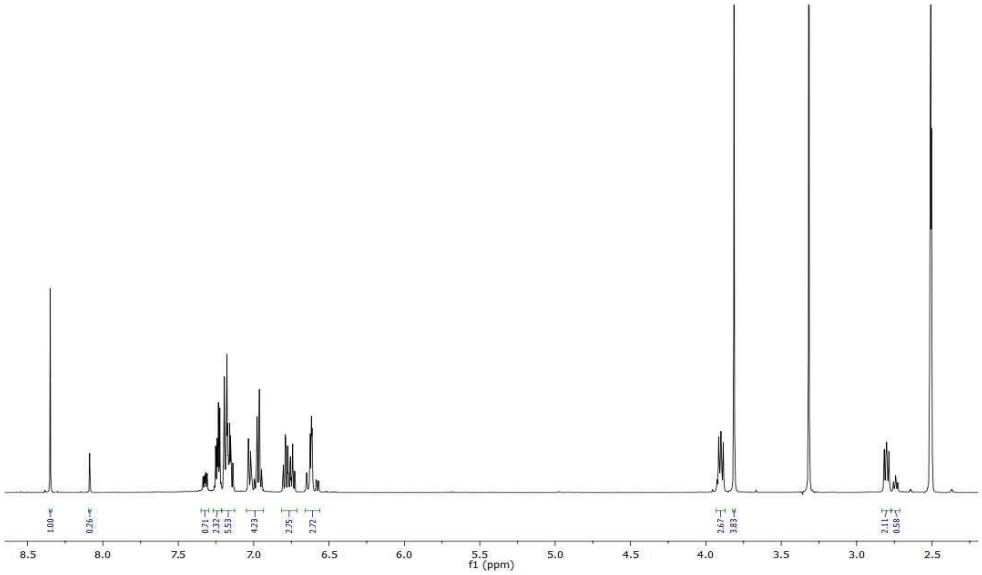

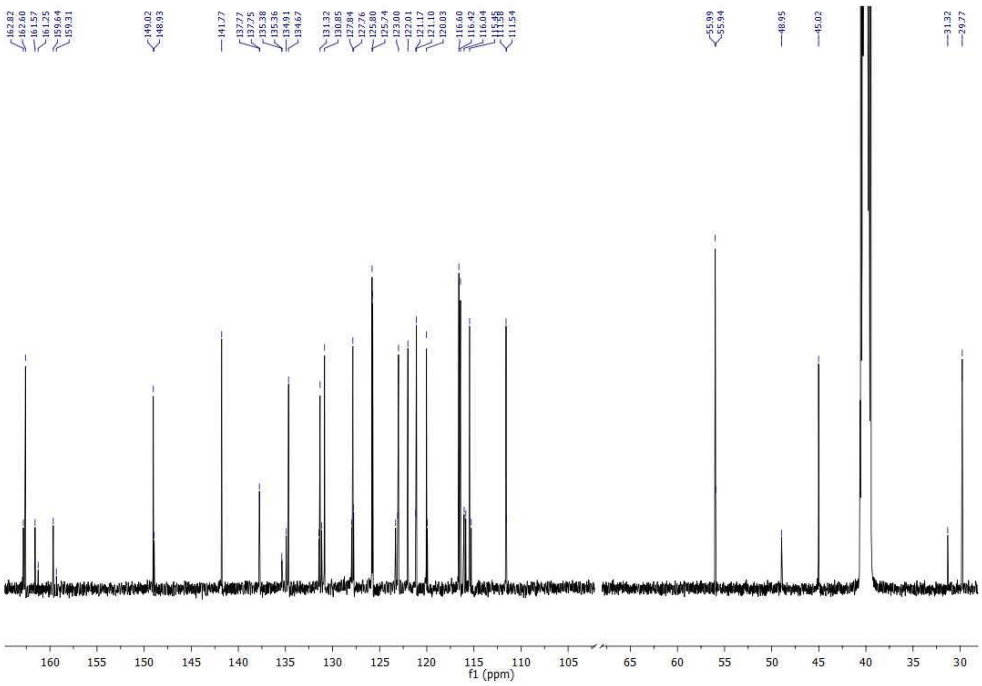

_N_-[2-[2-(2-cyanoanilino)phenyl]ethyl]-_N_-(4-fluorophenyl)formamide (22).

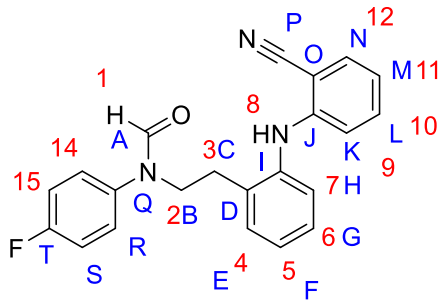

Prepared according to general method: Dioxane (10 mL), _N_-[2-(2-aminophenyl)ethyl]-_N_-(4-fluorophenyl)formamide (300 mg, 1.16 mmol), 2-iodobenzonitrile (453 mg, 1.98 mmol), Cs_2CO_3 (1.14 g, 3.48 mmol), XPhos (55.3 mg, 0.116 mmol) and $Pd_2(dba)_3$ (63.8 mg, 0.0697 mmol). Purification with column chromatography (1:1 EtOAc: _n_-Hex) yielded a yellow solid (337 mg, 81%).

^{1}H NMR (601 MHz, DMSO-d_6) δ 8.32 (1, s, 1H), 8.14 (1’, s, 1H), 7.96 (8’, s, 1H), 7.90 (8, s, 1H), 7.60 – 7.54 (12, m, 1H, 12’, m, 1H), 7.38 – 7.09 (15, m, 2H, 15’, m, 2H, 14, m, 2H, 14’, m, 2H, 6, m, 1H, 6’, m, 1H, 5, m, 1H, 5’, m, 1H, 4, m, 1H, 11, m, 1H, 11’, m, 1H, 10, m, 1H, 10’, m, 1H, 9, m, 1H, 9’, m, 1H), 6.85 – 6.80 (5, m, 1H, 5’, m, 1H), 6.47 – 6.44 (7, m, 1H, 7’, m, 1H), 3.92 – 3.86 (2, m, 2H, 2’, m, 2H), 2.76-2.73 (3, m, 2H), 2.70-2.67 (3’, m, 2H).

^{13}C NMR (126 MHz, DMSO-d_6) δ 162.81 (s), 162.49 (s), 160.60 (d, J = 243.0 Hz), 149.60 (s), 149.54 (s), 139.84 (s), 139.79 (s), 137.53 (d, J = 2.9 Hz), 135.23 (s), 134.72 (s), 134.70 (s), 134.60 (s), 134.24 (s), 134.18 (s), 134.13 (s), 131.45 (s), 131.11 (s), 128.45 (s), 128.30 (s), 127.79 (d, J = 8.4 Hz), 126.48 (s), 126.36 (s), 126.07 (s), 126.02 (s), 125.71 (d, J = 8.5 Hz), 119.12 (s), 119.00 (s), 118.22 (s), 118.18 (s), 116.58 (d, J = 22.5 Hz), 116.04 (d, J = 22.5 Hz), 115.68 (s), 115.55 (s), 98.04 (s), 97.99 (s), 49.26 (s), 44.87 (s), 31.27 (s), 29.75 (s).

EI HRMS: obtained m/z 359.14277 M+ (expected m/z 359.14284 M+).

MP: 102 – 104 °C.

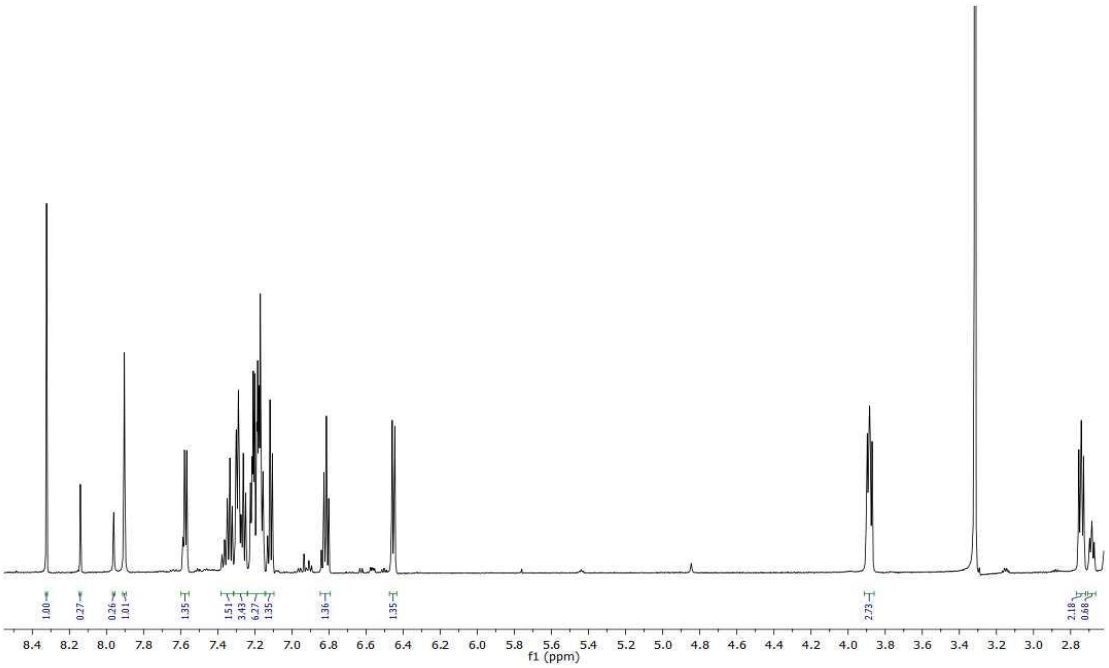
1.00
0.27
0.26
1.01
1.35
1.51
3.43
6.27
1.35
1.36
1.35
2.73
2.18
0.68
f1 (ppm)

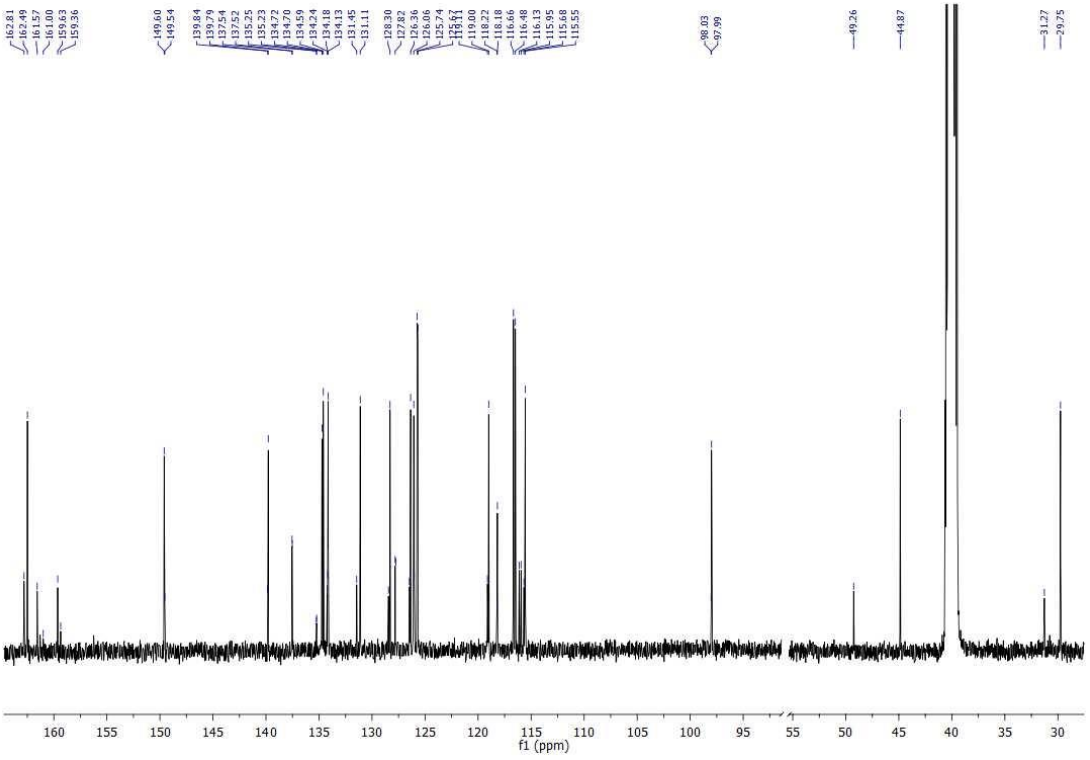
162.81
162.49
161.57
161.00
159.63
159.36
149.60
149.54
139.84
139.79
137.54
137.52
135.25
135.23
134.72
134.70
134.59
134.24
134.18
134.13
131.45
131.11
128.30
127.82
126.36
126.06
125.74
125.67
119.00
118.22
118.18
116.66
116.48
116.13
115.95
115.68
115.55
98.03
97.99
49.26
44.87
31.27
29.75
f1 (ppm)

Amide Couplings

General Method:

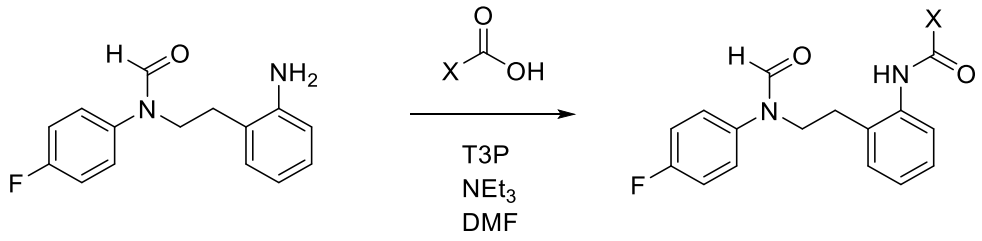

To a solution of aniline in dry DMF was added an appropriately substituted acid. Propylphosphonic anhydride solution was then added followed by triethylamine. The reaction mixture was stirred overnight at room temperature and then extracted with DCM, washed with 2M HCl, water and brine. The combined organic phases were then dried over $MgSO_4$ and concentrated *in vacuo*. The crude product was then purified by column chromatography.

_N_-[2-[2-(4-fluoro-_N_-formyl-anilino)ethyl]phenyl]acetamide (23)

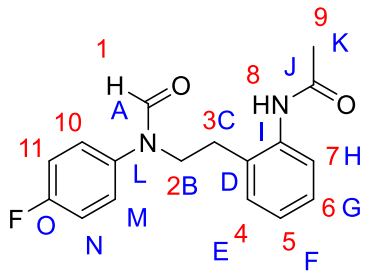

Prepared according to general method: DMF (4 mL), *N*-[2-(2-aminophenyl)ethyl]-*N*-(4-fluorophenyl)formamide (200 mg, 0.774 mmol), acetic acid (46.5 mg, 44.3 µL, 0.774 mmol), propylphosphonic anhydride (50%) in ethyl acetate (542 mg, 507 µL, 0.852 mmol), triethylamine (94.0 mg, 130 µL, 0.929 mmol). Purification with column chromatography (1:1 EtOAc: *n*-Hex) yielded a white solid (160 mg, 69%).

^{1}H NMR (601 MHz, DMSO-d_6) δ 9.35 (8, s, 1H), 8.37 (1, s, 1H), 8.14 (1', s, 1H), 7.41 – 7.34 (10, m, 2H, 10', m, 2H, 7, m, 1H, 7', m, 1H), 7.30 – 7.25 (11, m, 2H, 11', m, 2H), 7.23 – 7.18 (4, m, 1H, 4', m, 1H, 6, m, 1H, 6', m, 1H), 7.17 – 7.09 (5, m, 1H, 5',

m, 1H), 3.89 – 3.80 (2, m, 2H, 2', m, 2H), 2.81 – 2.76 (3, m, 2H), 2.72 (3', t, J = 7.5 Hz, 2H), 2.01 (9, s, 3H), 1.96 (9, s, 3H).

^{13}C NMR (126 MHz, DMSO-d_6) δ 169.07 (J, s), 162.84 (A', s), 162.70 (A, s), 160.79 (O, d, J = 243.18 Hz), 160.45 (O', d, J = 243.18 Hz), 137.76 (L, d, J = 2.5 Hz), 136.94 (I, s), 136.78 (I', s), 135.35 (L', d, J = 2.9 Hz), 133.44 (D', s), 133.11 (D, s), 130.67 (E', s), 130.39 (E, s), 128.10 (M', d, J = 8.5 Hz), 127.39 (G', s), 127.31 (G, s), 126.48 (H, s), 126.25 (F', s), 126.15 (M, d, J = 8.5 Hz), 125.96 (F, s), 116.65 (N, d, J = 22.6 Hz), 116.10 (N', d, J = 22.5 Hz), 49.40 (B', s), 45.52 (B, s), 31.27 (C', s), 29.86 (C, s), 23.62 (K, s), 23.48 (K', s).

^{19}F NMR (471 MHz, DMSO-d_6) δ -115.95 (minor), -116.36 (major).

EI HRMS: obtained m/z 300.12757 M+ (expected m/z 300.12686 M+).

MP: 110 – 113 °C

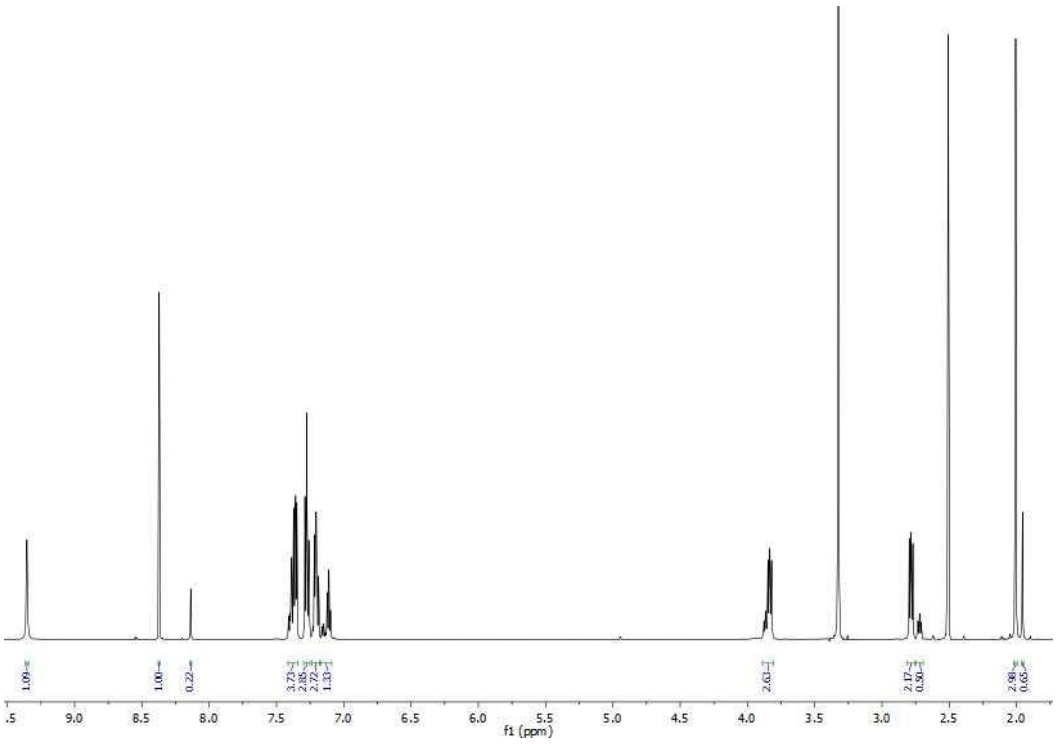

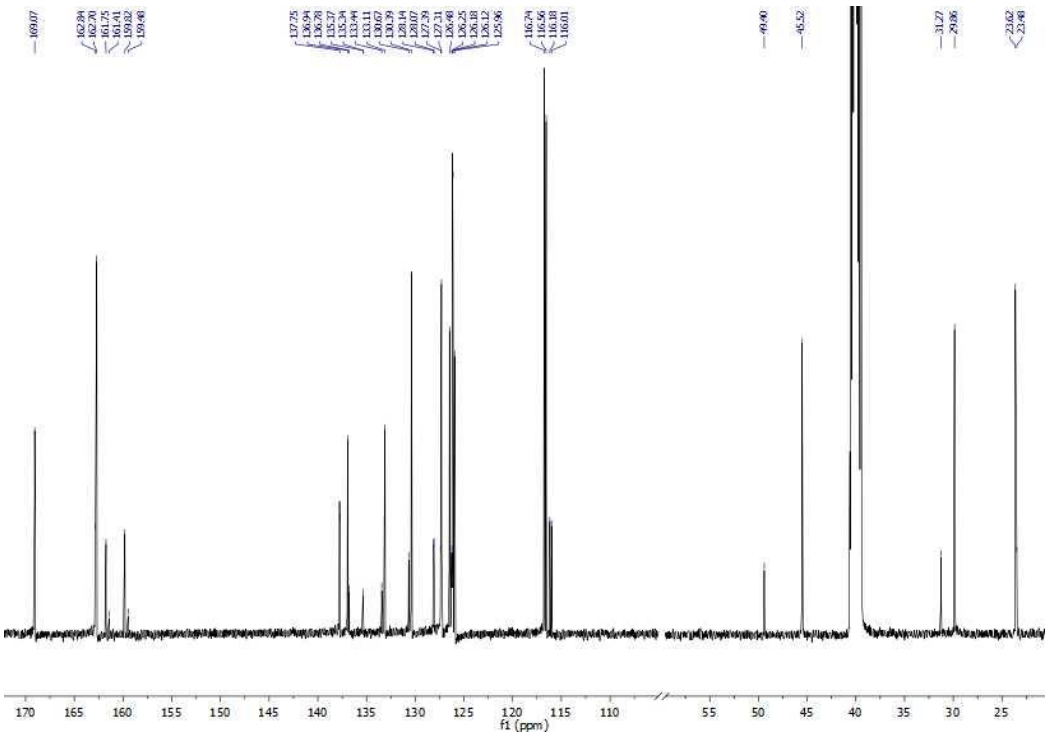

2,2,2-trifluoro-*N*-[2-[2-(4-fluoro-*N*-formyl-anilino)ethyl]phenyl]acetamide (24)

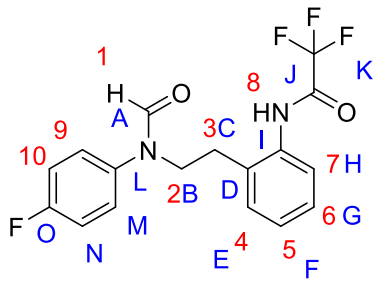

Prepared according to general method: DMF (4 mL), *N*-[2-(2-aminophenyl)ethyl]-*N*-(4-fluorophenyl)formamide (200 mg, 0.774 mmol), trifluoroacetic acid (88.3 mg, 59.3 µL, 0.774 mmol), propylphosphonic anhydride (50%) in ethyl acetate (542 mg, 507 µL, 0.852 mmol), triethylamine (94.0 mg, 130 µL, 0.929 mmol). Purification with column chromatography (1:1 EtOAc: *n*-Hex) yielded a white solid (195 mg, 71%).

^{1}H NMR (601 MHz, DMSO-d_6) δ 10.93 (8, s, 1H), 8.32 (1, s, 1H), 8.16 (1', s, 1H), 7.38 – 7.29 (9, m, 2H, 9', m, 2H, 7, m, 1H, 4, m, 1H, 7', m, 1H, 6, m, 1H, 6', m, 1H), 7.29 – 7.22 (10, m, 2H, 10', m, 2H, 5, m, 1H, 5', m, 1H), 3.90 – 3.83 (2, m, 2H, 2', m, 2H), 2.76 – 2.71 (3, m, 2H), 2.70 – 2.65 (3', m, 2H).

^{13}C NMR (126 MHz, DMSO-d6) δ 162.77 (s), 162.48 (s), 160.82 (d, J = 243.3 Hz), 160.57 (d, J = 243.18 Hz), 156.20 (q, J = 36.6 Hz), 137.56 (d, J = 2.9 Hz), 135.34 (s), 135.13 (d, J = 3.0 Hz), 134.87 (s), 133.83 (s), 131.01 (s), 130.74 (s), 128.44 (s), 128.23

(d, *J* = 8.5 Hz), 128.07 (s), 127.96 (s), 127.83 (s), 126.34 (d, *J* = 8.5 Hz), 119.92 (s), 117.63 (s), 116.61 (d, *J* = 22.6 Hz), 116.11 (d, *J* = 22.5 Hz), 115.33 (s), 113.04 (s), 49.39 (s), 45.30 (s), 30.93 (s), 29.42 (s).

^{19}F NMR (471 MHz, DMSO-d_6) δ -73.95 (C$\underline{F}_3$, major), -74.00 (C$\underline{F}_3$, minor), -115.89 (minor), -116.35 (major).

EI HRMS: obtained m/z 354.09803 M+ (expected m/z 354.09859 M+).

MP: 125 – 127 °C.

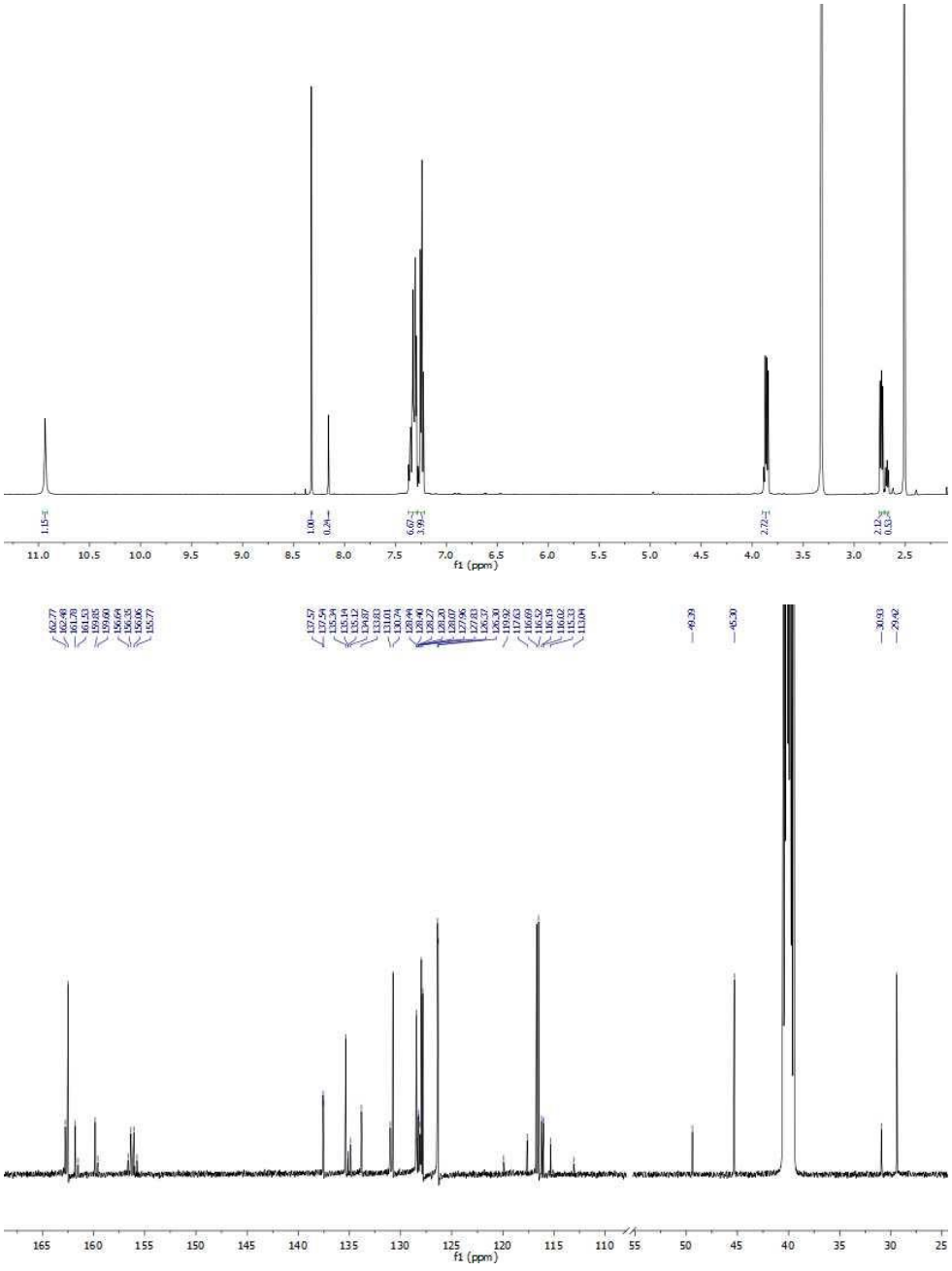

_N_-[2-[2-(4-fluoro-_N_-formyl-anilino)ethyl]phenyl]-2,2-dimethyl-propanamide (25)

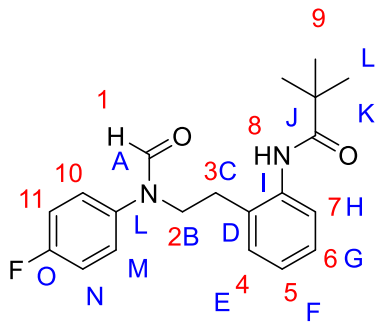

Prepared according to general method: DMF (4 mL), *N*-[2-(2-aminophenyl)ethyl]-*N*-(4-fluorophenyl)formamide (200 mg, 0.774 mmol), trimethylacetic acid (79 mg, 88.9 µL, 0.774 mmol), propylphosphonic anhydride (50%) in ethyl acetate (542 mg, 507 µL, 0.852 mmol), triethylamine (94.0 mg, 130 µL, 0.929 mmol). Purification with column chromatography (1:1 EtOAc: *n*-Hex) yielded a white solid (217 mg, 82%).

^{1}H NMR (500 MHz, DMSO-d_6) δ 8.95 (8', s, 1H), 8.87 (8, s, 1H), 8.31 (1, s, 1H), 8.14 (1', s, 1H), 7.38 – 7.32 (10, m, 2H, 10', m, 2H), 7.28 – 7.09 (11, m, 2H, 11', m, 2H, 4, m, 1H, 4', m, 1H, 5, m, 1H, 5', m, 1H, 6, m, 1H, 6', m, 1H, 7, m, 1H, 7', m, 1H), 3.90 – 3.84 (2, m, 2H, 2', m, 2H), 2.71 – 2.63 (3, m, 2H, 3', m, 2H), 1.12 (9, s, 9H, 9', s, 9H).

^{13}C NMR (126 MHz, DMSO-d_6) δ 177.42 (s), 177.35 (s), 162.90 (s), 162.46 (s), 160.91 (d, J = 243.18 Hz), 160.63 (d, J = 243.18 Hz), 137.66 (d, J = 2.8 Hz), 137.09 (s), 135.37 (s), 135.28 (s), 130.44 (s), 130.08 (s), 128.70 (s), 128.62 (s), 128.55 (s), 128.28 (s), 127.33 (s), 127.15 (s), 126.87 (d, J = 8.5 Hz), 126.73 (s), 116.62 (d, J = 22.4 Hz), 116.16 (d, J = 22.7 Hz), 67.49 (s), 56.50 (s), 49.52 (s), 45.54 (s), 38.99 (s), 31.31 (s), 29.57 (s), 27.66 (s), 25.60 (s), 19.03 (s).

^{19}F NMR (471 MHz, DMSO-d_6) δ -115.80– -115.86 (minor, m), -116.17 – -116.23 (major, m).

EI HRMS: obtained m/z 342.17408 M+ (expected m/z 342.17381 M+).

MP: 122 – 125 °C

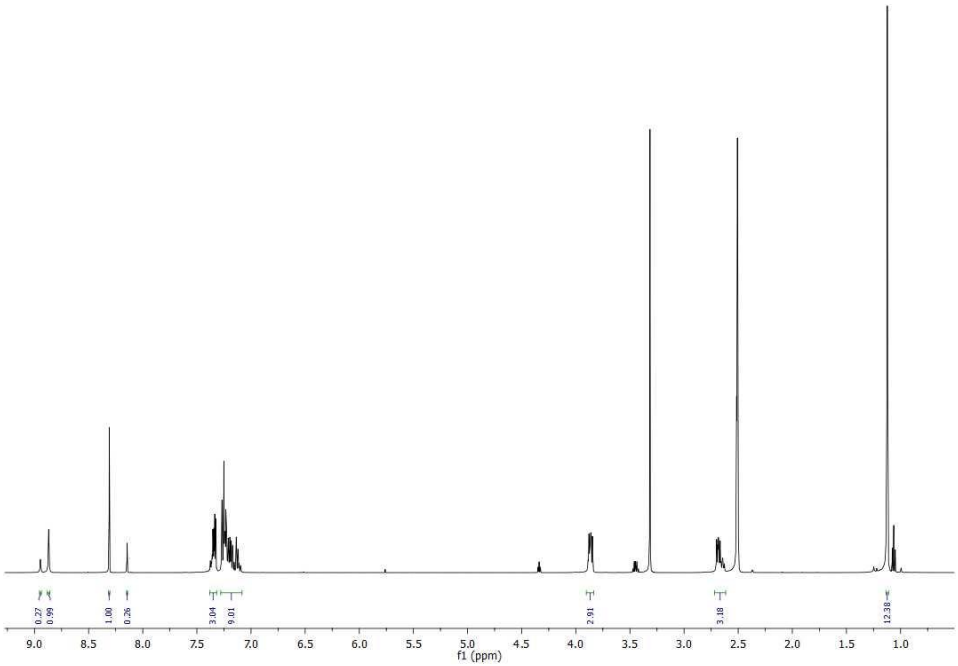
0.27
0.99
1.00
0.26
3.04
9.01
2.01
3.18
12.38
9.0 8.5 8.0 7.5 7.0 6.5 6.0 5.5 5.0 4.5 4.0 3.5 3.0 2.5 2.0 1.5 1.0
f1 (ppm)

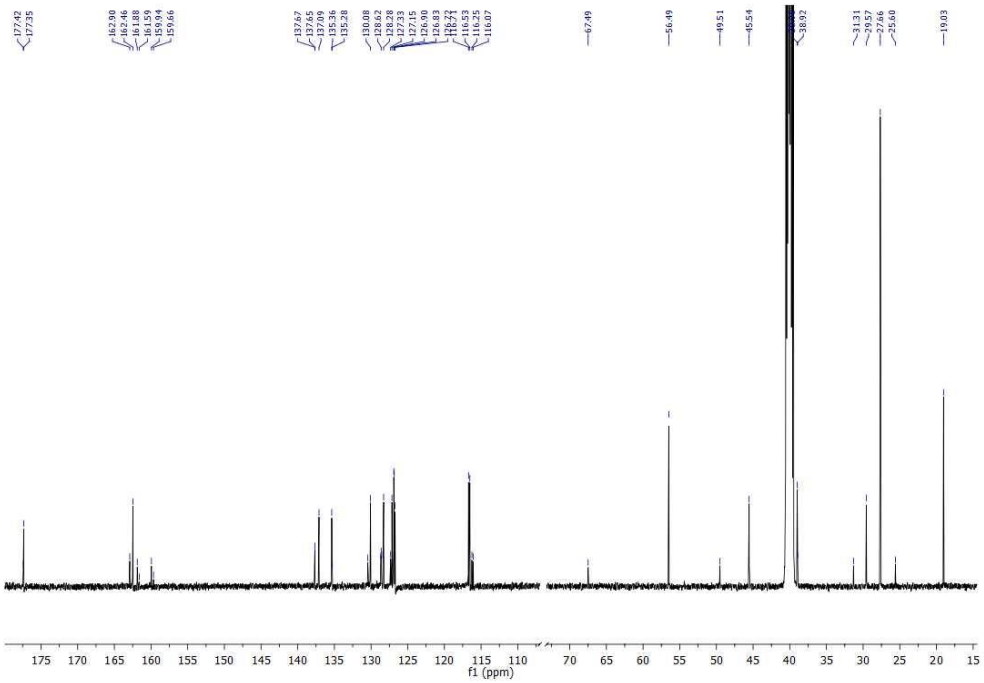
177.42
173.35
162.90
162.46
161.88
161.59
159.94
159.66
137.67
137.65
137.09
135.36
135.28
130.08
128.62
128.28
127.33
127.15
126.90
126.63
116.71
116.53
116.35
116.07
67.49
56.49
49.51
45.54
38.92
31.31
29.57
27.66
25.60
19.03
175 170 165 160 155 150 145 140 135 130 125 120 115 110 70 65 60 55 50 45 40 35 30 25 20 15
f1 (ppm)

_N_-[2-[2-(4-fluoro-_N_-formyl-anilino)ethyl]phenyl]benzamide (26)

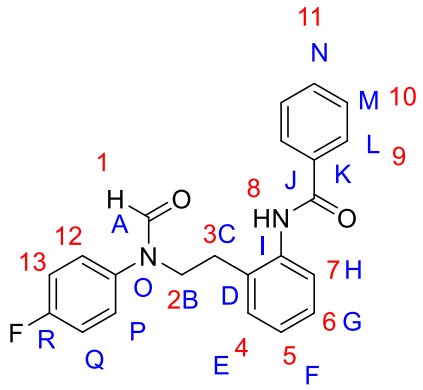

Prepared according to general method: DMF (4 mL), _N_-[2-(2-aminophenyl)ethyl]-_N_-(4-fluorophenyl)formamide (200 mg, 0.774 mmol), benzoic acid (94.5 mg, 0.774 mmol), propylphosphonic anhydride (50%) in ethyl acetate (542 mg, 507 µL, 0.852 mmol), triethylamine (94.0 mg, 130 µL, 0.929 mmol). Purification with column chromatography (1:1 EtOAc: _n_-Hex) yielded a white solid (205 mg, 73%).

^{1}H NMR (601 MHz, DMSO-d_6) δ 9.92 (8', s, 1H), 9.89 (8, s, 1H), 8.31 (1, s, 1H), 8.17 (1', s, 1H), 7.91 – 7.84 (9, m, 2H, 9', m, 2H), 7.64 – 7.58 (11, m, 1H, 11', m, 1H), 7.54 – 7.49 (10, m, 2H, 10', m, 2H), 7.34 – 7.21 (12, m, 2H, 12', m, 2H, 4, m, 1H, 4', m, 1H, 7, m, 1H, 7', m, 1H, 6, m, 1H, 6', m, 1H, 5, m, 1H, 5', m, 1H), 7.04 – 6.99 (13, m, 2H, 13', m, 2H), 3.92 – 3.86 (2, m, 2H, 2', m, 2H), 2.82 – 2.73 (3, m, 2H, 3', m, 2H).

^{13}C NMR (126 MHz, DMSO-d_6) δ 166.35 (J, s), 162.83 (A', s), 162.43 (A, s), 160.61 (R, d, J = 244.44 Hz), 160.32 (R', d, J = 243. 18 Hz), 137.49 (O, d, J = 2.6 Hz), 136.81 (I, s), 136.78 (I', s), 135.35 (D, s), 135.18 (O, d, J = 1.9 Hz), 134.75 (K, s), 134.60 (K', s), 132.06 (N', s), 131.95 (N, s), 130.81 (H', s), 130.47 (H, s), 128.82 (M', s), 128.74 (M, s), 128.62 (F', s), 128.34 (F, s), 128.09 (L, s), 127.96 (L', s), 127.58 (G', s), 127.44 (G, s), 127.14 (E, s), 127.11 (E', s), 126.09 (P, d, J = 8.5 Hz), 116.45 (Q, d, J = 22.6 Hz), 115.94 (Q', d, J = 22.5 Hz), 49.57 (B', s), 45.37 (B, s), 31.57 (C', s), 29.91 (C, s).

^{19}F NMR (471 MHz, DMSO-d_6) δ -115.90 (minor), -116.36 (major).

EI HRMS: obtained m/z 362.14178 M+ (expected m/z 362.14251 M+).

MP: 128 – 130 °C.

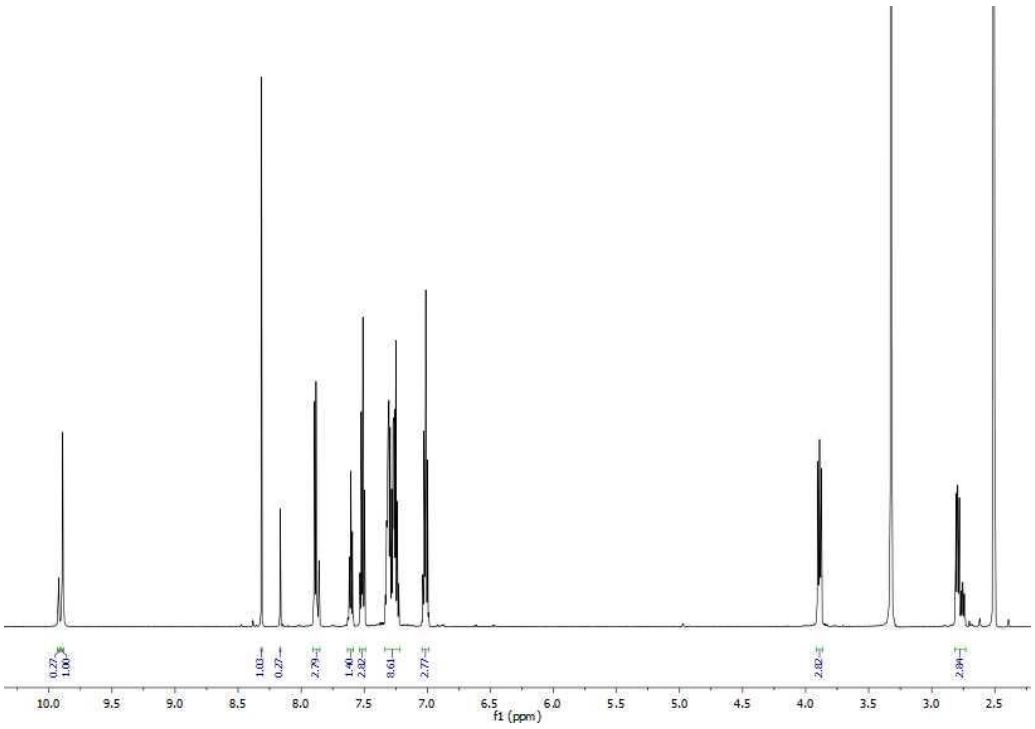
0.27
1.00
1.03
0.27
2.79
1.40
2.82
8.61
2.77
2.82
2.84
10.0
9.5
9.0
8.5
8.0
7.5
7.0
6.5
6.0
5.5
5.0
4.5
4.0
3.5
3.0
2.5
f1 (ppm)

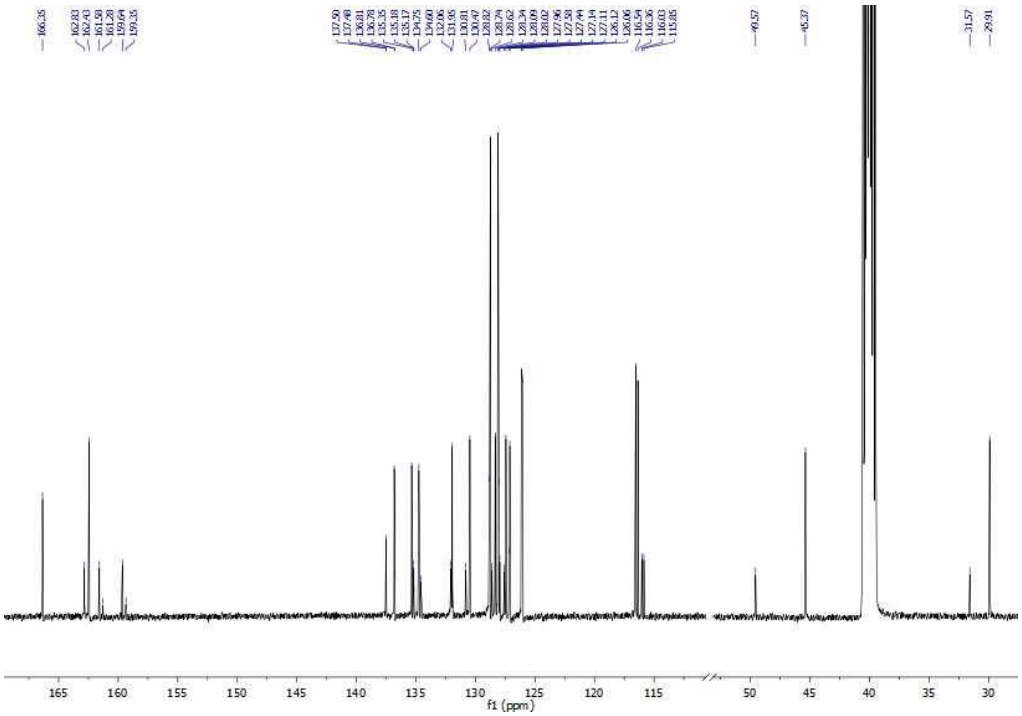
166.35
162.83
162.43
161.58
161.28
160.64
159.35
137.90
137.68
136.81
136.78
135.35
135.18
135.17
134.75
134.60
132.06
131.95
130.81
130.47
130.32
128.74
128.62
128.36
128.09
128.02
127.96
127.58
127.44
127.14
127.11
126.12
126.04
116.54
116.36
116.03
115.85
49.57
45.37
31.57
29.91
165
160
155
150
145
140
135
130
125
120
115
50
45
40
35
30
f1 (ppm)

_N_-[2-[2-(4-fluoro-_N_-formyl-anilino)ethyl]phenyl]-4-methoxy-benzamide (27)

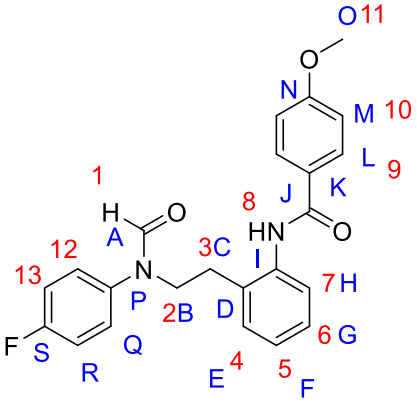

Prepared according to general method: DMF (4 mL), *N*-[2-(2-aminophenyl)ethyl]-*N*-(4-fluorophenyl)formamide (200 mg, 0.774 mmol), 4-methoxybenzoic acid (118 mg, 0.774 mmol), propylphosphonic anhydride (50%) in ethyl acetate (542 mg, 507 µL, 0.852 mmol), triethylamine (94.0 mg, 130 µL, 0.929 mmol). Purification with column chromatography (1:1 EtOAc: *n*-Hex) yielded a white solid (156 mg, 51 %).

^{1}H NMR (601 MHz, DMSO-d_6) δ 9.77 (8', s, 1H), 9.73 (8, s, 1H), 8.31 (1, s, 1H), 8.15 (1', s, 1H), 7.89 – 7.84 (9, m, 2H, 9', 2H), 7.32 – 7.20 (12', m, 2H, 12, m, 2H, 4, m, 1H, 5, m, 1H, 6, m, 1H, 7, m, 1H, 4', m, s, 5', m, s, 6', m, s, 7', m, s), 7.06 – 6.99 (13, m, 2H, 13', m, 2H, 10, m, 2H, 10', m, 2H), 3.90 – 3.85 (2, m, 2H, 11, m, 3H, 2', m, 2H, 11', m, 3H), 2.81 – 2.72 (3, m, 2H, 3', m, 2H).

^{13}C NMR (126 MHz, DMSO-d_6) δ 165.77 (J', s), 165.74 (J, s), 162.82 (A', s), 162.42 (A, s), 162.38 (N', s), 162.32 (N, s), 160.61 (S, d, J = 243.18 Hz), 160.32 (S', d, J = 243.18 Hz), 137.48 (P, d, J = 2.5 Hz), 137.01 (I, s), 136.99 (I', s), 135.34 (D, s), 135.21 (D', s), 135.18 (P', d, J = 2.5 Hz), 130.77 (H', s), 130.42 (H, s), 129.99 (L, s), 129.93 (L', s), 128.68 (F', s), 128.36 (F, s), 127.97 (Q', d, J = 8.4 Hz), 127.53 (G', s), 127.38 (G, s), 126.99 (E', s), 126.94 (E, s), 126.87 (K, s), 126.72 (K', s), 126.06 (Q, d, J = 8.5 Hz), 116.45 (R, d, J = 22.5 Hz), 115.95 (R', d, J = 22.5 Hz), 114.03 (M', s), 113.95 (M, s), 55.90 (O', s), 55.89 (O, s), 49.56 (B', s), 45.38 (B, s), 31.64 (C', s), 29.93 (C, s).

^{19}F NMR (471 MHz, DMSO-d_6) δ -115.92 (minor), -116.40 (major).

EI HRMS: obtained m/z 392.15346 M+ (expected m/z 392.15307 M+).

MP: 136 – 138 °C.

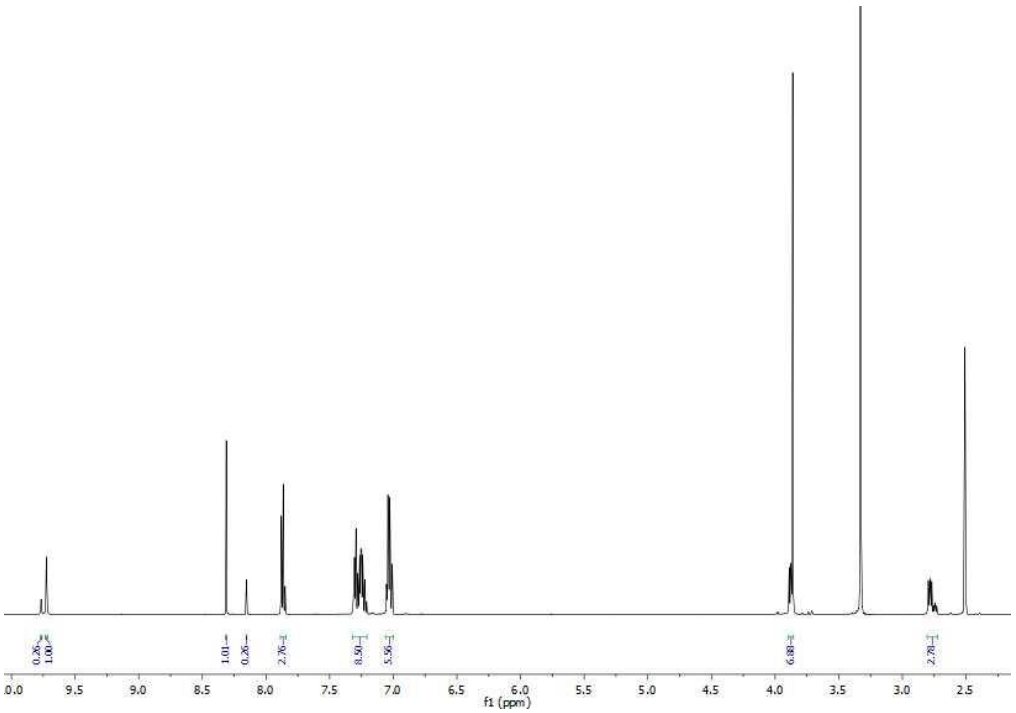
0.26
1.00
1.01
0.26
2.76
8.50
5.56
6.88
2.78
f1 (ppm)

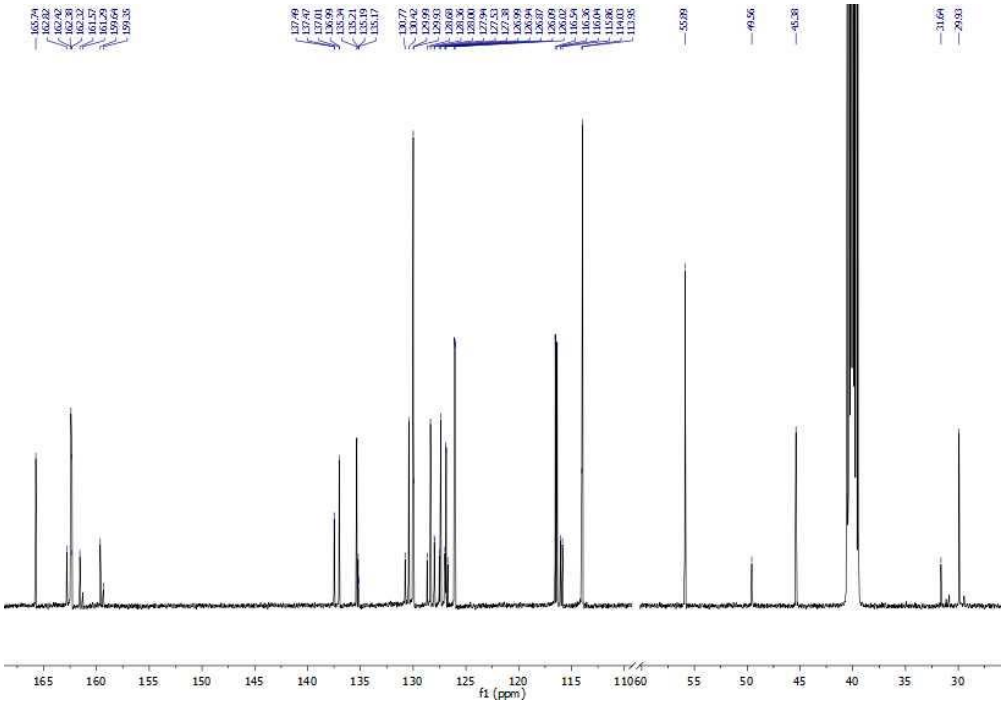
165.74
162.82
162.42
162.38
161.52
161.52
161.29
159.64
159.36
137.49
137.42
137.01
136.99
135.34
135.21
135.19
135.17
130.77
130.42
129.99
129.93
128.68
128.36
128.14
127.94
127.53
127.38
126.99
126.94
126.87
126.09
126.02
116.54
116.45
116.14
115.86
114.03
113.98
55.89
49.56
45.38
31.66
29.93
f1 (ppm)

_N_-[2-[2-(4-fluoro-_N_-formyl-anilino)ethyl]phenyl]pyridine-2-carboxamide (28)

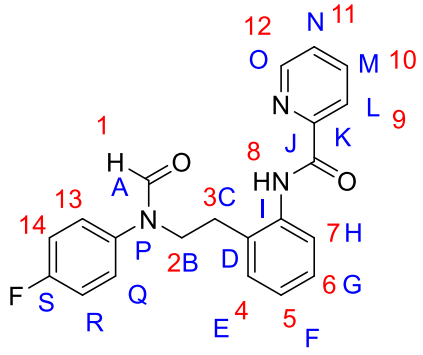

Prepared according to general method: DMF (4 mL), _N_-[2-(2-aminophenyl)ethyl]-_N_-(4-fluorophenyl)formamide (200 mg, 0.774 mmol), 2-picolinic acid (95.3 mg, 0.774 mmol), propylphosphonic anhydride (50%) in ethyl acetate (542 mg, 507 µL, 0.852 mmol), triethylamine (94.0 mg, 130 µL, 0.929 mmol). Purification with column chromatography (1:1 EtOAc: _n_-Hex) yielded a white solid (104 mg, 37%).

^{1}H NMR (601 MHz, DMSO-d_6) δ 10.31 (8', s, 1H), 10.30 (8, m, 1H), 8.70 – 8.65 (9, m, 1H, 9', m, 1H), 8.30 (1, s, 1H), 8.18 (1', s, 1H), 8.12 – 8.04 (11, m, 1H, 11', m, 1H, 12, m, 1H, 12', m, 1H), 7.72 – 7.68 (10, m, 1H, 10', m, 1H), 7.60 – 7.55 (7, m, 1H, 7', m, 1H), 7.34 – 7.18 (13, m, 2H, 13', m, 2H, 6, m, 1H, 6', m, 1H, 4, m, 1H, 5, m, 1H, 4', m, 1H, 5', m, 1H), 7.03 – 6.99 (14, m, 2H, 14', m, 2H), 3.96 – 3.89 (2, m, 2H, 2', m, 2H), 2.86 – 2.77 (3, m, 2H, 3', m, 2H).

^{13}C NMR (126 MHz, DMSO-d_6) δ 163.25 (J', s), 163.17 (J, s), 162.88 (A', s), 162.43 (A, s), 160.55 (S, d, J = 243.18 Hz), 160.25 (S', d, J = 243. 18 Hz), 150.04 (L', s), 148.88 (L, s), 138.54 (O', s), 138.50 (O, s), 137.36 (P, d, J = 2.9 Hz), 136.37 (I, s), 135.10 (P', d, J = 3.0 Hz), 133.45 (K, s), 133.20 (K', s), 130.78 (E', s), 130.53 (E, s), 127.87 (Q', d, J = 8.5 Hz), 127.64 (F', s), 127.53 (F, s), 127.38 (M', s), 127.33 (M, s), 126.50 (G, s), 126.22 (H, s), 125.95 (Q, d, J = 8.5 Hz), 122.72 (N', s), 122.68 (N, s), 116.38 (R, d, J = 22.8 Hz), 115.86 (R', d, J = 22.4 Hz), 49.35 (B', s), 44.85 (B, s), 31.41 (C', s), 29.80 (C, s).

^{19}F NMR (471 MHz, DMSO-d_6) δ -115.94 (minor), -116.39 (major).

EI HRMS: obtained m/z 363.13657 M+ (expected m/z 363.13665 M+).

MP: 85 – 86 °C.

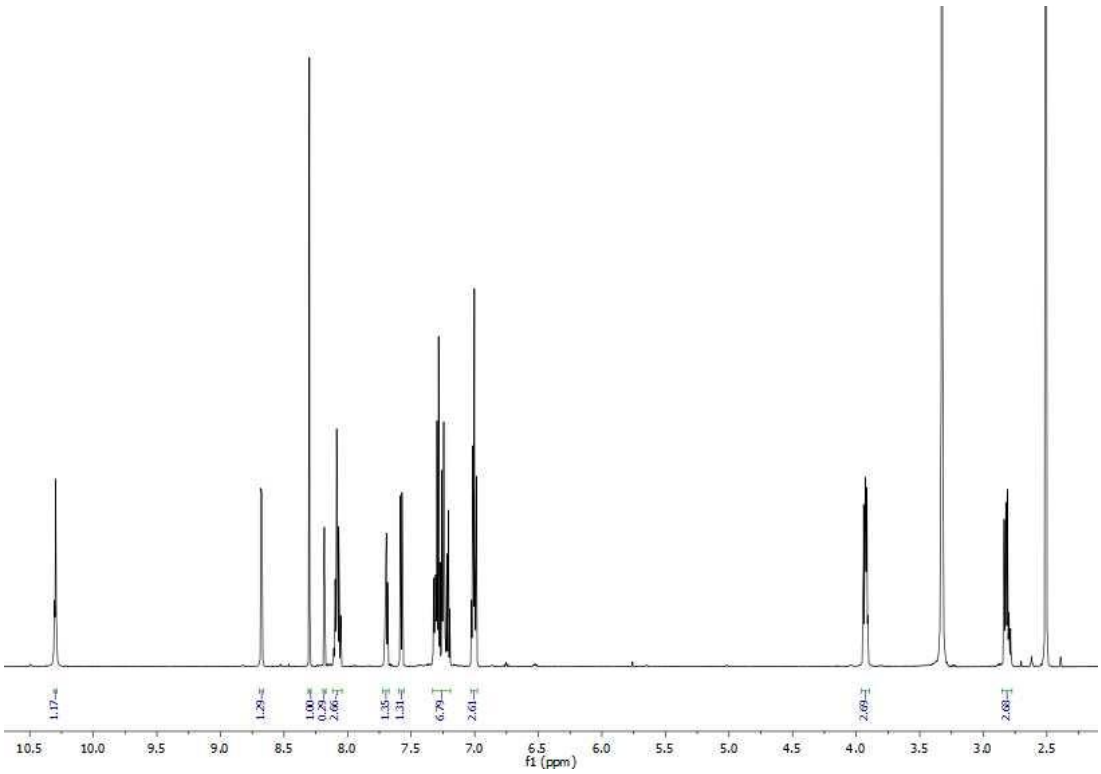
1.17
1.29
1.00
0.29
2.66
1.35
1.31
6.79
2.61
2.69
2.68
10.5 10.0 9.5 9.0 8.5 8.0 7.5 7.0 6.5 6.0 5.5 5.0 4.5 4.0 3.5 3.0 2.5
f1 (ppm)

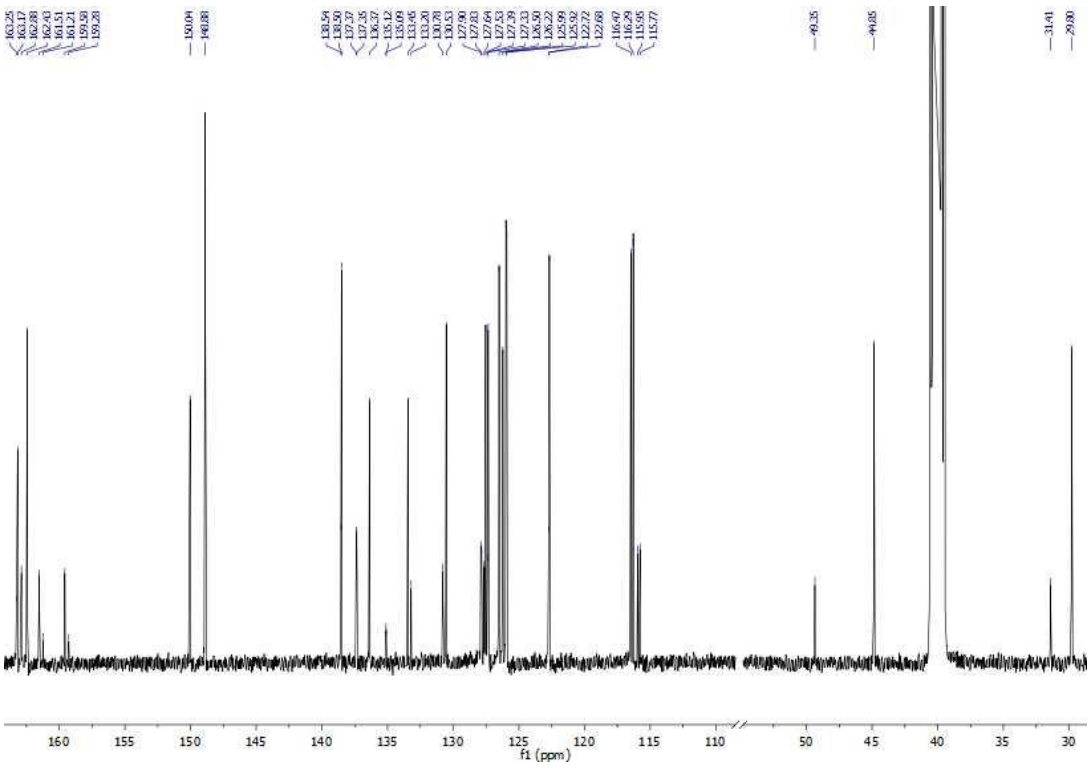
163.25
163.17
162.88
162.43
161.51
161.21
159.58
159.28
150.04
140.88
138.54
138.50
137.37
137.26
136.77
135.12
135.09
133.45
133.20
130.78
130.53
127.90
127.83
127.64
127.53
127.39
127.33
126.50
126.22
125.99
125.92
122.72
122.68
116.47
116.29
115.95
115.77
49.35
49.05
31.41
29.80
160 155 150 145 140 135 130 125 120 115 110 50 45 40 35 30
f1 (ppm)

5-fluoro-*N*-[2-[2-(4-fluoro-*N*-formyl-anilino)ethyl]phenyl]pyridine-2-carboxamide (29)

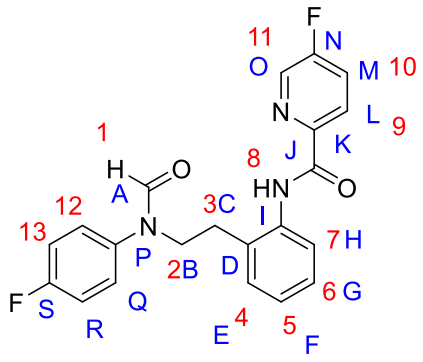

Prepared according to general method: DMF (4 mL), *N*-[2-(2-aminophenyl)ethyl]-*N*-(4-fluorophenyl)formamide (200 mg, 0.774 mmol), 5-fluoro-2-pyridinecarboxylic acid (109 mg, 0.774 mmol), propylphosphonic anhydride (50%) in ethyl acetate (542 mg, 507 µL, 0.852 mmol), triethylamine (94.0 mg, 130 µL, 0.929 mmol). Purification with column chromatography (1:1 EtOAc: *n*-Hex) yielded a white solid (100 mg, 34 %).

^{1}H NMR (601 MHz, DMSO-d_6) δ 10.22 (8', s, 1H), 10.21 (8, s, 1H), 8.65 (9, m, 1H, 9', m, 1H), 8.28 (1, s, 1H), 8.20 – 8.09 (11, m, 1H, 11', m, 1H), 8.03 – 7.93 (10, m, 1H, 10', m, 1H), 7.53 – 7.44 (7, m, 1H, 7', m, 1H), 7.33 – 7.26 (12', m, 2H, 6, m, 1H, 6', m, 1H, 5, m, 1H, 5', m, 1H), 7.26 – 7.19 (12, m, 2H, 4, m, 1H, 4', m, 1H), 7.05 – 7.00 (13, m, 2H, 13', m, 2H), 3.96 – 3.80 (2, m, 2H, 2', m, 2H), 2.86 – 2.68 (3, m, 2H, 3', m, 2H).

^{13}C NMR (126 MHz, DMSO-d_6) δ 162.85, 162.43, 162.40, 162.36, 160.58 (S, d, J = 243.18 Hz), 160.31, 160.29, 160.26 (S', d, J = 244.44 Hz),

146.82 (d, J = 3.8 Hz), 137.36, 137.34, 137.13, 136.31, 135.11 (d, J = 3.0 Hz), 133.99, 133.79, 130.75, 130.51, 127.96 (d, J = 8.5 Hz), 127.60, 127.50, 127.07, 126.78, 126.74, 126.13 (d, J = 8.5 Hz), 125.21, 125.16, 125.06, 124.98, 124.93, 116.38 (R, d, J = 22.8 Hz), 115.86 (R', d, J = 22.5 Hz), 49.47 (B', s), 45.02 (B, s), 31.37 (C', s), 29.79 (C, s).

EI HRMS: obtained m/z 381.12593 M+ (expected m/z 381.12451 M+).

MP: 95 – 96 °C.

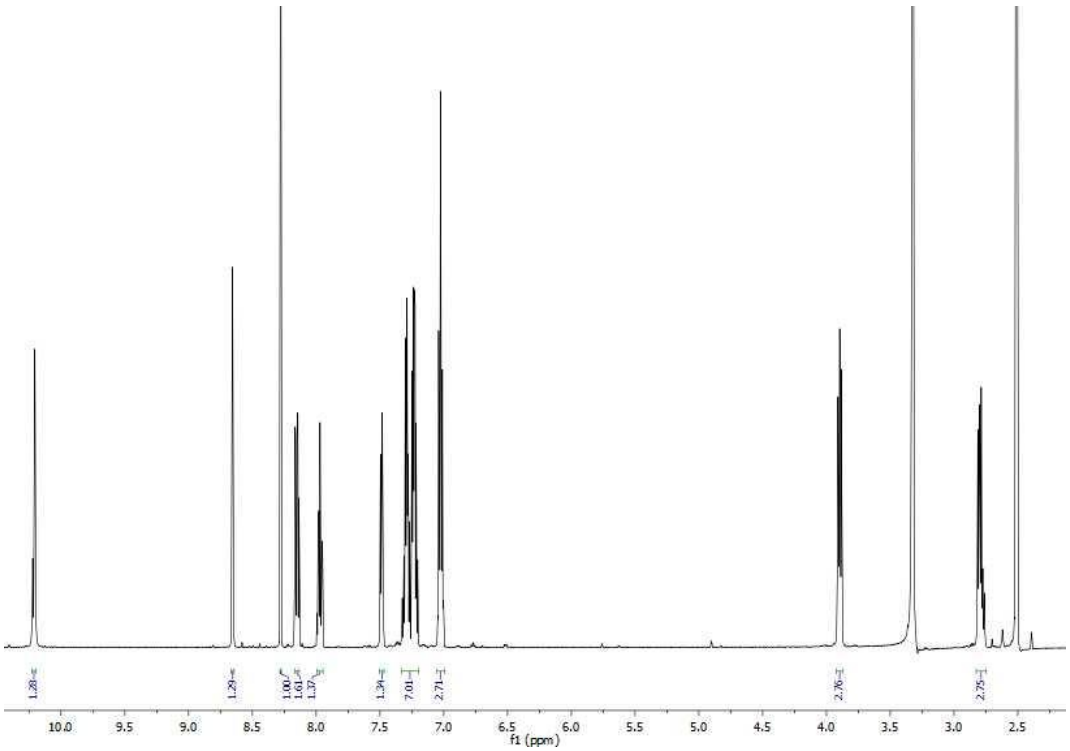
1.28
1.29
1.00
1.61
1.37
1.34
7.01
2.71
2.76
2.75
10.0
9.5
9.0
8.5
8.0
7.5
7.0
6.5
6.0
5.5
5.0
4.5
4.0
3.5
3.0
2.5
f1 (ppm)

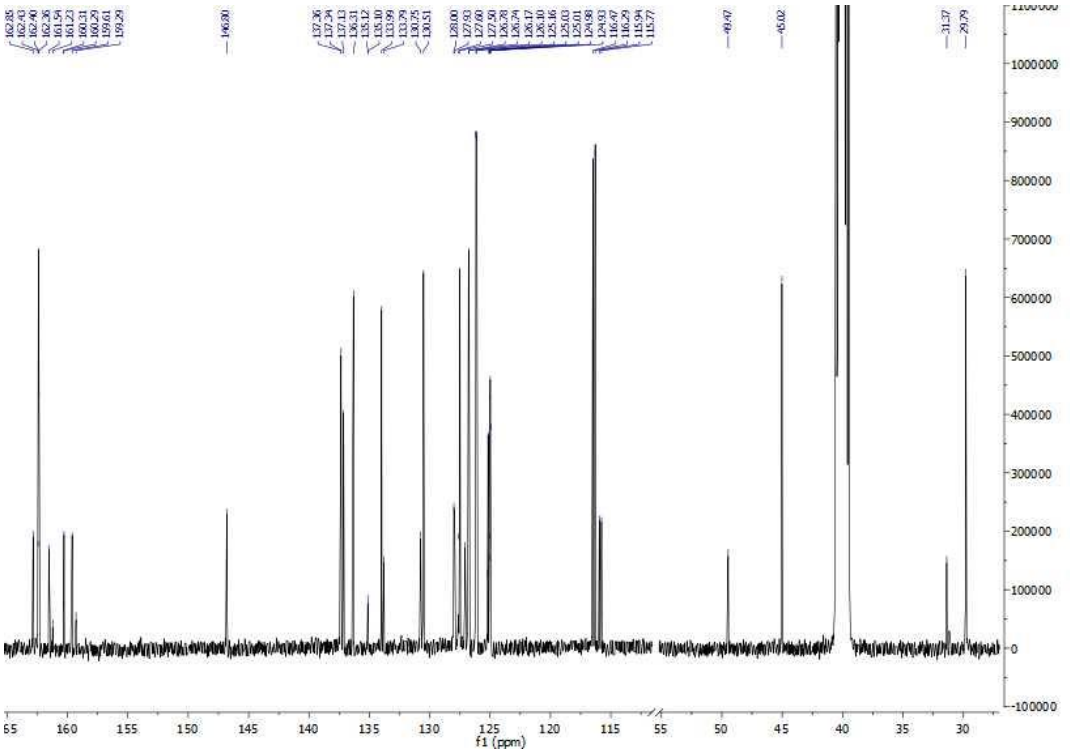
162.85
162.43
162.40
162.36
161.54
161.23
160.31
160.03
159.61
159.29
146.80
137.36
137.24
137.13
136.31
135.12
135.10
133.99
133.79
130.75
130.51
128.00
127.93
127.60
127.50
126.28
126.24
126.17
126.10
125.16
125.03
125.01
124.98
124.93
116.67
116.54
115.94
115.77
49.47
45.02
31.37
29.79
1000000
900000
800000
700000
600000
500000
400000
300000
200000
100000
0
-100000
65
160
155
150
145
140
135
130
125
120
115
55
50
45
40
35
30
f1 (ppm)

Water Soluble Series

General Scheme

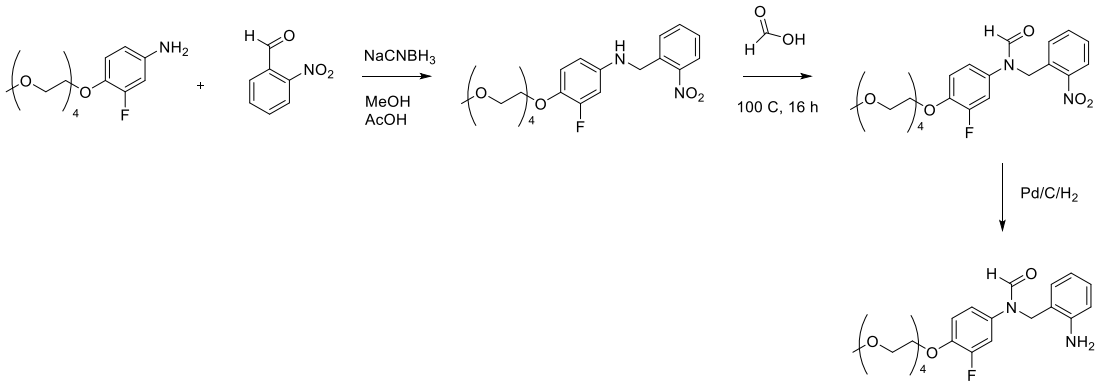

3-fluoro-4-[2-[2-[2-(2-methoxyethoxy)ethoxy]ethoxy]ethoxy]-*N*-[(2-nitrophenyl)methyl]aniline (42)

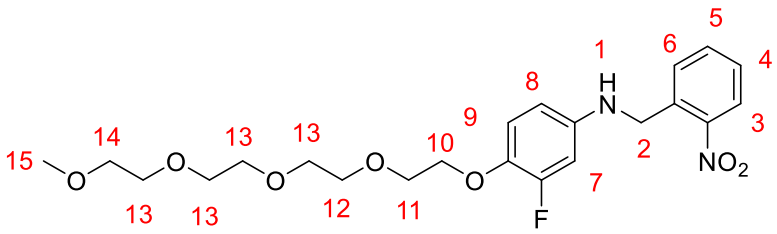

To a solution of 3-fluoro-4-[2-[2-[2-(2-methoxyethoxy)ethoxy]ethoxy]ethoxy]aniline (1.00 mL, 3.15 mmol) in dry methanol (10 mL) was added 2-nitrobenzaldehyde (619 mg, 4.10 mmol) and sodium cyanoborohydride (258 mg, 4.10 mmol). Acetic acid (946 mg, 902 µL, 15.8 mmol) was then added dropwise and the mixture heated to reflux overnight. The reaction mixture was then reduced under pressure and dissolved in diethyl ether (10 mL), washed with water (10 mL) and brine (10 mL). The reaction mixture was then concentrated, dried with $MgSO_4$ and purified using column chromatography (100% EtOAc) to yield a yellow oil (550 mg, 39%).

^{1}H NMR (500 MHz, Chloroform-*d*) δ 8.09 (3, m, 1H), 7.65 (5, m, 1H), 7.61 (6, m, 1H), 7.48 – 7.43 (4, m, 1H), 6.86 (7, m, 1H), 6.36 (8, m, 1H), 6.27 (9, m, 1H), 4.71 – 4.65 (2, m, 2H), 4.24 (1, s, 1H), 4.18 – 4.08 (10, m, 3H), 3.84 – 3.79 (11, m, 2H), 3.75 – 3.64 (13, 12, m, 10H), 3.59 – 3.54 (14, m, 2H), 3.39 (15, s, 3H).

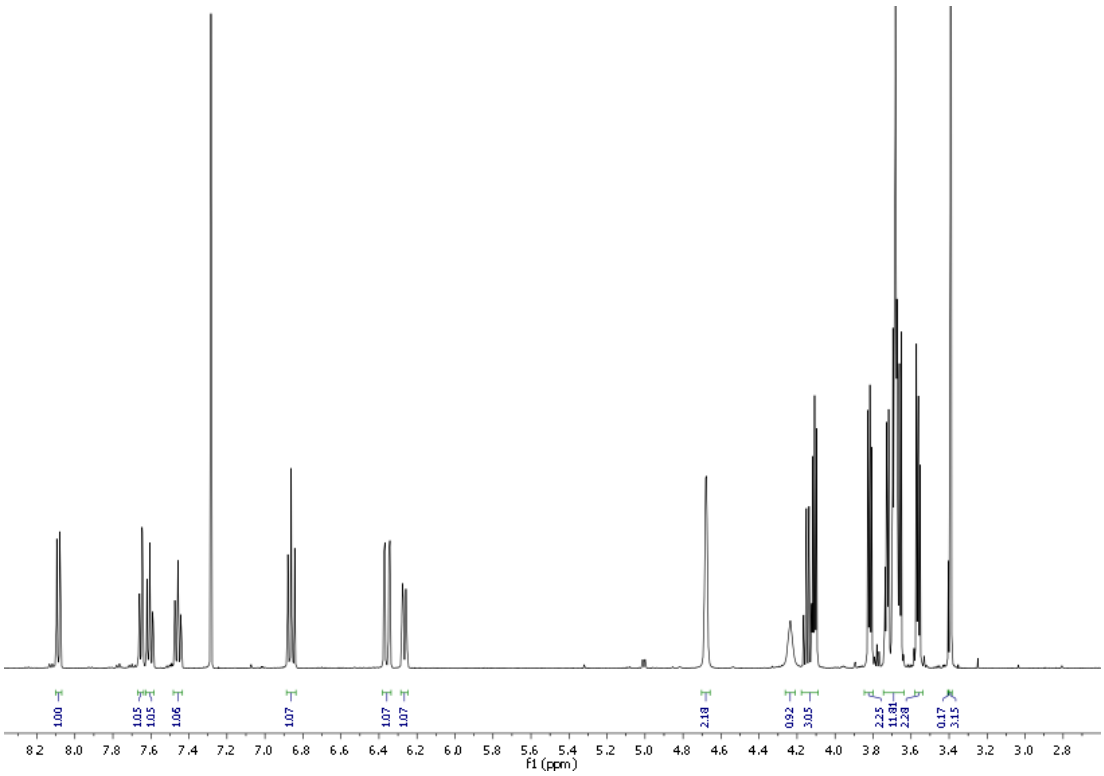
1.00
1.05
1.05
1.06
1.07
1.07
1.07
2.18
0.92
3.05
2.25
1.41
1.01
2.28
0.17
3.15
8.2 8.0 7.8 7.6 7.4 7.2 7.0 6.8 6.6 6.4 6.2 6.0 5.8 5.6 5.4 5.2 5.0 4.8 4.6 4.4 4.2 4.0 3.8 3.6 3.4 3.2 3.0 2.8
f1 (ppm)

_N_-[3-fluoro-4-[2-[2-[2-(2-methoxyethoxy)ethoxy]ethoxy]ethoxy]phenyl]-_N_-[(2-nitrophenyl)methyl]formamide (43)

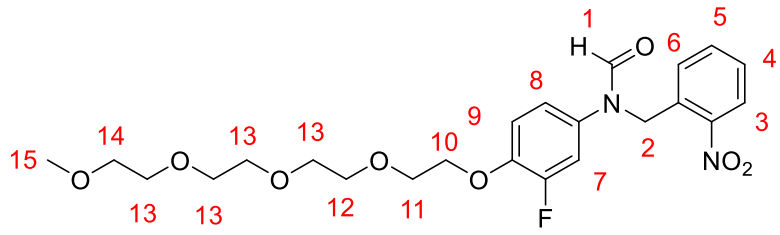

Formic acid was added to 3-fluoro-4-[2-[2-[2-(2-methoxyethoxy)ethoxy]ethoxy]ethoxy]-_N_-[(2-nitrophenyl)methyl]aniline (500 mg, 1.11 mmol) and the mixture was refluxed overnight. The reaction mixture was then extracted with diethyl ether (10 mL), quenched with Na_2CO_3 (10 mL), washed with water (10 mL), concentrated *in vacuo* and then dried with $MgSO_4$ and purified using column chromatography (100% EtOAc) to yield a colourless oil (330 mg, 66%).

^{1}H NMR (500 MHz, Chloroform-*d*) δ 8.60 (1, s, 1H), 8.06 (3, m, 1H), 7.62 (5, m, 1H), 7.49 – 7.42 (6, 4, m, 2H), 7.00 (7, m, 1H), 6.95 – 6.84 (8, 9, m, 2H), 5.36 (2, s, 2H), 4.21 – 4.18 (10, m, 2H), 3.90 – 3.84 (11, m, 2H), 3.75 – 3.72 (12, m, 2H), 3.71 – 3.64 (13, m, 8H), 3.58 – 3.55 (14, m, 2H), 3.39 (15, s, 3H).

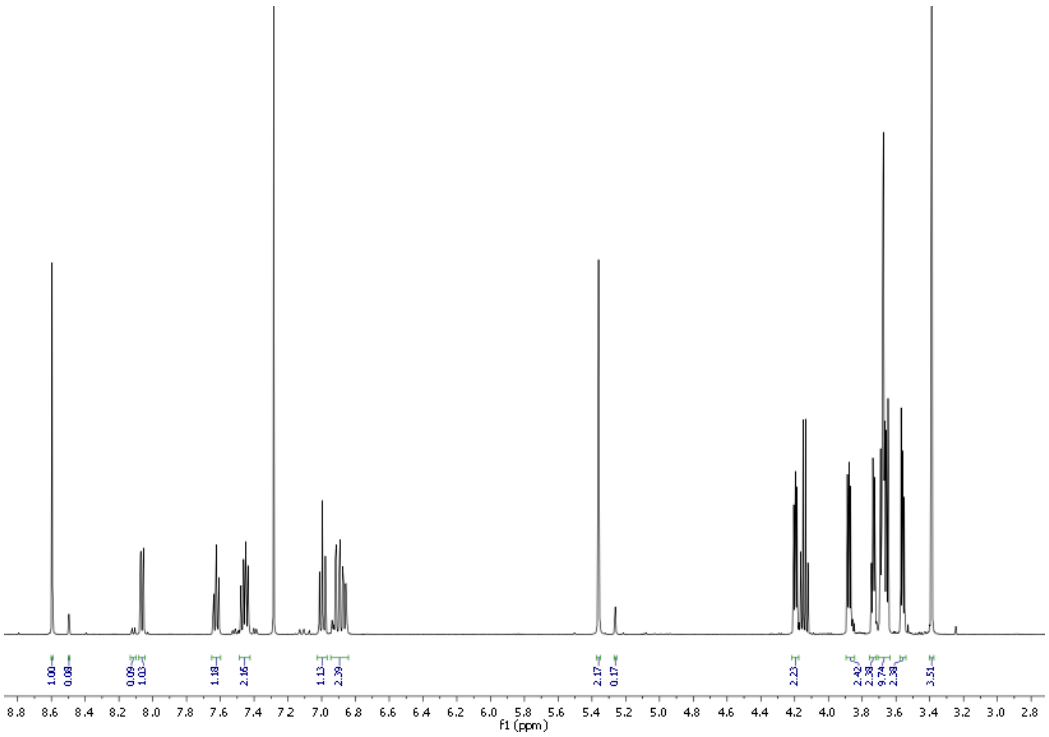

_N_-[(2-aminophenyl)methyl]-_N_-[3-fluoro-4-[2-[2-[2-(2-methoxyethoxy)ethoxy]ethoxy]ethoxy]phenyl]formamide (30)

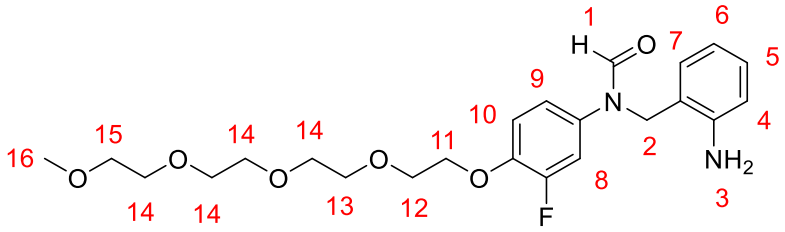

To a reaction flask under a nitrogen atmosphere was added a solution of _N_-[3-fluoro-4-[2-[2-[2-(2-methoxyethoxy)ethoxy]ethoxy]ethoxy]phenyl]-_N_-[(2-nitrophenyl)methyl]formamide (300 mg, 0.624 mmol) in EtOH (10 mL). Palladium on carbon (10 wt %) was then added and the reaction mixture placed under a hydrogen environment. The reaction mixture was monitored to completion via TLC and then filtered through Celite. The crude mixture was then reduced under pressure and purified using column chromatography (2% MeOH/EtOAc) to yield a colourless oil (230 mg, 82%).

^{1}H NMR (601 MHz, DMSO-d_6) δ 8.52 (1', s, 1H), 8.49 (1, s, 1H), 7.32 (8, dd, J = 12.6, 2.7 Hz, 1H), 7.24 (8', dd, J = 13.0, 2.5 Hz, 1H), 7.17 – 7.13 (10, s, 1H), 7.12 – 7.08 (10', s, 1H), 7.03 – 6.99 (9, m, 1H, 9', m, 1H), 6.96 – 6.90 (5, m, 1H, 5', m, 1H), 6.82 – 6.76 (7, m, 1H, 7', m, 2H), 6.65 – 6.59 (4, m, 1H, 4', m, 1H), 6.48 – 6.45 (6', m, 1H), 6.43 – 6.39 (6, m, 1H), 5.03 (3, s, 2H, 3', s, 2H), 4.80 (2, s, 2H), 4.77 (2', s, 2H), 4.15 – 4.11 (11, m, 2H, 11', m , 2H), 3.75 – 3.71 (12, m, 2H, 12', m, 2H), 3.60 – 3.56 (13, m, 2H, 13', m, 2H), 3.54 – 3.48 (14, m, 8H, 14', m, 8H), 3.44 – 3.39 (15, m, 2H, 15', m, 2H), 3.23 (16, s, 3H, 16', s, 3H).

^{13}C NMR (126 MHz, DMSO-d_6) δ 163.63 (s), 163.13 (s), 151.76 (d, J = 244.9 Hz), 151.27 (d, J = 244.9 Hz), 146.62, 145.24 (d, J = 10.5 Hz), 134.05 (d, J = 8.6 Hz), 129.57, 128.80, 128.61, 121.57, 120.48 (d, J = 3.4 Hz), 120.10, 119.14, 116.72, 116.30, 115.81, 115.66 (d, J = 2.7 Hz), 115.25, 115.00, 113.75, 113.58, 112.66, 112.50, 71.74, 70.40, 70.27, 70.24, 70.03, 69.22, 68.98, 68.88, 67.49, 58.50, 49.26, 44.46, 25.60.

^{19}F NMR (376 MHz, DMSO-d_6) δ -132.48 – -132.60 (major), -133.60 – -133.69 (minor).

EI HRMS: obtained m/z 450.21457 M+ (expected m/z 450.21607 M+).

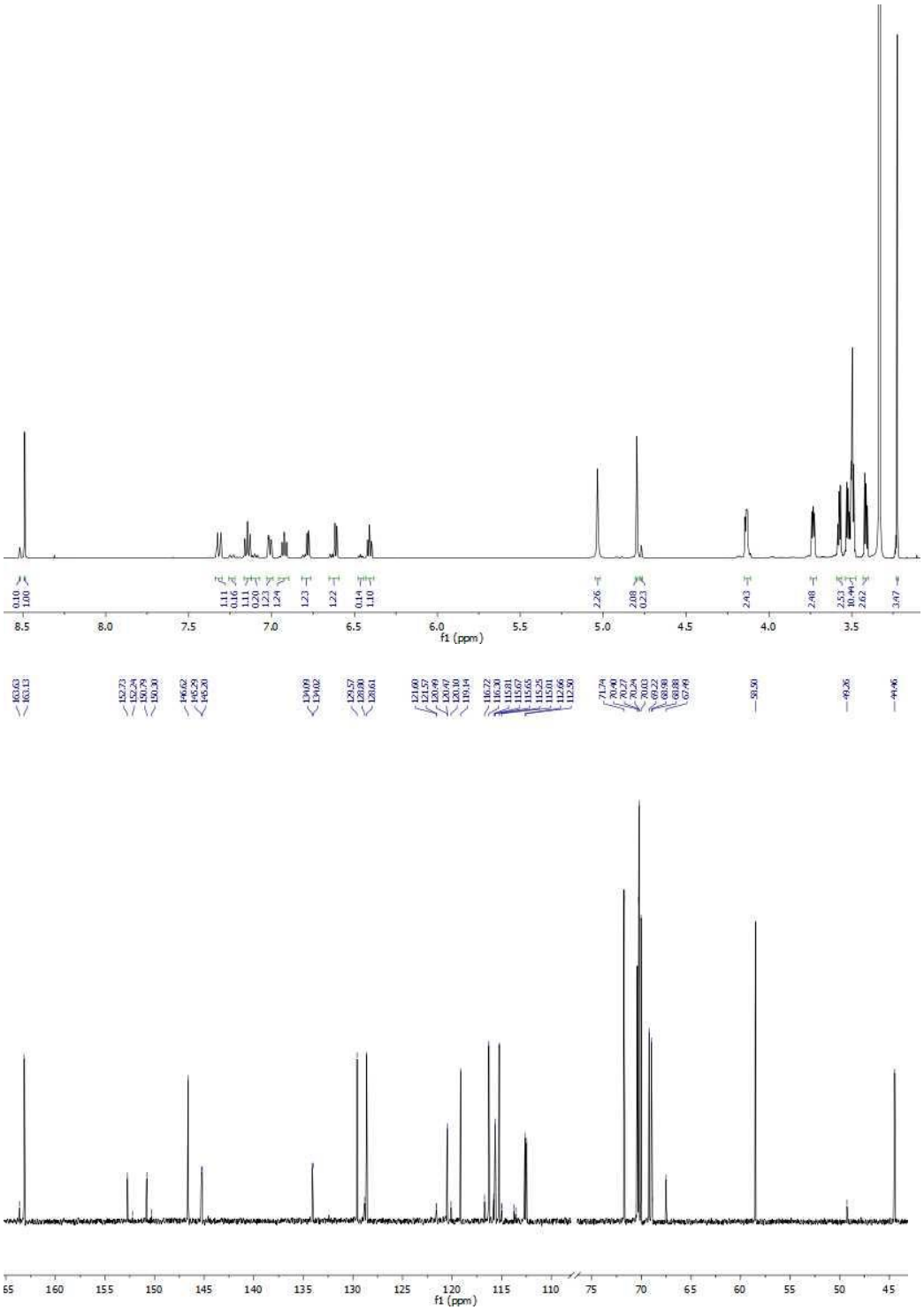

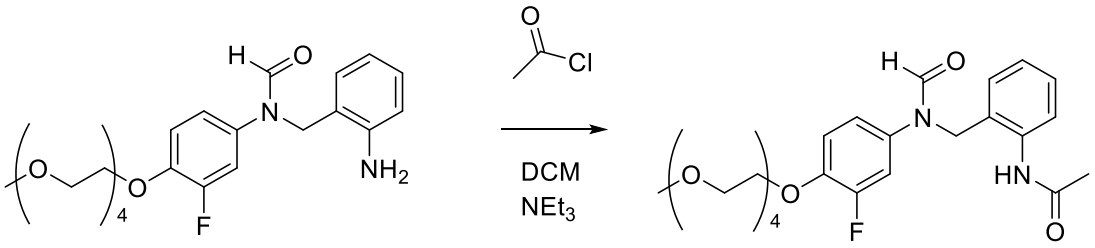

_N_-[2-[[3-fluoro-_N_-formyl-4-[2-[2-[2-(2-methoxyethoxy)ethoxy]ethoxy]ethoxy]anilino]methyl]phenyl]acetamide (31)

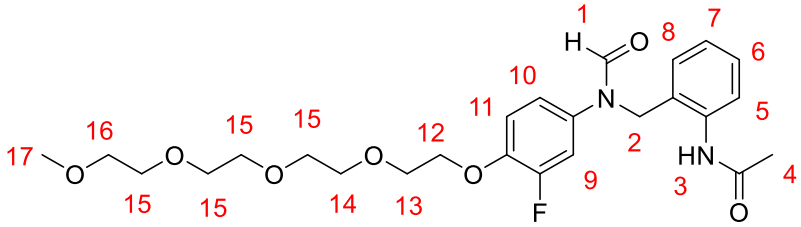

To a solution of *N*-[(2-aminophenyl)methyl]-*N*-[3-fluoro-4-[2-[2-[2-(2-methoxyethoxy)ethoxy]ethoxy]ethoxy]phenyl]formamide (300 mg, 0.666 mmol) in dry DCM (7 mL) was added acetyl chloride (62.7 mg, 57.0 µL, 0.799 mmol). Triethylamine (135 mg, 186 µL, 1.33 mmol) was then added and the reaction mixture heated to reflux. The reaction mixture was monitored to completion via TLC and then diluted with diethyl ether (10 mL) and washed with saturated Na_2HCO_3 (10 mL). The aqueous phase was extracted with diethyl ether (2x10 mL) and the combined organic phases were then washed with water (10 mL) and brine (10 mL), dried over $MgSO_4$ and concentrated *in vacuo*. The crude product was then purified by column chromatography (2% MeOH/EtOAc) to yield a colourless oil (280 mg, 71%).

^{1}H NMR (601 MHz, DMSO-d_6) δ 9.59 (3', s, 1H), 9.48 (3, s, 1H), 8.53 (1, s, 1H), 8.47 (1', s, 1H), 7.42 – 7.39 (5, m, 1H, 5', m, 1H), 7.34 – 7.30 (7, m, 1H, 7', m, 1H), 7.24 – 7.02 (11, m, 1H, m, 11', 1H, 9, m, 1H, 9', m, 1H, 10, m, 1H, 10', m, 1H, 8, m, 1H, 8', m, 1H, 6, m, 1H, 6', m, 1H), 4.92 (2, s, 2H), 4.88 (2', s, 2H), 4.15 – 4.10 (12, m, 2H, 12', m, 2H), 3.75 – 3.71 (13, m, 2H, 13', m, 2H), 3.59 – 3.56 (14, m, 2H, 14', m, 2H), 3.54 – 3.48 (15, m, 8H, 15', m, 8H), 3.43 – 3.40 (16, m, 2H, 16', m, 2H), 3.23 (17, s, 3H, 17', s, 3H), 2.05 (4, s, 3H, 4', s, 3H).

^{13}C NMR (126 MHz, DMSO-d6) δ 168.89, 163.18, 151.80 (d, J = 244.9 Hz), 145.23, 145.15, 136.48, 134.23, 134.16, 131.86, 130.45, 129.06, 128.60, 128.31, 127.98, 126.14, 125.64, 125.53, 120.23, 115.75 (d, J = 2.6 Hz), 112.48, 112.31, 71.74, 70.40, 70.27, 70.24, 70.03, 69.22, 69.02, 58.50, 44.51, 23.80, 23.54.

^{19}F NMR (471 MHz, DMSO-*d*$_6$) δ -132.39 (major), -133.52 (minor).

EI HRMS: obtained m/z 492.22734 M+ (expected m/z 492.22663 M+).

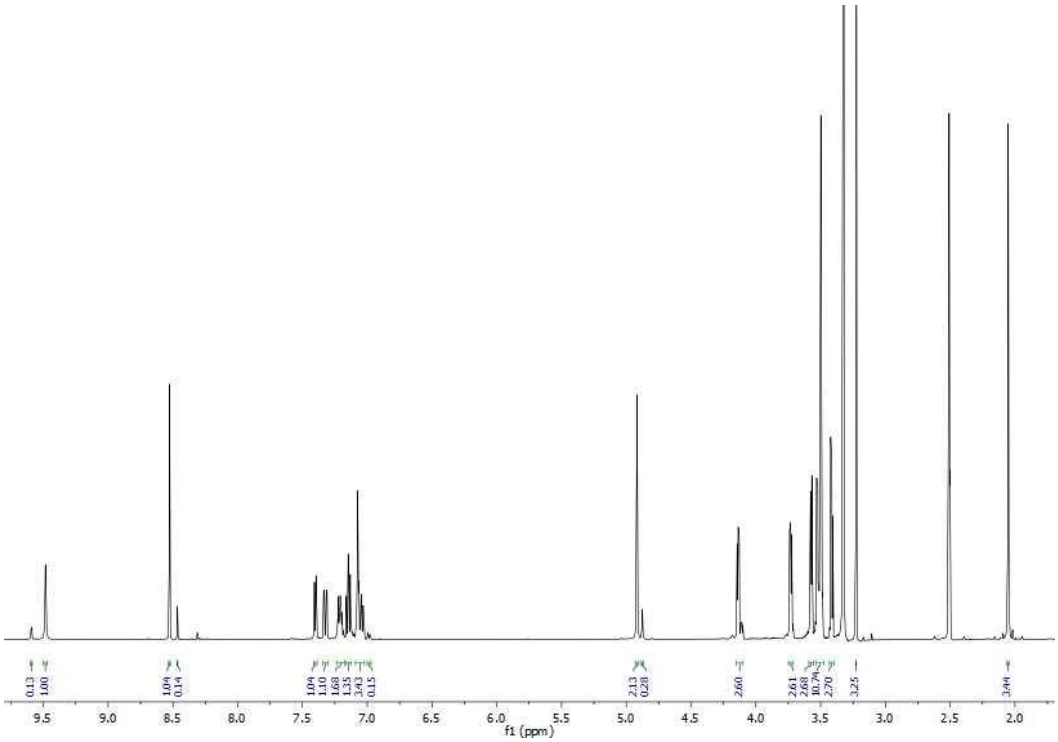

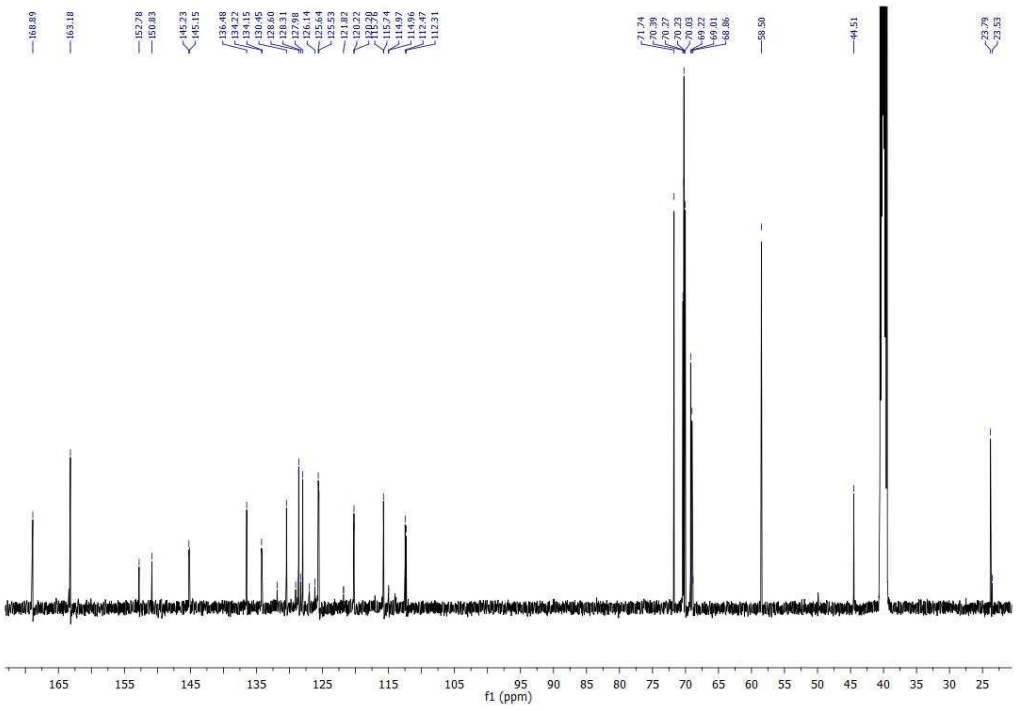
168.89
163.18
152.78
150.83
145.23
145.15
136.48
134.22
134.15
130.45
128.60
128.31
127.98
126.14
125.64
125.53
121.82
120.22
115.74
114.97
114.96
112.77
112.31
71.74
70.39
70.27
70.23
70.00
69.22
69.01
68.86
58.50
44.51
23.79
23.53
165
155
145
135
125
115
105
95
90
85
80
75
70
65
60
55
50
45
40
35
30
25
f1 (ppm)

General Scheme

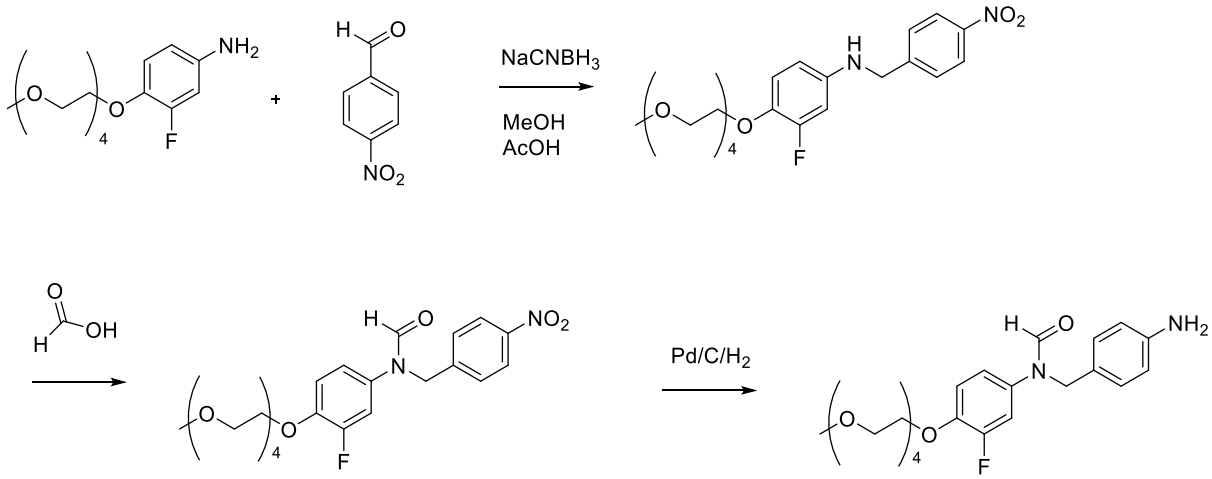

3-fluoro-4-[2-[2-[2-(2-methoxyethoxy)ethoxy]ethoxy]ethoxy]-*N*-[(4-nitrophenyl)methyl]aniline (44)

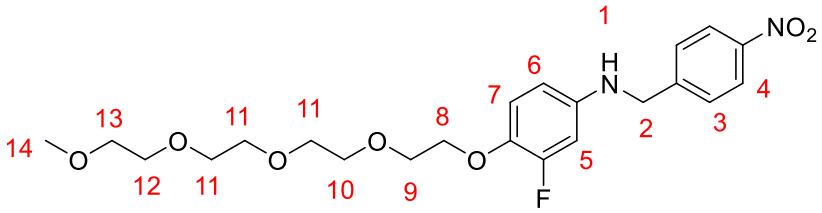

To a solution of 3-fluoro-4-[2-[2-[2-(2-methoxyethoxy)ethoxy]ethoxy]ethoxy]aniline (1.00 mL, 3.15 mmol) in dry methanol (10 mL) was added 4-nitrobenzaldehyde (619 mg, 4.10 mmol) and sodium cyanoborohydride (258 mg, 4.10 mmol). Acetic acid (946 mg, 902 µL, 15.8 mmol) was then added dropwise and the mixture heated to reflux overnight. The reaction mixture was then reduced under pressure and dissolved in diethyl ether (10 mL), washed with water (10 mL) and brine (10 mL). The reaction mixture was then concentrated, dried with $MgSO_4$ and purified using column chromatography (100 % EtOAc) to yield a yellow oil (600 mg, 42%).

_N_-[3-fluoro-4-[2-[2-[2-(2-methoxyethoxy)ethoxy]ethoxy]ethoxy]phenyl]-_N_-[(4-nitrophenyl)methyl]formamide (45)

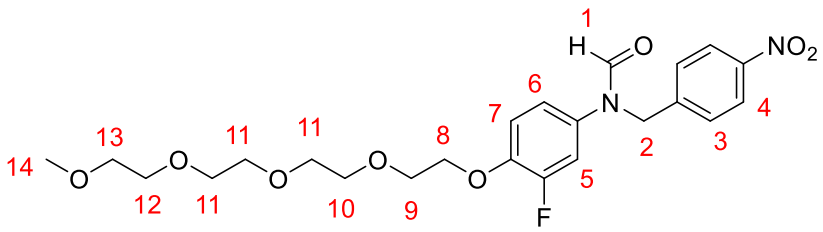

Formic acid (10 mL) was added to 3-fluoro-4-[2-[2-[2-(2-methoxyethoxy)ethoxy]ethoxy]ethoxy]-_N_-[(4-nitrophenyl)methyl]aniline (500 mg, 1.11 mmol) and the mixture was refluxed overnight. The reaction mixture was then extracted with diethyl ether (10 mL), quenched with Na_2CO_3 (10 mL), washed with water (10 mL), concentrated *in vacuo* and then dried with $MgSO_4$ and purified using column chromatography (100% EtOAc) to yield a colourless oil (450 mg, 84%).

^{1}H NMR (400 MHz, Chloroform-*d*) δ 8.44 (d, *J* = 0.7 Hz, 1H), 8.12 (4, m, 2H), 7.40 – 7.33 (3, m, 2H), 6.94 (7, m, 1H), 6.85 (5, m, 1H), 6.76 (6, m, 1H), 4.99 (2, s, 2H), 4.14 (8, m, 2H), 3.86 – 3.79 (9, m, 2H), 3.71 – 3.57 (10, 12, m, 10H), 3.54 – 3.47 (13, m, 2H), 3.33 (14, m, 3H).

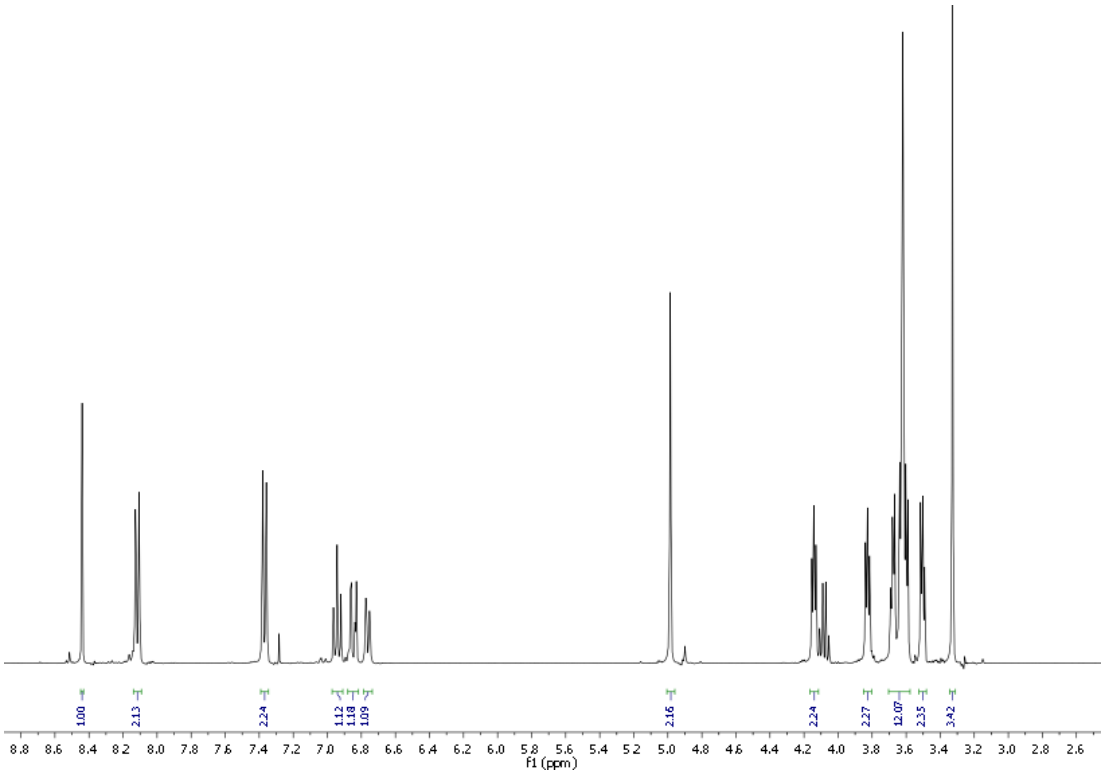

_N_-[(4-aminophenyl)methyl]-_N_-[3-fluoro-4-[2-[2-[2-(2-methoxyethoxy)ethoxy]ethoxy]ethoxy]phenyl]formamide (32)

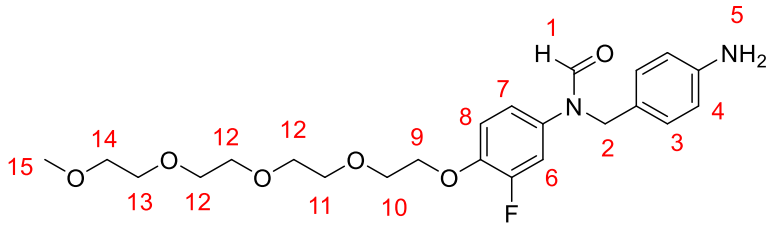

To a reaction flask under a nitrogen atmosphere was added a solution of _N_-[3-fluoro-4-[2-[2-[2-(2-methoxyethoxy)ethoxy]ethoxy]ethoxy]phenyl]-_N_-[(4-nitrophenyl)methyl]formamide (400 mg, 0.832 mmol) in EtOH (10 mL). Palladium on carbon (10 wt %) was then added and the reaction mixture put under a hydrogen environment. The reaction mixture was monitored to completion via TLC and then filtered through Celite. The crude mixture was then reduced under pressure and purified using column chromatography (2% MeOH/EtOAc) to yield a colourless oil (300 mg, 80%).

^{1}H NMR (500 MHz, DMSO-d_6) δ 8.51 (1', s, 1H), 8.46 (1, s, 1H), 7.30 – 7.25 (8, m, 1H) 7.22 – 7.18 (8', m, 1H), 7.16 – 7.07 (6, m, 1H, 6', m, 1H), 7.02 – 6.98 (7, m, 1H, 7', m, 1H) 6.94 – 6.87 (3', m, 2H, 3, m, 2H), 6.47 – 6.41 (4', m, 2H, 4, m, 2H), 4.78 (2, s, 2H), 4.72 (2', s, 2H), 4.15 – 4.11 (9, m, 2H, 9', m, 2H), 3.75 – 3.71 (10, m, 2H, 10', m, 2H), 3.59 – 3.56 (11, m, 2H, 11', m, 2H), 3.55 – 3.47 (12, m, 6H, 12, m, 6H), 3.44 – 3.39 (13, m, 2H, 13', m, 2H), 3.23-3.22 (15, s, 3H, 15', s, 3H), 2.99 – 2.93 (14, m, 2H, 14', m, 2H).

^{13}C NMR (126 MHz, DMSO-d_6) δ 163.17 (s), 162.59 (s), 151.80 (d, J = 244.8 Hz), 148.88 (s), 148.63 (s), 145.06 (s), 144.98 (s), 134.44 (d, J = 8.8 Hz), 129.05 (s), 128.93 (s), 123.73 (s), 123.69 (s), 122.01 (d, J = 3.4 Hz), 120.38 (d, J = 3.3 Hz), 115.68 (d, J = 2.6 Hz), 115.00 (s), 114.04 (s), 113.88 (s), 112.60 (s), 112.43 (s), 112.28 (s), 112.25 (s), 71.74 (s), 70.40 (s), 70.27 (s), 70.24 (s), 70.03 (s), 69.24 (s), 68.98 (s), 68.86 (s), 58.50 (s), 52.57 (s), 46.92 (s), 37.75 (s), 14.86 (s).

^{19}F NMR (471 MHz, DMSO-d_6) δ -132.57 (major), -133.63 (minor).

EI HRMS: obtained m/z 492.22473 M+ (expected m/z 492.22663 M+).

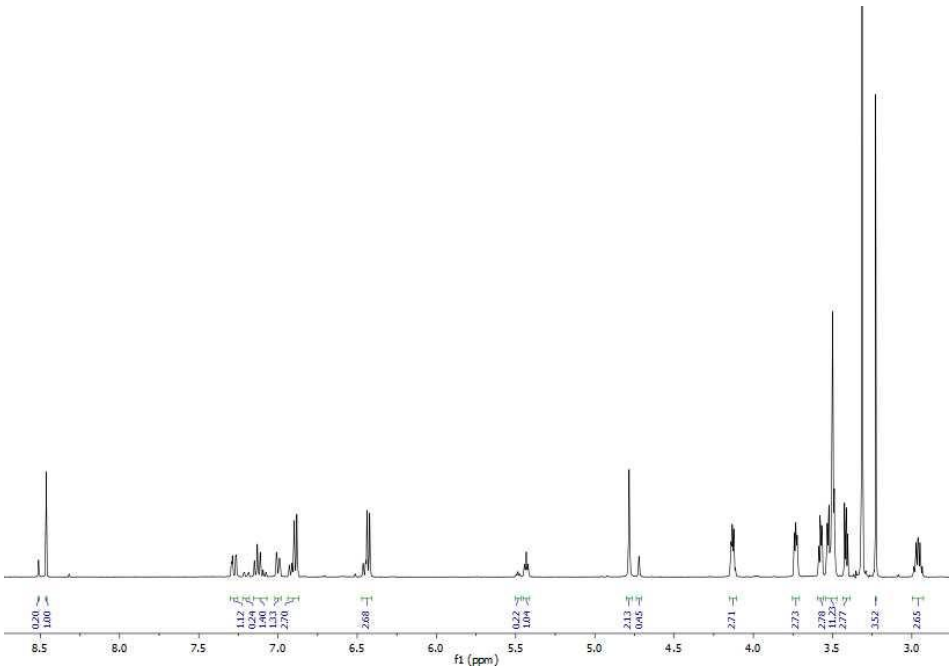
0.20
1.00
1.12
0.24
1.60
1.33
2.70
2.68
0.22
1.04
2.13
0.45
2.71
2.73
2.78
11.23
2.77
3.52
2.65
8.5
8.0
7.5
7.0
6.5
6.0
5.5
5.0
4.5
4.0
3.5
3.0
f1 (ppm)

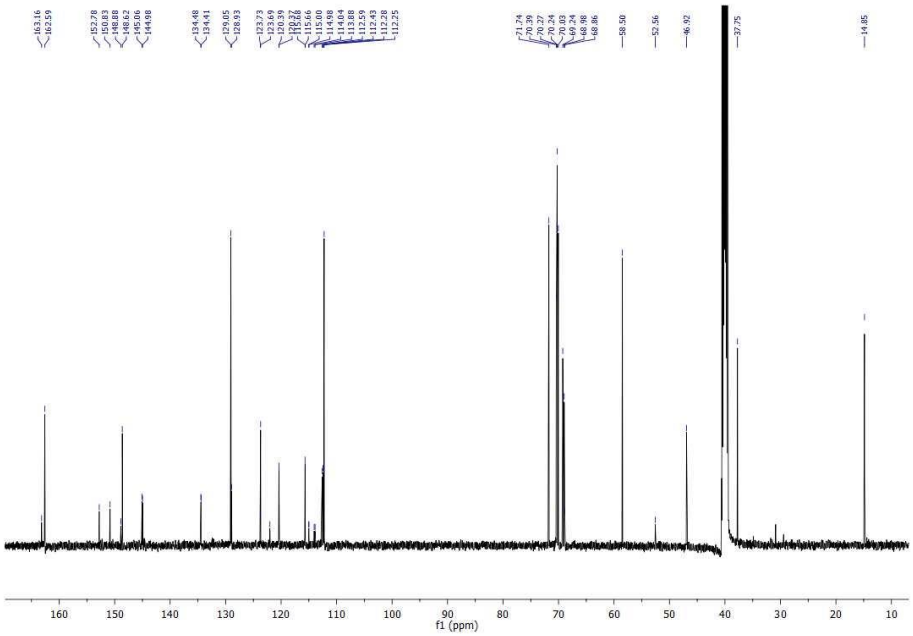
163.16
162.59
152.78
150.83
148.88
148.62
145.06
144.98
134.48
134.41
129.05
128.93
123.73
123.49
120.59
120.27
115.66
115.00
114.98
114.64
113.68
112.59
112.43
112.28
112.25
71.74
70.39
70.27
70.24
70.03
69.24
68.98
68.86
58.50
52.56
46.92
37.75
14.85
160
150
140
130
120
110
100
90
80
70
60
50
40
30
20
10
f1 (ppm)

Supporting Information C

Chapter 4: Solvent Effects on Cooperativity in H-Bond Chains

Table of Contents

Molecular torsion balances studied

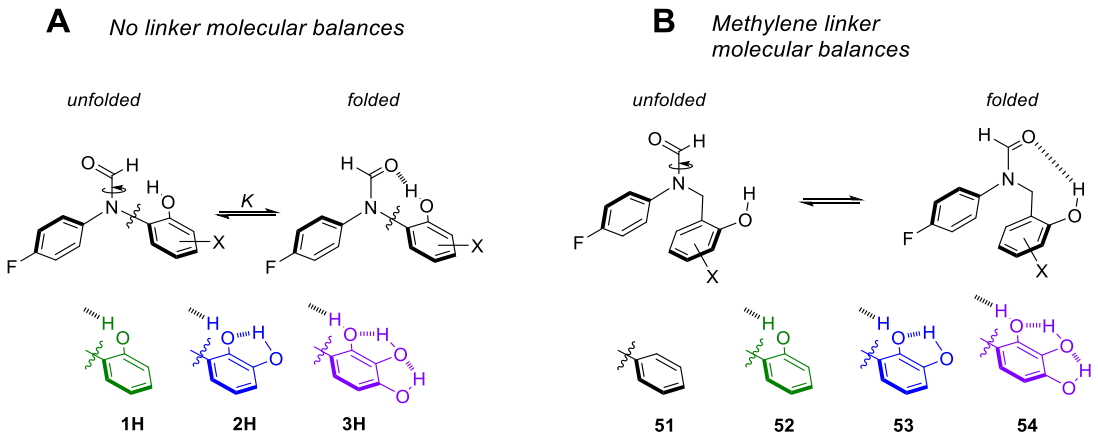

Figure S4.1. **A** Molecular balances without a linker group studied. **B** Methylene linker molecular balances studied.

α_s and β_s values of the solvents studied

Table S4.1. alpha and beta values of the solvents studied

Solvent	α_s	β_s
Chloroform-d	2.2	0.9
Ethyl acetate	1.5	5.3
Dichloromethane	1.9	1.1
Ethanol	2.7	5.3
Acetone	1.5	5.8
Methanol-d4	2.7	5.3
Acetonitrile-d3	1.7	5.1
DMSO-d6	2.2	8.7
DMF		7.7
THF	0.9	5.9
10 % H2O/THF	1.1	5.8
20 % H2O/THF	1.3	5.6
30 % H2O/THF	1.5	5.5
40 % H2O/THF	1.7	5.3
50 % H2O/THF	1.9	5.2
60 % H2O/THF	2.0	5.1
70 % H2O/THF	2.2	4.9
80 % H2O/THF	2.4	4.8
P=O/THF		9.9

Concentration study

Table S4.2. Concentration study of molecular balances

Compound	c/ mM	MeOH ΔG/ kJ mol^{-1}	EtOAc ΔG/ kJ mol^{-1}
52	1	-2.0	-6.0
	2	-2.0	-6.0
	4	-2.0	-6.0
53	1	-2.1	-7.0
	2	-2.1	-7.0
	4	-2.1	-7.0
54	1	-2.1	-7.4
	2	-2.1	-7.4
	4	-2.1	-7.4

Determination of experimental conformational free energies, ΔG_{EXP}

All molecular torsion balances were fully characterized in DMSO-d_6 by ^{1}H and ^{13}C-NMR, prior to the determination of experimental conformational free energies (see Conformer Characterisation section below). The NMR peaks corresponding to the folded and unfolded conformers were assigned using 2D NMR methods as detailed in the conformer assignment section below. NMR spectra used for conformational free energy calculation were determined by ^{19}F NMR spectroscopy using a Bruker Ultrashield 500 MHz, heteronuclear (512 scans). Conformer ratios were determined at balance concentrations of 3.5 mM and were found to be independent of concentration in a range of 1 – 4 mM (Figure). The conformational free energy differences measured in a range of solvents are provided in Tables

$$\Delta G_{EXP} = -RTlnK = -RTln\frac{[\text{Folded}]}{[\text{Unfolded}]}$$

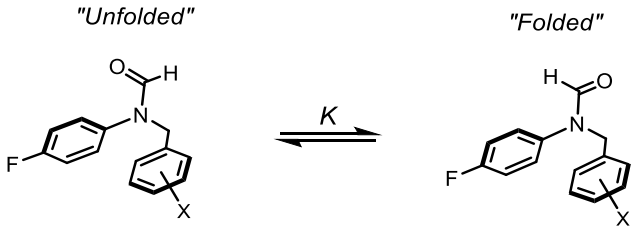

A conservative 3% estimate of the error in the integral of the minor conformer NMR peak was applied (e.g. the integration ratio was [∫major conformer = 1] / [∫minor conformer ± 0.03]), resulting in asymmetric ΔG_{EXP} error margins as listed in Tables S4.3-S4.9. All ^{19}F NMR measurements were carried out once to determine the integration ratios and the Gibbs free energies.

Table S4.3. Conformational free energies ΔG_{exp} of molecular balance **1H** determined at 298 K in various solvents.

1H			
		Error	
	ΔG / kJ mol^{-1}	-	+
Chloroform-d	–4.2	0.5	0.4
Acetone	0.4	0.1	0.1
Acetonitrile-d3	–0.5	0.1	0.1
Ethyl acetate	0.7	0.1	0.1
Tetrahydrofuran	1.5	0.1	0.1
Dichloromethane	–3.9	0.1	0.1
Ethanol	1.2	0.1	0.1
Methanol-d4	0.5	0.1	0.1
DMSO-d6	0.5	0.1	0.1

Table S4.4. Conformational free energies ΔG_{exp} of molecular balance **2H** determined at 298 K in various solvents.

2H			
		Error	
	ΔG / kJ mol^{-1}	-	+
Chloroform-d	–8.0	3.4	1.4
Acetone	0.8	0.1	0.1
Acetonitrile-d3	–0.5	0.1	0.1
Ethyl acetate	0.6	0.1	0.1
Tetrahydrofuran	2.0	0.2	0.2
Dichloromethane	–7.0	0.1	0.1
Ethanol	–	–	–
Methanol-d4	0.7	0.1	0.1
DMSO-d6	0.6	0.1	0.1

Table S4.5. Conformational free energies ΔG_{exp} of molecular balance **3H** determined at 298 K in various solvents.

3H			
		Error	
	ΔG / kJ mol^{-1}	-	+
Chloroform-d	–7.4	2.3	1.2
Acetone	1.4	0.1	0.1
Acetonitrile-d3	0.0	0.1	0.1
Ethyl acetate	1.3	0.1	0.1
Tetrahydrofuran	2.7	0.2	0.2
Dichloromethane	–6.3	0.1	0.1
Ethanol	1.9	0.2	0.2
Methanol-d4	1.0	0.1	0.1
DMSO-d6	1.1	0.1	0.1

Table S4.6. Conformational free energies ΔG_{exp} of molecular balance **51** determined at 298 K in various solvents.

51			
		Error	
	ΔG / kJ mol^{-1}	–	+
Chloroform-d	–5.7	0.9	0.6
Ethyl acetate	–5.5	0.8	0.6
Dichloromethane	–5.5	0.8	0.6
Ethanol	–5.1	0.7	0.5
Acetone	–5.1	0.7	0.5
Methanol-d4	–4.2	0.5	0.4
Acetonitrile-d3	–4.4	0.5	0.4
DMSO-d6	–4.2	0.5	0.4
DMF	–4.4	0.5	0.4
THF	–6.0	1.0	0.7
10 % H2O/THF	–4.9	0.6	0.5
20 % H2O/THF	–4.5	0.5	0.4
30 % H2O/THF	–4.2	0.5	0.4
40 % H2O/THF	–4.2	0.5	0.4
50 % H2O/THF	–3.6	0.4	0.3
60 % H2O/THF	–3.5	0.3	0.3
70 % H2O/THF	–3.1	0.3	0.2
80 % H2O/THF	–2.8	0.2	0.2
P=O/THF	–5.3	0.7	0.6

Table S4.7. Conformational free energies ΔG_{exp} of molecular balance **52** determined at 298 K in various solvents.

	52		
		Error	
	ΔG / kJ mol^{-1}	–	+
Chloroform-d	< –10	–	–
Ethyl acetate	–5.9	1.0	0.7
Dichloromethane	< –10	–	–
Ethanol	–2.1	0.2	0.2
Acetone	–3.8	0.4	0.3
Methanol-d4	–2.0	0.2	0.2
Acetonitrile-d3	–5.0	0.7	0.5
DMSO-d6	–2.8	0.2	0.2
DMF	–3.0	0.3	0.2
THF	–5.0	0.7	0.5
10 % H2O/THF	–3.2	0.3	0.3
20 % H2O/THF	–3.2	0.3	0.3
30 % H2O/THF	–3.0	0.3	0.2
40 % H2O/THF	–2.7	0.2	0.2
50 % H2O/THF	–2.3	0.2	0.2
60 % H2O/THF	–2.0	0.2	0.2
70 % H2O/THF	–1.8	0.2	0.2
80 % H2O/THF	–1.2	0.1	0.1
P=O/THF	–3.2	0.3	0.3

Table S4.8. Conformational free energies ΔG_{exp} of molecular balance **53** determined at 298 K in various solvents.

53			
		Error	
	ΔG / kJ mol^{-1}	–	+
Chloroform-d	< –10	–	–
Ethyl acetate	–7.4	1.7	1.0
Dichloromethane	< –10	–	–
Ethanol	–2.5	0.2	0.2
Acetone	–5.3	0.7	0.6
Methanol-d4	–2.1	0.2	0.2
Acetonitrile-d3	–6.0	1.0	0.7
DMSO-d6	–2.8	0.2	0.2
DMF	–3.0	0.3	0.2
THF	–5.5	0.8	0.6
10 % H2O/THF	–3.3	0.3	0.3
20 % H2O/THF	–3.2	0.3	0.3
30 % H2O/THF	–3.2	0.3	0.3
40 % H2O/THF	–2.7	0.2	0.2
50 % H2O/THF	–2.7	0.2	0.2
60 % H2O/THF	–2.8	0.2	0.2
70 % H2O/THF	–2.2	0.2	0.2
80 % H2O/THF	–1.7	0.2	0.1
P=O/THF	–3.0	0.3	0.2

Table S4.9. Conformational free energies ΔG_{exp} of molecular balance **54** determined at 298 K in various solvents.

	54		
		Error	
	ΔG / kJ mol^{-1}	–	+
Chloroform-d	< –10	–	–
Ethyl acetate	–7.4	2.3	1.2
Dichloromethane	< –10	–	–
Ethanol	–2.2	0.2	0.2
Acetone	–5.5	0.8	0.6
Methanol-d4	–2.1	0.2	0.2
Acetonitrile-d3	–6.3	1.2	0.8
DMSO-d6	–2.2	0.2	0.2
DMF	–2.3	0.2	0.2
THF	–5.5	0.8	0.6
10 % H2O/THF	–3.3	0.3	0.3
20 % H2O/THF	–2.7	0.2	0.2
30 % H2O/THF	–2.5	0.2	0.2
40 % H2O/THF	–2.6	0.2	0.2
50 % H2O/THF	–1.9	0.2	0.2
60 % H2O/THF	–1.8	0.2	0.2
70 % H2O/THF	–1.4	0.1	0.1
80 % H2O/THF	–1.0	0.1	0.1
P=O/THF	–2.5	0.2	0.2

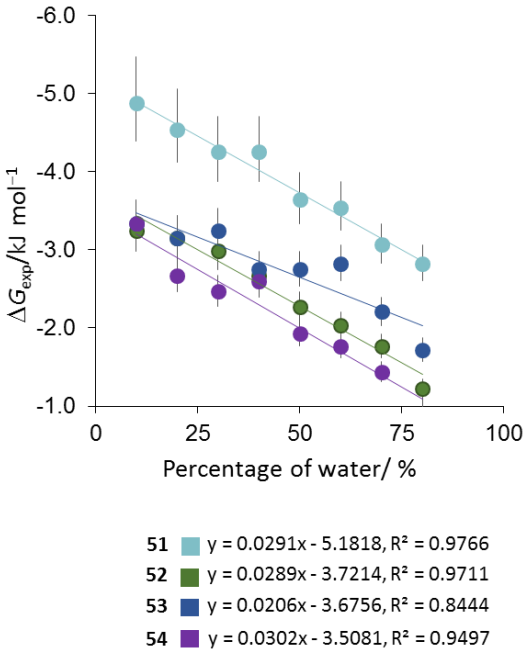

Figure S4.2. Percentage of water plotted against experimentally determined Gibbs free energies for molecular balances **51-54**.

Van't Hoff analyses of compounds 51, 52, 53 and 54

Van't Hoff analysis was carried out on ~3.5 mM samples of compounds **51-54** in EtOAc, MeCN, DMSO and 80% water/THF solvents. Samples were prepared and placed in an air-tight Wilmad-cap NMR tube. Spectra were obtained at a minimum of seven temperatures, beginning with the coldest. Samples were equilibrated at each temperature for 30 minutes within the spectrometer. Results are shown in Table S4.10-S4.14 and Figures S4.3-4.17 showing the derivation of thermodynamic parameters from the gradient and intercept according to the equation $\Delta G = \Delta H - T\Delta S$.

EtOAc

Table S4.10: Van't Hoff analysis for compounds 51-54 in EtOAc**.**

T/ K	1/ T	ln K_{51}	ln K_{52}	ln K_{53}	ln K_{54}
300	0.00333	2.244	2.442	2.442	3.037
305	0.00328	2.226	2.419	2.419	2.957
310	0.00323	2.235	2.430	2.430	2.957
315	0.00317	2.216	2.419	2.419	2.957
320	0.00313	2.198	2.397	2.375	2.882
325	0.00308	2.180	2.397	2.397	2.865
330	0.00303	2.180	2.419	2.397	2.847

MeCN

Table S4.11: Van't Hoff analysis for compounds 51-54 in MeCN.

T/ K	1/ T	ln K_{51}	ln K_{52}	ln K_{53}	ln K_{54}
300	0.00333	1.778	1.973	2.430	2.564
305	0.00328	1.749	1.959	2.419	2.513
310	0.00323	1.709	1.981	2.430	2.526
315	0.00317	1.715	1.973	2.408	2.513
320	0.00313	1.645	1.973	2.386	2.526
325	0.00308	1.645	1.981	2.386	2.465
330	0.00303	1.604	2.040	2.375	2.465

DMSO

Table S4.12: Van't Hoff analysis for compounds 51-54 in DMSO.

T/ K	1/ T	ln K_{51}	ln K_{52}	ln K_{53}	ln K_{54}
300	0.00333	1.715	1.139	1.136	0.899
305	0.00328	1.677	1.127	1.118	0.892
310	0.00323	1.687	1.121	1.109	0.887
315	0.00317	1.645	1.094	1.091	0.872
320	0.00313	1.630	1.088	1.079	0.875
325	0.00308	1.614	1.085	1.076	0.875
330	0.00303	1.604	1.070	1.076	0.872

80% water/THF

Table S4.13: Van't Hoff analysis for compounds 51-54 in 80% water/THF.

T/ K	1/ T	ln K_{51}	ln K_{52}	ln K_{53}	ln K_{54}
300	0.00333	1.287	0.587	0.799	0.751
305	0.00328	1.306	0.603	0.823	0.781
310	0.00323	1.313	0.631	0.842	0.770
315	0.00317	1.324	0.660	0.853	0.753
320	0.00313	1.321	0.673	0.879	-
325	0.00308	1.324	0.705	0.870	-
330	0.00303	1.336	0.722	0.901	-

80% water/THF

Table S4.14: Dissection of ΔH and $T\Delta S$ at 300 K for compounds 51-54 in 80% water/THF solvent system.

Balance	$-T\Delta S$/ kJ mol^{-1}	ΔH/ kJ mol^{-1}	ΔG/ kJ mol^{-1}
51	-4.3	1.10	-3.21
52	-5.3	3.80	-1.46
53	-4.6	2.60	-1.99
54	-	-	-1.87

EtOAc

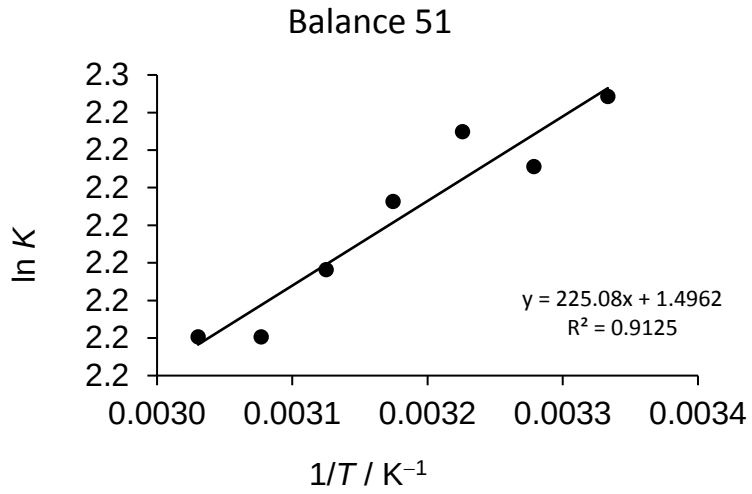

Figure S4.3: Van't Hoff analysis of compound 51 in EtOAc

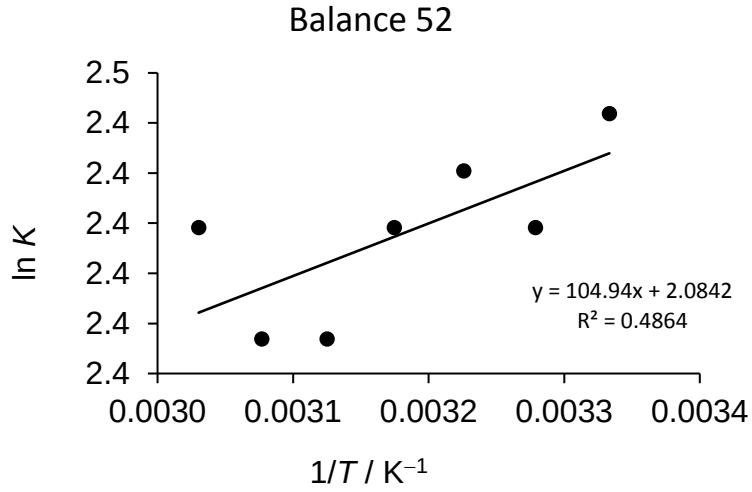

Figure S4.4: Van't Hoff analysis of compound 52 in EtOAc

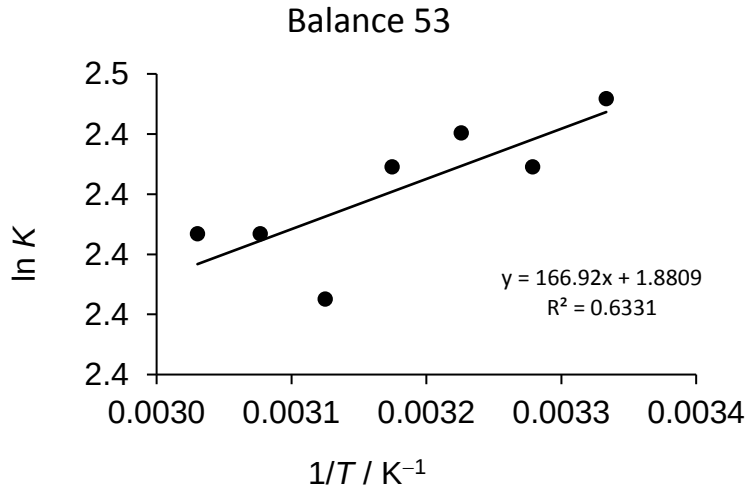

Figure S4.5: Van't Hoff analysis of compound 53 in EtOAc.

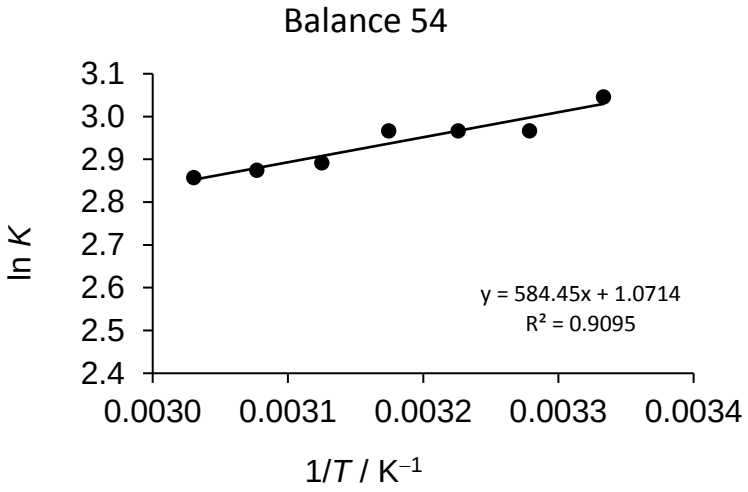

Figure S4.6: Van't Hoff analysis of compound 54 in EtOAc.

MeCN

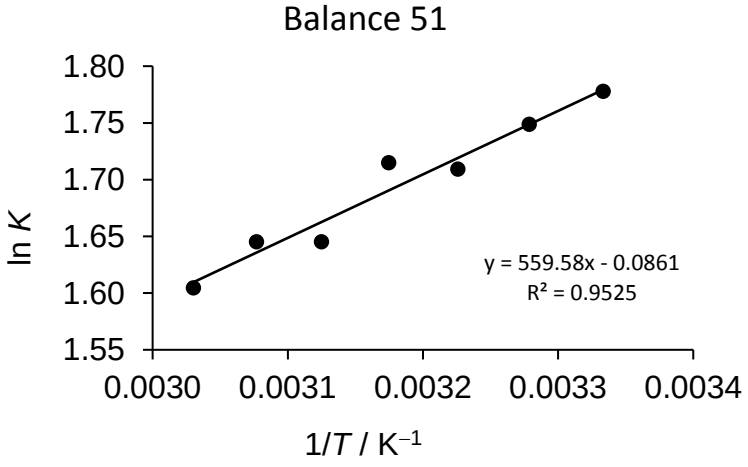

Figure S4.7: Van't Hoff analysis of compound 51 in MeCN.

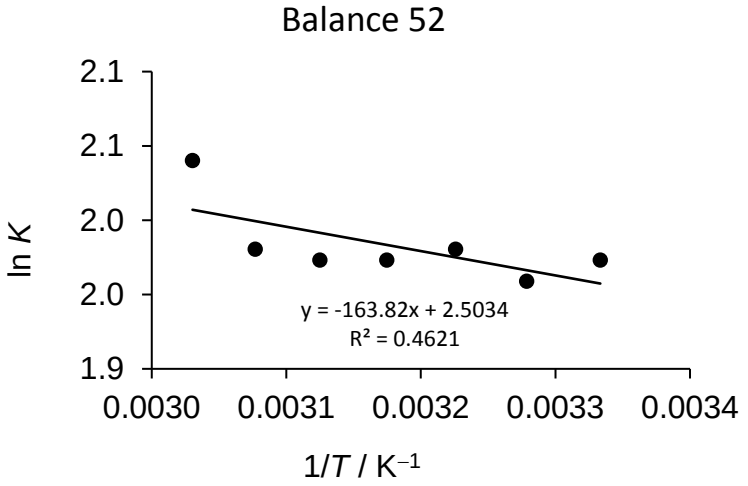

Figure S4.8: Van't Hoff analysis of compound 52 in MeCN.

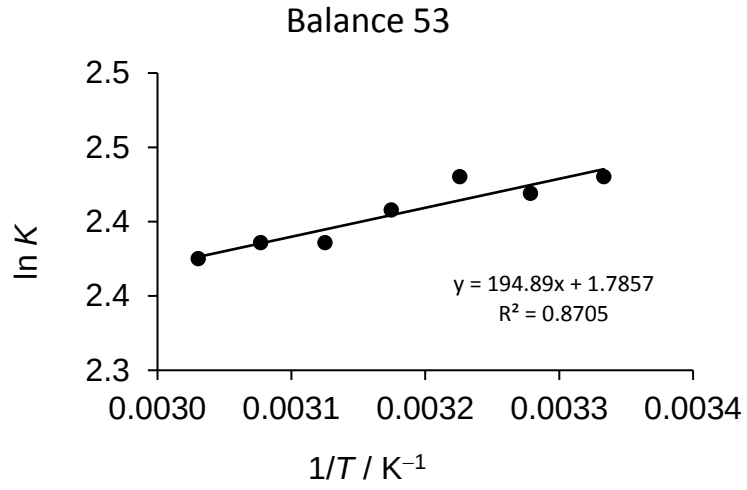

.

Figure S4.9: Van't Hoff analysis compound 53 in MeCN.

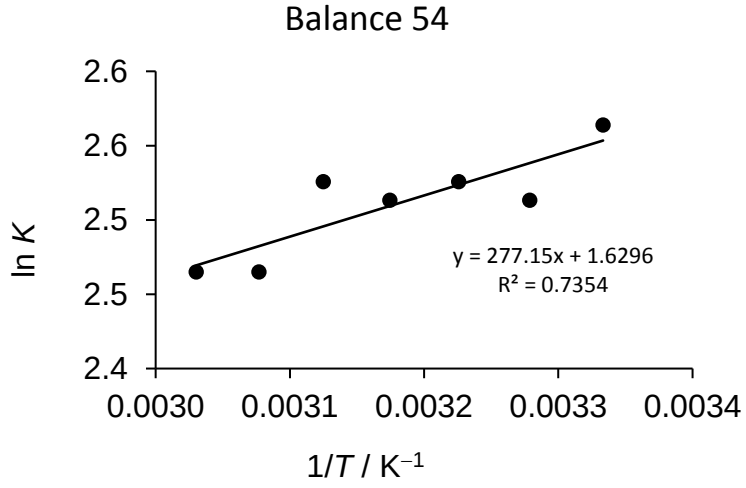

Figure S4.10: Van't Hoff analysis compound 54 in MeCN.

DMSO

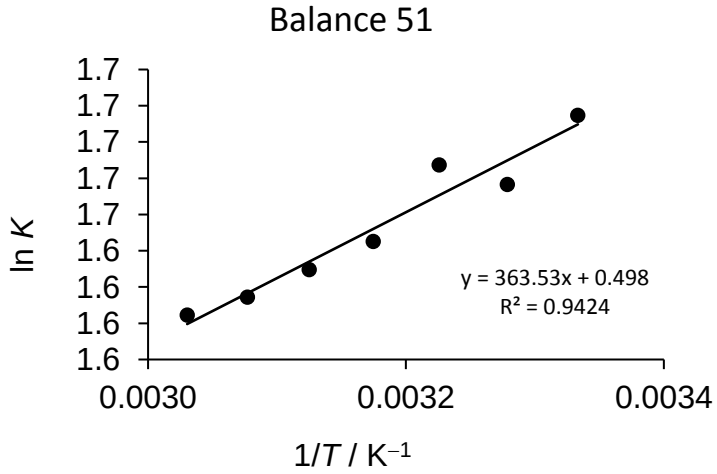

Figure S4.11: Van't Hoff analysis of compound 51 in DMSO.

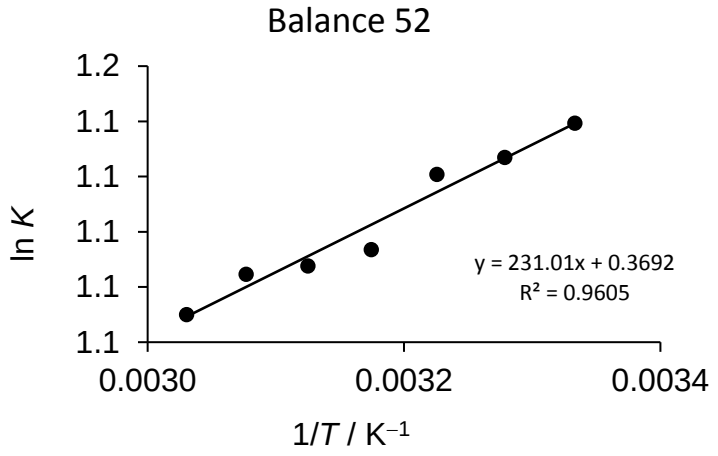

Figure S4.12: Van't Hoff analysis of compound 52 in DMSO.

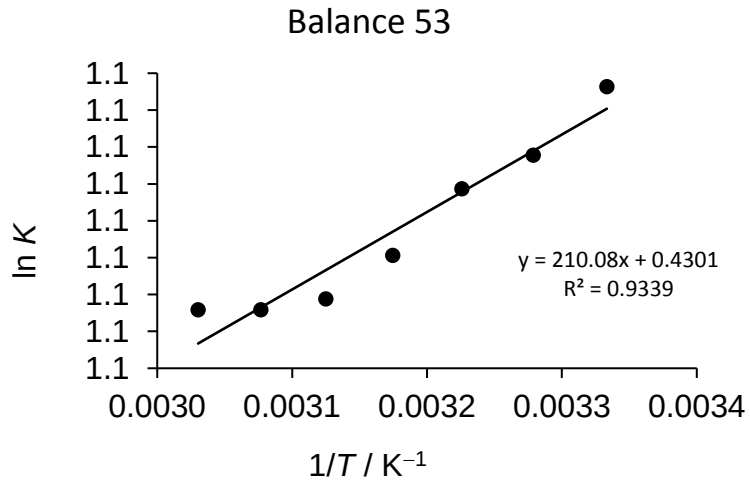

Figure S4.13: Van't Hoff analysis of compound 53 in DMSO.

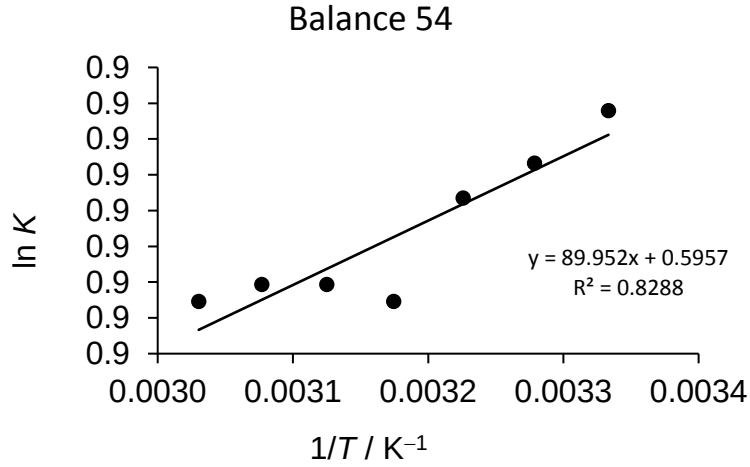

Figure S4.14: Van't Hoff analysis of compound 54 in DMSO.

80% water/THF

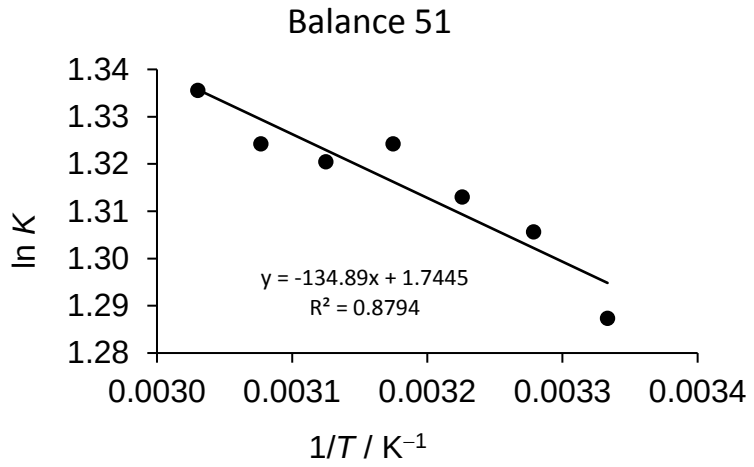

Figure S4.15: Van't Hoff analysis of compound 51 in 80% water/THF.

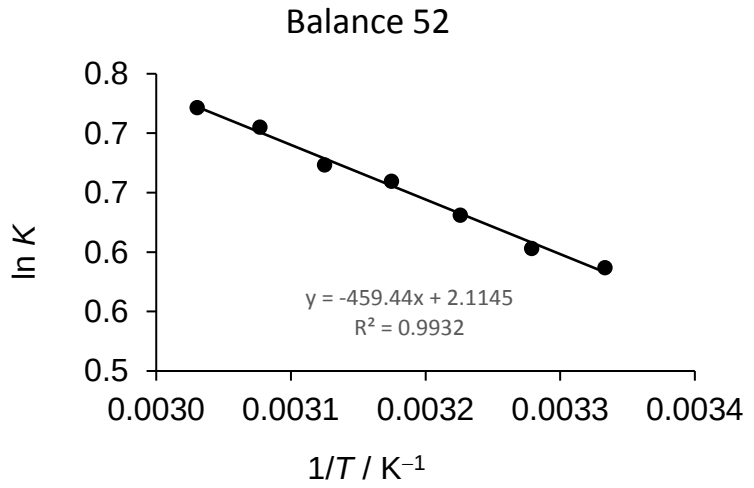

Figure S4.16: Van't Hoff analysis of compound 52 in 80% water/THF.

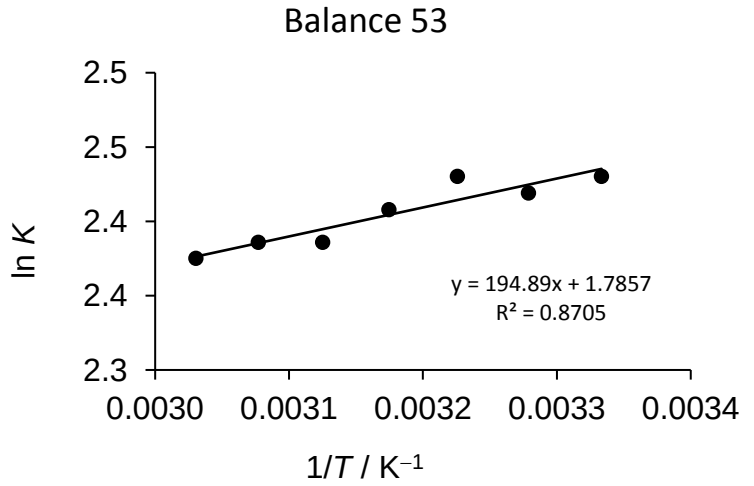

Figure S4.17: Van't Hoff analysis of compound 53 in 80% water/THF.

Computational methods and data

Geometry minimization and calculated conformational energies

Conformer distribution searches were performed on full molecular balances using Spartan '14 with DFT/B3LYP/6-311G* to obtain the minimised geometries of the unfolded and folded conformers. The resulting gas phase energies and corresponding energy differences, ΔG_{DFT} in each conformer are reported in Table S4.15. The minimized B3LYP/6-311G* geometries of the folded and unfolded are presented in Figure S4.17.

Table S4.15. Calculated energies of folded and unfolded conformers and the calculated conformational free energy, ΔG_{DFT}, performed using DFT/B3LYP/6-311G*.

Compound	Energy folded conformer/ kJ mol^{-1}	Energy unfolded conformer/ kJ mol^{-1}	ΔG_{DFT}/ kJ mol^{-1}
51	–2023509.13	–2023499.46	–9.67
52	–2221073.02	–2221042.73	–30.29
53	–2418623.72	–2418585.05	–38.67
54	–2616168.21	–2616127.21	–41.00

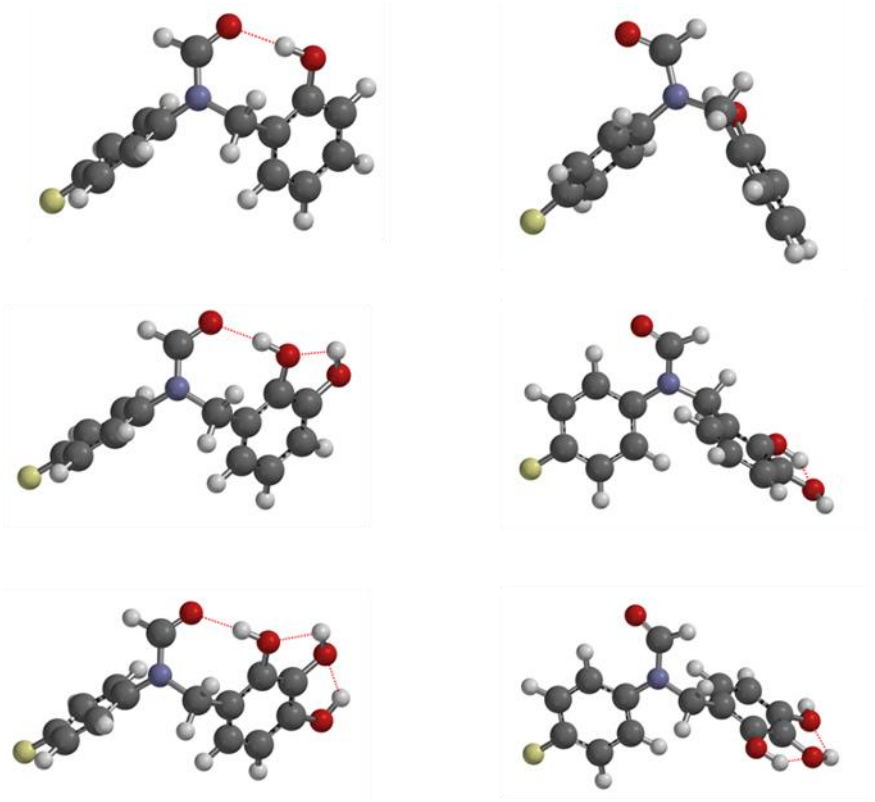

Figure S4.17. Calculated optimised geometries of 'unfolded' and 'folded' conformers using DFT/6-311G*/B3LYP.

Calculated conformational energies employing polarizable continuum model (PCM) implicit solvation model

Table S4.16. Calculated conformational energies (DFT/B3LYP/6-311G*) in DMSO employing the PCM solvation model.

Compound	Energy folded conformer/ kJ mol^{-1}	Energy unfolded conformer/ kJ mol^{-1}	ΔE_{DMSO}/ kJ mol^{-1}
52	–2199530.32	–2199503.267	–27.05
53	–2395162.513	–2395130.681	–31.83
54	–2590789.965	–2590756.392	–33.57

Table S4.17. Calculated conformational energies (DFT/B3LYP/6-311G*) in MeOH employing the PCM solvation model.

Compound	Energy folded conformer/ kJ mol^{-1}	Energy unfolded conformer/ kJ mol^{-1}	ΔE_{MEOH}/ kJ mol^{-1}
52	–2199529.982	–2199502.898	–27.08
53	–2395162.172	–2395130.274	–31.90
54	–2590789.608	–2590755.967	–33.64

Conformer assignment by NMR spectroscopy

The following figures present the NMR spectra (^{1}H, ^{13}C, HSQC, COSY, NOESY and HMBC) of N-[2-[(4-fluoro-N-formyl-anilino)methyl]phenyl]-2,2-dimethyl-propanamide in DMSO-d_6, showing the full spectral assignment for both conformers. The proton resonances have been labelled numerically and carbon resonances alphabetically. Red peaks with prime notation (') denotes a minor conformer, while blue indicates the major conformer.

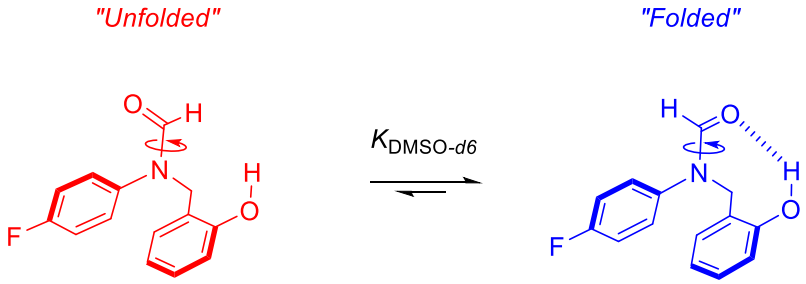

Figure S4.18. Equilibrium of molecular balance, 52, in DMSO-d_6

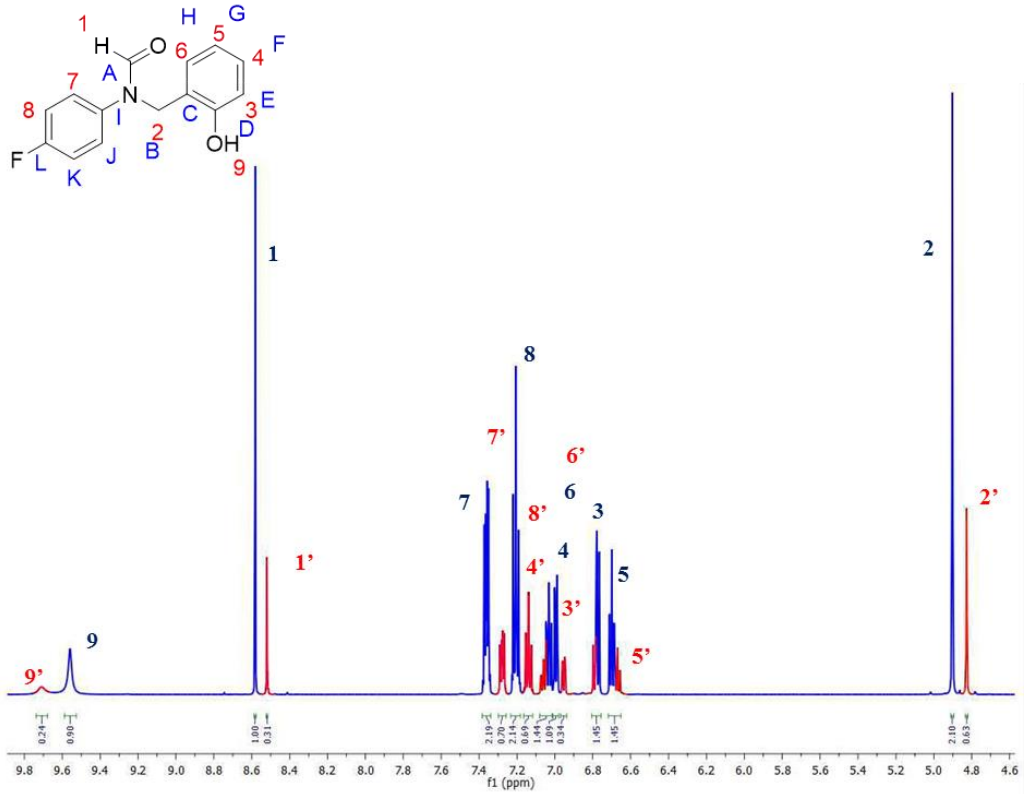

Figure S4.19: ^{1}H NMR spectrum of molecular balance 52 in DMSO-d_6.

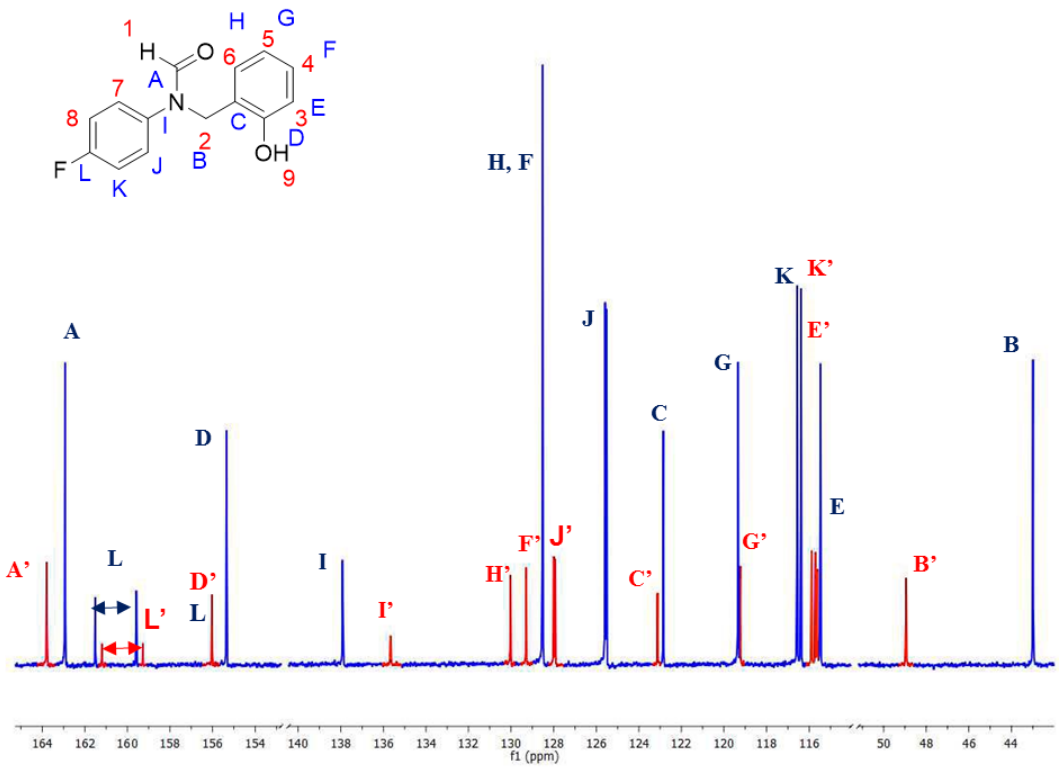

Figure S4.20: ^{13}C NMR spectrum of molecular balance 52 in DMSO-d_6.

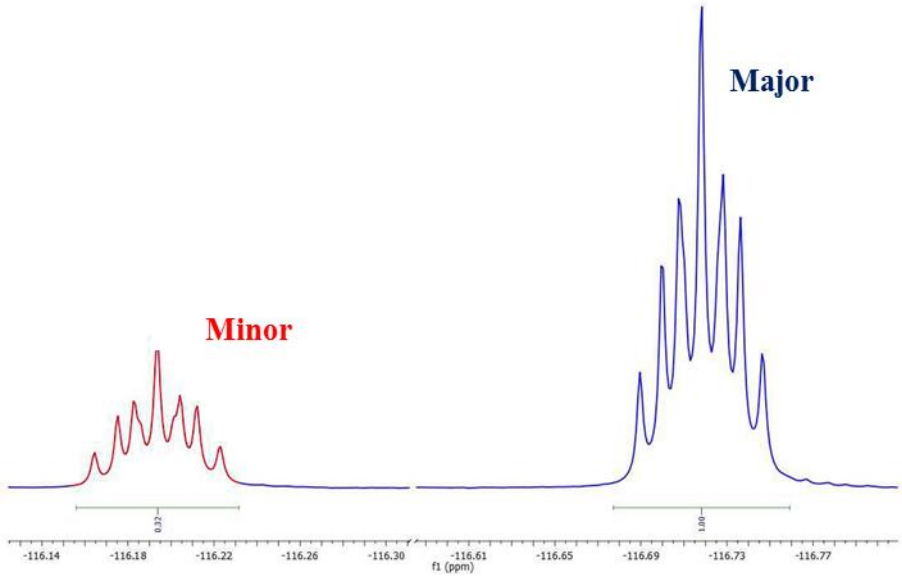

Figure S4.21: ^{19}F NMR spectrum of molecular balance 52 in DMSO-d_6.

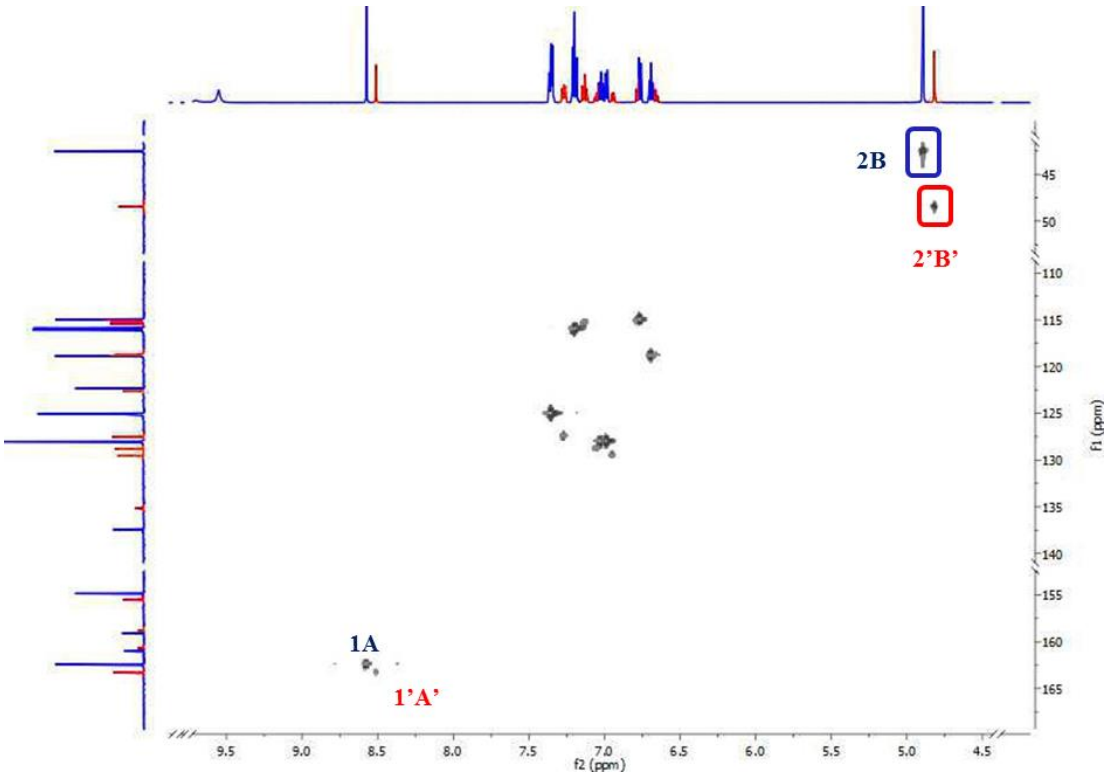

Figure S4.22: HSQC spectrum of molecular balance 52 in DMSO-d_6.

The major and minor conformers were unambiguously distinguished by analysing the HMBC spectra (Figure 4.23); H-C correlation through multiple bonds. The formyl proton has a cross peak with the *trans*-CH_2 carbon in the H-bonded conformer, whereas in the unbound conformer the formyl proton has a *trans*-cross peak with trans-quaternary aromatic carbon.

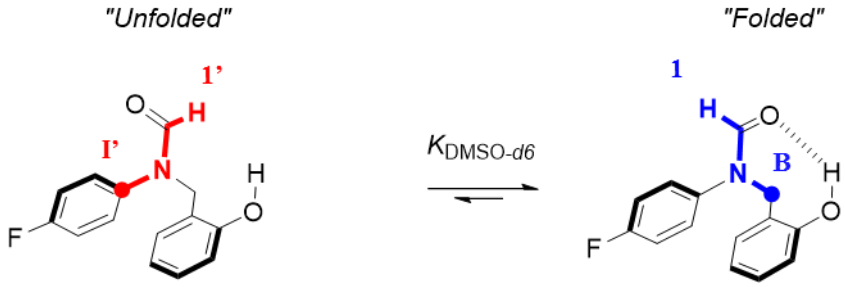

Figure S4.23: Coupling of the formyl proton 1 to carbon B in the major conformer. Coupling of formyl proton 1' to carbon I in the minor conformer.

In the example depicted in Figure S4.24, the major formyl proton 1 couples to carbon B, and the minor formyl proton 1' couples with I'.

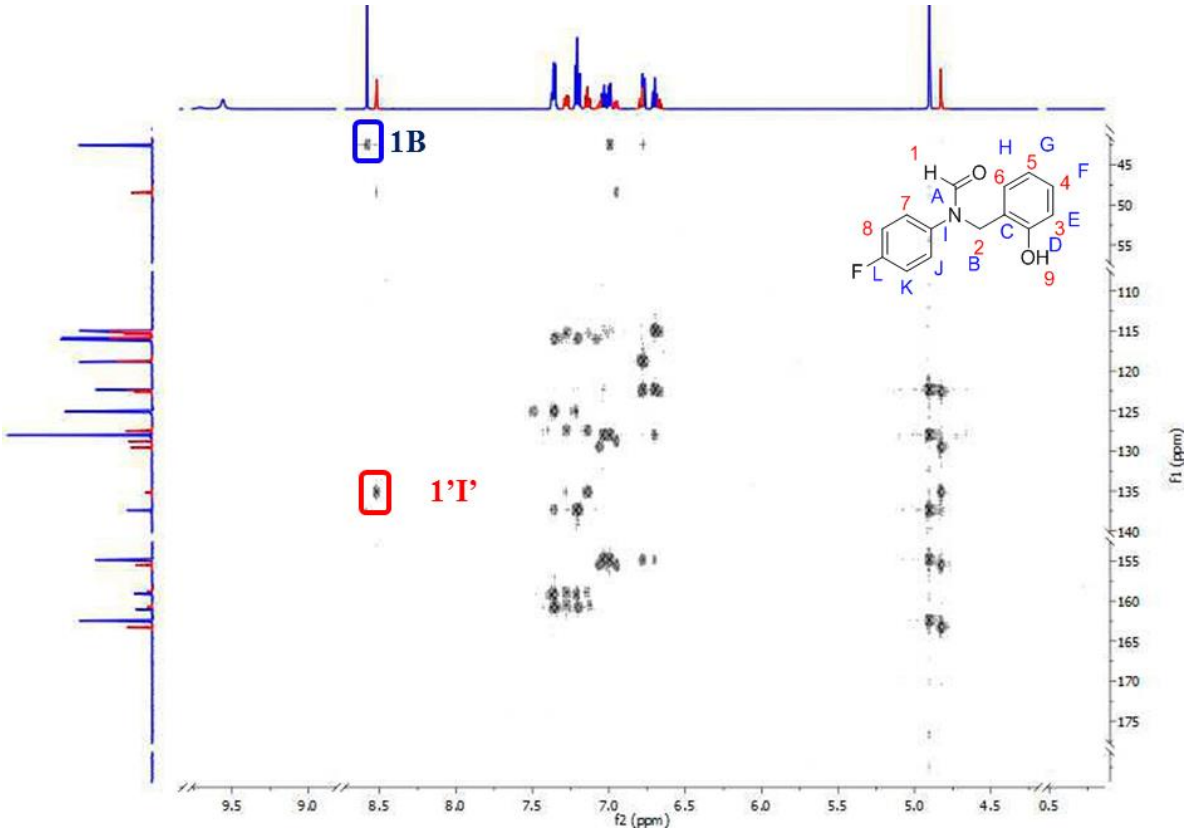

Figure S4.24: HMBC spectrum of molecular balance 52 in DMSO-d_6.

Experimental

Synthesis of *N*-benzyl-*N*-(4-fluorophenyl)formamide (51)

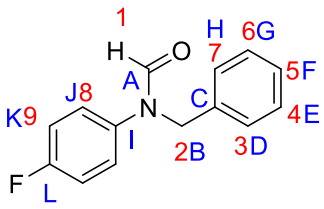

To a flask under a nitrogen atmosphere was added a solution of *N*-(4-fluorophenyl) formamide (200 mg, 1.44 mmol), in dry DMF (5 mL), benzyl bromide (171 µL, 1.44 mmol) was then added and the mixture cooled to 0 °C. Sodium hydride (0.070 mg, 1.73 mmol) was then carefully added and the mixture allowed to warm to room temperature. The reaction mixture was stirred overnight, diluted with DCM (5 mL) and quenched with water (5 mL). The organics were then reduced *in vacuo*, dried with $MgSO_4$ and purified using column chromatography (30 % EtOAc/*n*-Hex) to yield a colourless oil (267 mg, 81%).

^{1}H NMR (601 MHz, DMSO-d_6) δ 8.60 (1', s, 1H), 8.57 (1, s, 1H), 7.39 – 7.36 (9, m, 2H, 9', m, 2H), 7.35 – 7.27 (6, m, 1H, 6', m, 1H, 4, m, 1H, 4', m, 1H), 7.26 – 7.13 (8, m, 2H, 8', m, 2H, 7, m, 1H, 7', m, 1H, 3, m, 1H, 3', m, 1H, 5, m, 1H, 5', m, 1H), 5.01 (2, s, 2H), 4.96 (2', s, 2H).

^{13}C NMR (151 MHz, DMSO-d_6) δ 163.48, 162.89, 160.62 (d, J = 243.0 Hz), 160.62 (d, J = 243.1 Hz), 137.54 (d, J = 2.6 Hz), 137.23, 135.47, 129.02, 128.94, 128.50, 127.99, 127.86, 127.80, 127.61, 127.08, 126.88, 125.82 (d, J = 8.6 Hz), 116.59 (d, J = 22.7 Hz), 115.90 (d, J = 22.4 Hz), 52.72, 47.39.

^{19}F NMR (471 MHz, DMSO-d_6) δ -116.00 (minor), -116.46 (major).

EI HRMS: obtained 229.09078 m/z M+ (expected m/z 229.08974 M+).

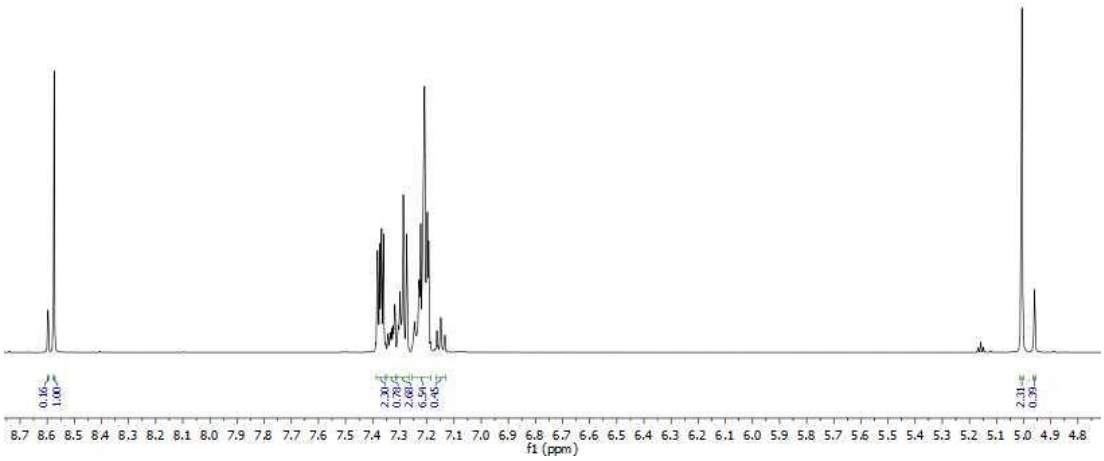
0.16
1.00
2.30
0.78
2.68
6.54
0.45
2.31
0.39
8.7 8.6 8.5 8.4 8.3 8.2 8.1 8.0 7.9 7.8 7.7 7.6 7.5 7.4 7.3 7.2 7.1 7.0 6.9 6.8 6.7 6.6 6.5 6.4 6.3 6.2 6.1 6.0 5.9 5.8 5.7 5.6 5.5 5.4 5.3 5.2 5.1 5.0 4.9 4.8
f1 (ppm)

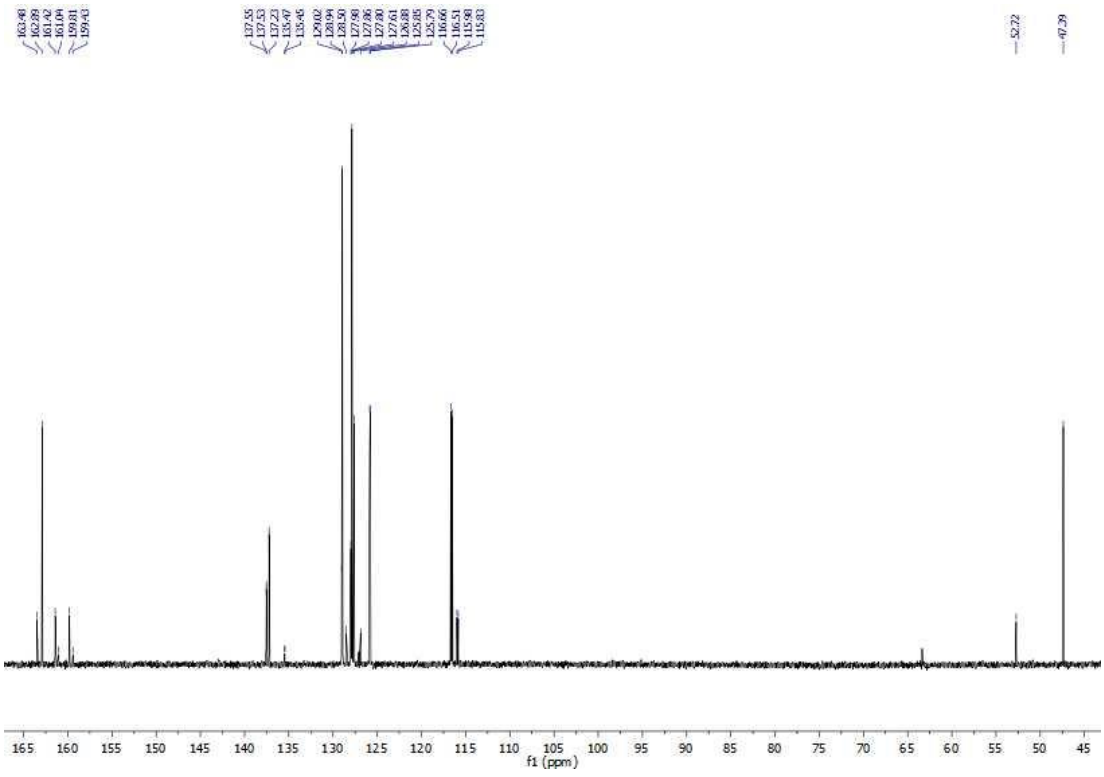
163.48
162.89
161.42
161.04
159.81
159.43
137.55
137.53
137.23
135.47
135.45
129.02
128.94
128.50
127.98
127.86
127.80
127.61
126.68
125.95
125.79
116.66
116.51
115.98
115.83
52.72
47.39
165 160 155 150 145 140 135 130 125 120 115 110 105 100 95 90 85 80 75 70 65 60 55 50 45
f1 (ppm)

Synthesis of *N*-(4-fluorophenyl)-*N*-[(2-hydroxyphenyl)methyl]formamide

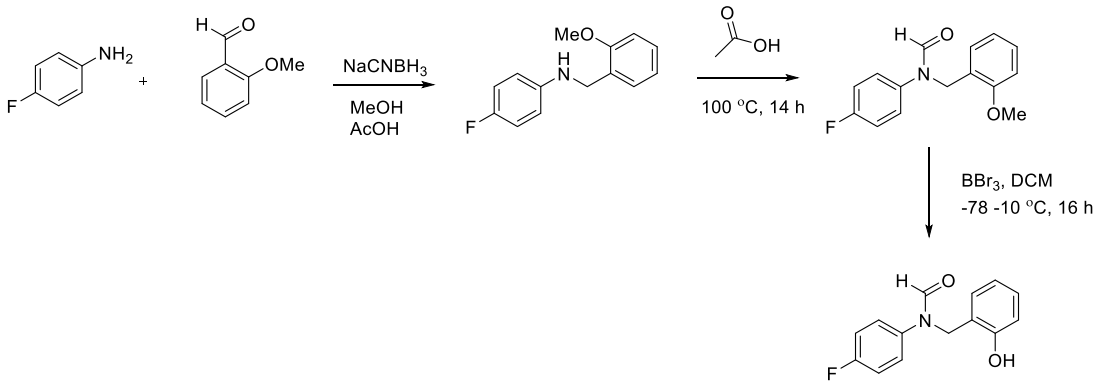

4-fluoro-*N*-[(2-methoxyphenyl)methyl]aniline (55)

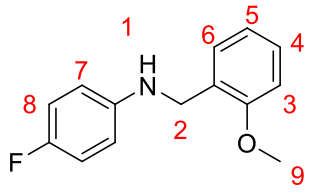

To a solution of 4-fluoroaniline (1.00 mL, 10.5 mmol) in dry methanol (10 mL) was added methoxybenzaldehyde (1.86 g, 13.7 mmol) and sodium cyanoborohydride (860 mg, 13.7 mmol). Acetic acid (3.00 mL, 52.6 mmol) was then added dropwise and the mixture heated to reflux overnight. The reaction mixture was then reduced under pressure and dissolved in ethyl acetate (10 mL), washed with water (10 mL) and brine (10 mL). The reaction mixture was then concentrated, dried with $MgSO_4$ and purified using column chromatography (30 % EtOAc/*n*-Hex) to yield a white solid (1.67 g, 69 %).

N-(4-fluorophenyl)-*N*-[(2-methoxyphenyl)methyl]formamide (56)

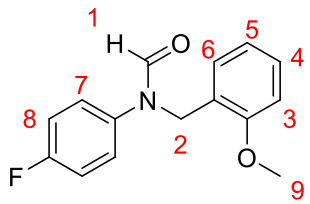

Formic acid (10 mL) was added neat to 4-fluoro-*N*-[(2-methoxyphenyl)methyl]aniline (1.67 g, 7.22 mmol) and the reaction mixture refluxed overnight. The mixture was then diluted in DCM (10 mL) and quenched with saturated Na_2CO_3 (10 mL), washed with water (5 mL) and brine (5 mL), dried over $MgSO_4$, concentrated under reduced pressure and purified using column chromatography (1:1 EtOAc:*n*-Hex) to yield a white solid (630 mg, 34 %).

^{1}H NMR (601 MHz, Chloroform-*d*) δ 8.56 (1', s, 1H), 8.51 (1, s, 1H), 7.26 – 7.19 (5, 5', 6, 6', m, 4H), 7.14 – 7.08 (7, 7', m, 4H), 7.05 – 6.99 (8, 8', m, 4H), 6.90 (4, 4', m, 2H), 6.88 – 6.81 (3, 3', m, 1H), 5.02 (2, s, 2H), 4.79 (2', s, 2H), 3.86 (9', s, 3H), 3.73 (9, s, 3H).

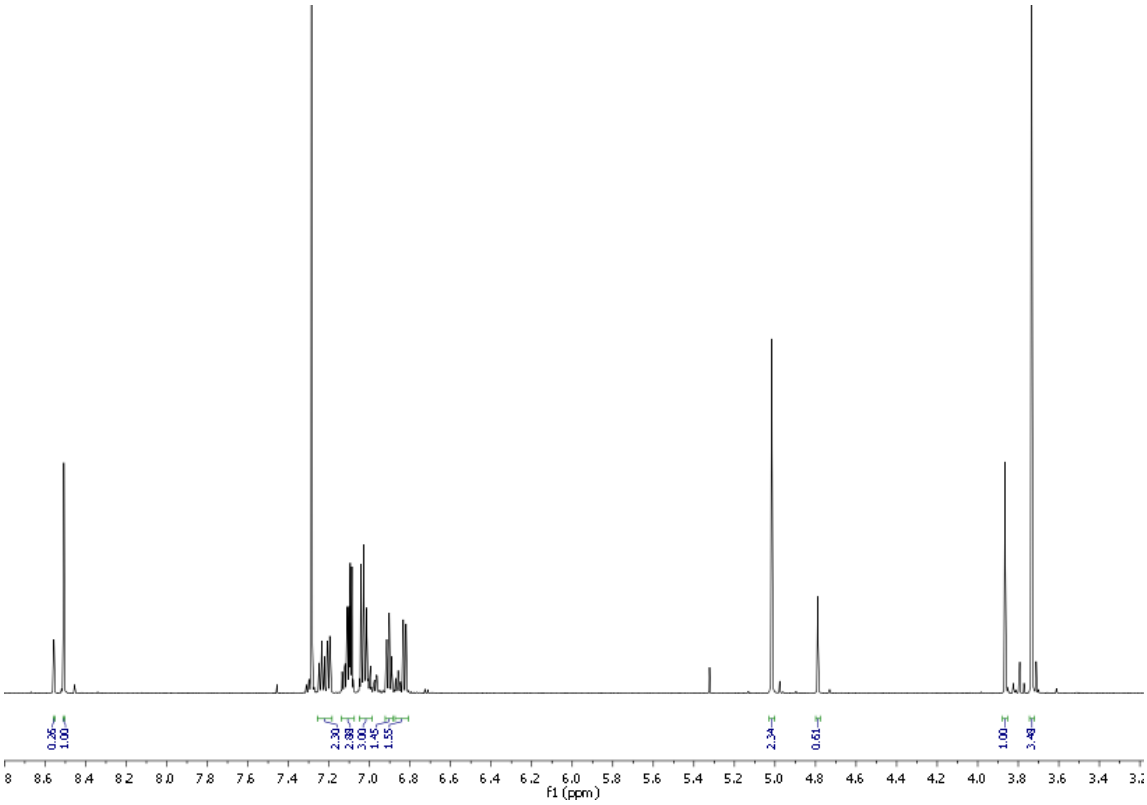

N-(4-fluorophenyl)-*N*-[(2-hydroxyphenyl)methyl]formamide (52)

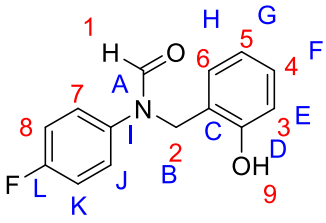

To a flask under a nitrogen atmosphere was added a solution of *N*-(4-fluorophenyl)-*N*-[(2-methoxyphenyl)methyl]formamide (700 mg, 2.70 mmol) in DCM (10 mL). The reaction mixture was cooled to -78 °C and boron tribromide (33 % wt. 1.56 mL, 16.2 mmol) in DCM was carefully added dropwise. The reaction mixture was then allowed to warm to room temperature and stirred overnight. The reaction mixture was quenched with water (10 mL) and extracted with DCM (2 x 10 mL), dried over $MgSO_4$,

concentrated under reduced pressure and purified by column chromatography (1:4 EtOAc:*n*-Hex) to yield a white solid (310 mg, 47%).

^{1}H NMR (601 MHz, DMSO-d_6) δ 9.71 (9', s, 1H), 9.56 (9, s, 1H), 8.58 (1, s, 1H), 8.52 (1', s, 1H), 7.39 – 7.34 (7, m, 2H), 7.29 – 7.26 (7', m, 2H), 7.23 – 7.18 (8, m, 2H), 7.16 – 7.12 (8', m, 2H), 7.08 – 7.01 (4, m, 2H, 4', m, 2H), 7.01 – 6.98 (6, m, 1H), 6.97 – 6.94 (6', m, 1H), 6.81 – 6.76 (3, m, 1H, 3', m, 1H), 6.72 – 6.65 (5, m, 1H, 5, m, 1H), 4.90 (2, s, 2H), 4.83 (2', s, 1H).

^{13}C NMR (126 MHz, DMSO-d_6) δ 163.79 (A', s), 162.93 (A, s), 160.55 (L, d, J = 243.18 Hz), 160.23 (L', d, J = 243.32 Hz), 156.03 (D', s), 155.34 (D, s), 137.91 (I, d, J = 2.7 Hz), 135.66 (I', d, J = 3.1 Hz), 130.03 (H', s), 129.29 (F', s), 128.52 (H, s), 128.52 (F, s), 127.96 (J', d, J = 8.4 Hz), 125.55 (J, d, J = 8.5 Hz), 123.12 (C', s), 122.85 (C, s), 119.34 (G, s), 119.24 (G', s), 116.47 (K, d, J = 22.5 Hz), 115.80 (K', d, J = 22.4 Hz), 115.63 (E', s), 115.47 (E, s), 48.95 (B', s), 42.99 (B, s).

^{19}F NMR (471 MHz, DMSO-d_6) δ -116.19 (minor), -116.72 (major).

EI HRMS: obtained m/z 245.08539 M+ (expected m/z 245.08466 M+).

MP: 91 – 93 °C.

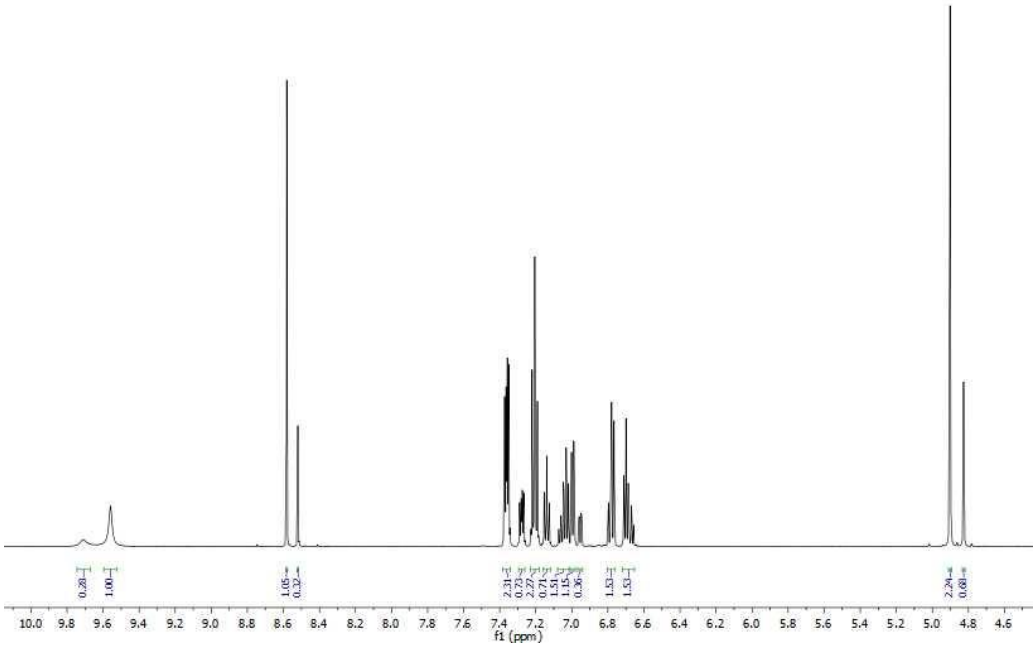
0.28
1.00
1.05
0.32
2.31
0.73
2.27
0.71
1.51
1.15
0.36
1.53
1.53
2.24
0.68
10.0 9.8 9.6 9.4 9.2 9.0 8.8 8.6 8.4 8.2 8.0 7.8 7.6 7.4 7.2 7.0 6.8 6.6 6.4 6.2 6.0 5.8 5.6 5.4 5.2 5.0 4.8 4.6
f1 (ppm)

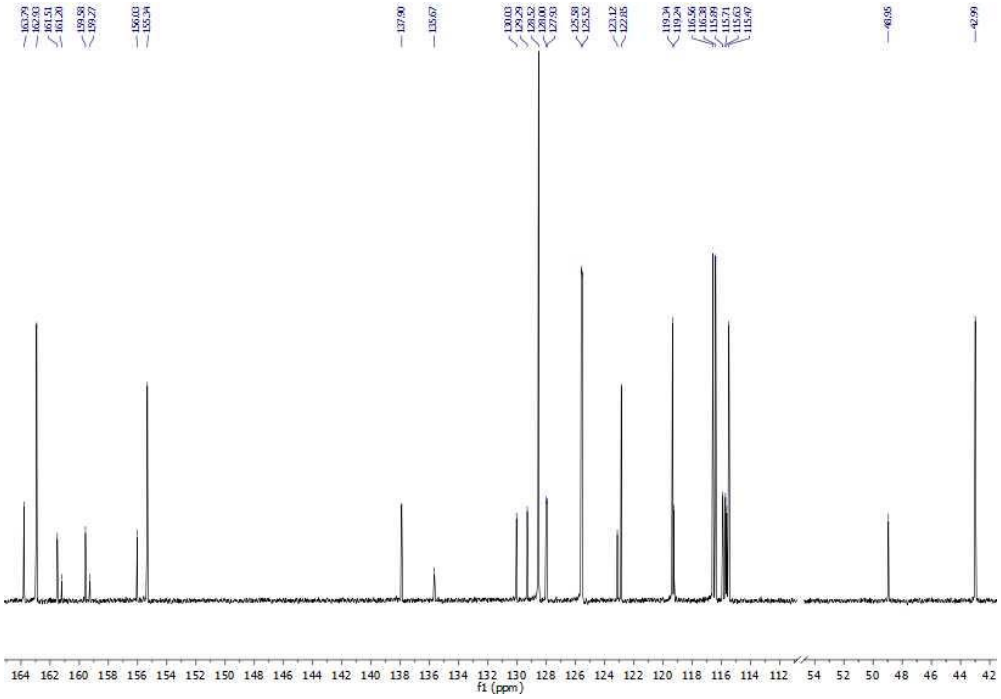
163.29
162.93
161.51
161.20
159.88
159.27
156.03
155.34
137.90
135.67
130.03
129.59
128.52
128.01
127.93
125.58
125.52
123.12
122.85
119.24
119.24
116.56
116.38
115.99
115.71
115.61
115.47
49.95
42.99
164 162 160 158 156 154 152 150 148 146 144 142 140 138 136 134 132 130 128 126 124 122 120 118 116 114 112 54 52 50 48 46 44 42
f1 (ppm)

Synthesis of *N*-[(2,3-dihydroxyphenyl)methyl]-*N*-(4-fluorophenyl)formamide

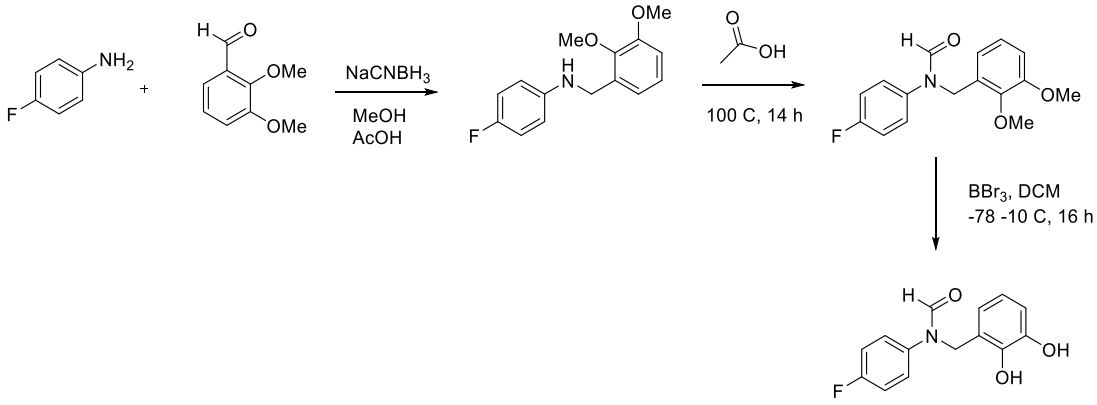

N-[(2,3-dimethoxyphenyl)methyl]-4-fluoro-aniline (57)

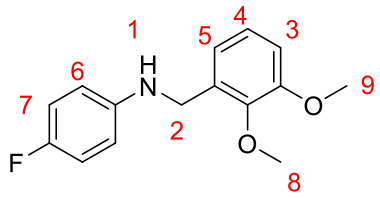

To a solution of 4-fluoroaniline (1.00 mL, 10.5 mmol) in dry methanol (10 mL) was added 2,3-dimethoxybenzaldehyde (2.28 g, 13.7 mmol), and sodium cyanoborohydride (860 mg, 13.7 mmol). Acetic acid (3.00 mL, 52.6 mmol) was then added dropwise and the mixture heated to reflux overnight. The reaction mixture was then reduced under pressure and dissolved in ethyl acetate (10 mL), washed with water (10 mL) and brine (10 mL). The reaction mixture was then concentrated, dried with $MgSO_4$ and purified using column chromatography (30 % EtOAc/*n*-Hex) to yield a colourless oil (2.03 g, 86 %).

^{1}H NMR (500 MHz, Chloroform-*d*) δ 7.04 (5, m, 1H), 6.96 – 6.94 (4, m, 1H), 6.92 – 6.87 (7, 3, m, 3H), 6.63 – 6.59 (6, m, 2H), 4.34 (2, s, 2H), 4.01 (1, s, 1H), 3.90 (8, 9, s, 6H)

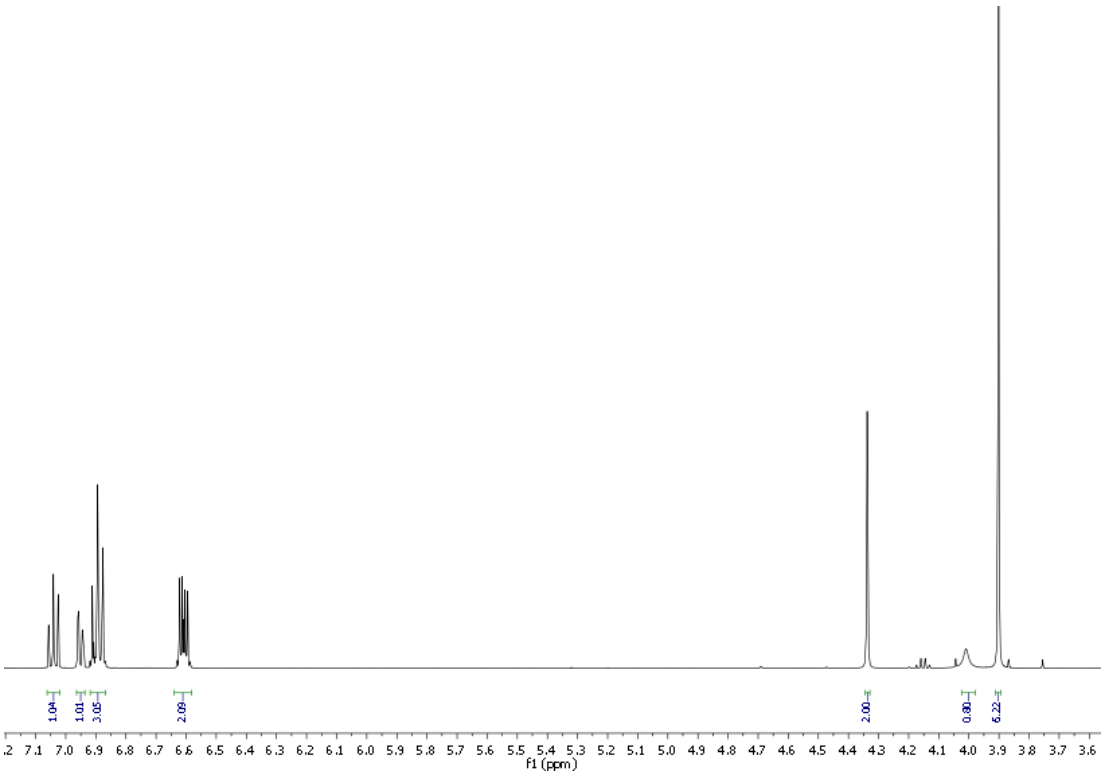

N-[(2,3-dimethoxyphenyl)methyl]-*N*-(4-fluorophenyl)formamide (58)

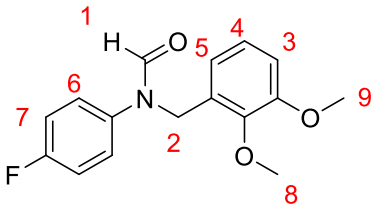

Formic acid (10 mL) was added neat to amine (1.67 g, 7.22 mmol) and the reaction mixture refluxed overnight. The mixture was then diluted in DCM (10 mL) and quenched with saturated Na_2CO_3 (10 mL), washed with water (5 mL) and brine (5 mL), dried over $MgSO_4$, concentrated under reduced pressure and purified using column chromatography (40 % EtOAc:*n*-Hex) to yield a colourless oil (1.32 g, 60%).

^{1}H NMR (601 MHz, Chloroform-*d*) δ 8.56 (1', s, 1H), 8.50 (1, s, 1H), 7.19 – 7.15 (6', m, 2H), 7.12 – 7.07 (6, m, 2H), 7.03 – 6.95 (5, 4, 3, 4', 7', m, 6H), 6.88 (3', m, 1H), 6.85 – 6.80 (7, m, 2H), 6.67 – 6.64 (5', m, 1H), 5.06 (2, s, 2H), 4.82 (2', s, 2H), 3.86 (8', s, 3H), 3.83 (8, s, 3H), 3.81 (9', s, 3H), 3.72 (9, s, 3H).

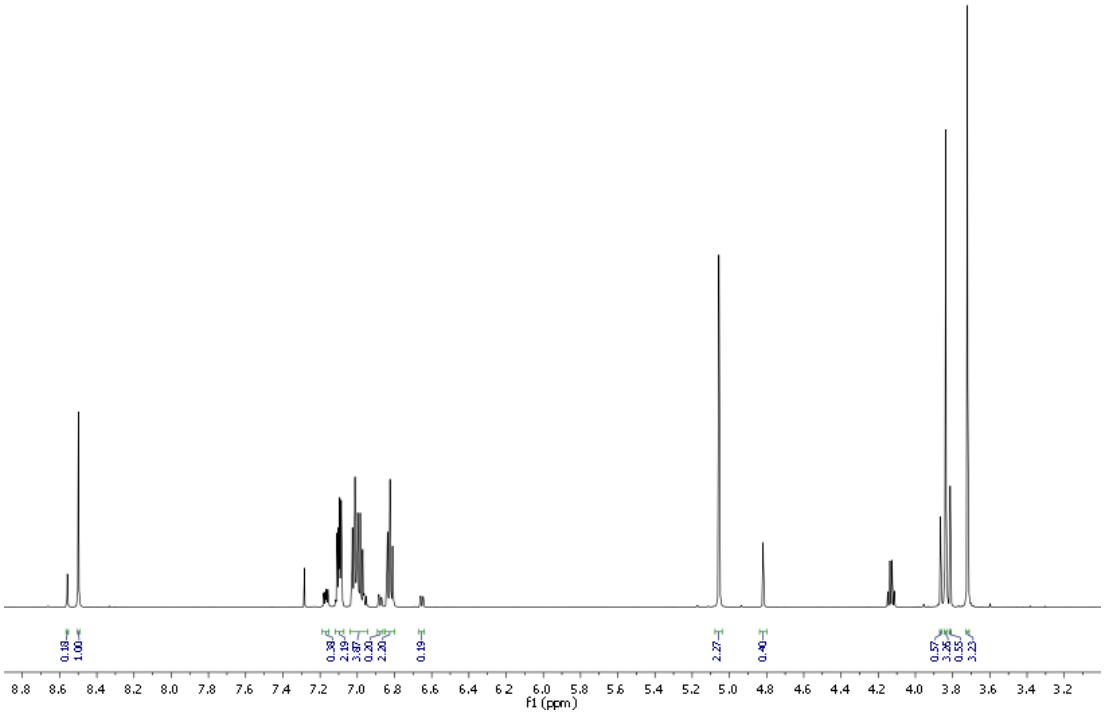
0.18
1.00
0.38
2.19
3.87
0.20
2.20
0.19
2.27
0.40
0.57
3.26
0.55
3.23
8.8 8.6 8.4 8.2 8.0 7.8 7.6 7.4 7.2 7.0 6.8 6.6 6.4 6.2 6.0 5.8 5.6 5.4 5.2 5.0 4.8 4.6 4.4 4.2 4.0 3.8 3.6 3.4 3.2
f1 (ppm)

N-[(2,3-dihydroxyphenyl)methyl]-*N*-(4-fluorophenyl)formamide (53)

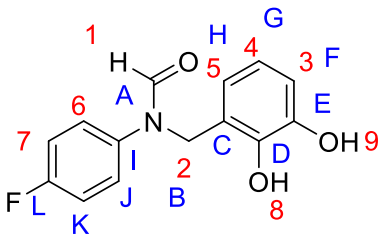

To a flask under a nitrogen atmosphere was added a solution of *N*-(4-fluorophenyl)-*N*-[(2,3,4-trimethoxyphenyl)methyl]formamide (700 mg, 2.41 mmol) in DCM (10 mL). The reaction mixture was cooled to -78 °C and boron tribromide (wt. 33 %. 1.39 mL, 14.5 mmol) in DCM was carefully added dropwise. The reaction mixture was then allowed to warm to room temperature and stirred overnight. The reaction mixture was then quenched with water and extracted with DCM (2 x 10 mL), dried over $MgSO_4$, concentrated under reduced pressure and purified by column chromatography (1:4 EtOAc:*n*-Hex) to yield a white solid (0.60 g, 95 %).

^{1}H NMR (601 MHz, DMSO-d_6) δ 8.57 (1, s, 1H), 8.51 (1', s, 1H), 7.36 – 7.32 (6, m, 2H), 7.30 – 7.27 (6', m, 1H), 7.22 – 7.18 (7, m, 2H), 7.16 – 7.12 (7', m, 2H), 6.67 (3', dd, J = 7.9, 1.6 Hz, 1H), 6.64 (3, dd, J = 7.8, 1.6 Hz, 1H), 6.54 – 6.49 (4, m, 2H, 4', m, 2H), 6.46 (5, dd, J = 7.8, 1.5 Hz, 1H), 6.43 (5', dd, J = 7.7, 1.5 Hz, 1H), 4.90 (2, s, 2H), 4.82 (2', s, 1H).

^{13}C NMR (126 MHz, DMSO-d_6) δ 163.74 (A', s), 162.92 (A, s), 160.54 (L, d, J = 243.18 Hz), 160.20 (L', d, J = 243.18 Hz), 145.51 (E, s), 145.50 (E', s), 144.16 (D', s), 143.50 (D, s), 137.90 (I, d, J = 2.8 Hz), 135.77 (I', d, J = 3.0 Hz), 127.83 (J', d, J = 8.5 Hz), 125.49 (J, d, J = 8.6 Hz), 123.94 (C', s), 123.72 (C, s), 120.14 (H', s), 119.24 (G, s), 119.09 (G', s), 118.79 (H, s), 116.45 (K, d, J = 22.5 Hz), 115.76 (K', d, J = 22.4 Hz), 115.31 (F', s), 114.65 (F, s), 48.87 (B', s), 42.95 (B, s).

^{19}F NMR (471 MHz, DMSO-d_6) δ -116.28 (minor), -116.75 (major).

EI HRMS: obtained m/z 261.07893 M+ (expected m/z 261.07957 M+).

MP: 155 – 157 °C.

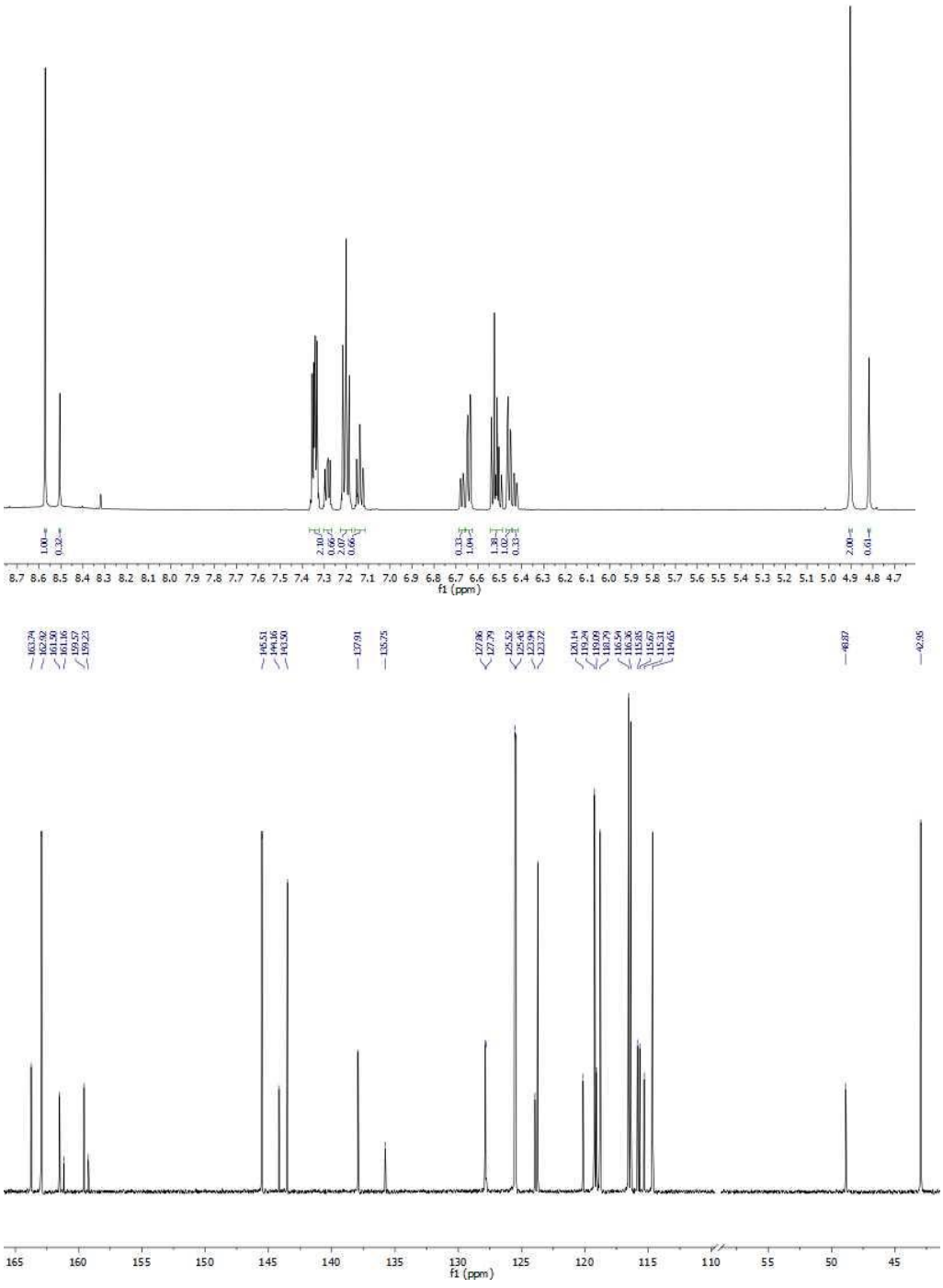
1.00
0.32
2.10
2.66
2.07
0.66
0.33
1.04
1.38
1.02
0.33
2.00
0.61
f1 (ppm)
163.74
162.92
161.90
161.16
159.57
159.23
145.51
144.16
143.50
137.91
130.75
127.86
127.79
125.52
125.45
123.94
123.72
120.14
119.24
119.09
118.79
116.54
116.36
115.98
115.67
115.31
114.65
49.87
42.95
f1 (ppm)

Synthesis of *N*-[(2,3-dihydroxyphenyl)methyl]-*N*-(4-fluorophenyl)formamide

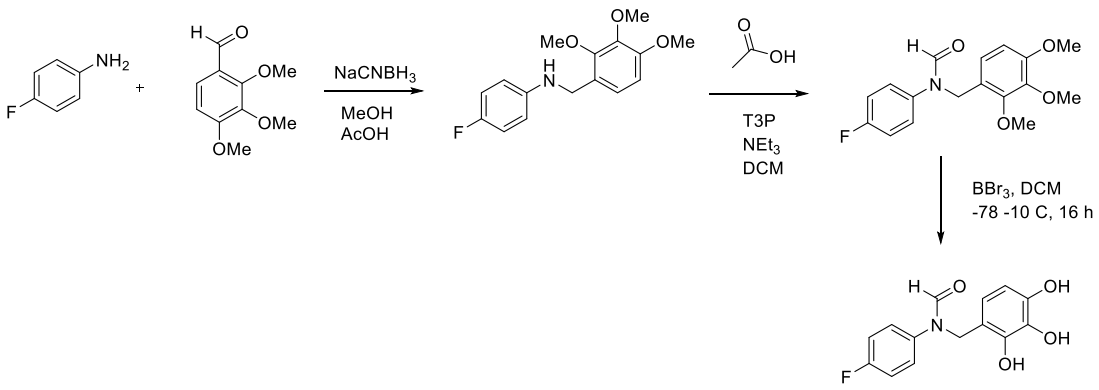

4-fluoro-*N*-[(2,3,4-trimethoxyphenyl)methyl]aniline (59)

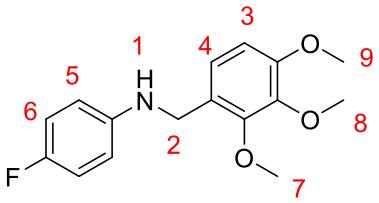

To a solution of 4-fluoroaniline (1.00 mL, 10.5 mmol) in dry methanol (10 mL) was added 2,3,4-trimethoxybenzaldehyde (2.69 g, 13.7 mmol), and sodium cyanoborohydride (860 mg, 13.7 mmol). Acetic acid (3.00 mL, 52.6 mmol) was then added dropwise and the mixture heated to reflux overnight. The reaction mixture was then reduced under pressure and dissolved in ethyl acetate (10 mL), washed with water (10 mL) and brine (10 mL). The crude product yielded a white solid (2.26 g, 74 %) that was used without further purification.

^{1}H NMR (500 MHz, Chloroform-*d*) δ 7.00 (4, m, 1H), 6.92 – 6.88 (6, m, 2H), 6.66 – 6.59 (5, 3, m, 3H), 4.24 (2, s, 2H), 3.95 (7, s, 3H), 3.91 (8, s, 4H), 3.87 (9, s, 3H).

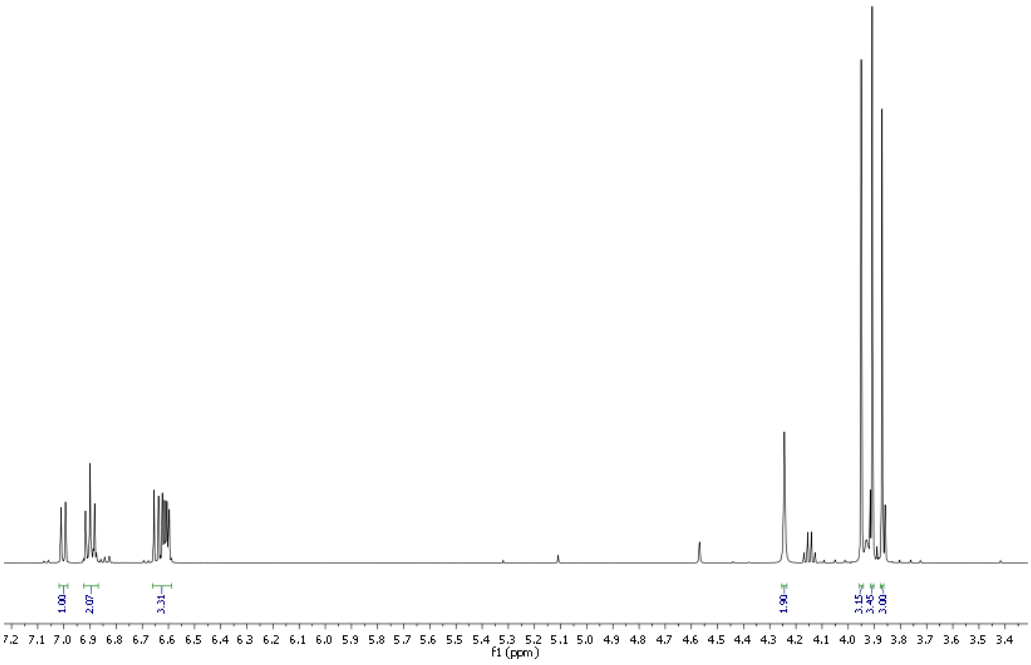

N-(4-fluorophenyl)-*N*-[(2,3,4-trimethoxyphenyl)methyl]formamide (60)

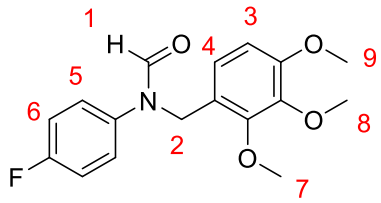

To a solution of 4-fluoro-*N*-[(2,3,4-trimethoxyphenyl)methyl]aniline (400 mg, 1.37 mmol) in dry DCM (10 mL) was added formic acid (63.2 mg, 51.8 µL, 1.37 mmol). Propylphosphonic anhydride solution (960 mg, 897 µL, 1.51 mmol) was then added followed by trimethylamine (166 mg, 229 µL, 1.64 mmol). The reaction mixture was stirred overnight at room temperature and then extracted with DCM (10 mL), washed with 2M HCl (10 mL), water (10 mL) and brine (10 mL). The combined organic phases were then dried over $MgSO_4$ and concentrated *in vacuo*. The crude product yielded a colourless oil (200 mg, 64%) and was used further without purification.

^{1}H NMR (500 MHz, Chloroform-*d*) δ 8.55 (1', s, 1H), 8.45 (1, s, 1H), 7.15 – 6.99 (5, 6, 5', 6', m, 8H), 6.92 (4, m, 1H), 6.67 (4', m, 1H), 6.60 (3, m, 1H), 6.55 (3', m, 1H), 4.96 (2, s, 2H), 4.73 (2', s, 2H), 3.90 (7', s, 3H), 3.86 (8', s, 3H), 3.85 (9', s, 3H), 3.84 (7, s, 3H), 3.82 (8, s, 3H), 3.74 (9, s, 3H).

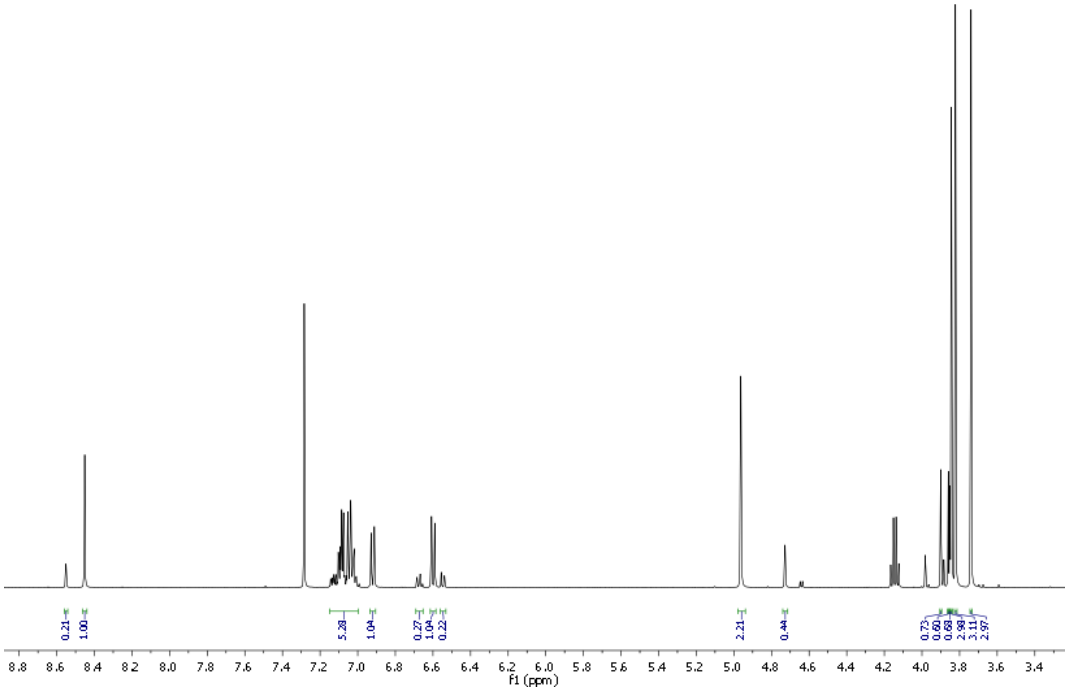

N-(4-fluorophenyl)-*N*-[(2,3,4-trihydroxyphenyl)methyl]formamide (54)

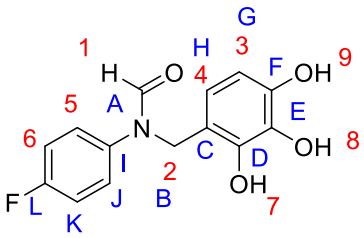

To a flask under a nitrogen atmosphere was added a solution of (200 mg, 0.626 mmol) in DCM (10 mL). The reaction mixture was cooled to -78 °C and boron tribromide (wt. 33 %. 1.88 g, 723 µL, 7.52 mmol) in DCM was carefully added dropwise. The reaction mixture was then allowed to warm to room temperature and stirred overnight. The reaction mixture was then quenched with water (5 mL) and extracted with DCM (2 x 10 mL), dried over $MgSO_4$, concentrated under reduced pressure and purified by column chromatography (1:1 EtOAc:*n*-Hex) to yield a white solid (90.0 mg, 52 %).

^{1}H NMR (500 MHz, DMSO-d_6) δ 8.51 (1, s, 1H), 8.47 (1', s, 1H), 7.33 – 7.28 (5, m, 2H), 7.26 – 7.22 (5', m, 2H), 7.21 – 7.16 (6, m, 2H), 7.15 – 7.11 (6', m, 2H), 6.29 (4, d, J = 8.3 Hz, 1H), 6.24 (4', d, J = 8.3 Hz, 1H), 6.18 (3, d, J = 8.3 Hz, 1H), 6.15 (3', d, J = 8.2 Hz, 1H), 4.81 (2, s, 2H), 4.71 (2', s, 1H).

^{13}C NMR (126 MHz, DMSO-d6) δ 163.59 (s), 162.89 (s), 160.56 (d, *J* = 243.23 Hz), 160.21 (d, *J* = 243.15 Hz), 146.29 (s), 145.70 (s), 145.41 (s), 144.70 (s), 137.84 (d, *J* = 2.8 Hz), 135.82 (s), 133.41 (s), 133.39 (s), 128.08 (d, *J* = 8.5 Hz), 125.85 (d, *J* = 8.5 Hz), 119.85 (s), 118.66 (s), 116.36 (d, *J* = 22.7 Hz), 115.69 (d, *J* = 22.1 Hz), 114.86 (s), 114.55 (s), 107.01 (s), 106.68 (s), 49.14 (s), 42.88 (s).

^{19}F NMR (471 MHz, DMSO-d_6) δ -116.34 (minor), -116.70 (major).

EI HRMS: obtained m/z 277.07314 M+ (expected m/z 277.07449 M+).

MP: 155 – 156 °C.